NAVAL POSTGRADUATE SCHOOL

MONTEREY, CALIFORNIA

THESIS

AN ANALYSIS OF NUMERICAL WEATHER PREDICTION OF THE DIABATIC ROSSBY VORTEX

by

Matthew W. McKenzie

June 2014

Thesis Advisor:	Richard W. Moore
Second Reader:	Michael T. Montgomery

Approved for public release; distribution is unlimited

THIS PAGE INTENTIONALLY LEFT BLANK

REPORT DOCUMENTATION PAGE

Form Approved OMB No. 0704-0188

1. AGENCY USE ONLY *(Leave blank)*	2. REPORT DATE	3. REPORT TYPE AND DATES COVERED
	June 2014	Master's Thesis

4. TITLE AND SUBTITLE
AN ANALYSIS OF NUMERICAL WEATHER PREDICTION OF THE DIABATIC ROSSBY VORTEX

5. FUNDING NUMBERS

6. AUTHOR(S) MATTHEW W. MCKENZIE

7. PERFORMING ORGANIZATION NAME(S) AND ADDRESS(ES)
Naval Postgraduate School
Monterey, CA 93943-5000

8. PERFORMING ORGANIZATION REPORT NUMBER

9. SPONSORING /MONITORING AGENCY NAME(S) AND ADDRESS(ES)
N/A

10. SPONSORING/MONITORING AGENCY REPORT NUMBER

11. SUPPLEMENTARY NOTES The views expressed in this thesis are those of the author and do not reflect the official policy or position of the Department of Defense or the U.S. Government. IRB Protocol number ____N/A____.

12a. DISTRIBUTION / AVAILABILITY STATEMENT
Approved for public release; distribution is unlimited

12b. DISTRIBUTION CODE

13. ABSTRACT (maximum 200 words)

This work examines diabatic Rossby vortex (DRV) predictability through the examination of 12 cases of DRV genesis and evolution that undergo explosive deepening. An objective DRV identification script is created and applied to European Center for Medium Range Forecasting (ECMWF) ensemble data.

The script is verified via an examination of the observed lifecycle of a DRV associated with recurving tropical cyclone Chaba. An assessment of the control forecast indicated significant uncertainty regarding the predictability of the DRV with no explosive deepening predicted.

The evaluation of the 12 control forecasts identified two good forecasts, indicating generally poor performance. The DRV identification script was then applied to the ECMWF ensemble data. The analysis of the perturbed member forecasts exhibited similar characteristics to those of the 12 control forecasts and large uncertainty in the vicinity of the observed DRVs was found.

The analysis of ensemble data in the selected cases is shown to provide valuable information. It is possible to quantify the uncertainty and to identify a subset of members that provide a disturbance genesis and evolution that is similar to the observed. Given the large initial condition uncertainty in such cases, it is apparent that a probabilistic approach should be incorporated when examining DRV predictability.

14. SUBJECT TERMS	15. NUMBER OF PAGES
Diabatic Rossby Vortex	225
	16. PRICE CODE

17. SECURITY CLASSIFICATION OF REPORT	18. SECURITY CLASSIFICATION OF THIS PAGE	19. SECURITY CLASSIFICATION OF ABSTRACT	20. LIMITATION OF ABSTRACT
Unclassified	Unclassified	Unclassified	UU

NSN 7540-01-280-5500

Standard Form 298 (Rev. 2-89)
Prescribed by ANSI Std. 239-18

THIS PAGE INTENTIONALLY LEFT BLANK

Approved for public release; distribution is unlimited

AN ANALYSIS OF NUMERICAL WEATHER PREDICTION OF THE DIABATIC ROSSBY VORTEX

Matthew W. McKenzie
Lieutenant Commander, United States Navy
B.S., University of South Carolina, 2003

Submitted in partial fulfillment of the
requirements for the degree of

MASTER OF SCIENCE IN METEOROLOGY

from the

NAVAL POSTGRADUATE SCHOOL
June 2014

Author: Matthew W. McKenzie

Approved by: Richard W. Moore
Thesis Advisor

Michael T. Montgomery
Second Reader

Wendell A. Nuss
Chair, Department of Meteorology

THIS PAGE INTENTIONALLY LEFT BLANK

ABSTRACT

This work examines diabatic Rossby vortex (DRV) predictability through the examination of 12 cases of DRV genesis and evolution that undergo explosive deepening. An objective DRV identification script is created and applied to European Center for Medium Range Forecasting (ECMWF) ensemble data.

The script is verified via an examination of the observed lifecycle of a DRV associated with recurving tropical cyclone Chaba. An assessment of the control forecast indicated significant uncertainty regarding the predictability of the DRV with no explosive deepening predicted.

The evaluation of the 12 control forecasts identified two good forecasts, indicating generally poor performance. The DRV identification script was then applied to the ECMWF ensemble data. The analysis of the perturbed member forecasts exhibited similar characteristics to those of the 12 control forecasts and large uncertainty in the vicinity of the observed DRVs was found.

The analysis of ensemble data in the selected cases is shown to provide valuable information. It is possible to quantify the uncertainty and to identify a subset of members that provide a disturbance genesis and evolution that is similar to the observed. Given the large initial condition uncertainty in such cases, it is apparent that a probabilistic approach should be incorporated when examining DRV predictability.

THIS PAGE INTENTIONALLY LEFT BLANK

TABLE OF CONTENTS

THIS PAGE INTENTIONALLY LEFT BLANK

LIST OF FIGURES

LIST OF TABLES

LIST OF ACRONYMS AND ABBREVIATIONS

APE	available potential energy
CAA	cold air advection
CSV	comma separated values
DRV	diabatic Rossby vortex
DRW	diabatic Rossby wave
EC	extratropical cyclone
ECMWF	European Center for Medium-Range Forecasting
FCST	forecast
GIS	geographic information system
HPA	hectopascals
HR	hour
K	kelvin
KM	kilometer
LAT	latitude
LLJ	low-level jet
LON	longitude
M	meter
NH	Northern Hemisphere
PT	potential temperature
PVA	positive vorticity advection
PV	potential vorticity
Q	relative humidity
RH	relative humidity
SG	semigeostrophic
SLP	sea level pressure
WAA	warm air advection
2D	two-dimensional
3D	three-dimensional

THIS PAGE INTENTIONALLY LEFT BLANK

ACKNOWLEDGMENTS

I would like to thank my second reader, Professor Michael Montgomery. His hard work and insightful revisions helped me complete the work presented in this thesis. His subject-matter expertise was greatly appreciated.

I would like to express thanks and appreciation to my classmates. I owe them more than I could ever repay. They became my family while I was at NPS.

Above all, I would like to thank my advisor, Rich, for his encouragement and patience. I am absolutely certain that without his unwavering support I would not have been able to complete this thesis.

THIS PAGE INTENTIONALLY LEFT BLANK

I. INTRODUCTION

The diabatic Rossby vortex (DRV) is a small-scale cyclonic disturbance that forms in the absence of upper-level forcing. Besides being of a smaller scale than a typical extratropical cyclone (EC), the DRV also differs in the method of formation. Instead of being primarily driven by upper-level positive vorticity advection (PVA), DRV genesis is dominated by the diabatic generation of low-level potential vorticity (PV) in the vicinity of both sufficient baroclinicity and moisture. (Moore and Montgomery 2004)

In more general terms, a DRV is initially formed when a large amount of condensation, occurs in a very moist atmosphere along a strong temperature gradient. The condensation releases a large amount of latent heat, which sets up a strong positive lapse rate with a warmed air mass aloft sitting above an air mass being cooled by precipitation and downdrafts. This arrangement of warm air over cool forms a positive PV anomaly that generates a localized cyclonic rotation of winds, which begin to move the moist air meridionally up along the temperature gradient wedge. As the moist air rises along the thermal wedge it cools adiabatically until it reaches saturation, at which point it condenses, releases latent heat, and begins to form a new PV anomaly. In the Northern Hemisphere (NH), the cyclonic flow of warm, moist air generally occurs to the east/northeast of the original PV anomaly. The formation of the new PV anomaly on the downstream side, and the weakening of the original anomaly from cold air advection and subsidence on the upstream side, begins a cycle of self-regeneration and propagation of the DRV east/northeast along the temperature gradient. (Parker and Thorpe 1995) This propagation of the DRV will continue until the disturbance comes into contact with a pre-existing upper-level trough or extratropical cyclone and intensifies, or moves into an area with insufficient moisture or baroclinicity and decays. (Moore and Montgomery 2004, Boettcher and Wernli 2013)

The requirement for a substantial amount of moisture in the atmosphere dictates that the vast majority of DRVs will form over oceans; more specifically over the warm currents on the western boundaries of the Atlantic and Pacific basins. Combined with the general east-northeast propagation pattern (in the NH), it is apparent that the genesis and

propagation phases of a DRV lifespan occur in observation-sparse areas of the globe. DRV genesis also often occurs in dynamically complex situations such as the remnants or outflow of extratropical cyclones, mesoscale convective systems (MCS), and tropical cyclones (TC). (Boettcher and Wernli 2013) The sparse observational data of the regions of genesis and propagation and the complex environments in which DRVs spawn, as can be observed in Figure 1, make identifying and forecasting the disturbances very challenging.

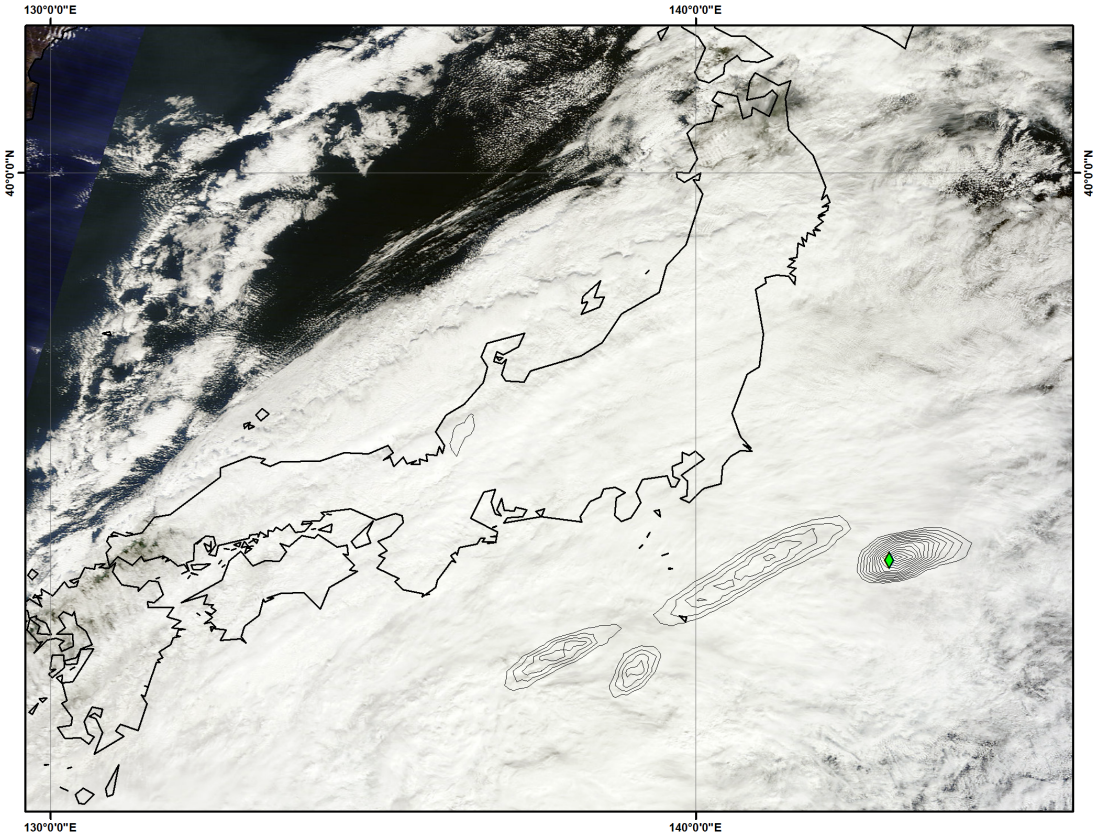

Figure 1. MODIS true color satellite imagery of outflow of TC Chaba 0120 UTC 28 October 2010 (NASA/GSFC, Rapid Response). The green diamond represents the location of a DRV at time 00 UTC 28 October 2010 (climatology data from Boettcher and Wernli 2013), and the thin black lines are contours of positive relative vorticity (first contour at 3.5 x 10^{-4} s^{-1}, additional contours every 0.5 x 10^{-5}) (derived from TIGGE ECMWF ensemble forecast data).

A DRV that undergoes explosive deepening has three distinct phases in its lifecycle: genesis, propagation, and intensification/decay. (Boettcher and Wernli 2011) While the genesis and propagation phases are relatively benign, with only moderate surface level pressure falls and localized convection, it is the intensification stage of the DRV lifecycle that drives much of the urgency for better understanding of these storm systems. As low-level DRV disturbances approach the North American and European continents from the west, there exists the possibility of interaction with an upper-level trough or other synoptic scale disturbance. The likely outcome of this interaction is referred to as a meteorological "bomb"; an explosive intensification and rapid fall in surface pressure that often generate devastating storm systems. (Boettcher and Wernli 2011, 2013)

In his thesis, Shih (2012) linked "bombing" DRVs to extreme weather events (Figure 2), including explosive cyclones (Gyakum et al. 1992; Wernli 02; Moore, Montgomery, and Davies 2008; Boettcher and Wernli 2011; CB11), mesoscale convective vortices (Raymond and Jiang 1990; Davis and Weisman 1994; Jiang and Raymond 1995; Conzemius et al. 2007; Conzemius and Montgomery 2010), squall lines (Parker and Thorpe 1995), and polar lows (Montgomery and Farrell 1992; Fantini and Buzzi 1993; Mak 1994).

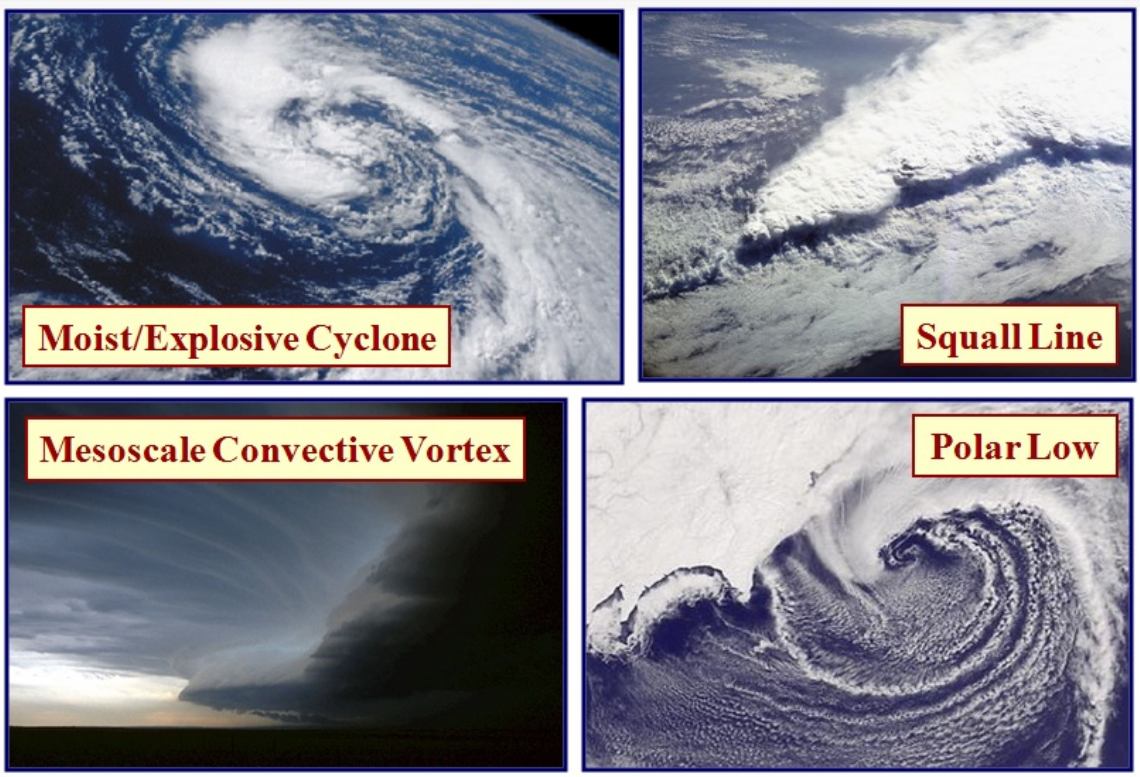

Figure 2. High impact weather with precursor/pathway linked to DRVs (from Shih 2012).

While more than 100 diabatic Rossby vortices occur on average every year, the subset that "bomb" is a relatively small percentage (roughly 15 percent). Yet despite the prevalent nature of both intensifying and non-intensifying DRVs, Numerical weather prediction (NWP) models struggle with all three DRV lifecycle phases. The first two phases of the DRV are challenging due to the small-scale and fast propagation characteristics of a DRV given the spatial and temporal limitations of current NWP models. Furthermore, forecasting DRV interactions with upper-level features can also prove to be problematic for NWP models, with either underrepresentation of the strength of the DRV or upper-level trough or phasing errors of the converging storm systems. (Boettcher and Wernli 2011, 2013)

The intent of this thesis is to investigate both control and probabilistic NWP forecast skill with respect to diabatic Rossby vortices. The primary analysis for this study will be conducted on 12 test cases selected from a 10-year DRV climatology (developed

by Boettcher and Wernli 2013) and the European Centre for Medium-Range Weather Forecasting (ECMWF) ensemble forecast data covering those events. The scope of this study will be to objectively analyze the ECMWF model's ability to forecast the genesis and early propagation phases of the selected DRV case studies.

THIS PAGE INTENTIONALLY LEFT BLANK

II. BACKGROUND

A. PREVIOUS RESEARCH

1. Type A Cyclogenesis

In 1971, Petterssen and Smebye (hereafter referred to as PS71) postulated that cyclogenesis for extratropical cyclones begins in one of two ways. Using the naming convention Type A and Type B, PS71 distinguished the two from the perspective of upper-level forcing at genesis. Type B cyclogenesis is typical of most EC disturbances with an upper-level trough and positive vorticity advection serving as a lifting mechanism and initiating a low-level baroclinic zone. Type A cyclogenesis, conversely, begins with a low-tropospheric cyclonic disturbance and subsequently develops upper-level support for growth.

Though the two cyclogenesis regimes were in regards to synoptic scale extratropical cyclones, the "bottom-up" growth mechanic would later form the foundation for DRV dynamics.

2. The Meteorological "Bomb"

Sanders and Gyakum (1980, hereafter referred to as SG80) coined the meteorological term "bomb" after adapting Tor Bergeron's work on "rapidly deepening" extratropical cyclones. Tor Bergeron originally defined "rapidly deepening" as a pressure fall of 1hpa/hr for a minimum of 24 hours. While Bergeron's initial equation for falling pressure was conceived for cyclones at around 60° N, SG80 modified it to be applicable across all latitudes by geostrophic adjustment, which resulted in Equation 1.

$$1Bergeron = 24 * (\sin\phi / \sin 60°)\,\text{hPa}/\,24hr \tag{1}$$

Despite being devised as a metric for extratropical cyclones, this calculation is also a useful benchmark when applied to DRVs. A DRV is considered a "bomb" if it deepens at least one Bergeron during the intensification phase of its lifecycle. Extreme weather associated with a DRV is almost always the result of a "bomb," but it is worth

noting that the majority of DRVs do not "bomb." Finally, all DRV cases studied for this thesis were identified as "bombs."

3. Moist Baroclinic Instability

Laying the groundwork for the mechanics of DRV genesis, Raymond and Jiang (1990; hereafter referred to as RJ90) postulated the existence of self-sustaining moist baroclinic processes at work within a subset of mesoscale convective systems (MCS). Within these specific MCSs, examples that include supercell thunderstorms and squall lines, RJ90 theorized that the condensation of water vapor within the column of convection release tremendous amounts of latent heat. This localized heating of the lower troposphere then establishes a pocket of warm air relative to both the cooler air below and above the level of convection.

The warm air mass at mid-tropospheric levels produces a positive lapse rate above the cooler air located near the surface and a negative lapse rate between the warm air mass and the cooler air above. Ertel's equation for PV (Equation 2) indicates that an increasing positive lapse rate would result in an increase to the static stability and therefore generate positive PV. The reverse would also hold true for a decreasing negative lapse rate.

$$PV = (\zeta_\theta + f)(-g\frac{\delta\theta}{\delta p}) \tag{2}$$

The result would be the development of a positive PV anomaly in the lower troposphere and a negative PV anomaly aloft at the tropopause. The low-level PV anomaly would then initiate cyclonic circulation (or intensify a preexisting circulation) as seen in Figure 3.

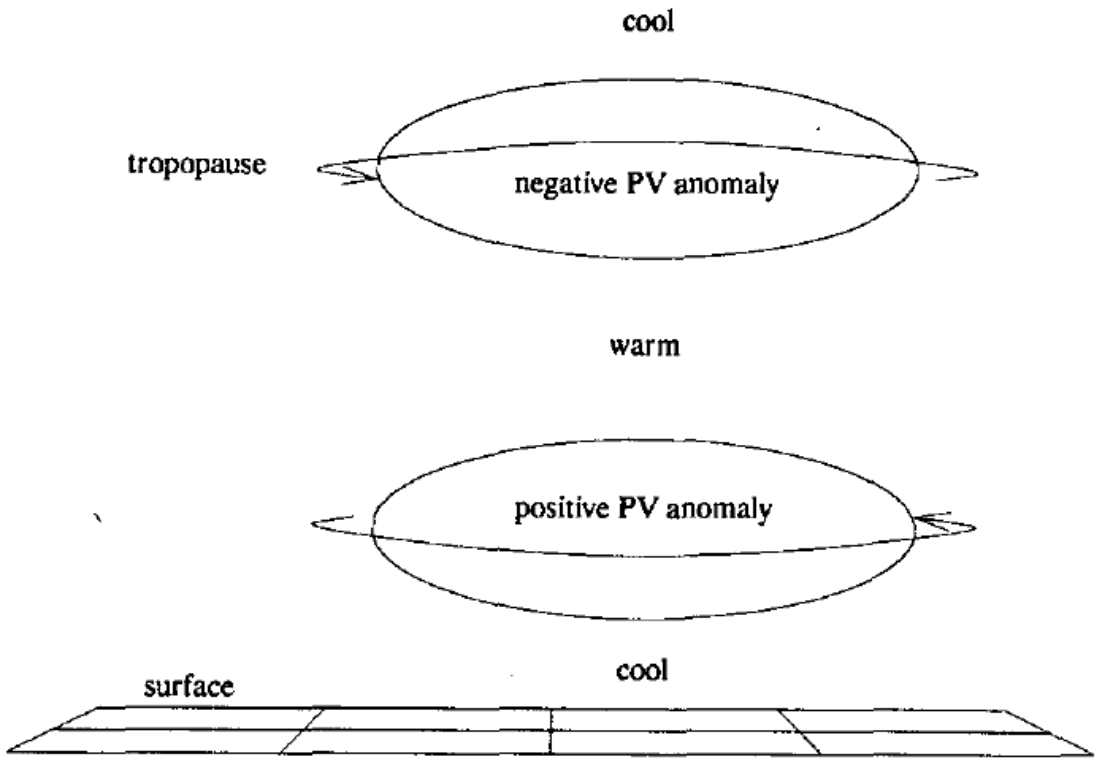

Figure 3. Postulated structure of potential vorticity anomalies produced by a region of convection and the associated changes in temperature and wind structure. The circulation is cyclonic around the lower, positive anomaly, and anticyclonic around the upper anomaly as shown by arrows (from RJ90).

If the lower-tropospheric positive PV anomaly was located along a baroclinic zone, the cyclonic circulation would then further increase convective activity through isentropic lifting. Figure 4 illustrates the movement of warm, moist air up along the isentropic surfaces ahead of the PV anomaly and the descent of cool, dry air behind. In this manner, convection, condensation, and latent heat release are triggered ahead (to the east) of the system. Behind the system air parcels are descending and cooling, depressing convection to the west of anomaly. Through these strengthening and weakening mechanics ahead and behind the disturbance, the positive PV anomaly propagates eastward.

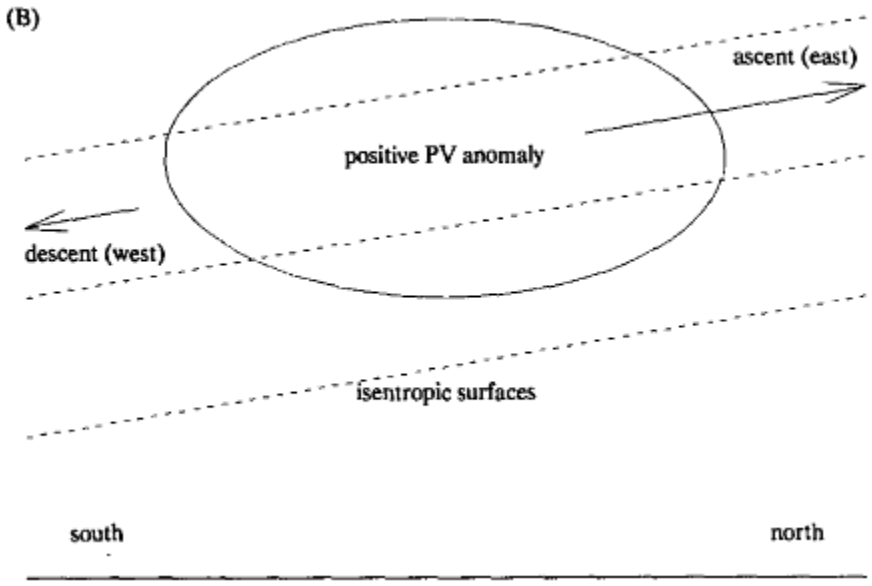

Figure 4. A diagram of a positive PV anomaly from the east. The dotted lines represent isentropic surfaces with warm air to the south and cool air to the north. As cyclonic circulation increase, air parcels will ascend meridionally ahead of the PV anomaly and descend behind (after RJ90).

The moist baroclinic instability research conducted by RJ90 was focused on MCS disturbances, but the mechanics of the self-sustaining, low-tropospheric positive PV anomaly would later form the framework for understanding DRV dynamics.

4. The Diabatic Rossby Wave

Parker and Thorpe (1995; hereafter referred to as PT95) continued the research of moist baroclinic disturbances using a highly idealized model setup. Utilizing a semigeostrophic (SG), two-dimensional (2D) model in a moist baroclinic atmosphere, PT95 identified a system uniquely different from the typical dry baroclinic Rossby wave. PT95 would name this newly discovered convective system the diabatic Rossby wave (DRW).

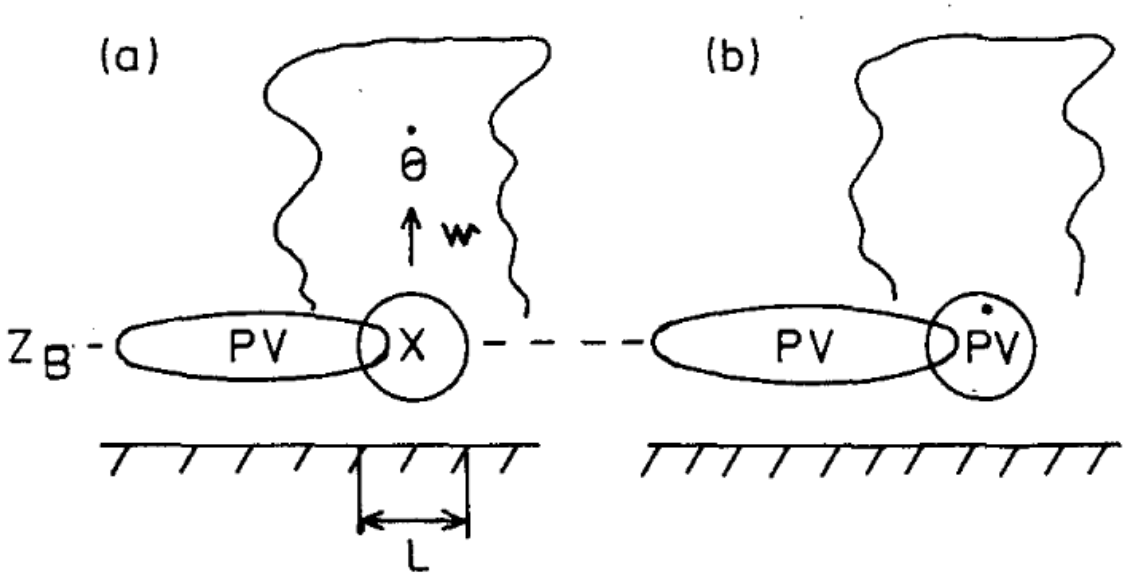

Figure 5. Schematic representations of the dynamics of the diabatic Rossby wave. Here L is the horizontal scale of the jet on the eastern side of the PV anomaly. (a) The poleward jet (marked by "X") associated with the lower tropospheric PV anomaly gives positive thermal advection, leading to upward motion and diabatic heating. (b) This diabatic heating leads to a PV tendency to the east of the low-level PV anomaly (from PT95).

The growth and intensification dynamics of the DRW (viewed from the south) are illustrated above in Figure 5. Figure 5(a) portrays a low-level PV anomaly with an inherent cyclonic circulation initiates a meridional low-level jet (LLJ). The meridional LLJ, depicted in the figure above with an "X" is traveling north (into the page) and advecting warm, moist air. This warm, moist air is rising along isentropic surfaces as identified the by the ascending *w*. As the air parcels rise, cool, and condense they release large amounts of latent heat, represented by θ in the figure. These dynamics serve to increase the positive lapse rate and static stability, in the same manner as described in section 3, and form an increasing PV anomaly to the east of the original as depicted in Figure 5(b).

The process of PV generation and growth to the east is the functional mechanic of propagation for the DRW. The newly formed PV anomaly grows in strength forming its own cyclonic circulation pattern which weakens the original PV anomaly to the west and

begins to form a growing PV anomaly further to the east. As long as the regenerating PV anomalies continue to exist in a moist, baroclinic atmosphere the process acts as a self-sustaining growth mechanism.

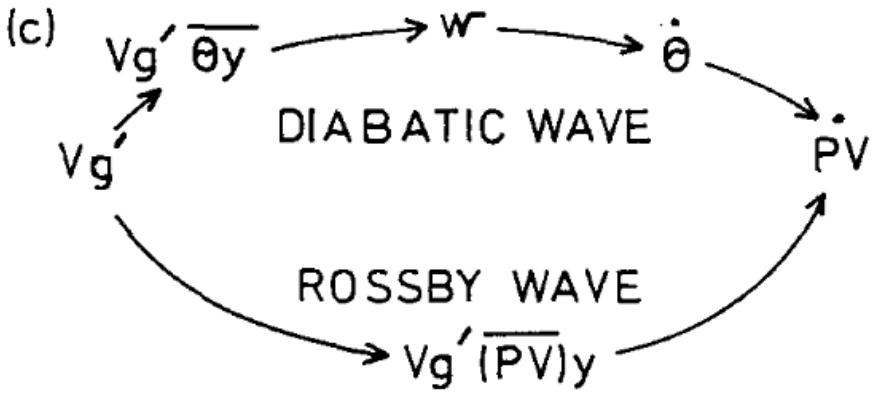

Figure 6. A comparison between the dynamical processes involved in the diabatic wave and the classical Rossby wave, linking the meridional advection with the PV tendency (from PT95).

To differentiate between a classic Rossby wave and the newly identified diabatic Rossby wave PT95 created the flow diagram represented in Figure 6. While a classic Rossby wave PV tendency the result of meridional advection of PV (lower path of Figure 6), the diabatic Rossby wave undergoes meridional thermal advection, leading to rising motion, latent heat release, a growing PT anomaly aloft, and finally the resulting PV tendency (upper path of Figure 5). The end result is opposite propagation orientations for the two waves. Due to the meridional advection of positive PV occurring to the west in a classical Rossby wave, the propagation direction (before introducing background flow) is westward, while meridional thermal advection to the east of the low level PV disturbance in a diabatic Rossby vortex propagates the disturbance eastward (for phenomenon in the northern hemisphere).

5. The Diabatic Rossby Vortex

Moore and Montgomery (2004), hereafter referred to as MM04, employed a semi geostrophic (SG), two-dimensional (2D) model with a parameterization of latent heat release in pursuit of better understanding of growth-rates, wavelength cut-offs, energetics, and the structures of diabatic normal modes in moist, baroclinic environments.

a. Growth Rate and Wavelength

MM04 modeled the growth rates of both dry and moist disturbances and evaluated them against non-dimensional wavenumber (k) and wavelength (km), as seen in Figure 7. While the growth regimes of the dry and moist disturbances are similar in shape at larger wavelengths, it was calculated that a moist system exhibits a larger maximum growth rate 1.14 times the dry maximum, yet peaks at a slightly shorter wavelength of 3490 km (moist) compared to 3900 km (dry). The moist system also clearly displays two distinct growth regimes, whereas the dry mode has a single growth regime with a distinct shortwave cut-off at around 3000 km.

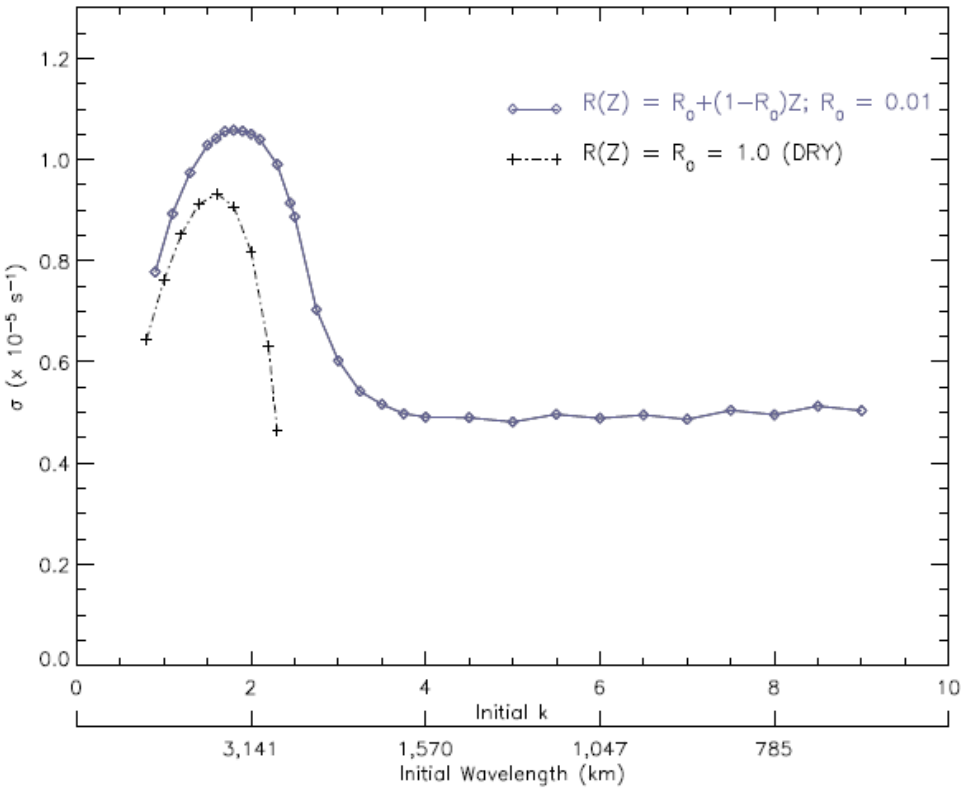

Figure 7. Growth rate (σ; $\times 10^{-5}$ s^{-1}) as a function of initial nondimensional wavenumber and dimensional wavelength (km) of a dry system (dot-dash line) and a moist system (solid line) (after MM04).

As described above, at longer wavelengths the moist mode behaves in a similar manner to a dry baroclinic wave that has been modified by diabatic effects, but below wavelengths of around 1900 km the disturbance growth rate levels off and becomes independent of zonal wavelength. MM04 adopted the convention of Eady (1949) and thereafter refer to the two regimes as long-wave (those with zonal wavelengths larger than 1900 km) and cyclone wave (those with zonal wavelengths less than 1900 km) disturbances. The long-wave can be related to a typical baroclinic wave that relies on upper-level forcing, while the cyclone wave can be equated to the diabatic Rossby wave (identified in section 4), as it is diabatically dominated and has no reliance on an upper-level disturbance for development.

b. Phase Speed and Wavelength

Similar to the growth regimes identified in section 5a, the phase speed of moist disturbances also fall into two distinct regimes. Figure 8 demonstrates the phase speed changes of a moist system across a wavelength spectrum. When observing the phase speed of long-wave (baroclinic) disturbances, a relatively flat decay rate is displayed. As wavelengths decrease and cross below the previously identified boundary of the cyclone wave, phase speeds transition to more of an exponential decay.

With both growth rate and phase speed adhering to two distinct regimes, and with both regimes having similar wavelength cut-offs, it is intuitive that long-wave and cyclone wave disturbances are being driven by distinctly different dynamics.

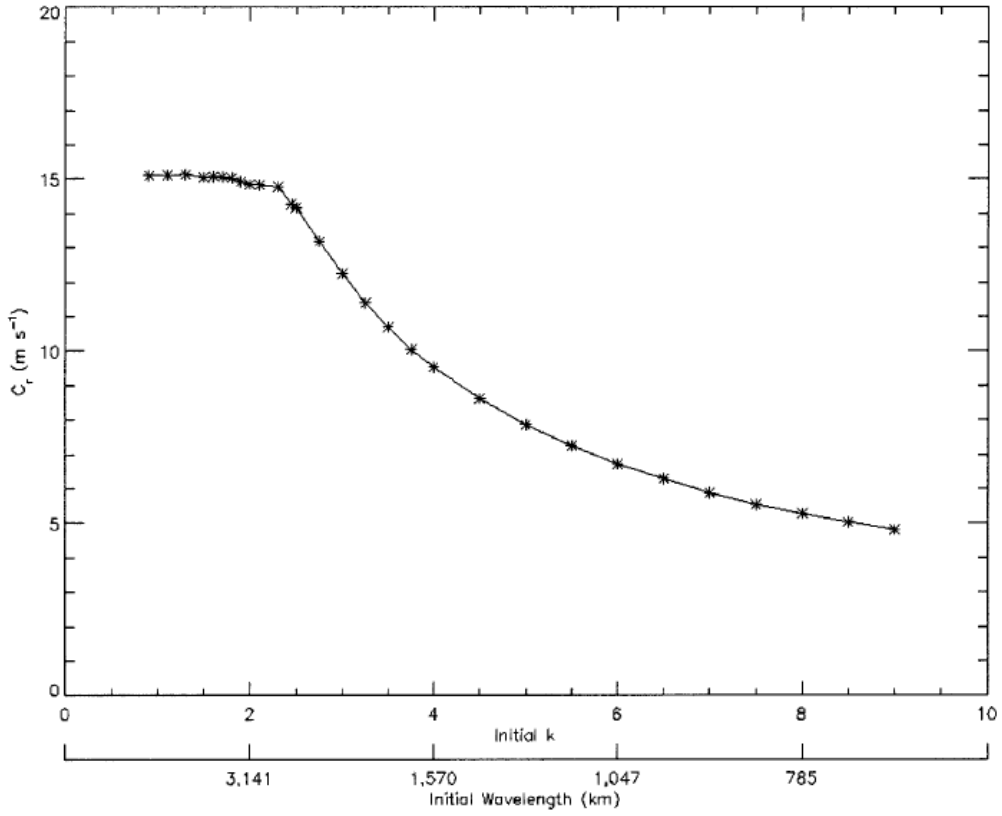

Figure 8. The real part of the phase speed (C_r; m s^{-1}) as a function of initial nondimensional wavenumber and dimensional wavelength (km) for a system with a vertically varying moisture parameter for the exponentially unstable disturbance at a given zonal wavenumber k (from MM04).

c. Energetics

MM05 further differentiated the dynamics of long-wave and cyclone wave disturbances through their respective growth energetics. The diagnostic eddy available potential energy (APE) equation was defined by Lorenz (1955) and Norquist et al. (1977) as:

$$\frac{\delta A_E}{\delta t} = C_A - C_E + G_E \tag{3a}$$

$$A_E = \int_{P1}^{P2} \frac{[\overline{T'^2}]}{2\overline{\sigma}} dp \tag{3b}$$

The LHS of Equation 3 represents the change in eddy APE (A_E) over time, while the RHS variables can be expressed as:

$$C_A = -\int_{P1}^{P2} \frac{[\overline{\upsilon' T'}]}{\overline{\sigma}} \frac{\overline{\partial [T]}}{\partial y} dp - \int_{P1}^{P2} \frac{[\overline{\omega' T'}]}{\overline{\sigma}} \frac{\overline{\partial [T]}^*}{\partial p} dp \tag{4}$$

$$C_E = -\frac{1}{g} \int_{P1}^{P2} \frac{R}{p} [\overline{\omega' T'}] dp \tag{5}$$

$$G_E = \int_{P1}^{P2} \frac{[\overline{Q' T'}]}{c_p \overline{\sigma}} dp \tag{6}$$

All above variables represent conventional meteorological symbology; an apostrophe denotes a perturbation and an overbar represents a spatially integrated quantity. Of special note *Q'* is representing the diabatic heating perturbation. In this manner C_A is the conversion from basic-state APE, C_E is the conversion from eddy APE to eddy kinetic energy, and G_E is the conversion from diabatic heat sources.

Analyzing the corresponding importance of baroclinic and diabatic processes on wave growth, MM05 then calculated the ratio of G_E (diabatic heating production of eddy APE) to C_A (baroclinic production of eddy APE) as a function of wavenumber (and therefore wavelength), graphed in Figure 9.

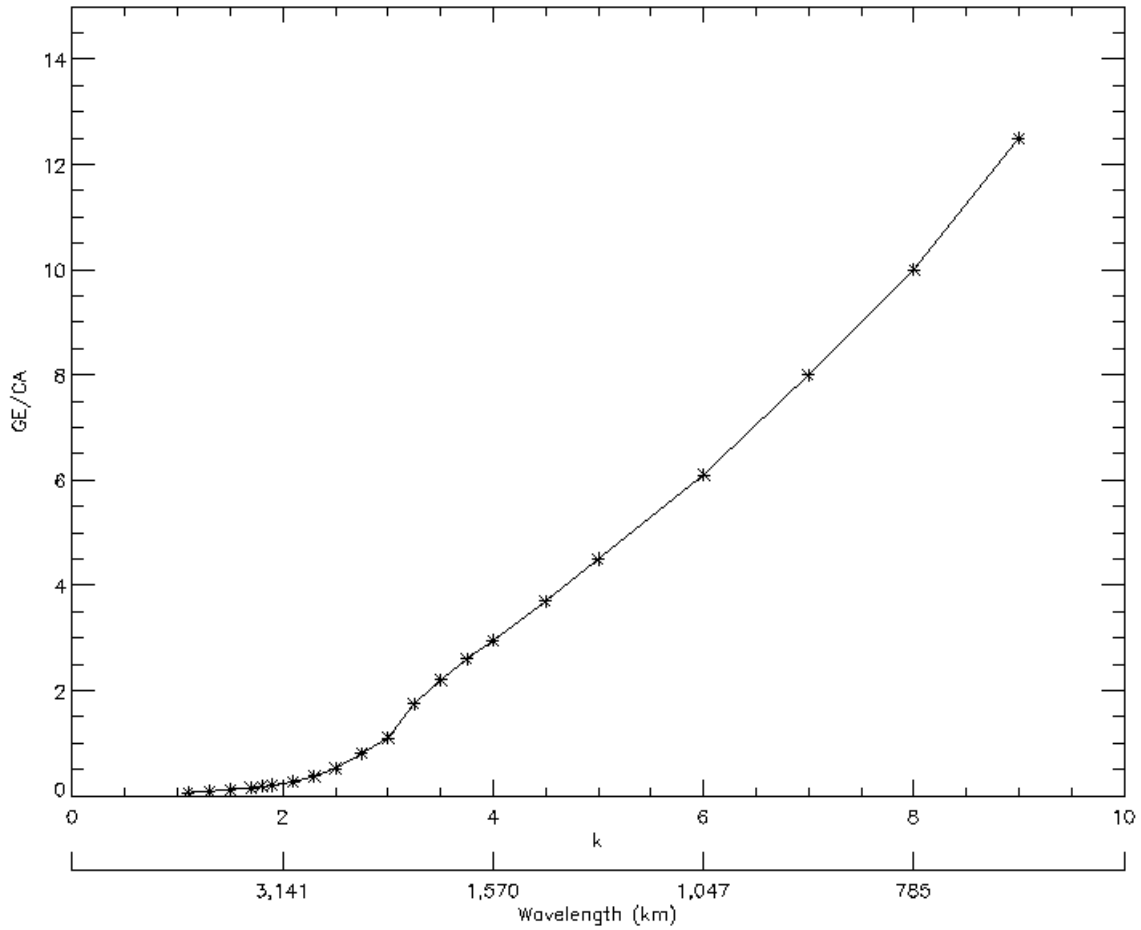

Figure 9. Ratio of the conversion of diabatic heat sources to eddy APE (G_E) over the conversion of basic-state APE to eddy APE (C_A) as a function of initial nondimensional wavenumber and dimensional wavelength (km) for a vertically varying moisture parameter (from MM04).

When analyzed from the perspective of dominating eddy APE production, as with growth rate and phase speed, two distinct regimes emerge. Long-wave disturbances, using the previously defined 1900 km cut-off, have G_E/C_A ratios less than one and decreasing with increasing wavelength, highlighting the increasing domination of C_A, the baroclinic eddy APE conversion variable. Cyclone wave (DRW) scale disturbances, conversely, exhibit an increasing domination of $G_{E,}$ the diabatic eddy APE conversion variable, in other words, the domination of diabatic versus baroclinic increases with decreasing wavelength.

d. Wave Structure

The wave structures of both long-wave and cyclone wave regimes were explored by MM05. Using zonal wavelengths of 3490 km (long-wave) and 1047 km (cyclone wave), MM05 created longitudinal cross-sections (vs height) of geostrophic meridional wind (v_g) and potential temperature (PT) (Figure 10), and vertical velocity (w) and anomalous dry vorticity (q) (Figure 11) at a 92.5 hr lifespan.

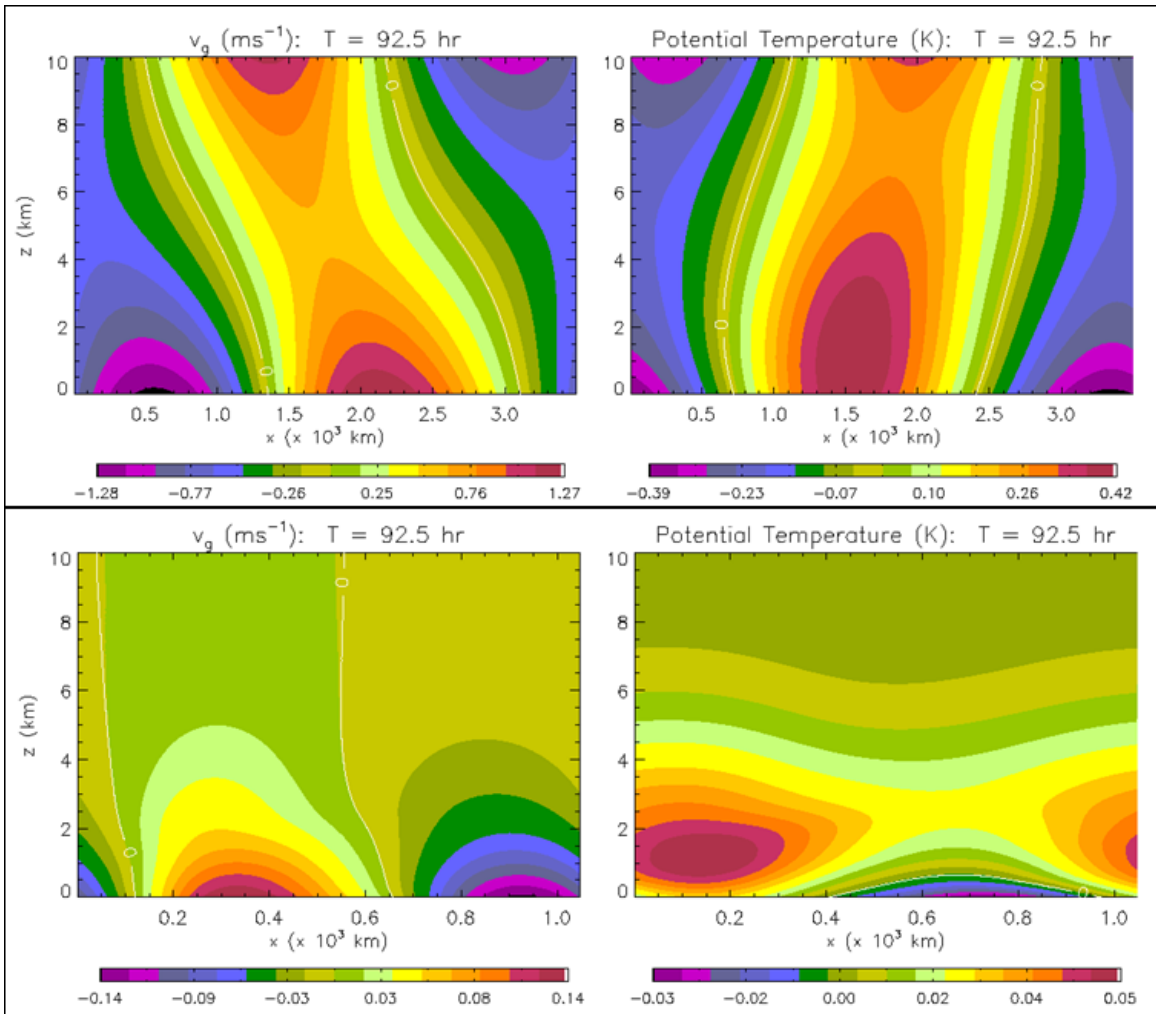

Figure 10. Longitude vs height cross sections at time T = 92.5 hrs of (top) the most unstable moist mode (wavelength = 3490 km) and (bottom) a previously neutral wave (wavelength = 1047 km). Geostrophic meridional wind (v_g; m s^{-1}) is shaded on the right hand plots and potential temperature (PT; K) is shaded on the left hand plots (after MM04).

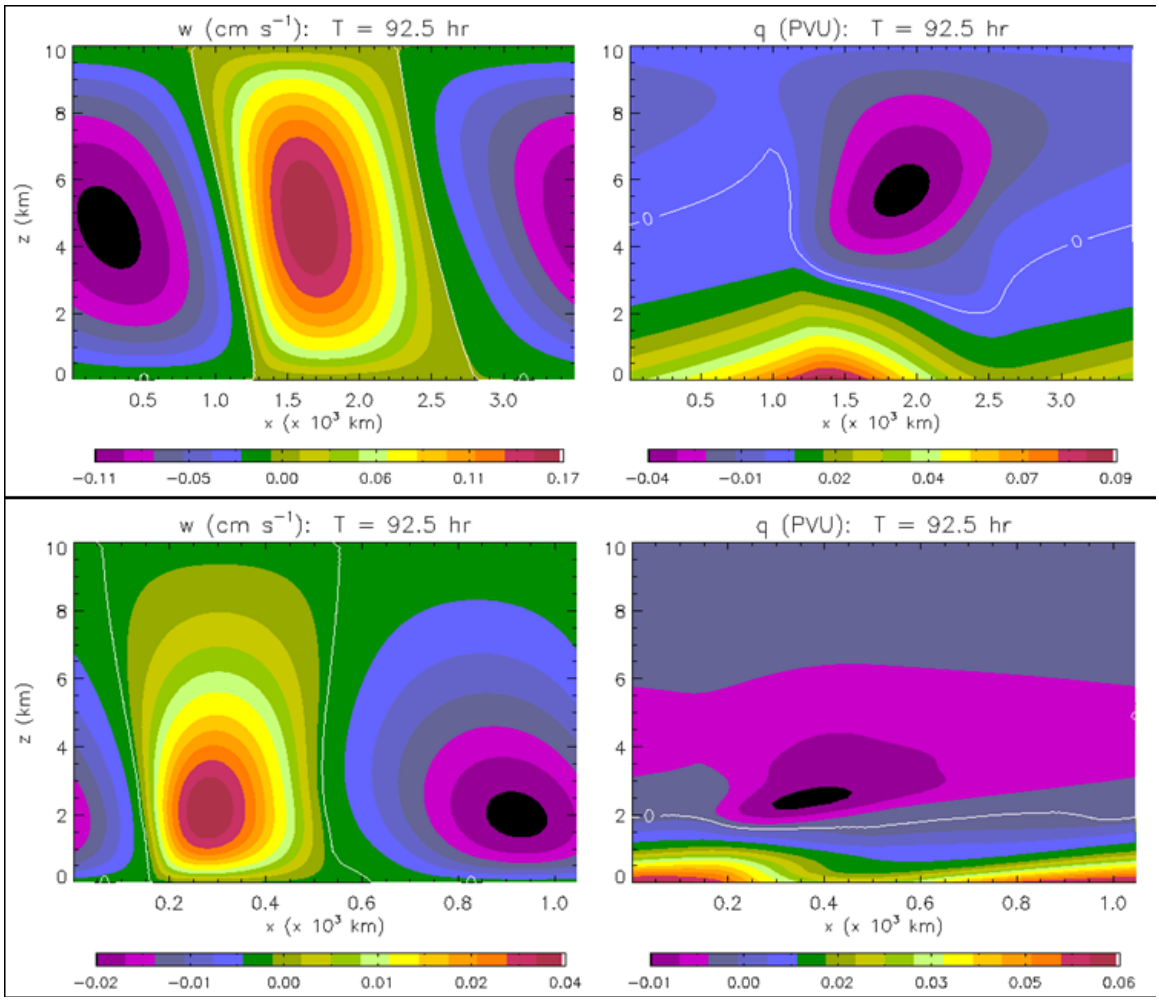

Figure 11. Longitude vs height cross sections at time T = 92.5 hrs of (top) the most unstable moist mode (wavelength = 3490 km) and (bottom) a previously neutral wave (wavelength = 1047 km). Vertical velocity (w; cm s^{-1}) is shaded on the right hand plots and anomalous dry vorticity (q; PVU) is shaded on the left hand plots (after MM04).

Immediately apparent in Figures 10 and 11 is the westward tilt with height of the geostrophic meridional winds and vertical wind velocities of the long-wave disturbance. This westward tilt with height is a defining characteristic of a developing dry baroclinic wave (Holton 1992). Similarly, the eastward tilt with height of PT is modeled as expected for a typical extratropical cyclone. These factors together are evidence of baroclinic conversion of APE to kinetic energy, as outlined above in the exploration of energetics of the long-wave disturbance.

Comparatively, examining the cyclone wave cross sections in figures 10 and 11 reveals a disturbance that is surface-concentrated in nature. Geostrophic meridional winds occur only at the surface and vertical wind maximums are located in the lower troposphere and only extend weakly into the upper levels of the atmosphere. Potential temperature anomalies are oriented at 90 degrees with the long-wave cross section and are co-located with meridional wind maximums giving strong indication of diabatic heating resulting from a poleward low-level jet. With no upper level support for the cyclone wave evident, it is intuitive that a low level growth mechanism must be responsible for the evolution of the DRW.

e. Wave versus Vortex

Finally, MM05 proposed that diabatic Rossby waves, when represented in a 3-dimensional (3D) framework, behave in several ways as coherent vortices. The lack of an alternating high/low wave-like structure and the closed circulation of the disturbances are more depictive of a vortex than a wave. BW13 confirms the existence of both wave and vortex-like characteristics in DRWs, and notes the particular hybrid nature of the disturbances. For the purpose of this study the terms diabatic Rossby wave and diabatic Rossby vortex are considered the same phenomena, but diabatic Rossby vortex (DRV) will be used from this point forward for consistency.

B. ILLUSTRATIVE CASE STUDIES

The previous background section of this thesis was an overview of the history of the meteorological research problem and the refinement of understanding of the mechanics and dynamics of DRVs. The majority of the discussed literature was limited to idealized or model-based frameworks. The following two case studies are highlighted to link the body of work summarized above with real world extreme weather events that were the result of an explosively intensifying DRV.

1. Extreme Winter Storm Lothar

When winter storm Lothar (Figure 12) swept across Europe from 24 to 26 December 1999, it left a path of destruction from France to Switzerland (Wernli et al. 2002, hereafter referred to as W02). Winter storm Lothar would result in more than 50 deaths and damage invaluable sites of historical importance including Versailles and the church of Notre Dame.

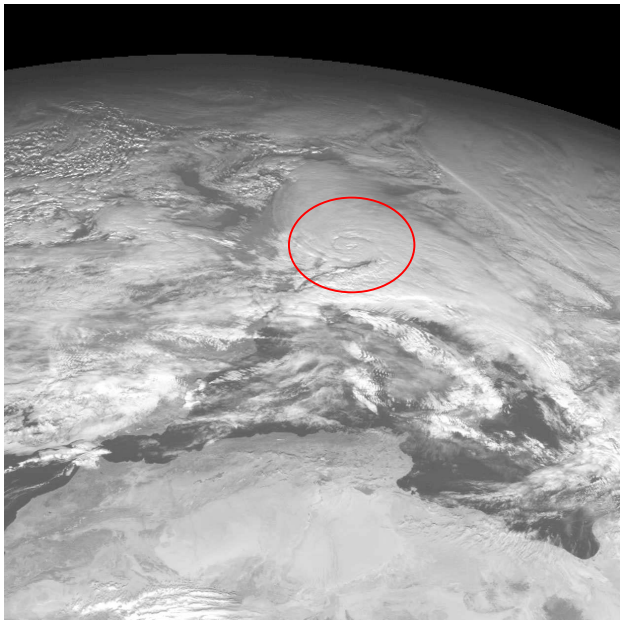

Figure 12. Visible satellite imagery of winter storm Lothar (identified by red circle) 25 December 1999 (after Shih 2013).

Winter storm Lothar was a watershed event for DRV research because it was one of the first definitive studies of a low-level, small-scale cyclone (DRV) interacting with a strong upper-level jet that resulted in extreme weather. The lower tropospheric cyclone was determined to have been formed in the western Atlantic with no discernable upper-level feature before rapidly propagating to the European continent. Using both ECMWF and high resolution model (HRM) hindcast analysis, W02 captured and traced the lifecycle of the DRV and resulting explosive cyclogenesis.

ECMWF analysis of the DRV structure prior to interaction with the upper-level jet is diagrammed in Figure 13. The two cross sections in Figure 13 display an almost perfect DRV structure. In the left diagram, a strong positive PV anomaly is located to the west of a low-level poleward jet. The low-level jet is located within a warm PT anomaly, implying strong thermal advection. In the right diagram, to the east of the PV anomaly strong PV generation is taking place, the result of the thermal advection and diabatic heat release of the poleward jet. Concurrent PV depletion is occurring at the location of the DRV center. The PV generation/depletion dipole indicates the anomaly will continue to propagate to the east. Finally, all observed dynamics are occurring in the lower troposphere with no discernable upper-level interaction.

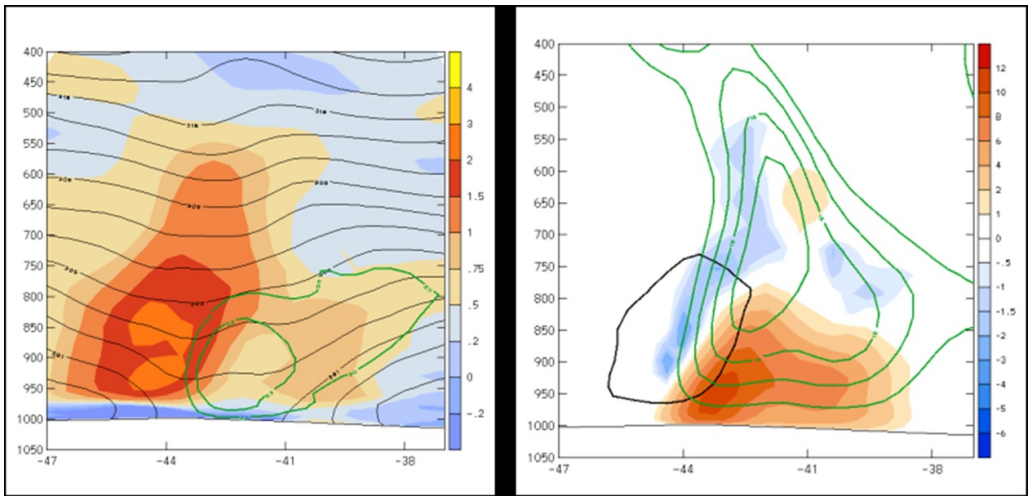

Figure 13. ECMWF cross section (longitude vs height) analysis of the DRV at 00 UTC 25 December 1999. Left: PV (in PVU; shaded), PT (every 3° K; black lines), and meridional wind (v; 20 and 23 m s^{-1}; green lines). Right: diabatic PV generation rate (in PVU/hr; shaded), positive vertical velocity (w; cm s^{-1}; green lines), and the 1.5 PVU anomaly superimposed from the right panel (black line) (after W02).

Using in-situ observations, ECMWF analyses, and HRM hindcast simulations, W02 were able to capture the DRV transition from propagation to intensification stage. As can be observed in Figure 14, from 12 UTC 25 December 1999 to 18 UTC 25 December 1999 the DRV experienced only a moderate drop in SLP, indicating it was still within the propagation phase of its lifecycle. After 18 UTC 25 there was a precipitous drop in SLP of almost 30 hPa the following twelve hour period, exceeding the 1 Bergeron criteria for a "bomb." The extreme pressure fall combined with the storm meeting the "bomb" criteria gives an estimate of the timeframe of the DRV interaction with an upper-level feature.

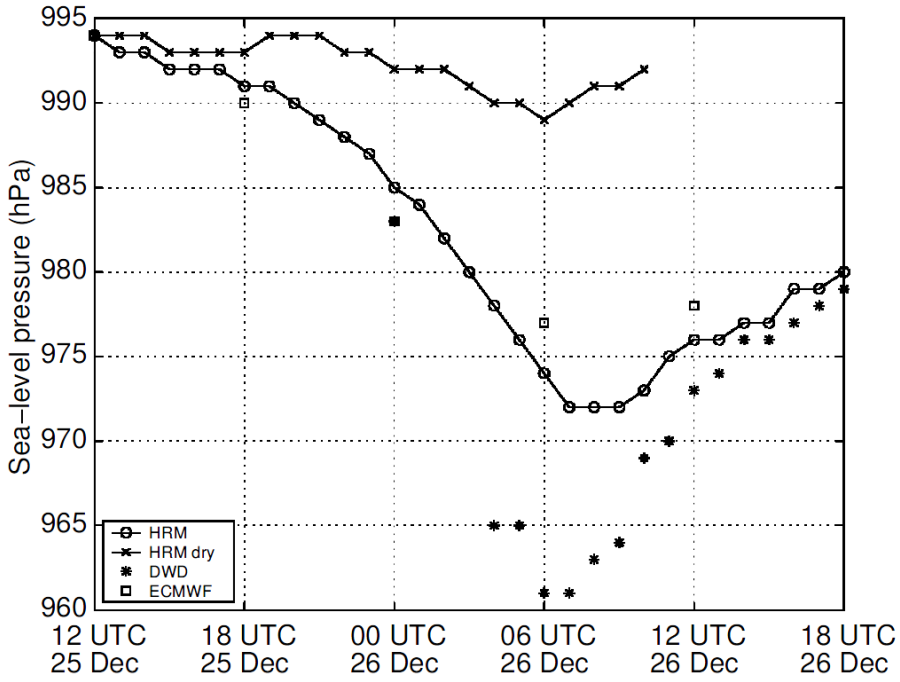

Figure 14. Time series of the minimum sea-level pressure in the core of cyclone Lothar, showing in-situ observations (German Weather Service; DWD), ECMWF analyses, and HRM (moist and dry) mesoscale hindcast simulations (after W02).

To further investigate the Lothar DRV propagation and upper-level interaction dynamics, WO2 used the HRM hindcast to create a 3D 2 PVU isosurface at 6-hour intervals (Figure 15). The time steps for the 3D model are 18 UTC 25 December 1999, 00 UTC 26 December 1999, and 06 UTC 26 December 1999, which cover the period of

rapid pressure fall, as noted above in Figure 14. In Figure 15(a) the DRV can be observed as a low-level disturbance approximately 1000 km west of the European continent. Of note there is no evidence of upper level interaction at this time step. As the model projects 6 hours ahead, Figure 15(b) displays an increase in height and intensity of the DRV as it moves just off the coast of Europe. Above the DRV a kink in the 2 PVU surface of the tropopause has begun to develop, indicating that upper level interaction has been triggered by the strength of the DRV at lower levels. By the final time step, Figure 15(c), the DRV has greatly intensified into a "PV tower" and the tropopause fold has deepened enough to form a continuous column of cyclonic PV. The bottom-up intensification observed throughout this 18 hour time span is an excellent example of both the Type A cyclogenesis (PS71) and "bomb" dynamics detailed in Chapter 2.1 and 2.2 of this study.

The bottom-up cyclogenesis outlined above was found to be the key dynamic in the development of winter storm Lothar. W02 surmised that the DRV intensification and subsequent growth into the mid-troposphere initiated cyclonic circulation aloft resulting in a wave perturbation along the tropopause. Meanwhile, strong baroclinicity to the north of the DRV initiated a strong upper level jet. The proximity of the DRV to the jet and the folding and lowering of the tropopause introduced an injection of high PV stratospheric air into the DRV, resulting in a PV tower, the rapid intensification of Lothar, and the resulting extreme storm system over Europe.

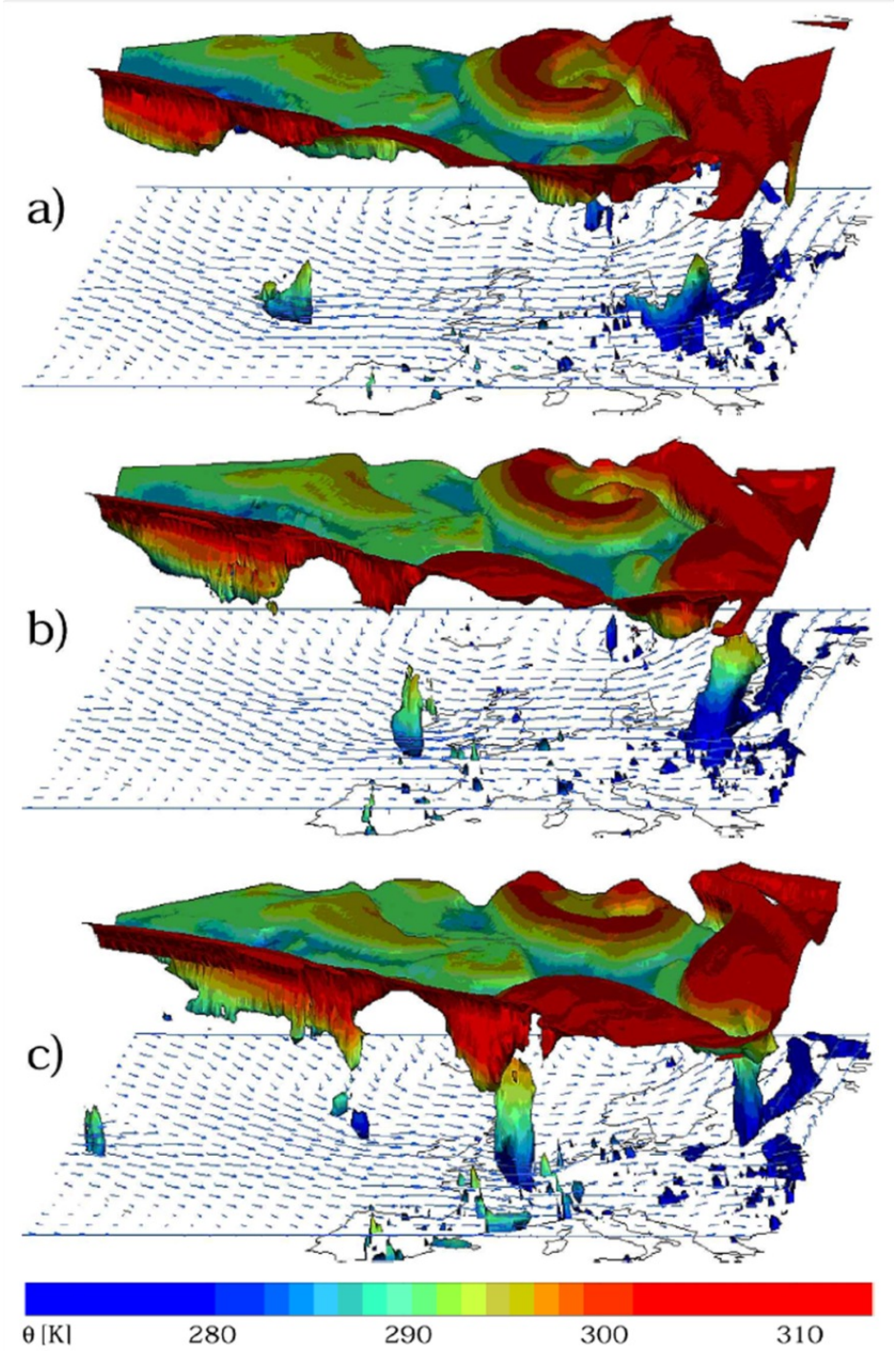

Figure 15. HRM hindcast simulation 2 PVU isosurface of the winter storm Lothar DRV at times (a) 18 UTC 25 December 1999, (b) 00 UTC 26 December 1999, and (c) 06 UTC 26 December 1999. The 2 PVU isosurface is shaded according to PT values and vectors represent 850 hPa horizontal winds (from W02).

2. North Atlantic Cyclone in December 2005

a. Operational Analysis of the DRV

Boettcher and Wernli (2011; hereafter referred to as BW11), utilizing operational analysis data from the ECMWF, investigated a North Atlantic cyclone with the goal of further exploration of the dynamics of each phase of the DRV lifecycle (Figure 16). The particular cyclone event, which occurred in December 2005, was an ideal candidate for study, as it began with a DRV precursor that led to an eventual explosive intensification. The DRV precursor began as remnants of an MCV that had formed in the Gulf of Mexico, then propagated to the northeast over the Atlantic, and eventually experienced explosive intensification that culminated in a strong extratropical cyclone in the North Atlantic.

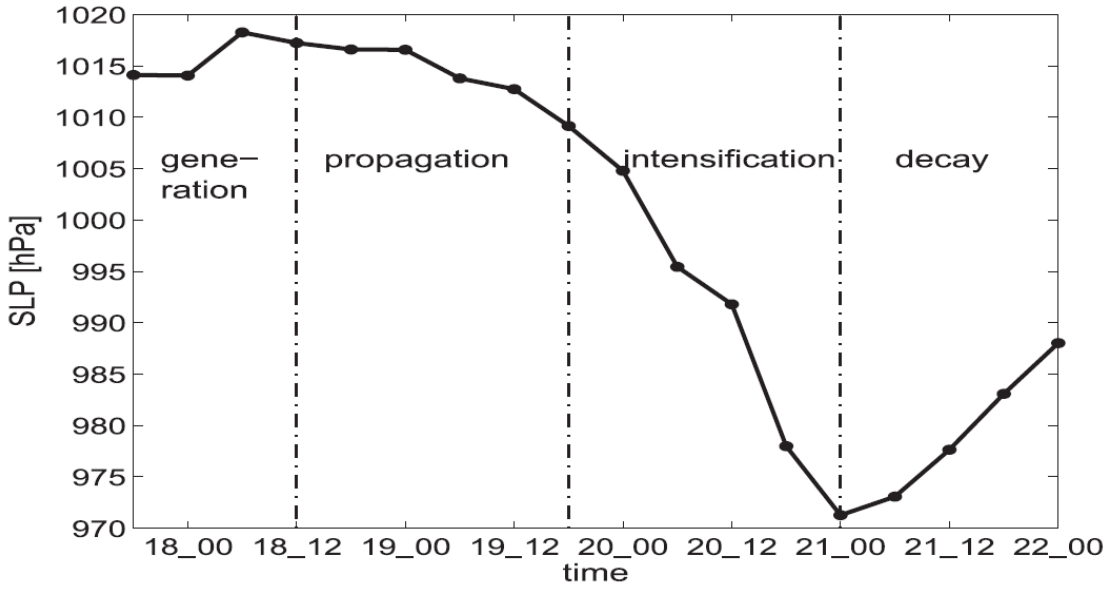

Figure 16. Minimum SLP (hPa) time development of the DRW 17 – 22 Dec 2005 defining the development phases (from BW11).

BW11 traced the generation of the DRV to a MCS that developed over the Gulf of Mexico. The MCS generated a strong low-level positive PV anomaly that was supported by an upper-level trough while traversing the Gulf. As the MCS transitioned to the North Atlantic, upper-level support was lost. While the system decayed and dispersed

into an elongated region of moderate convection, the low-level PV anomaly remained coherent. A strong horizontal temperature gradient existed downstream of the PV anomaly, and through continued diabatic PV production along the southern border of the baroclinic front the PV anomaly propagated rapidly to the east at roughly twice the speed of the prevailing wind. Additionally, no upper-level forcing could be associated with the low-level PV anomaly, as the nearest upper-level jet was approximately 900 km to the north. The diabatic PV generation in a baroclinic environment and lack of upper-level forcing combine to establish the disturbance as a DRV.

The DRV then continued to propagate eastward for roughly 28 hours with only a minor fall in sea-level pressure. Max PV values diluted from 2.5 to 2 PVU (the result of weakening convection) but remained at the 900 hPa level. Latent heat release was half the strength of the precursor MCS event, yet occurred at the same height of 750 hPa. As a result, the PV anomaly didn't reach the vertical extent of the precursor storm system and the maximum meridional winds were weaker than the precursor storm system, as well. These characteristics, along with the lack of upper-level support noted above, led BW11 to conclude that throughout the propagation phase the DRV can best be described as a shallow, diabatically driven low-level cyclonic system.

The transition to the intensification phase of the DRV began with the interaction of the disturbance with an upper-tropospheric wave. A rapid deepening of the SLP, the evolution of fronts, change in cloud structure, and growth of horizontal extent are all indications of the transformation from DRV to synoptic-scale extratropical cyclone. Infrared (IR) satellite imagery captured the rapid growth and transformation of the disturbance over the course of 18 hours (Figure 17). An explosive deepening of 34 hPa over a 24 hr period, low-level PV values upwards of 6 PVU, and meridional winds exceeding 30 m s^{-1} all give example to the extreme nature of the resulting cyclone, which was stronger in all regards when compared to the originating MCS.

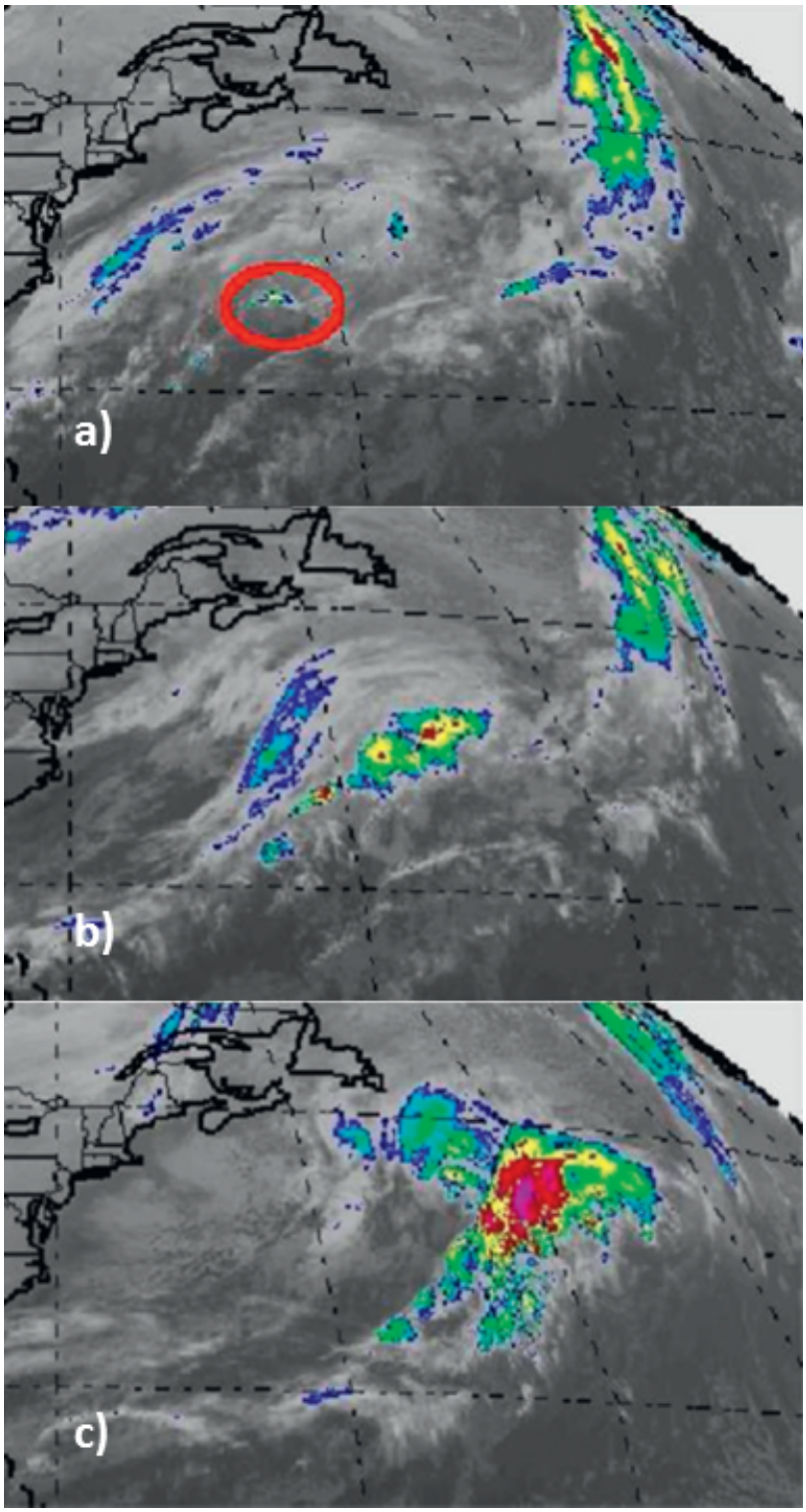

Figure 17. IR satellite image (Meteosat) of (a) the DRV (red circle) at 12 UTC 19 December 2005, (b) and (c) the developing extratropical cyclone at 18 UTC 19 December 2005 and 06 UTC 20 December 2005, respectively (after BW11)

b. ECMWF Forecast Evaluation

After analyzing the growth dynamics of North Atlantic cyclone, BW11 then conducted an evaluation of ECMWF control forecasts of the storm system. Four operational forecasts were selected for study, ranging from 0 to 36 hours prior to the propagation phase of the DRV (12 UTC 18 December 2005). The evaluation of the control forecasts had two goals: to analyze the forecasting skill of the model to capture the rapid propagation and strength of intensification and to further examine the dynamics throughout the DRV lifecycle.

BW11 designed a tracking algorithm to identify the location and attributes of the DRV as well as environmental characteristics for each forecast at 6 hr time steps through the life of the cyclone. Collected attributes of the DRV included PV, SLP, precipitation, and distance from upper-level forcing, while the recorded environmental factors consisted of baroclinicity and specific humidity.

While all four ECMWF forecasts identified the generation and propagation of the DRV, the attributes of the DRVs were found to be a mix of strong and weak signatures. Tracking the low-level PV anomaly maximum, used in this case as a proxy for the overall strength of the disturbance, the forecasts were divided equally between overestimating and underestimating growth. Similarly, rapid SLP drops were found to be split with two forecasts predicting explosive deepening, while the remaining two showed only moderate SLP falls.

Examination of the forecasted environmental characteristics explained the dipole of PV anomaly maximums. A strong weakening of downstream baroclinicity and decreasing moisture to the south of the DRV track were responsible for both underestimations. Conversely, the forecasts that overestimated PV anomaly maximums predicted only minor weakening of baroclinicity and decreasing moisture. The overall effect of the poorly forecasted environmental factors led to very little amplification of PV growth for the two under-predicted forecasts. As such, the two forecasts missed the explosive deepening of the DRV and transition to extratropical cyclone. When re-

examined, the poorly forecasted PV anomalies were found to have too weak an interaction with the midlatitude upper-tropospheric trough.

Finally, BW11 noted that the interaction problem between lower and upper level features is similar to the midlatitude transitioning of tropical cyclones. Both DRV intensification and tropical cyclone reintensification share general features that can be dynamically difficult for NWP model forecasts.

C. CLIMATOLOGY

Boettcher and Wernli (2013, hereafter referred to as BW13) developed an objective DRV identification and tracking algorithm in an effort to compile the first DRV climatology. Previous to this study, there was no clear understanding of how often DRVs occur, their geographical distribution, or the number of disturbances that result in explosive intensification. While this climatology was limited to a 10 year period from 2001 to 2010, and was confined to the Northern Hemisphere, the resulting data set was large enough for BW13 to produce a comprehensive look into annual DRV occurrence, formation dynamics, propagation tracks, distributions, and explosive deepening.

1. The Identification Algorithm

Applied to operational analysis data from the ECMWF, the algorithm developed by BW13 makes a first pass to identify two co-located criteria:

- A Local SLP Minimum: Local SLP minima grid points enveloped by a closed SLP contour at least 0.5 hPa higher than the local minima are identified.

- Large Positive Lower-Tropospheric PV: The average value of PV within a box centered on the SLP minimum and including the eight surrounding grid points. If the average value is greater than 0.8 PVU the SLP minima grid point is accepted.

- Persistence: All grid points that have fulfilled the SLP/PV co-location requirements are then tested for persistence. The above two-step process is run in succession in 6hr intervals within a box extending 12° to the east, 2° to the south, and 4° to the north from each identified grid point. In the case of multiple grid points meeting the criteria within a box the grid point with the highest PV value is kept. SLP/PV grid points that successfully meet the requirements at each time step for a 24 hour period are then considered for further examination.

Due to the pervasiveness of positive lower-tropospheric PV anomalies in mid-latitude ocean basins, and based on an understanding of the fundamental aspects of DRV dynamics, the meeting of the following criteria for three consecutive 12-hour time steps were deemed necessary for DRV identification:

- Fast Propagation: The SLP/PV maxima grid points must propagate faster than 11.6 m s^{-1} (250 km in a 6 hour period).

- Considerable Downstream Low-Level Baroclinicity: Baroclinicity ($\Delta\theta$) is calculated by averaging the 10 percent lowest and 10 percent highest 950 hPa PT values in a box with dimensions two to eight grid points to the east of the SLP/PV maxima, three grid points to the south, and eight grid points to the north. The calculated $\Delta\theta$ must be greater than or equal to 5° K.

- Sufficient Moisture for Saturation and Condensational Latent Heating: Atmospheric moisture is calculated by averaging the 10 percent highest 850 hPa relative humidity (RH) values in a box extending eight grid points to the west, eight grid points to the east, six grid points to the south, and five grid points to the north of the SLP/PV maxima. The calculated relative humidity value must be greater than 90 percent.

- Extremely Weak Upper-Level Forcing: The 650 – 100 hPa induced Quasi-geostrophic (QG) ascent is averaged and calculated at the 700 hPa level and PV is averaged at the 250 hPa level using the same search box as relative humidity. The calculated QG ascent rate must be smaller than 0.5 x 10^{-2} m $^{s-1}$ and the average PV must be less than 1 PVU.

An example of a DRV identified using the above algorithm can be observed in Figure 18. The large low-level positive PV anomaly can be seen at its original and 6 hour time step (closed black contours and shaded regions, respectively). The small, vertically oriented box represents the search area for downstream low-level baroclinicity, while the large horizontally oriented box represents the search area for sufficient moisture, QG ascent, and upper-level forcing (250 hPa PV represented by thick black lines north of the PV anomaly; 1.5 and 2 PVU).

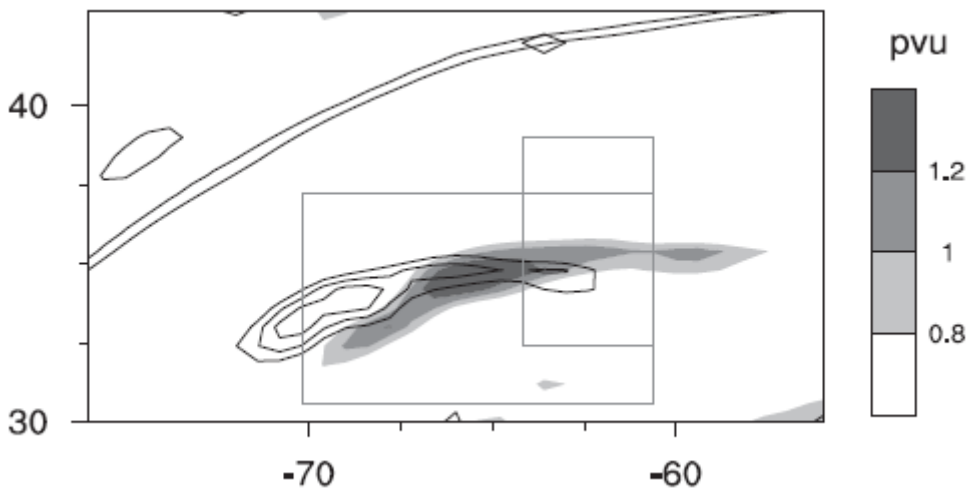

Figure 18. An example DRV at 12 UTC 19 December 2005 (after BW11).

2. Results

Limited to the Northern Hemisphere and covering a 10-year period (2001-2010), the compiled climatology consists of 1240 total DRV tracks. The geographic distribution of DRV formation was skewed heavily toward the North Pacific. Of the total 1240 DRV tracks, 809 occurred in the North Pacific, while 431 occurred in the North Atlantic. This equates to approximately 124 DRVs developing annually with a geographic distribution of 81 DRVs per year in the North Pacific and 43 in the North Atlantic. DRVs also were found to form most frequently in summer months, though explosive intensification was more likely in the spring and fall.

Five distinct synoptic-scale flow patterns were identified as favorable for DRV development, as illustrated in Figure 19. Impinging low-level flow from either an anticyclone or cyclone against a baroclinic zone can trigger large-scale ascent or moist convection (scenarios [a] and [b]). Scenario (c) has a low-level positive PV anomaly initially created by an upper-level trough, but through weakening of the upper-level support, continues to exist and propagate on its own via diabatic PV generation along the baroclinic zone. The final two scenarios ([d] and [e]) are similar in that both are diabatically produced PV anomalies (the former exemplified as a MCS and the latter as a tropical cyclone undergoing extratropical transition) formed in areas of weak baroclinicity, that then move into a region of strong low-level baroclinicity and begin propagation as DRVs.

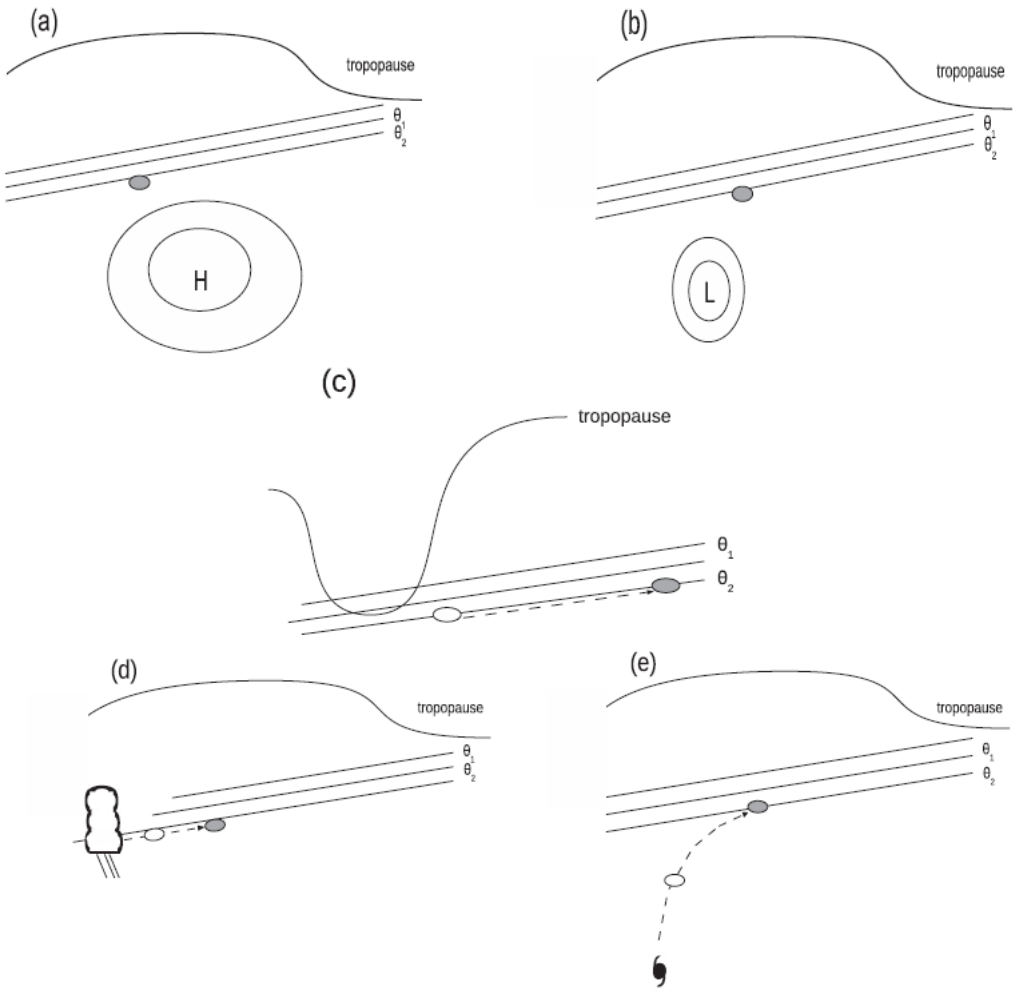

Figure 19. Schematics of typically observed synoptic-scale configurations for DRW genesis. White ellipses denote DRW track starting positions and gray ellipses indicate the start of the DRW propagation phase (a gray ellipse is shown if the two coincide). The scenarios are (a) flow around a subtropical high against the baroclinic zone; (b) flow around a cyclone against the baroclinic zone; (c) surface cyclone formation induced by forcing from upper-level trough; and (d),(e) PV remnants from a mesoscale convective system or tropical cyclone, respectively, moving into the baroclinic zone (from BW13).

Despite the seemingly large number of annual DRV events, the percentage of disturbances that were found to explosively deepen or "bomb" (as outlined in chapter 2.A.1) was relatively small, at slightly less than 15 percent. However, of significant note, 'DRV bombs' were responsible for 20 percent and 15 percent of all explosively

deepening cyclones in the Pacific and Atlantic basins, respectively, further illustrating their importance in extreme weather development.

THIS PAGE INTENTIONALLY LEFT BLANK

III. DATA AND METHODOLOGY

A. DATA

1. DRV Test Cases

Thirteen DRV test cases were objectively selected from the BW13 climatology data set discussed in Chapter 2.C. The selection criteria were that the DRV must undergo explosive deepening and occur in 2010. The former was chosen to highlight cases with probable significant sensible weather impact, while the latter resulted from an increase in ECMWF TIGGE data that was implemented January 2010 (described below). One of these cases was thrown out due to missing TIGGE data (BW13 climatology storm number 730).

For each of the remaining 12 DRV test cases the climatology provided latitude, longitude, and pressure in six-hour time steps from genesis through intensification/decay. The DRV locations obtained from the climatology will be considered "truth" against which the ensemble forecasts will be evaluated.

2. Ensemble Data

a. Overview

The meteorological analysis data used for this thesis was archived ECMWF ensemble forecasts retrieved from the historical THORPEX Interactive Grand Global Ensemble (TIGGE; http://tigge.ecmwf.int/#info). The TIGGE archive is an aggregate of 10 global numerical weather prediction model's ensemble forecast data. The ensemble forecast data is available from October 2006 to the present.

Although 10 global NWP ensembles are available in the TIGGE archives, this study will only utilize ECMWF ensemble data in an effort to be consistent with the DRV climatology (which used ECMWF operational analyses). In January 2010, the ECMWF ensemble data was upgraded to have a much higher horizontal resolution, which due to the small-scale nature of DRVs was determined to be of significant benefit to this study, and as a result only data from that year was utilized.

The ECMWF ensemble consists of 1 control and 50 perturbed members, for a total of 51 ensemble members. Horizontal resolution is 0.45 degrees in both latitude and longitude. Vertically resolution is eight pressure levels (1000, 925, 850, 700, 500, 300, 250, and 200 hPa). Ensemble initialization occurs every twelve hours at 00 and 12 UTC. Forecast data is projected every 6 hours from 0 to 15 days from initialization time.

b. Initialization Time of Forecast Data

The initialization time of all ensemble data is chosen so that the 48 hour forecast is valid at the time of DRV genesis as identified in the BW13 climatology. TIGGE ensemble data is only available at 0000 and 1200 UTC initialization times, therefore if the BW13 climatology indicates a genesis time of 0600 or 1800 UTC, the initialization time is moved to six hours after (1200 or 0000 UTC, respectively).

For clarity going forward, the 48 hour ensemble forecast corresponds to DRV genesis, the 60 hour forecast corresponds to 12 hours into the DRV lifecycle, and the 72 hour forecast corresponds to 24 hours into the DRV lifecycle. All three forecasts share the same initialization time.

c. Available TIGGE Ensemble Data

Ensemble data sets collected into the TIGGE archives are required to provide the following output fields in GRIB2 data format:

- Pressure Level Parameters
- Potential Temperature Level Parameters
- Potential Vorticity Level Parameters
- Single Level Parameters

The GRIB2 data outputs above are available at each initialization time as a separate Network Common Data Form (NetCDF) file. A review of the available parameters for each subset indicated that only the pressure level, potential vorticity level, and single level parameters from TIGGE ECMWF ensemble NetCDF data files would be

necessary to identify DRVs and their surrounding environmental characteristics. The required parameters for each data set are outlined below.

d. Pressure Level Parameters

Table 1 lists the extracted parameters from the pressure level NetCDF file (pressure level files will hereafter be referred to as pl-files). Pl-file parameters are available on eight pressure levels (1000, 925, 850, 700, 500, 300, 250, and 200 hPa).

Name	Abbreviation	Unit
Specific humidity	q	kg kg^{-1}
Temperature	T	K
U-velocity	u	m s^{-1}
V-velocity	v	m s^{-1}

Table 1. Variables extracted from ECMWF pressure level files.

e. Single Level Parameters

Table 2 lists the sole extracted parameter from the single level NetCDF file (single level files will hereafter be referred to as sl-files). Sl-file parameters are, as the name implies, only available on a single level.

Name	Abbreviation	Unit
Mean sea level pressure	msl	Pa

Table 2. Variables extracted from ECMWF single level files.

f. Potential Vorticity Level Parameters

Table 3 lists the sole extracted parameter from the potential vorticity level NetCDF file (potential vorticity level files will hereafter be referred to as pv-files). Pv-file parameters are available on the 2 PVU potential vorticity level. The pv-files were used to identify the dynamic tropopause and its features during research and model verification for this study.

Name	Abbreviation	Unit
Potential Temperature	pt	K

Table 3. Variables extracted from ECMWF potential vorticity level files.

B. METHODOLOGY

1. Selection of Test Cases

Having already limited the selection pool of possible test cases to those occurring in 2010 (following the reasoning laid out in Chapter 3.A.2.a), the selection was then narrowed further by distinguishing DRVs that underwent explosive cyclogenesis and were located in the North Pacific. From this much diminished list the following 12 DRVs were selected for study:

Test ID	Date	Time (UTC)	Longtitude	Latitude	Initial SLP	Min. SLP
1	20100304	1200	139.2	37.2	1013.87	966.83
2	20100324	1200	130.8	32.4	1010.79	965.27
3	20100404	1800	129.6	28.2	1008.91	971.24
4	20100906	1200	134.4	39.6	1006.99	974.72
5	20100914	0000	159.0	39.0	1003.13	970.06
6	20100923	1200	150.0	39.0	1007.03	970.47
7	20101005	1200	168.0	45.6	1008.57	972.37
8	20101009	0600	166.2	34.8	1008.21	970.62
9	20101020	1800	192.6	39.0	1009.51	981.11
10	20101020	1800	142.8	33.0	1011.04	959.81
11	20101028	0600	136.2	30.6	1005.50	935.51
12	20101213	0000	127.2	33.0	1007.21	967.76

Table 4. DRV Test Cases. Columns from left to right: test case identification number, date of initial detection (YYYYMMDD), time of initial detection (UTC), longitude of initial detection (DD), latitude of initial detection (DD), initial SLP (hPa), and minimum SLP (hPa).

2. Primary DRV Identification Script

The primary DRV identification script created for this study was coded in MATLAB and was designed to have a simple user interface for the selection of a test case and forecast hour for evaluation. The script then ingests the corresponding global ECMWF ensemble forecast NetCDF file and runs multiple algorithms designed to narrow the search area to a more manageable location and search for a candidate DRV within an area centered on the observed DRV location. After the script completes all computations, it outputs both text and csv (comma separated value) files containing the

results of the analysis. Other outputs include csv files containing the climatological location of the DRV at the evaluated time (hereafter referred to as the observed DRV location), the DRV search box, and lat/lon associated values of SLP, temperature, relative humidity, and potential temperature, which will be utilized for plotting and assessment using geographic information system (GIS) software.

Within the script, multiple algorithms exist to identify and assess characteristics of potential DRV candidates for each of the 51 ensemble members of a given forecast. The original algorithms were adapted to MATLAB from Interactive Data Language (IDL) script created to assess the probabilistic prediction of a DRV that originated in response to the impingement of warm, moist advection associated with recurving tropical cyclone Chaba on a low-level baroclinic zone (Moore et al. 2012, hereafter referred to as M12). The resulting code contained four unique algorithms that were designed to locate the most DRV-like feature in each ensemble member given the known location of the observed DRV. The algorithms can be simply described as calculating maximum relative vorticity, distance from observed DRV, poleward baroclinicity, and local specific humidity content. Minor tweaks to the first two algorithms were made to translate the code from IDL to MATLAB, but the baroclinicity and specific humidity algorithms were further adapted to be more in-line with the calculation methods of BW13. The final algorithms are described as follows:

a. Relative Vorticity Maxima

A box is initially created around the observed DRV location with dimensions of +/- five degrees latitude and +/- seven degrees longitude. Relative vorticity is then calculated at each grid point (GP) of the 850 and 925 hPa pressure levels (using the ensemble values for *u* and *v* and Equation 7) and then averaged between the two pressure levels. Finally the maximum value of averaged relative vorticity is identified and the location and magnitude are recorded. If the magnitude of the relative vorticity maximum is less than 3.5×10^{-4} s^{-1} the DRV candidate is rejected as a "miss." As an example, Figure 20 graphically represents the observed DRV location (from the BW13

climatology), search box, calculated relative vorticity values, and identified relative vorticity maximum for the 48 hour forecast of test case 11.

$$\zeta = \frac{\delta v}{\delta x} - \frac{\delta u}{\delta y} \tag{7}$$

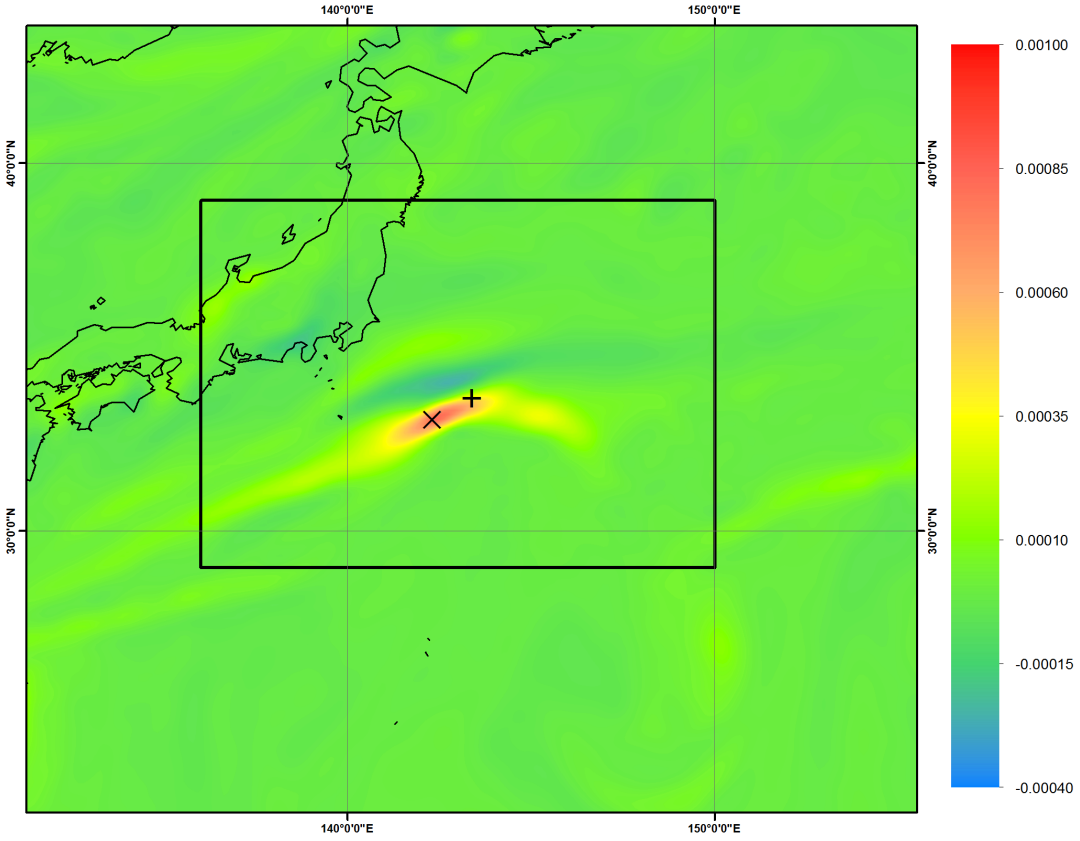

Figure 20. Relative vorticity maximum search box for the 48 hour forecast of ECMWF ensemble member 2 (valid time 12 UTC 28 October 2010). Relative vorticity values are shaded with warm colors indicating high levels of positive relative vorticity. The (+) symbol represents the observed DRV location and the (X) symbol represents the identified relative vorticity maxima and potential ensemble forecast DRV location. (Test case 11)

b. Ensemble Forecast Distance from the Observed DRV

A calculation is then run to determine the distance of the ensemble forecast's relative vorticity maxima from the location of the observed DRV. The distance is

recorded and a threshold value of 500 km from the observed DRV is enforced. If outside of the 500 km radius the DRV candidate is rejected as a "miss." Figure 21 displays the superimposed 500 km radius around the observed DRV for the same case and ensemble member.

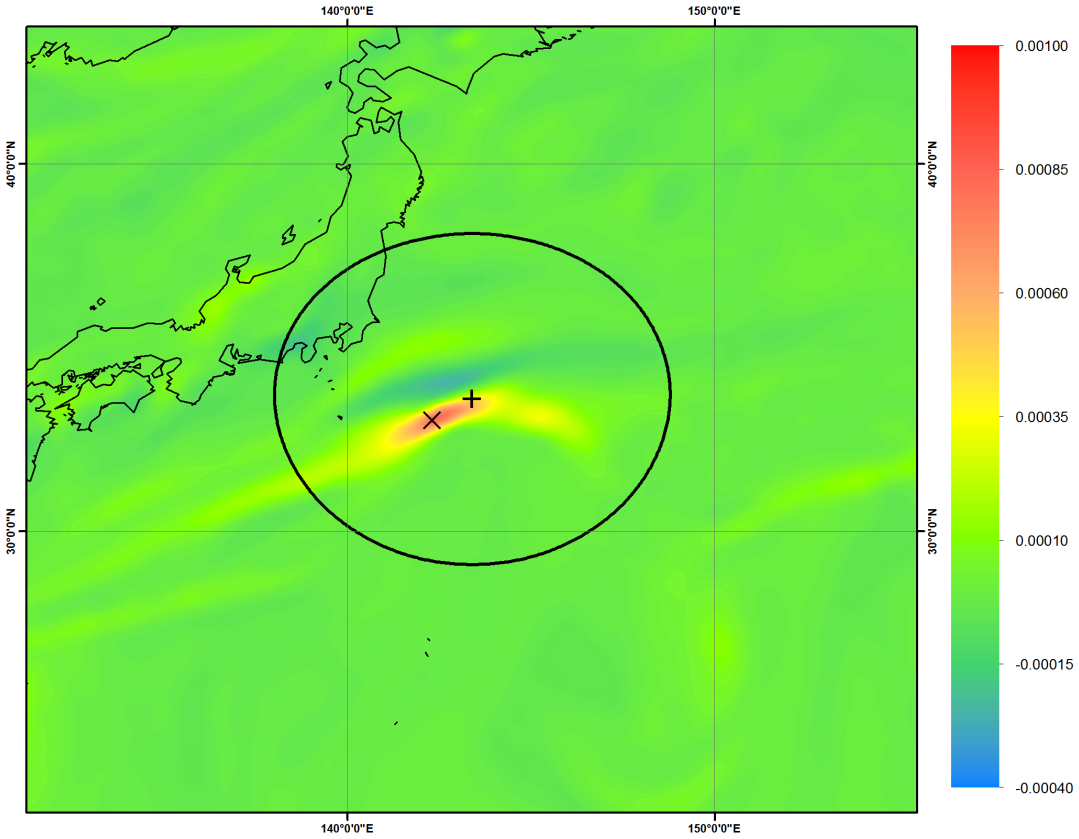

Figure 21. Same initial plot as Figure 20 (valid time 12 UTC 28 October 2010). The black circle represents a 500 km range ring. Relative vorticity values are shaded with warm colors indicating high levels of positive relative vorticity. The (+) symbol represents the "truth" DRV location and the (X) symbol represents the identified relative vorticity maxima. (Test case 11)

c. Downstream Low-Level Baroclinicity

The algorithm used for determining downstream low-level baroclinicity was designed after the methodology of BW13. A box is created from two to eight GP to the

east, three GP to the south, and eight GP to the north of the relative vorticity maxima. Within the box the mean of the 10 percent highest and 10 percent lowest temperatures at the 925 hPa level are calculated and the differences of the two values recorded. If the ΔT_{avg} is below a 5 K threshold, the DRV candidate is rejected as a "miss." The downstream orientation of the baroclinicity calculation box with respect to the relative vorticity maxima for test case 11 can be observed in Figure 22 (an example of a "hit").

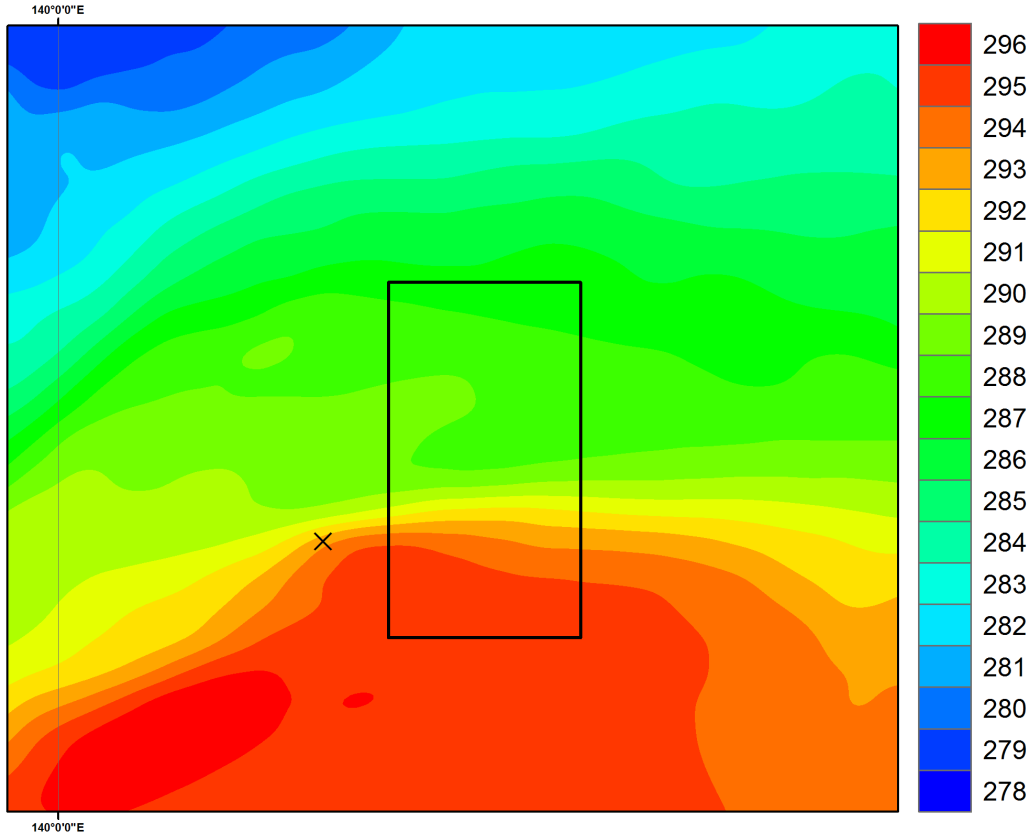

Figure 22. The baroclinicity calculation box for the 48 hour forecast of ECMWF ensemble member 2 (valid time 12 UTC 28 October 2010). 925 hPa temperature values are shaded (K). The (X) symbol represents the identified relative vorticity maxima and potential ensemble forecast DRV location. (Test case 11)

d. Sufficient Moisture

As with the baroclinicity calculations, the algorithm to determine sufficient moisture is adopted from BW13. Specific humidity (q) values from the 850 hPa pressure level are converted to relative humidity (RH) in a box extending eight GP to the west, eight GP to the east, six GP to the south, and five GP to the north of the forecast relative vorticity maxima. The top 10 percent of the relative humidity values are then averaged and recorded. If the calculated RH value is below 90 percent the DRV candidate is rejected as a "miss." Figure 23 gives example of the location and orientation of the RH evaluation box around the forecast relative vorticity maxima for test case 11 (another example of a "hit").

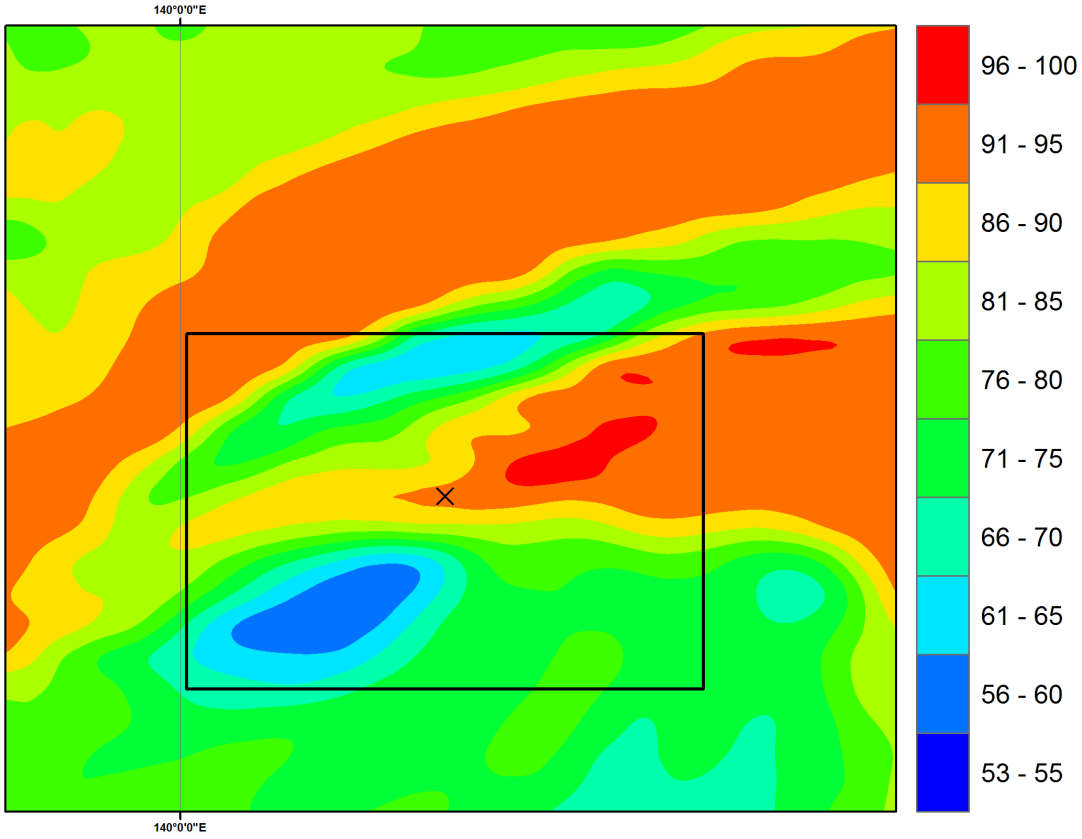

Figure 23. The relative humidity calculation box for the 48 hour forecast of ECMWF ensemble member 2 (valid time 12 UTC 28 October 2010). 850 hPa RH values are shaded (percent). The (X) symbol represents the identified relative vorticity maxima and potential ensemble DRV location. (Test case 11)

3. Testing and Results

All 12 test cases will be run through the DRV identification script and have the 51 ensemble members (1 control and 50 perturbed) tested by each of the four algorithms at forecasts times of 48, 60, and 72 hours. For an ensemble forecast to be considered successful it must meet the requirements of all four tests, a single miss in any category disqualifies the disturbance from identification as a DRV.

The script outputs a record of all 51 ensemble calculations for each forecast time to include a hit/miss check for a DRV, relative vorticity maxima lat/lon, relavitve vorticity maxima magnitude, distance from the climatology DRV, the calculated baroclinicity value, the calculated relative humidity value, and hit/miss checks for the four algorithms.

4. Necessary Alterations from the BW13 Algorithm

a. Relative Vorticity as Proxy for PV

The majority of previous research, and the climatology that this study builds on, identifies DRV location by enhanced low-level PV co-located with SLP minima. However, the minimal vertical resolution available with the TIGGE precludes an accurate calculation of PV. Previous studies calculated PV using 25 hPa height intervals, yet the TIGGE ECMWF ensemble data only contains 8 pressure levels.

Additionally, the identification of SLP minima as the sole determinant of DRV location would likely be an unsatisfactory condition because of the minor pressure falls associated with the early phases of the DRV lifecycle.

The substitution of relative vorticity for PV was inherited from the research of M12. M12 used relative vorticity maxima to identify DRV genesis associated with the recurving TC Chaba (test case 11). When considered further, the use of relative vorticity seems intuitive, as a strong low-level positive PV anomaly will be typically be associated a strong cyclonic circulation, which would in turn result in a highly-positive, low-level relative vorticity maxima.

To further confirm the correlation of low-level positive PV anomalies, SLP minima, and relative vorticity maxima, 7 DRV locations identified in the BW13 climatology storm number 795 (the TC Chaba case) were plotted against relative vorticity maxima identified with the DRV identification script (outlined above) run on the analysis data of the TIGGE ECMWF dataset. In all cases, the PVU-identified storm centers and relative vorticity maxima were located less than 70 km apart (Figure 24). A graphical example of the co-located features at DRV genesis is plotted in Figure 25.

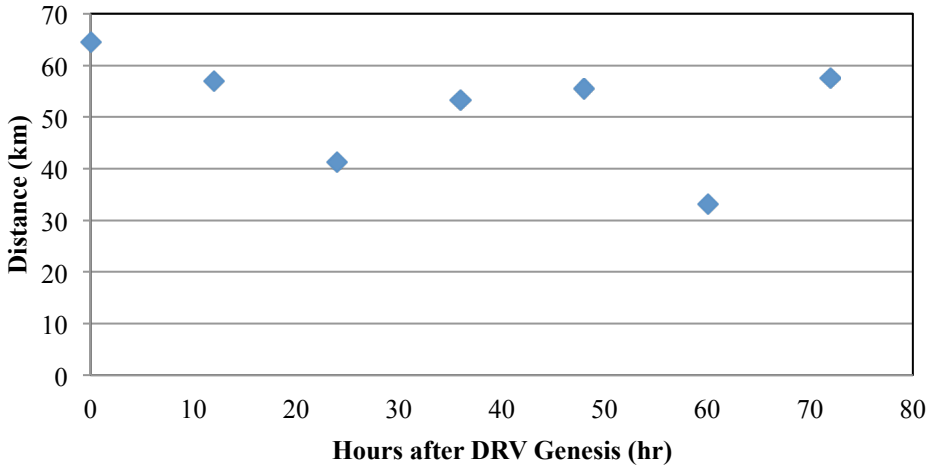

Figure 24. Distance between the observed DRV and the identified relative vorticity maxima at twelve hour intervals after formation (Climatology storm number 795, thesis test case 11).

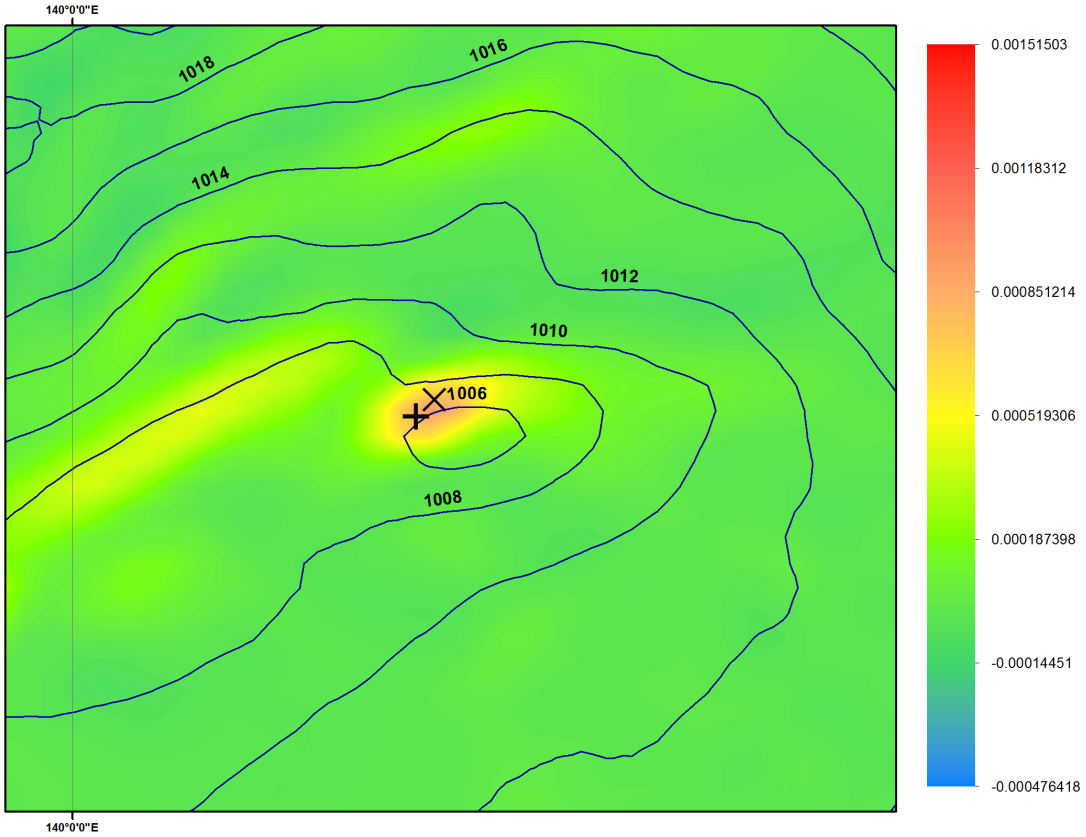

Figure 25. A plot showing the co-location of the PV identified DRV location (+) from the BW13 climatology, the relative vorticity maxima identified DRV (X), and the closed SLP contour from the DRV identification script evaluating the TIGGE ECMWF analysis data for 12 UTC 28 October 2010. Shading represents relative vorticity value (warmer colors indicate strong positive relative vorticity) and the contours are SLP (hPa)

b. Fast Propagation Assumption

The DRV identification script does not contain an algorithm to determine fast propagation of the disturbance, as was done in the climatology of BW13. The assumption made is thus: if successive ensemble forecast DRVs continue to fall within 500 km of the observed fast-propagating DRV, then the ensemble forecast DRV is also propagating at the minimum required speed.

c. Baroclinicity Calculation Using 925 hPa Temperature

The DRV identification script follows as closely as possible the algorithm developed by BW13 in determining downstream, low-level baroclinicity. However, by the necessity of the available TIGGE ensemble parameter data, 925 hPa temperature values are used in place of 950 hPa potential temperature values. This substitution should not result in any degradation of the DRV identification script.

IV. STUDY OF ECMWF TIGGE ANALYSIS AND CONTROL FORECASTS OF THE DRV ASSOCIATED WITH TYPHOON CHABA

A. INTRODUCTION

The study of M12 attempted to evaluate the probabilistic predictability of an observed DRV that occurred in October 2010 in the western North Pacific. The case was notable for a number of reasons. Trajectory analyses confirmed that the DRV formed as a result of warm moist advection impinging upon a baroclinic zone. It was found that the advection was in large part associated with recurving tropical cyclone (TC) Chaba. Subsequent work has shown that approximately 31 percent of recurving TCs in the western North Pacific generate DRVs (Moore et al. 2013). Given this relatively high fraction, it is of interest to examine the case of TC Chaba in detail to better understand the dynamical processes at work.

In addition to this unique pathway to DRV genesis, the case is of interest in that the incipient DRV subsequently underwent explosive cyclogenesis (deepening rate exceeding 2.75 Bergerons). The sea-level pressure trace for the case is shown in Figure 26. It captures a two-phase structure, with a period of modest growth followed by explosive deepening.

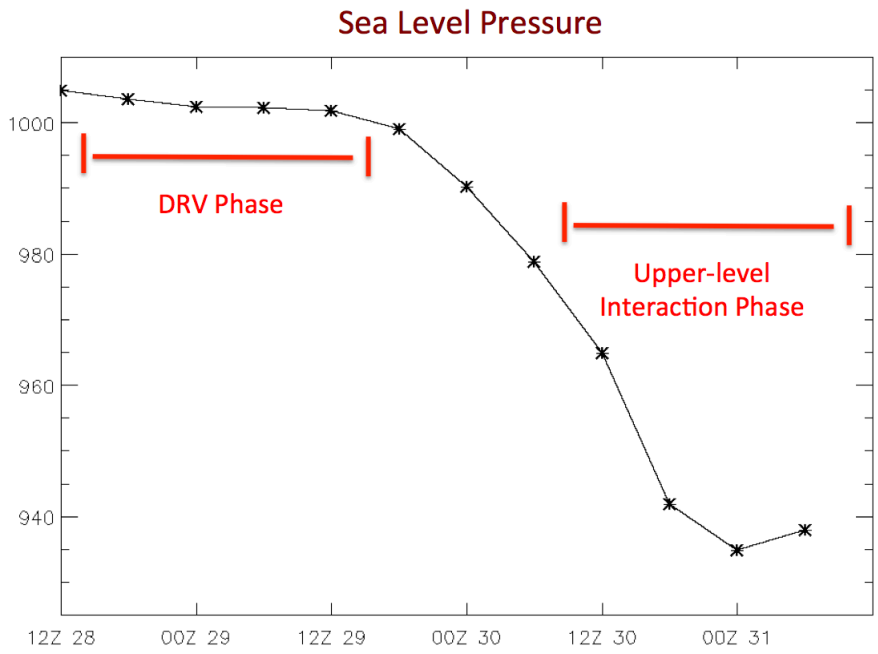

Figure 26. A time series of the sea level pressure (SLP) at the location of the TC Chaba associated DRV. The distinct two-phase lifecycle of the DRV can be observed with minimal pressure drop over the initial 30 hours followed by the subsequent rapid pressure fall (12 UTC October 2010 – 06 UTC 31 October 2010).

Via an analysis of the energetics, M12 found that, during the early phase, the diabatic generation of eddy APE was the dominant source (consistent with a DRV as a diabatically-dominated disturbance). As explosive cyclogenesis ensued baroclinic processes took on a great role, indicating the emergence of a troposphere deep disturbance. The observed, evolving structure of the disturbance was examined in detail and was consistent with the above conclusion. This two-phase structure has been found in previous studies of significant cyclones associated with DRVs (Wernli et al. 2002, Moore et al. 2008, Boetccher and Wernli 2011)

As noted, the formation of the observed DRV resulted from the southerly flow impinging upon the low-level baroclinic zone. This provided significant lifting resulting in deep convection along the frontal band (as seen in the MTSAT-IR image from 1330 UTC 28 October – Figure 27). Within a general band of convection, there are a number of more intense regions of convection observed, one of which is associated with the incipient DRV (annotated in Figure 27).

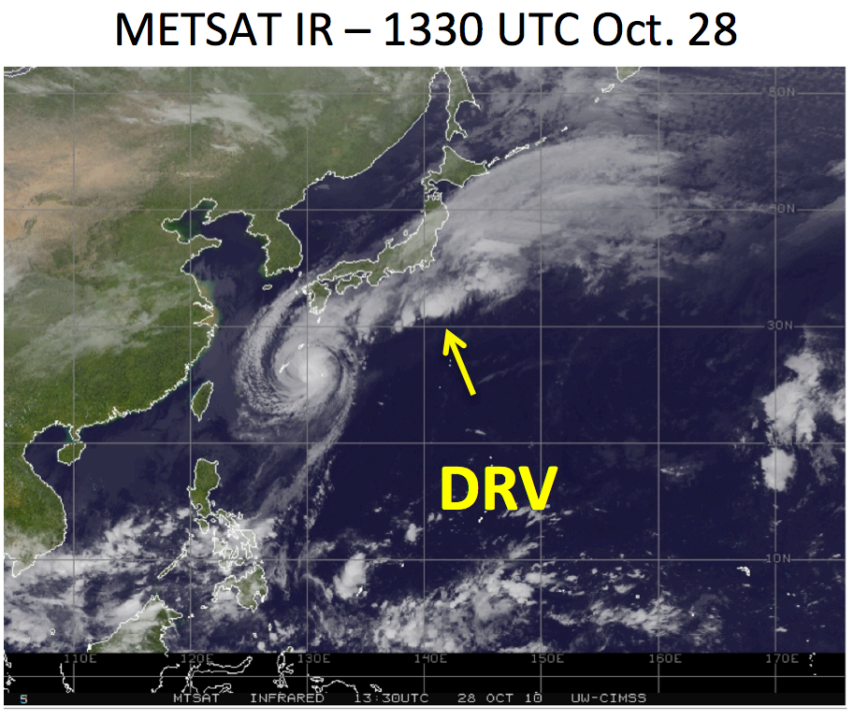

Figure 27. Infrared satellite imagery highlighting TC Chaba and associated outflow. The location of the DRV near the time of genesis is annotated on the imagery (MTSAT IR; 1330 UTC 28 October 2010).

Subsequent to this time, the DRV propagated quickly to the east northeast and strengthened. A series of surface analyses at relevant times from the Ocean Prediction Center are provided here to document the evolution (Figure 28). The explosive cyclone reached a minimum sea level pressure of 939 hPa and generated winds exceeding hurricane force.

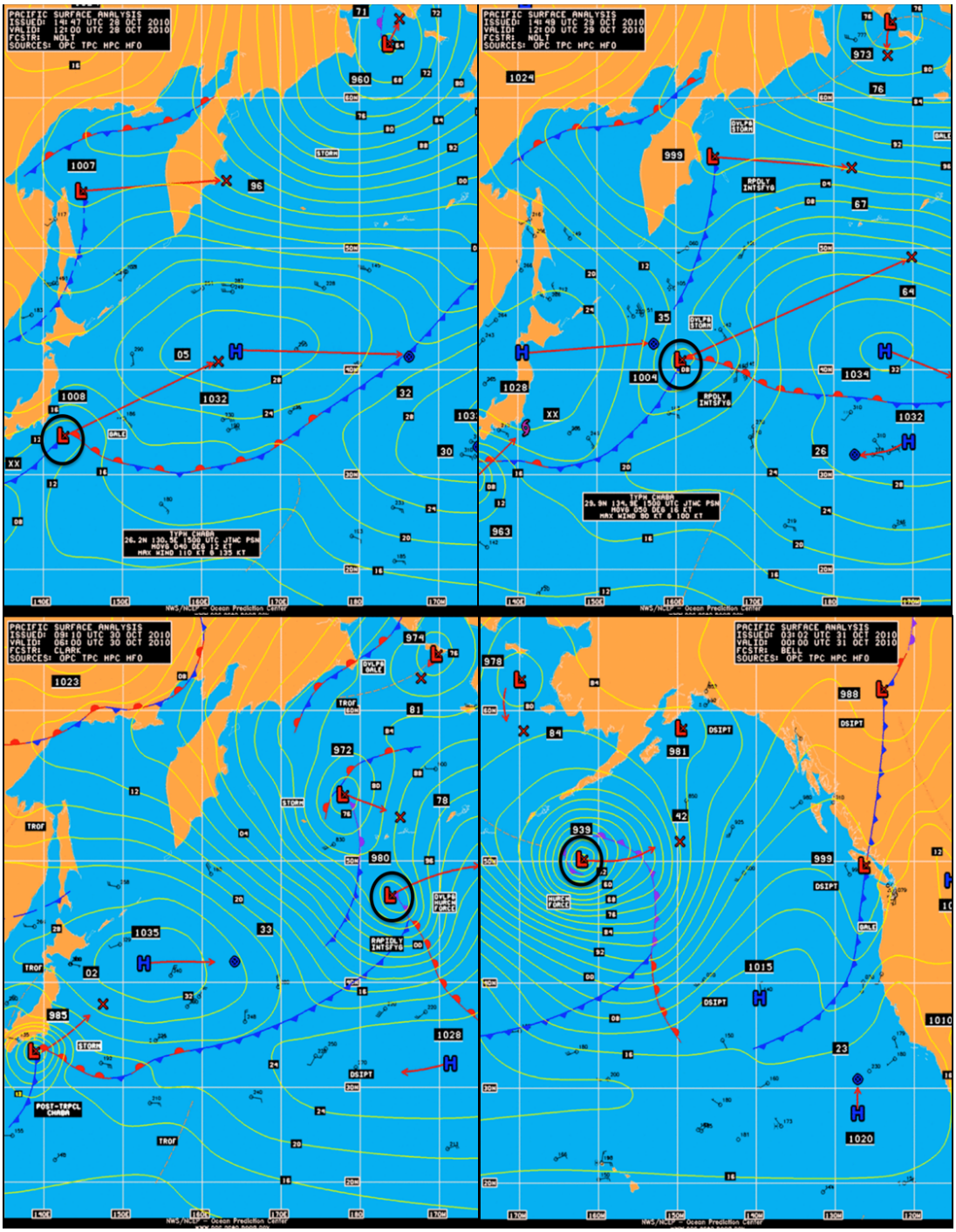

Figure 28. Surface analysis of the genesis, propagation, and subsequent upper-level interaction and explosive deepening of the TC Chaba related DRV [surface analysis provided by the Ocean Prediction Center; valid times: 12 UTC 28 October 2010 (upper left), 12 UTC 29 October 2010 (upper right), 0600 UTC 30 October 2010 (lower left), 00 UTC 31 October 2010 (lower right)].

In terms of the predictability of the DRV, the M12 study authors focused on the genesis phase by incorporating TIGGE data from a number of operational centers and multiple forecast lead times. The validation time was chosen to be six hours after the identification of the DRV in the objective climatology of BW13 at 12 UTC 28 October. The results indicated, as would be expected, that the so-called hit rate increased with decreasing forecast lead time.

With that said, there were low hit rates for even relatively short forecast lead times. For a 48-hour forecast, the ECMWF TIGGE ensemble prediction system found a hit rate of only 45 percent, indicating significant uncertainty in the forecast. The cause of the uncertainty, however, was not readily apparent. The sensitivity of the hit rate to the magnitude of the low-level baroclinicity, low-level relative humidity, and the intensity of tropical cyclone Chaba was examined. The results showed no clear signal.

A primary goal of the work presented herein is to expand the scope of the work presented in M12. In contrast to M12, forecast hit or miss will be evaluated up to 54 hours beyond DRV genesis. Zero, 12, 24, 36, and 48 hour analyses and 40, 60, 72, 84, and 96 hour forecasts for the same initialization time of the ECWMF TIGGE ensemble prediction system will be examined in detail for the TC Chaba associated DRV. The in depth analysis of the TC Chaba case presented in this chapter is designed to evaluate the efficacy of the DRV identification script described in Chapter 3.

B. 48 HOUR FORECAST AND ANALYSIS SUMMARY

1. Location and Intensity of Relative Vorticity Maxima

a. DRV Identification Script Performance

Figure 29 presents the analysis low-level relative vorticity (shading) valid at 12 UTC 28 October. This time corresponds to six hours after the first identification of the DRV in the BW13 climatology. Superposed on the map are the locations of the BW13 DRV (+) and that from the DRV identification script when applied to the analysis data (*). The DRV identification script did a credible job of locating and placing the center of the DRV. It is found within 65 km of that identified in BW13, an error that may in part

be due to the coarser resolution of the ECMWF TIGGE dataset (as opposed to the ECMWF operational analysis). The calculated value of maximum relative vorticity is well above threshold (8.95×10^{-4} s^{-1}) and supports the threshold value of 3.5×10^{-4} s^{-1} used in the DRV identification script at forecast lead times at or near DRV genesis.

b. Control Forecast Performance

Also shown in Figure 29 is the location of a DRV-like feature from the DRV identification script for the 48 hour control forecast valid at the same time (X). The contours represent lines of constant low-level relative vorticity, with the red contour being the threshold value. The 48 hour control forecast relative vorticity maximum was misplaced from the observed DRV location by 446.3 km, which is within the threshold limits for distance. Intensity also met threshold values and was calculated to be 3.81×10^{-4} s^{-1}. While both met the threshold criteria (the location and intensity were both registered as "hits" by the DRV identification script), the intensity value is considerably less than in the analysis and the displacement is quite large (meeting the 500 km threshold by a little more than 50 km).

M12 noted that the impingement of warm moist air upon the low-level baroclinic zone associated with recurving tropical cyclone Chaba resulted in a band of intense convection. As can be seen in Figure 29, a band of enhanced relative vorticity results, with four distinct maxima within the band. In contrast, a single relative vorticity maximum is identified in the control run.

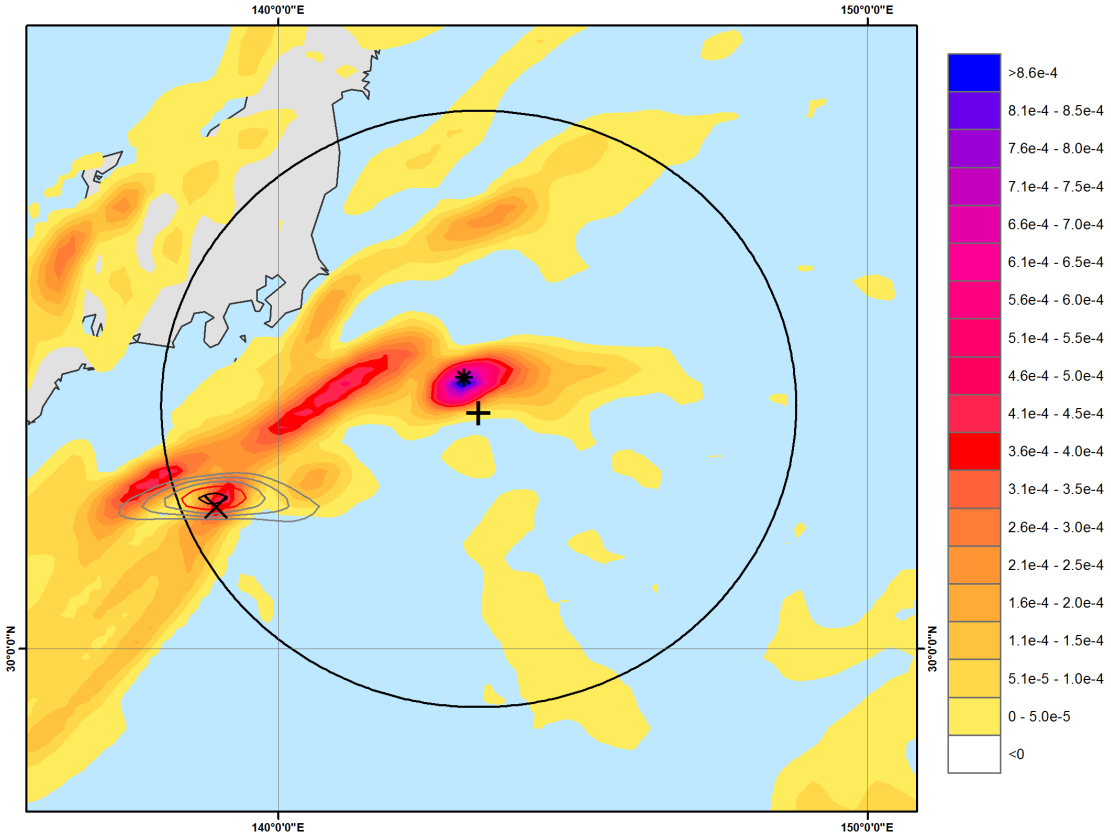

Figure 29. DRV11 00 hour analysis and 48 hour forecast (12 UTC 28 October 2010) plot of positive relative vorticity in the region of observed and forecast DRV locations. Shaded regions indicated areas of positive relative vorticity (magnitude identified by colorbar; s^{-1}), observed DRV location represented by (+), validation DRV location represented by (*), forecast relative vorticity maximum location represented by (X), contours represent control forecast positive relative vorticity (grey: 2.0 – 3.0 x 10^{-4} s^{-1}, red: 3.5 x 10^{-4} s^{-1}, black: >4.0 x 10^{-4} s^{-1}), black circle represents 500 km radius around the observed DRV.

2. Low-Level Baroclinicity

a. DRV Identification Script Performance

The DRV identification script calculated a baroclinicity value of 5.7 K downstream of the analysis DRV location, meeting the threshold minimum of 5 K. Visual inspection of the analysis plot (Figure 30; left panel) reveals a moderate temperature gradient to the east of the observed DRV position and the calculated value presents a

good indication of the relatively weak gradients that can be found at DRV genesis, but again confirms that even at this early forecast lead time, the threshold value used by the DRV identification script is sound. It should be noted, that there is considerable discrepancy between the observed and predicted structure of the low-level temperature gradient both in orientation and intensity.

b. Control Forecast Performance

Visual comparison of the analysis and control forecasts (Figure 30) provides insight into the location of the control forecast placement of the disturbance. The temperature gradient in the control forecast does not extend as far to the north and is generally zonal east of the control forecast disturbance. The analysis plot baroclinic zone visibly extends and strengthens to the north of the location of the observed DRV. The control forecast calculation of baroclinicity was a "hit" (5.9 k), but the placement of the baroclinic zone did not extend far enough to the northeast and likely resulted in the overall placement error of the disturbance.

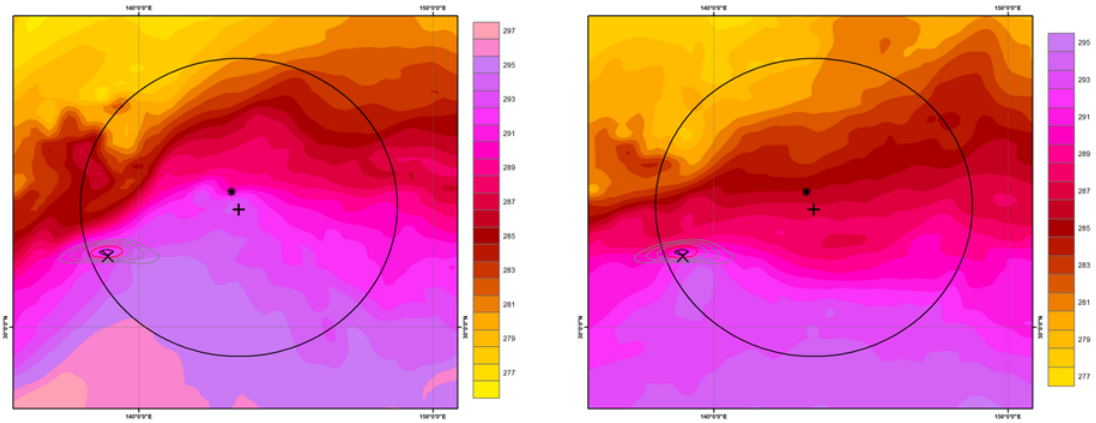

Figure 30. DRV11 00 hour analysis (left panel) and 48 hour forecast (right panel) (12 UTC 28 October 2010) plot of 925 hPa temperatures. Shaded regions represent temperatures (magnitude identified by colorbar; K), observed DRV location represented by (+), validation DRV location represented by (*), forecast relative vorticity maximum location represented by (X), contours represent control forecast positive relative vorticity (grey: 2.0 – 3.0 x 10^{-4} s^{-1}, red: 3.5 x 10^{-4} s^{-1}, black: >4.0 x 10^{-4} s^{-1}), black circle represents 500 km radius around the observed DRV.

3. Sufficient Moisture

a. DRV Identification Script Performance

The DRV identification script calculated a relative humidity value of 93.5 percent for the region around the analysis identified DRV location (Figure 31; left panel). This value is above the threshold and, as with the values noted above, further supports that the threshold in use by the DRV identification script is valid even at or near DRV genesis.

b. Control Forecast Performance

The control forecast calculated relative humidity value of 93.8 percent was above threshold and registered as a "hit" (Figure 31; right panel). Comparing the control forecast relative humidity field with the analysis reveals similar outputs, but the regions of higher values of relative humidity are more widespread in the analysis plot, indicating an under-forecast of relative humidity in the region. Supporting that argument, a strong band of highly saturated air to the southwest of the control forecast relative vorticity maximum that is visible in the analysis plot, but absent in the control forecast. This result is consistent with the zone of enhanced relative vorticity seen in the analysis data as opposed to the more isolated relative vorticity maximum in the control forecast. The implication is that the deep convection (ascent) along the baroclinic zone is more spread in the analysis than in control.

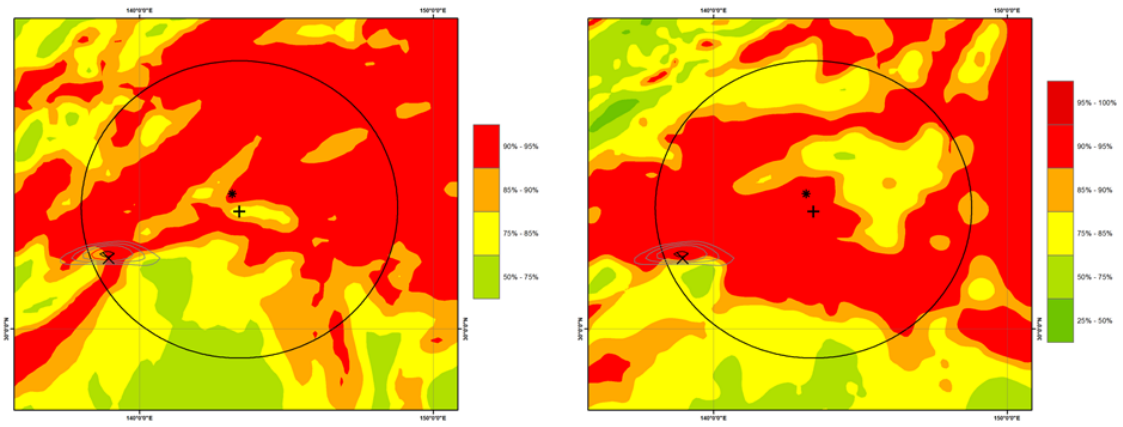

Figure 31. DRV11 00 hour analysis (left panel) and 48 hour forecast (right panel) (12 UTC 28 October 2010) plot of 850 hPa relative humidity. Shaded regions represent relative humidity (magnitude identified by colorbar; percent), observed DRV location represented by (+), validation DRV location represented by (*), forecast relative vorticity maximum location represented by (X), contours represent control forecast positive relative vorticity (grey: 2.0 – 3.0 x 10^{-4} s^{-1}, red: 3.5 x 10^{-4} s^{-1}, black: >4.0 x 10^{-4} s^{-1}), black circle represents 500 km radius around the observed DRV.

4. 00 Hour Analysis and 48 Hour Forecast Performance

The DRV identification code was successful in locating the DRV very close to the climatology position and calculated intensity, baroclinicity, and relative humidity values all above threshold, corroborating the threshold values in use. This is especially useful as the DRV is at genesis, so should be relatively weak and hardest to detect.

The control forecast was identified as a "hit" by meeting the thresholds of all four identification criteria, and without the in-depth cross-examination with the analysis above would have been considered a successfully identified DRV. The displacement of the disturbance was large, though, and likely due to the baroclinic front not extending far enough to the north. Further examination of the evolution of the control forecast will hopefully highlight the developmental impacts of this displacement.

C. 60 HOUR FORECAST AND ANALYSIS SUMMARY

1. Location and Intensity of Relative Vorticity Maxima

a. DRV Identification Script Performance

The 00 hour analysis run provides the DRV identification script a good opportunity to demonstrate it can reasonably locate the DRV center even from within a strong band of relative vorticity. The existence of the elongated bands of relative vorticity in the vicinity of DRVs has already been noted by the work of M12, but the performance of locating the DRV within such bands has not been thoroughly explored before this study. The results on display in Figure 32 give confidence to the identification technique, as given the wide band of intensely positive relative vorticity, the DRV identification script location was only displaced by 57 km. The calculated value of intensity of 7.49 x 10^{-4} s^{-1} is well above threshold and again reinforces the threshold value at an early stage in the DRV lifecycle.

b. Control Forecast Performance

The location of the 60 hour control forecast was 633 km to the southwest of the observed DRV, exceeding the 500 km threshold and registering as a "miss." The intensity was above threshold with a value of 3.90 x 10^{-4} s^{-1}, registering as a "hit," but well below that identified in the analysis. The further increase in distance from the control forecast identified disturbance to the observed DRV indicates the forecast disturbance is moving more slowly than observed. Idealized studies of DRV dynamics have shown that the propagation speed of a DRV is a function of the depth of the system, the strength of the baroclinic zone, and the amplitude of the DRV (MM04, MM05). The lower intensity of the control forecast storm is therefore likely the root cause of the disproportionate propagation of the control forecast to the observed DRV. It is also possible there is a lag in terms of the DRV formation in the control forecast. There is some similarity between the relative vorticity structures of the 12 UTC 28 October analysis and the 00 UTC 29 October control forecast. It will be interest to note going forward if this is simply a phasing issue.

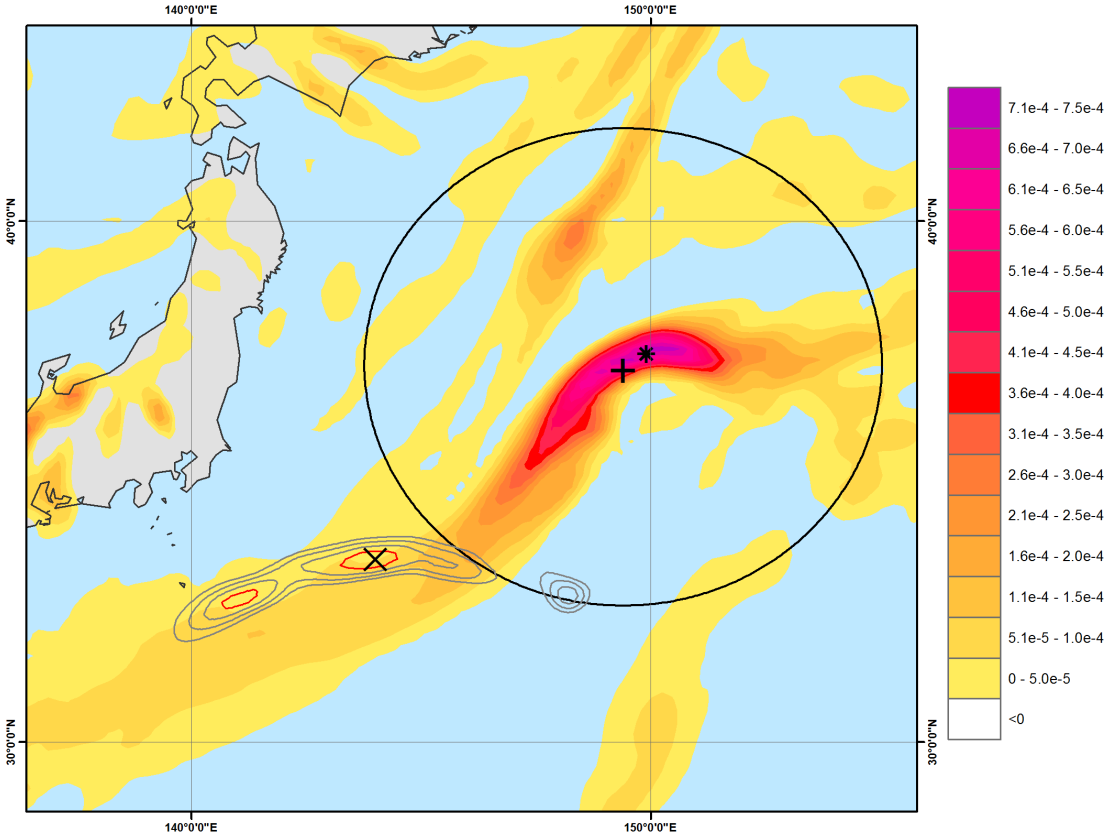

Figure 32. DRV11 12 hour analysis and 60 hour forecast (00 UTC 29 October 2010) plot of positive relative vorticity in the region of observed and forecast DRV locations. Shaded regions indicated areas of positive relative vorticity (magnitude identified by colorbar; s^{-1}), observed DRV location represented by (+), validation DRV location represented by (*), forecast relative vorticity maximum location represented by (X), contours represent control forecast positive relative vorticity (grey: 2.0 – 3.0 x 10^{-4} s^{-1}, red: 3.5 x 10^{-4} s^{-1}, black: >4.0 x 10^{-4} s^{-1}), black circle represents 500 km radius around the observed DRV.

2. Low-Level Baroclinicity

a. DRV Identification Script Performance

Strong frontogenesis is visible when comparing the 00 hour and 12 hour analysis fields (Figures 30 and 33; left panels). The frontogenesis is taking place in the vicinity of the DRV identification script located DRV. As such, a dramatic increase would be expected in downstream baroclinicity from the 00 hour to the 12 hour analysis. The DRV

identification script baroclinicity calculation of 9.6 K (an increase from 5.7 K at 00 hours) is an indication of the script performing as intended.

b. Control Forecast Performance

In contrast to the analysis, only minimal frontogenesis is predicted in the control run (Figure 33). The control forecast calculation for baroclinicity downstream of the identified location of maximum relative vorticity is above threshold (6.2 K), exceeding the threshold and indicating a small increase for 12 hours prior. Again, it is possible a time lag is an issue and the frontogenesis has yet to ramp up.

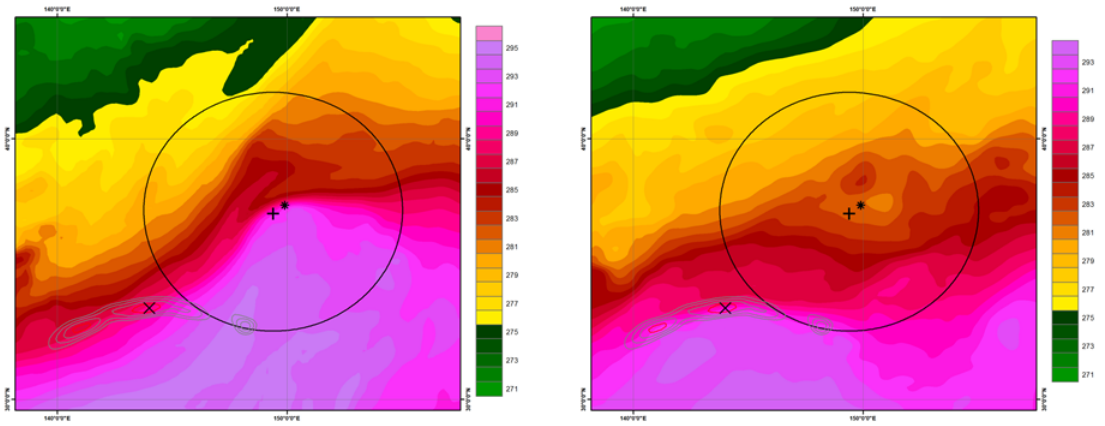

Figure 33. DRV11 12 hour analysis (left panel) and 60 hour forecast (right panel) (00 UTC 29 October 2010) plot of 925 hPa temperatures. Shaded regions represent temperatures (magnitude identified by colorbar; K), observed DRV location represented by (+), validation DRV location represented by (*), forecast relative vorticity maximum location represented by (X), contours represent control forecast positive relative vorticity (grey: 2.0 – 3.0 x 10^{-4} s^{-1}, red: 3.5 x 10^{-4} s^{-1}, black: >4.0 x 10^{-4} s^{-1}), black circle represents 500 km radius around the observed DRV.

3. Sufficient Moisture

a. DRV Identification Script Performance

The DRV identification script calculates sufficient moisture for both the analysis (Figure 34; left panel) and the 60 hour forecast (Figure 34; right panel). Visual inspection

of both plots confirms abundant levels of high relative humidity air in the vicinity of both and the script appears to continue to calculate relative humidity as expected.

b. Control Forecast Performance

The 60 hour control forecast calculation of 93.5 percent is well above threshold. Visual comparisons of the locations of the regions of moisture saturation indicate that the 60 hour control forecast and the 12 hour analysis do not share much agreement about placement of the regions of high relative humidity. The strong frontogenesis occurring around the observed DRV location likely has a lot to do with the analysis distribution of highly saturated air.

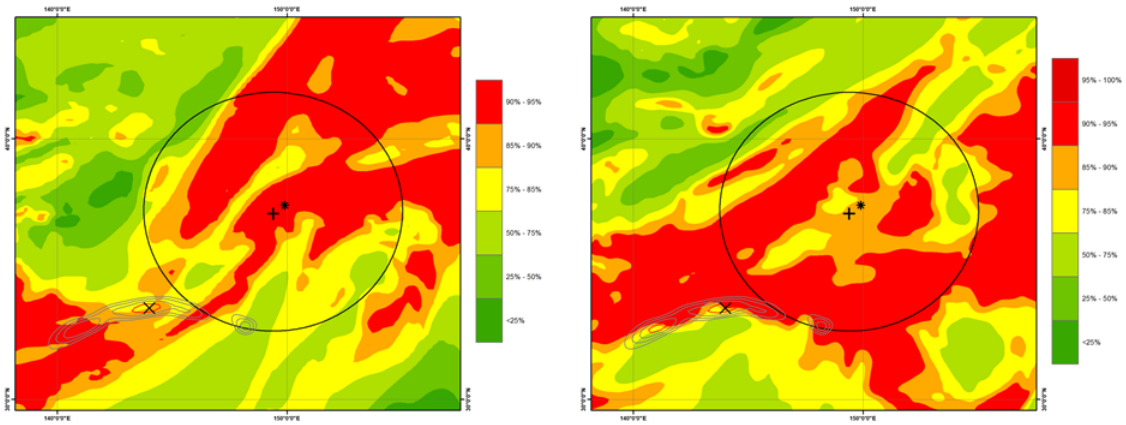

Figure 34. DRV11 12 hour analysis (left panel) and 60 hour forecast (right panel) (00 UTC 29 October 2010) plot of 850 hPa relative humidity. Shaded regions represent relative humidity (magnitude identified by colorbar; percent), observed DRV location represented by (+), validation DRV location represented by (*), forecast relative vorticity maximum location represented by (X), contours represent control forecast positive relative vorticity (grey: 2.0 – 3.0 x 10^{-4} s^{-1}, red: 3.5 x 10^{-4} s^{-1}, black: >4.0 x 10^{-4} s^{-1}), black circle represents 500 km radius around the observed DRV.

4. 12 Hour Analysis and 60 Hour Forecast Performance

The DRV identification code was again successful in locating the DRV very close to the observed position and calculated intensity, baroclinicity, and relative humidity

values all above threshold, corroborating the threshold values in use. The DRV identification script also managed to locate the DRV within a structured band of highly positive relative vorticity. This is just a first-case basis, but a good initial indication of ability.

The 60 hour control forecast was classified a "miss" after being located above the threshold distance from the observed DRV. It does appear the control forecast is identifying a DRV-like feature. Again, it will be interesting to note the subsequent evolution to discern if DRV genesis did take place, but was out of phase in time. It also begs the question as to repercussions in regards to the observed explosive deepening as phasing is typically important in such cases (BW11).

D. 72 HOUR FORECAST AND ANALYSIS SUMMARY

1. Location and Intensity of Relative Vorticity Maxima

a. DRV Identification Script Performance

As the 24 hour analysis displays in Figure 35, the structure of the band of intense positive relative vorticity continues to spread around the location of observed DRV. This is consistent with the emerging frontal structure seen in the surface analysis. The DRV identification script continues to do an exceptional job of locating the maximum relative vorticity in the vicinity of the climatology DRV. The calculated distance is down to 41 km despite the banding. The intensity is decreased again from the 12 hour analysis to $6.91 \times 10^{-4}\ s^{-1}$.

Also apparent in Figure 35 is the presence of a secondary system with high values of low-level relative vorticity. This represents the extratropical disturbance identified to the north of the DRV in the surface analysis (Figure 28).

b. Control Forecast Performance

The 72 hour control forecast continues to forecast a weak disturbance to the south of the observed DRV position. Distance at this lead time is outside of the 500 km threshold at 537 km. The intensity is weak at a calculated relative vorticity maximum of $2.92 \times 10^{-4}\ s^{-1}$. As a result, both metrics are registered as "misses."

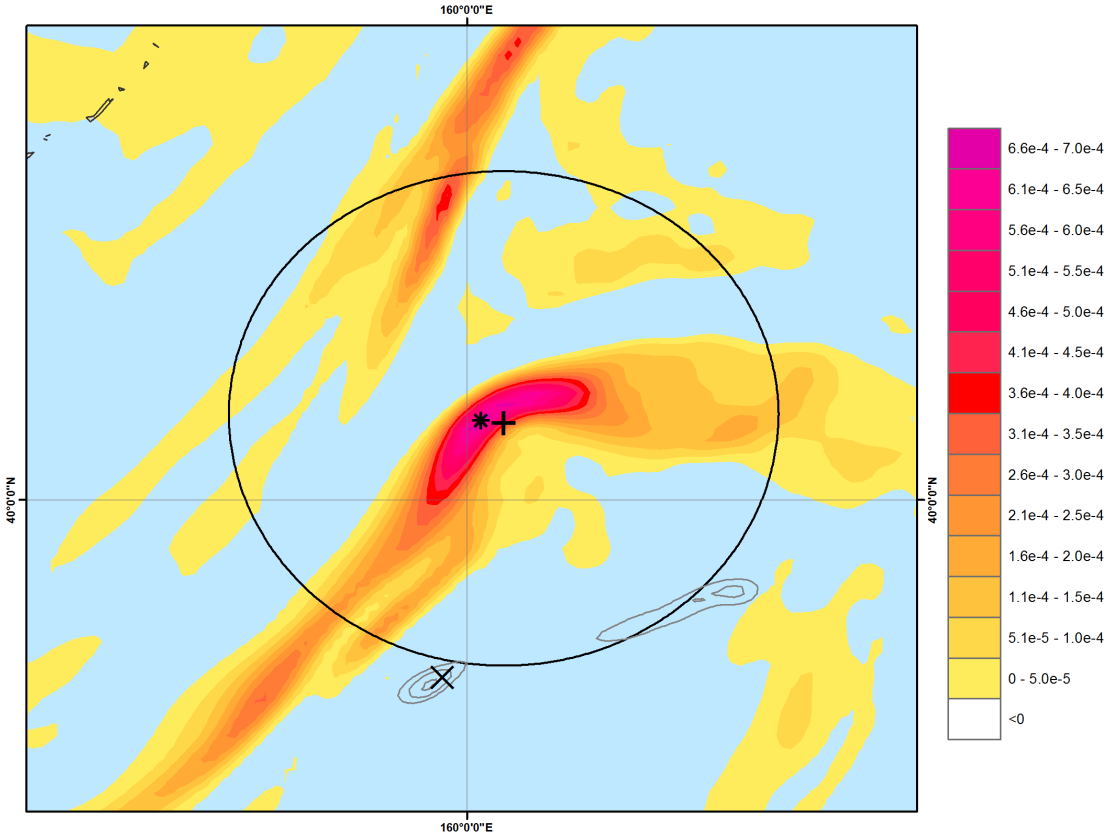

Figure 35. DRV11 24 hour analysis and 72 hour forecast (12 UTC 29 October 2010) plot of positive relative vorticity in the region of observed and forecast DRV locations. Shaded regions indicated areas of positive relative vorticity (magnitude identified by colorbar; s^{-1}), observed DRV location represented by (+), validation DRV location represented by (*), forecast relative vorticity maximum location represented by (X), contours represent control forecast positive relative vorticity (grey: 2.0 – 3.0 x 10^{-4} s^{-1}, red: 3.5 x 10^{-4} s^{-1}, black: >4.0 x 10^{-4} s^{-1}), black circle represents 500 km radius around the observed DRV.

2. Low-Level Baroclinicity

a. DRV Identification Script Performance

Strong frontogenesis continues to take place in the 24 hour analysis plot, as observed in Figure 36 (left panel). The frontogenesis is still centrally located around the positions of the DRV as located by the identification script and climatology. The slightly increased calculated baroclinicity value of 9.9 K supports the hypothesis of growth and

gives confidence to the continued success of DRV identification code itself when evaluating "real world" DRV conditions.

b. Control Forecast Evaluation

The 72 hour control forecast continues to miss the frontogenesis occurring to the north. The baroclinic zone continues to exhibit a moderate gradient and an east-west orientation. The control forecast has moved the disturbance slightly too far to the south of the baroclinic zone for the calculation to reach threshold at this lead time, though, and a "miss" is registered with a calculated value of 4.3 K. What is evident is that the control forecast is continually identifying a disturbance on the southern side of the baroclinic zone. What is not readily apparent is if this represents a growing disturbance or simply the generation of new relative vorticity features along the baroclinic front. Further study (ideally an attempt to track a coherent feature and conduct an energetics analysis) would be of interest in this case.

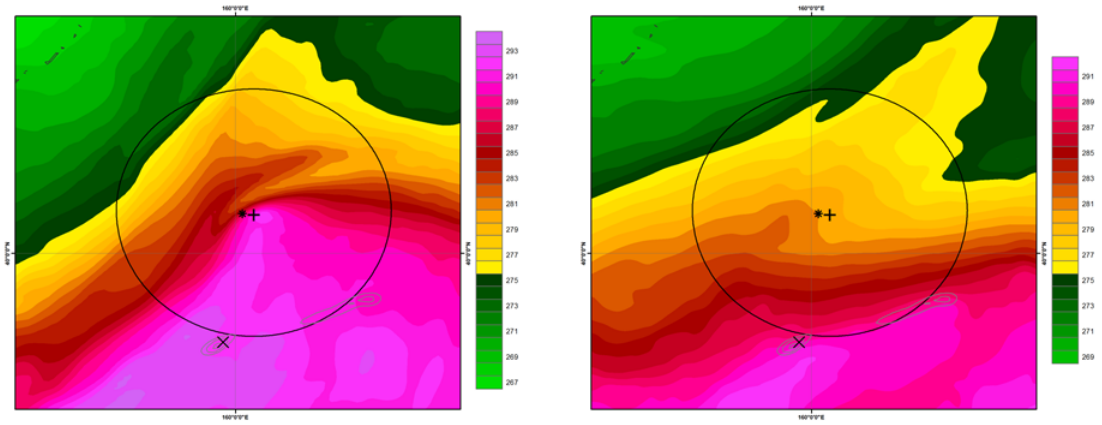

Figure 36. DRV11 24 hour analysis (left panel) and 60 hour forecast (right panel) (12 UTC 29 October 2010) plot of 925 hPa temperatures. Shaded regions represent temperatures (magnitude identified by colorbar; K), observed DRV location represented by (+), validation DRV location represented by (*), forecast relative vorticity maximum location represented by (X), contours represent control forecast positive relative vorticity (grey: 2.0 – 3.0 x 10^{-4} s^{-1}, red: 3.5 x 10^{-4} s^{-1}, black: >4.0 x 10^{-4} s^{-1}), black circle represents 500 km radius around the observed DRV.

3. Sufficient Moisture

a. DRV Identification Script Performance

Both the 24 hour analysis and the 72 hour control forecast relative humidity calculations are above threshold (93.4 percent and 93.7 percent, respectively). Visual analysis of both (Figure 37) gives no reason to suspect the identification code is making erroneous calculations.

b. Control Forecast Performance

The 72 hour control forecast places a band of moisture over the identified relative vorticity maximum (Figure 37; right panel) that also exists in the 24 hour analysis (Figure 37; left panel). The analysis, however, indicates a band of saturated air wrapping around the observed DRV location and starting to resemble the structure of growing, strong convective system. The 72 hour control forecast is far less structured with no visible systems or cohesion.

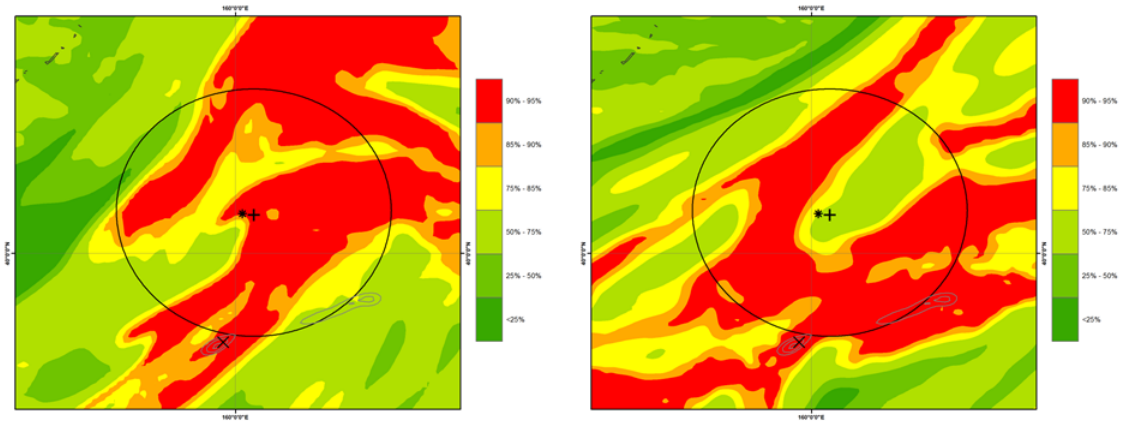

Figure 37. DRV11 24 hour analysis (left panel) and 72 hour forecast (right panel) (12 UTC 29 October 2010) plot of 850 hPa relative humidity. Shaded regions represent relative humidity (magnitude identified by colorbar; percent), observed DRV location represented by (+), validation DRV location represented by (*), forecast relative vorticity maximum location represented by (X), contours represent control forecast positive relative vorticity (grey: 2.0 – 3.0 x 10^{-4} s^{-1}, red: 3.5 x 10^{-4} s^{-1}, black: >4.0 x 10^{-4} s^{-1}), black circle represents 500 km radius around the observed DRV.

4. 24 Hour Analysis and 72 Hour Forecast Performance

The DRV identification script continues to do an admirable job of identifying and calculating reasonable values given the plots of the 24 hour analysis. All threshold values continue to be met for analysis of a "real world" DRV.

The 72 hour control forecast continued under-forecasting disturbance intensity and placement of both the disturbance and the baroclinic front too far to the south. The result is a generally weak system that continues to decay.

E. 84 HOUR FORECAST AND ANALYSIS SUMMARY

1. Location and Intensity of Relative Vorticity Maxima

a. DRV Identification Script Evaluation

The DRV identification script again locates the analysis DRV extremely close to the observed DRV (53 km), as seen in Figure 38. The strong relativity vorticity banding continues to spread and weaken the highest levels of relative vorticity, with the 36 hour analysis maximum at $5.08 \times 10^{-4}\ s^{-1}$, but still well above the threshold value. It should be noted that the explosive deepening has begun by this time in the observations.

b. Control Forecast Performance

A strong disturbance is developed to the south of the observed DRV in the 84 hour control forecast. The strength and proximity of the newly emerging disturbance appears to have caused the DRV identification script to have abandoned the weaker previously tracked disturbance that can be identified to the southwest of the new disturbance. This indicates that future forecasts will be tracking a new disturbance, not an evolution of initial disturbance. The new disturbance meets both distance (465 km) and intensity ($6.07 \times 10^{-4}\ s^{-1}$) thresholds.

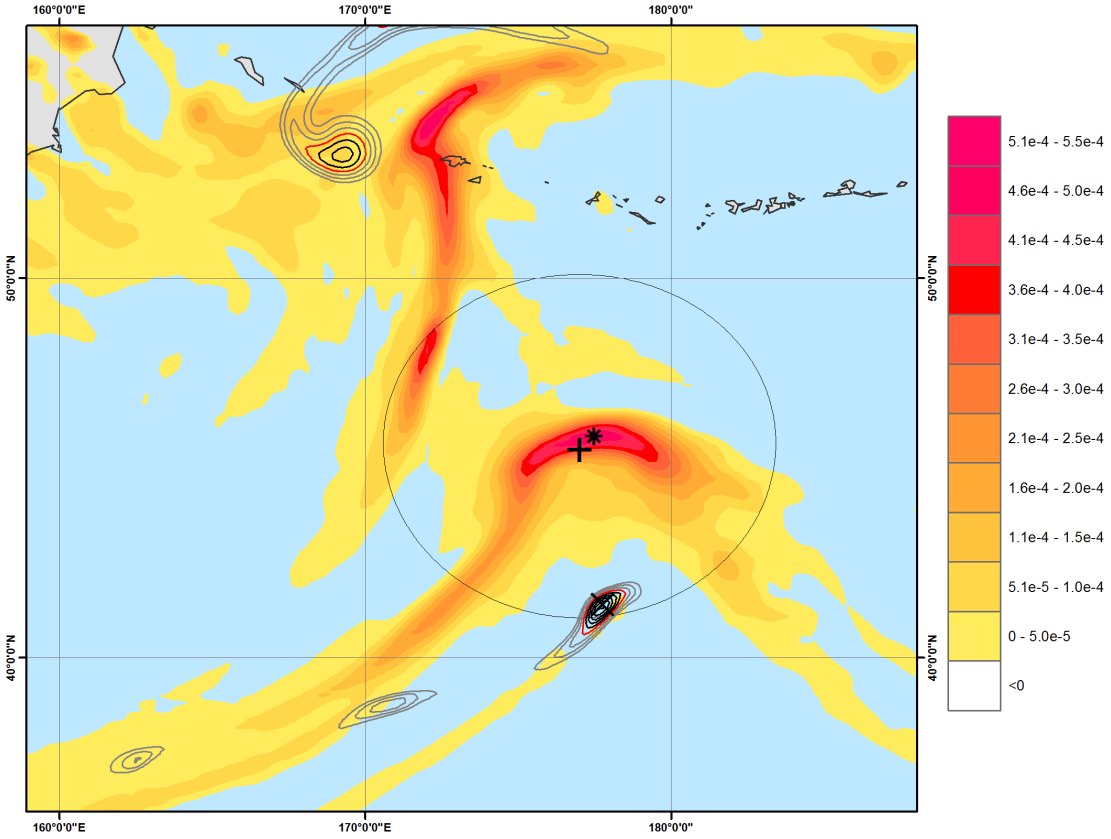

Figure 38. DRV11 36 hour analysis and 84 hour forecast (00 UTC 30 October 2010) plot of positive relative vorticity in the region of observed and forecast DRV locations. Shaded regions indicated areas of positive relative vorticity (magnitude identified by colorbar; s^{-1}), observed DRV location represented by (+), validation DRV location represented by (*), forecast relative vorticity maximum location represented by (X), contours represent control forecast positive relative vorticity (grey: 2.0 – 3.0 x 10^{-4} s^{-1}, red: 3.5 x 10^{-4} s^{-1}, black: >4.0 x 10^{-4} s^{-1}), black circle represents 500 km radius around the observed DRV.

2. Low-Level Baroclinicity

a. DRV Identification Script Performance

Frontogenesis continues in the 36 hour analysis, as can be seen in Figure 39 (left panel), as well as in the 84 hour control forecast in in the vicinity of the newly identified relative vorticity maximum (Figure 39; right panel). Increased baroclinicity calculations

confirm the visible trends in Figure 39 with calculations of 12.8 K and 8.0 K, respectively.

b. Control Forecast Performance

A weak disturbance observed downstream of the initially tracked disturbance in the 72 hour control forecast can be observed in the 84 hour control forecast to have moved into a strong baroclinic zone (Figure 39; right panel), likely initiated forecasted frontogenesis and intensification. As noted in the previous section, this is most likely not the initially tracked system.

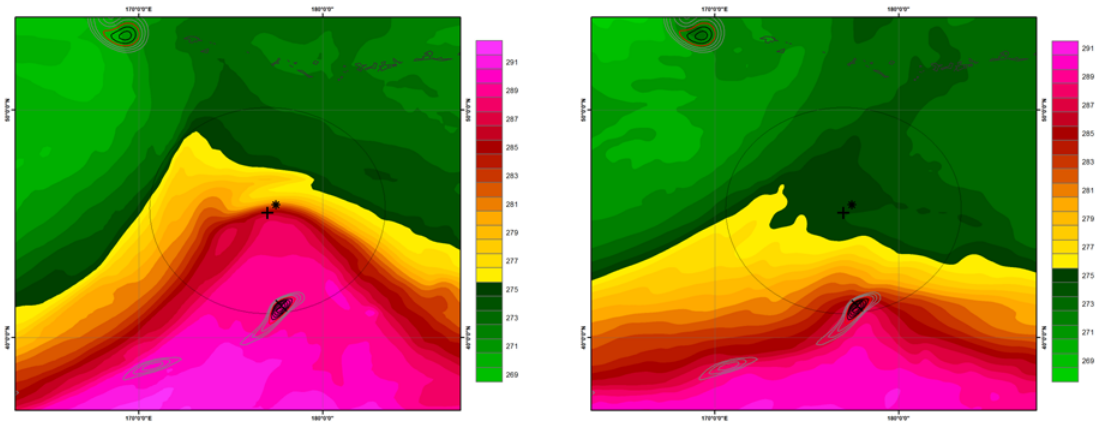

Figure 39. DRV11 36 hour analysis (left panel) and 84 hour forecast (right panel) (00 UTC 30 October 2010) plot of 925 hPa temperatures. Shaded regions represent temperatures (magnitude identified by colorbar; K), observed DRV location represented by (+), validation DRV location represented by (*), forecast relative vorticity maximum location represented by (X), contours represent control forecast positive relative vorticity (grey: 2.0 – 3.0 x 10^{-4} s^{-1}, red: 3.5 x 10^{-4} s^{-1}, black: >4.0 x 10^{-4} s^{-1}), black circle represents 500 km radius around the observed DRV.

3. Sufficient Moisture

a. DRV Identification Script Performance

The DRV identification script calculated relative humidity values of 93.2 and 94.6 percent for the 36 hour analysis and the 84 hour control forecast respectively. Given the

plotted distributions of relative humidity in Figure 40 these figures seem reasonable and there is no reason to question the output of the identification script.

b. Control Forecast Performance

The banding of relative humidity observed in the 84 hour control forecast is likely the result of the flow fields given the layout of the forecast baroclinic front examined in the section above. The 84 hour control forecast calculated relative humidity registered as a "hit." The strong convective system observed in the 36 hour analysis is more cohesive and more in line with the strengthening convective system observed over the previous 24 hours.

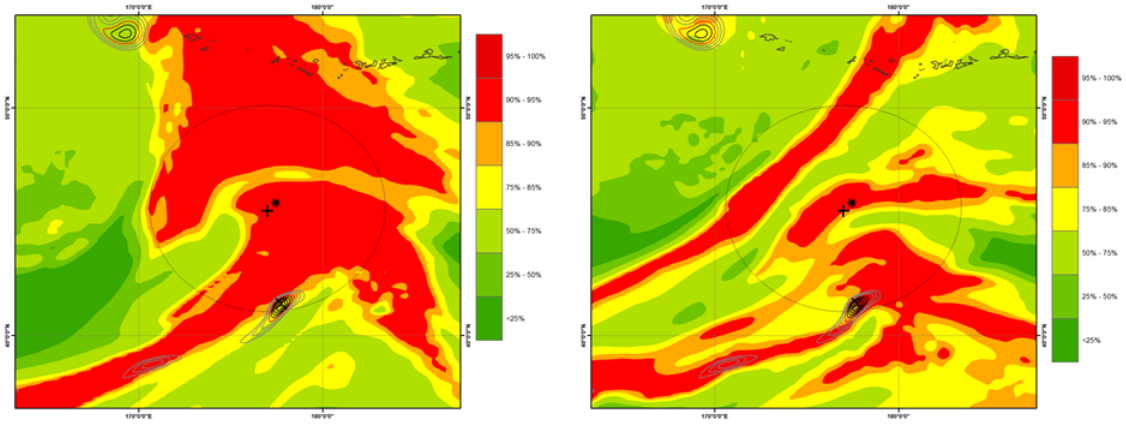

Figure 40. DRV11 36 hour analysis (left panel) and 84 hour forecast (right panel) (00 UTC 30 October 2010) plot of 850 hPa relative humidity. Shaded regions represent relative humidity (magnitude identified by colorbar; percent), observed DRV location represented by (+), validation DRV location represented by (*), forecast relative vorticity maximum location represented by (X), contours represent control forecast positive relative vorticity (grey: 2.0 – 3.0 x 10^{-4} s^{-1}, red: 3.5 x 10^{-4} s^{-1}, black: >4.0 x 10^{-4} s^{-1}), black circle represents 500 km radius around the observed DRV.

4. 36 Hour Analysis and 84 Hour Forecast Performance

The DRV identification script continued to do a good job at identifying and calculating reasonable values given the plots of the 24 hour analysis. The relative

vorticity continued to change structure and stretch in banding, but the location remained less than 60 km from the observed DRV location, further confirming the DRV identification scripts ability.

At the 84 hour control forecast lead time a previously weak disturbance to the east of the originally tracked disturbance appears to have intensified and been picked up by the DRV identification script. The DRV identification script, much like the BW13 climatology script, only locates the strongest disturbance within the area being searched and has no ability to at this time to perform feature tracking. This example highlights a specific instance were the 84 hour control forecasts registers as a "hit," but in reality is a "miss," since it is no longer tracking the original disturbance.

F. 96 HOUR FORECAST AND ANALYSIS SUMMARY

1. Location and Intensity of Relative Vorticity Maxima

a. DRV Identification Script Performance

The observed DRV began rapid intensification over the previous 12 hour and as a result the 48 hour analysis displays a very intense disturbance structure (Figure 41). The observed sea level pressure minimum is approximately 980 hPa at this time. The DRV identification script once again locates the analysis DRV within 60km of the climatology DRV position and intensity has increased to $8.90 \times 10^{-4}\ s^{-1}$.

b. Control Forecast Performance

The identified disturbance in the 84 hour control forecast has moved out of detection range to the south and has weakened over the previous 12 hours. What appears to be a weak outer band of vorticity associated with the previously mentioned extratropical cyclone to the northwest is the only positive relative vorticity feature to identify and track within the search area. For the second time in two forecast lead times, the identification script has jumped features, highlighting the weakness of not being able to actively track features. The newly tracked feature is too weak to weak to meet threshold ($2.57 \times 10^{-4}\ s^{-1}$) and is registered as a "miss."

The southern disturbance does still resemble a DRV like feature and one might question whether the DRV identification script is properly functioning. The primary reason for the distance criteria is to evaluate the atmosphere within a reasonable distance of the observed feature. A forecast feature, even if it is a DRV in the forecast, is not well predicted if it is not within a distance of 500 km of the observed representing a significant track error. It might be useful to make a corollary with TC track errors. Five hundred km would be quite large in that scenario.

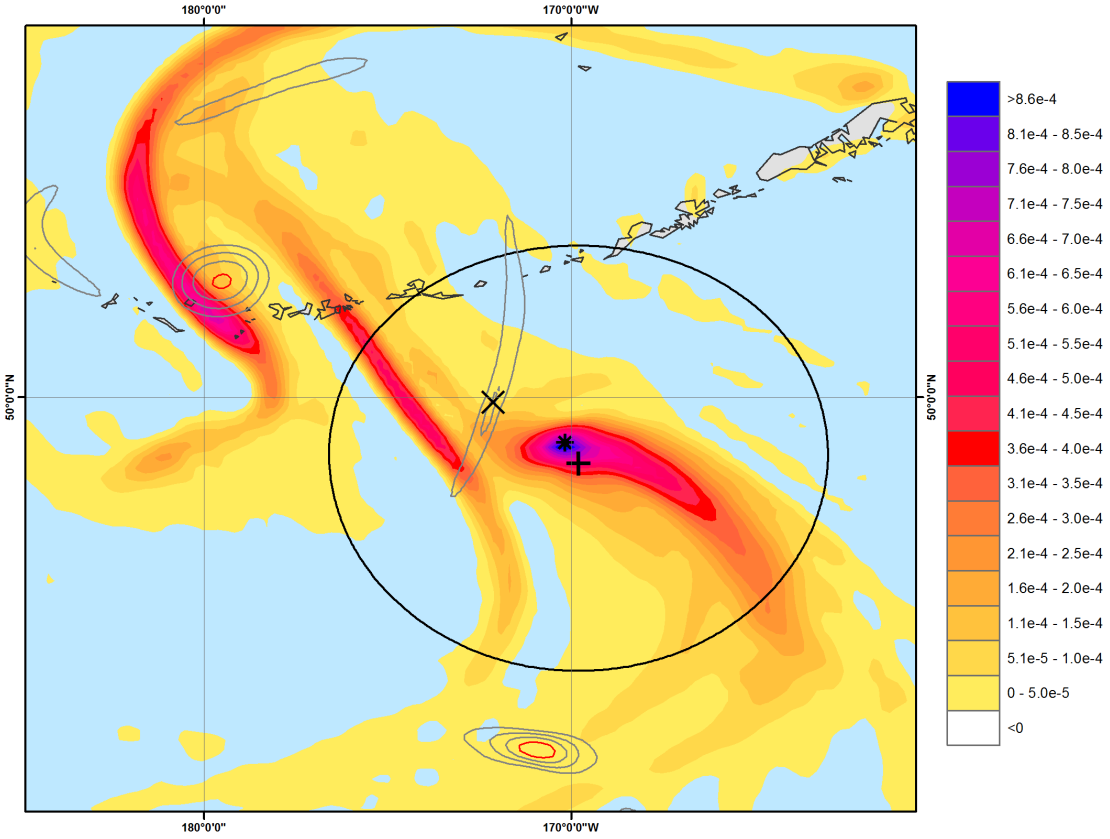

Figure 41. DRV11 48 hour analysis and 96 hour forecast (12 UTC 30 October 2010) plot of positive relative vorticity in the region of observed and forecast DRV locations. Shaded regions indicated areas of positive relative vorticity (magnitude identified by colorbar; s^{-1}), observed DRV location represented by (+), validation DRV location represented by (*), forecast relative vorticity maximum location represented by (X), contours represent control forecast positive relative vorticity (grey: 2.0 – 3.0 x 10^{-4} s^{-1}, red: 3.5 x 10^{-4} s^{-1}, black: >4.0 x 10^{-4} s^{-1}), black circle represents 500 km radius around the observed DRV.

2. Low-Level Baroclinicity

a. DRV Identification Script Performance

The 48-hour analysis reveals the front is starting to get wrapped into the rapidly deepening system, but still exhibits a downstream baroclinic front. The DRV identification script calculates an 8.0 K temperature gradient, which registers as a "hit." The 96-hour control forecast location of maximum relative vorticity is located in an area of almost uniform temperatures and the DRV identification script calculation reflects this with a calculated value of 1.7 K.

b. Control Forecast Performance

As the feature being identified in the 96 hour control forecast is certainly not the original feature, nor is it the observed DRV, there is not much concern about the downstream baroclinicity of the feature that has been identified. It is worth noting the similarities in structure of the baroclinic front. Though not matching one-to-one, the location of the temperature ridging appears well forecast; although the intensity appears under-forecast (Figure 42).

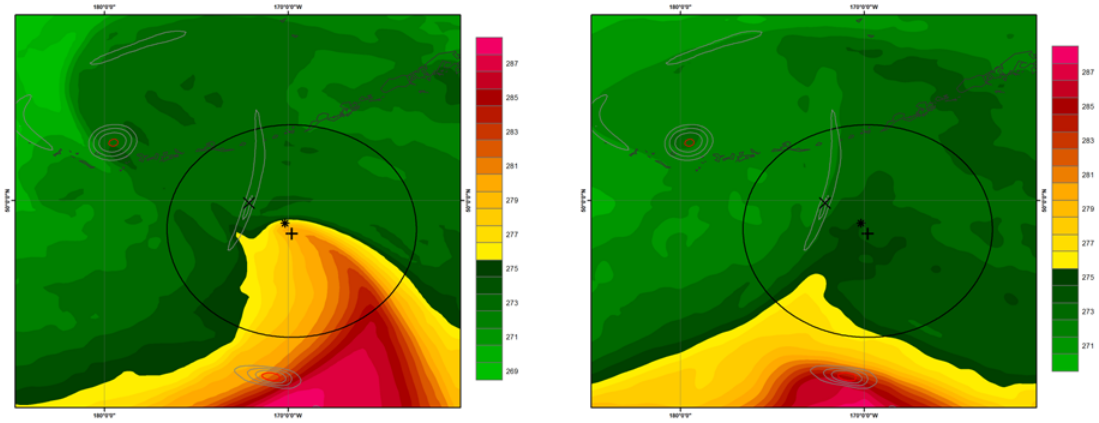

Figure 42. DRV11 48 hour analysis (left panel) and 96 hour forecast (right panel) (12 UTC 30 October 2010) plot of 925 hPa temperatures. Shaded regions represent temperatures (magnitude identified by colorbar; K), observed DRV location represented by (+), validation DRV location represented by (*), forecast relative vorticity maximum location represented by (X), contours represent control forecast positive relative vorticity (grey: 2.0 – 3.0 x 10^{-4} s^{-1}, red: 3.5 x 10^{-4} s^{-1}, black: >4.0 x 10^{-4} s^{-1}), black circle represents 500 km radius around the observed DRV

3. Sufficient Moisture

a. DRV Identification Performance

The DRV identification script calculated relative humidity values of 92.8 and 93.4 percent for the 48 hour analysis and the 96 hour control forecast respectively. Given the plotted distributions of relative humidity in Figure 43 these figures seem reasonable and there is no reason to question the output of the identification script.

b. Control Forecast Performance

The 96 hour control forecast relative humidity structure gives appears to represent an occluded system far to the north (Figure 43, right panel). This feature is also evident in the analysis field although it is significantly displaced to the west. Comparing to the moisture structures in the 48 hour analysis where the interactions of multiple cyclones are observed including the wrapping of saturated air into the observed explosively deepening DRV (Figure 43; left panel).

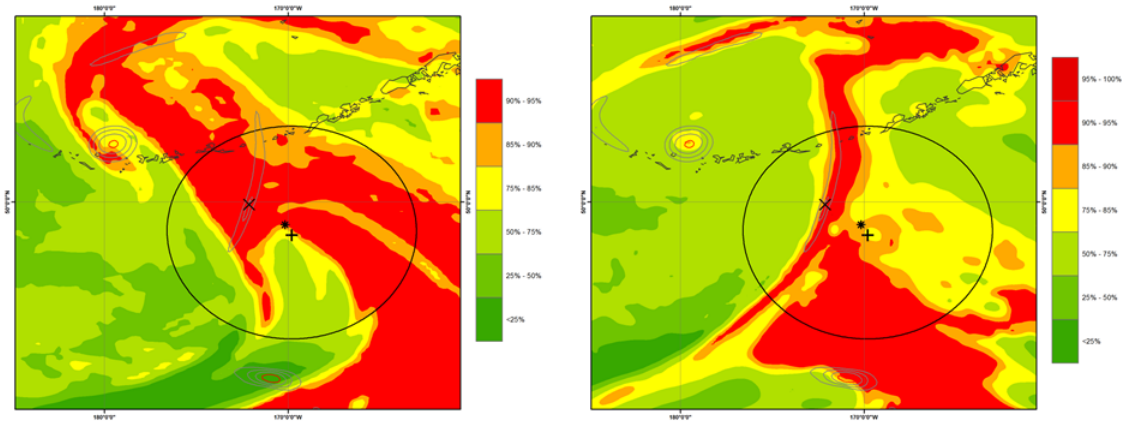

Figure 43. DRV11 48 hour analysis (left panel) and 96 hour forecast (right panel) (12 UTC 30 October 2010) plot of 850 hPa relative humidity. Shaded regions represent relative humidity (magnitude identified by colorbar; percent), observed DRV location represented by (+), validation DRV location represented by (*), forecast relative vorticity maximum location represented by (X), contours represent control forecast positive relative vorticity (grey: 2.0 – 3.0 x 10^{-4} s^{-1}, red: 3.5 x 10^{-4} s^{-1}, black: >4.0 x 10^{-4} s^{-1}), black circle represents 500 km radius around the observed DRV.

4. 48 Hour Analysis and 96 Hour Forecast Performance

Given an explosively deepening system, the DRV identification script did an outstanding job of locating the DRV in the final analyzed analysis of this study. All conditions to identify the disturbance as a DRV were met and, again, all variable thresholds were exceeded by a wide margin.

When analyzing the 96 hour control forecast, the DRV identification script again jumped to a new feature, as the previous feature moved too far south to be included in the search. This again highlights the shortfalls of not being able to do perform feature tracking, a feature that would require much higher temporal resolution in a tracking algorithm. The TIGGE data (specifically the very low vertical resolution) likely precludes the development of a robust tracking feature when considering the scale of the features in question.

5. Explosive Deepening in the Control Forecast

A final question of interest in regards to the control forecast is whether the observed explosive deepening occurred. For this particular case, the answer is no. Figure 44 shows a 108-hour forecast dynamic tropopause map valid at 00 UTC 31 October [potential temperature on the 2.0 PVU surface (shaded), sea level pressure (white contours), (*) is the location of explosive cyclogenesis, (diamond) is the observed location of TC Chaba]. The forecast valid time coincides with the minimum sea level pressure observation.

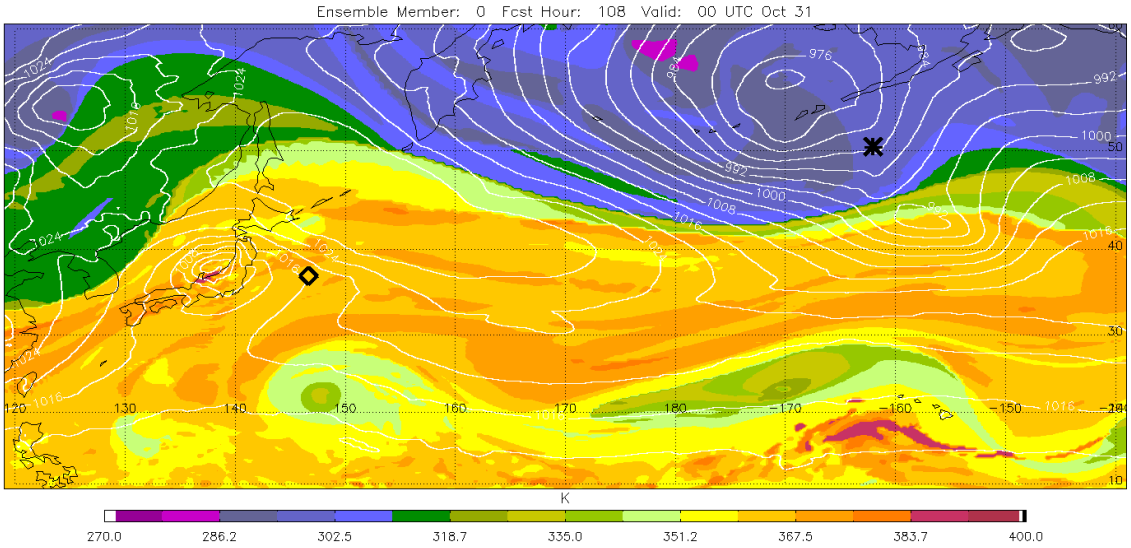

Figure 44. Dynamic tropopause map for the 108 hour control forecast, valid time 00 UTC 31 October 2010 [potential temperature on the 2.0 PVU surface (shaded), sea level pressure (white contours), (*) is the location of explosive cyclogenesis, (diamond) is the observed location of TC Chaba].

Two observed cyclonic features (sea level pressure minima) are observed, the DRV-like feature to the south of the largest potential temperature gradient and the occluded cyclone to the north. Neither has exhibited explosive deepening over the time period examined here. This is an important result, as it illustrates that misforecasts at and shortly after genesis time can be sufficient to preclude the accurate prediction of explosive deepening and, hence, possible high impact weather.

G. VERIFICATION AND FORECAST OF DRV ASSOCIATED WITH TYPHOON CHABA DISCUSSION

The M12 study represented a 'first look' into the predictability of DRV genesis in a probabilistic framework. The approach entailed an ingredients-based identification method that was applied to TIGGE ensemble data from a number of operational centers for different lead-time forecasts, all of which were applied to the genesis of the TC Chaba DRV case. As such, the scope of the work was quite limited. It represented a single case study and only examined the predictability of the incipient DRV disturbance.

The work presented in this chapter is an attempt to assess and validate improvements on the M12 study. Firstly, the objective analysis technique was altered to be more consistent with the methodology of BW13. This is not insignificant. Much of this work is leveraged on the efficacy of the BW13 study (i.e. that the location and environmental conditions associated with the identified DRVs are 'truth'). Therefore, any effort to provide a consistent approach is justified. The improved consistency largely involves the environmental factors (baroclinicity and moisture), which have been adapted to precisely match the BW13 approach.

The performance of the improved identification methodology is assessed via a comparison of the location and characteristics of the observed DRV (from the BW13 climatology) to that obtained by applying the DRV identification script to the analysis data. Within a reasonable measure, the results were entirely consistent, thusly providing a measure of confidence in the improved identification code.

Given this positive result, the identification code was subsequently used to evaluate the control simulation of the ECMWF TIGGE ensemble. To first order, the control simulation represents a deterministic approach to numerical weather prediction in that it takes the best guess of the initial condition and integrates forward. The performance of the control simulation was evaluated beginning at genesis time and the subsequent 48 hours of evolution.

While certain shortcomings of the objective identification script were identified, it was apparent the control (deterministic) forecast performed quite poorly in the case of the TC Chaba DRV. An in depth analysis of the parameter values provided by the identification script combined with a visual inspection of the simulated fields illustrated that, while there were instantaneous examples of a disturbance that had DRV-like characteristics, there was no coherent disturbance over the observed time period.

For the most part, the identification script deemed the assessment as a miss, indicating a poor representation of the observed disturbance (although there were spurious hits during the investigation time period). What was entirely clear is that the erroneous forecast at genesis time resulted in the complete lack of explosive deepening.

THIS PAGE INTENTIONALLY LEFT BLANK

V. DETAILED ANALYSIS OF SELECT CONTROL ECMWF DRV FORECASTS

The study of M12 attempted to evaluate the probabilistic predictability of an observed DRV associated with recurving tropical cyclone Chaba in October 2010. The DRV subsequently underwent explosive cyclogenesis, exhibiting a deepening rate of greater than 2.75 Bergerons. Sanders and Gyakum (1980) proposed a threshold value of one to define explosive cyclogenesis.

M12 focused on the predictability of the genesis phase of the DRV by incorporating TIGGE data from a number of operational centers and multiple forecast lead times. The validation time was chosen to be six hours after the identification of the DRV in the objective climatology of BW13. The results indicated, as would be expected, that the so-called hit rate increased with decreasing forecast lead time.

With that said, there were surprisingly low hit rates for even relatively short forecast lead times. For a 48-hour forecast, the ECMWF TIGGE ensemble prediction system found a hit rate of only 45 percent, indicating significant uncertainty in the forecast. The cause of the uncertainty, however, was not readily apparent. The sensitivity of the hit rate to the magnitude of the low-level baroclinicity, low-level relative humidity, and the intensity of tropical cyclone Chaba were examined. The results showed no clear signal.

A primary goal of the work presented herein is to expand the scope of the work presented in M12 via the examination of multiple cases of explosive cyclogenesis associated with a DRV at different stages of DRV evolution. In contrast to M12, forecast hit or miss will be evaluated up to 30 hours beyond DRV genesis. Forty eight, 60 and 72 hour forecasts for the same initialization time of the ECWMF TIGGE ensemble prediction system will be examined. The evaluation in this chapter only pertains to the control forecast of the ensemble prediction system.

A. SUMMARY OF TEST CASE SELECTIONS FOR DETAILED STUDY

Three test cases were selected from the original 12 (test cases numbered and detailed in Chapter 3.B.1) for detailed analysis. The selections were made to highlight examples of control forecasts that ranged from excellent to poor. The intention is two-fold: (1) to illustrate in detail some aspects of success and failure of the forecast output and (2) to demonstrate the effectiveness of the model assessment script and assess its ability to identify forecasted DRVs within the model runs. The evaluation terms used to describe tests cases as "good," "fair," or "poor" will be discussed in depth in Chapter 5.

1. Selected Test Cases

A brief summary of the test cases selected for in depth analysis of the control forecast is provided below, while detailed analyses are presented in Section B of this chapter.

a. Test Case 1: An Examination of a "Poor" Forecast

Test case 1 was ultimately deemed a poor forecast. As will be shown below, the control forecast did not meet the requirements for a hit at all forecast lead times. The formation of the DRV occurred over land (Japan). This represents a somewhat unique occurrence, as the vast majority of DRVs form over the ocean. It is therefore of interest to examine model performance in such a scenario.

b. Test Case 2: An Examination of a "Fair" Forecast

Test case 2 is of interest due to the fact that the initial forecast of DRV genesis at a 48-hour lead time was very poor, yet the subsequent forecasts at 60 and 72 hours were quite good. It is hoped the examination of this case will shed light on the possible reasons for such a forecast evolution.

c. Test Case 7: An Examination of a Good "" Forecast

Test case 7 provides an interesting contrast to test case 2. The initial forecast is excellent in location, intensity, and environmental conditions. As the forecast lead time advances, the location continues to be remarkably close to the observed, but the intensity

drops below minimum DRV threshold as defined here. The ensemble control forecast appears to have performed adequately in a qualitative sense, yet failed the DRV identification script. Given this, examination of this case should provide additional information regarding the efficacy of the identification scheme presented in this study.

B. TEST CASE 1

The test case 1 DRV (hereafter referred to as DRV01) was first observed over the Japanese mainland at 12 UTC on 4 March 2010. After a slight deviation to the southeast, DRV01 propagated east-northeast across the Northern Pacific for 48 hours before transitioning to the intensification phase at around 170E. During intensification, which lasted an additional 48 hours, the DRV traced a path just south of the Aleutian Islands. A deepening rate of 1.02 Bergerons and a SLP minimum of 968.8 hPa were recorded. The DRV01 observed propagation and intensification path is plotted in Figure 45.

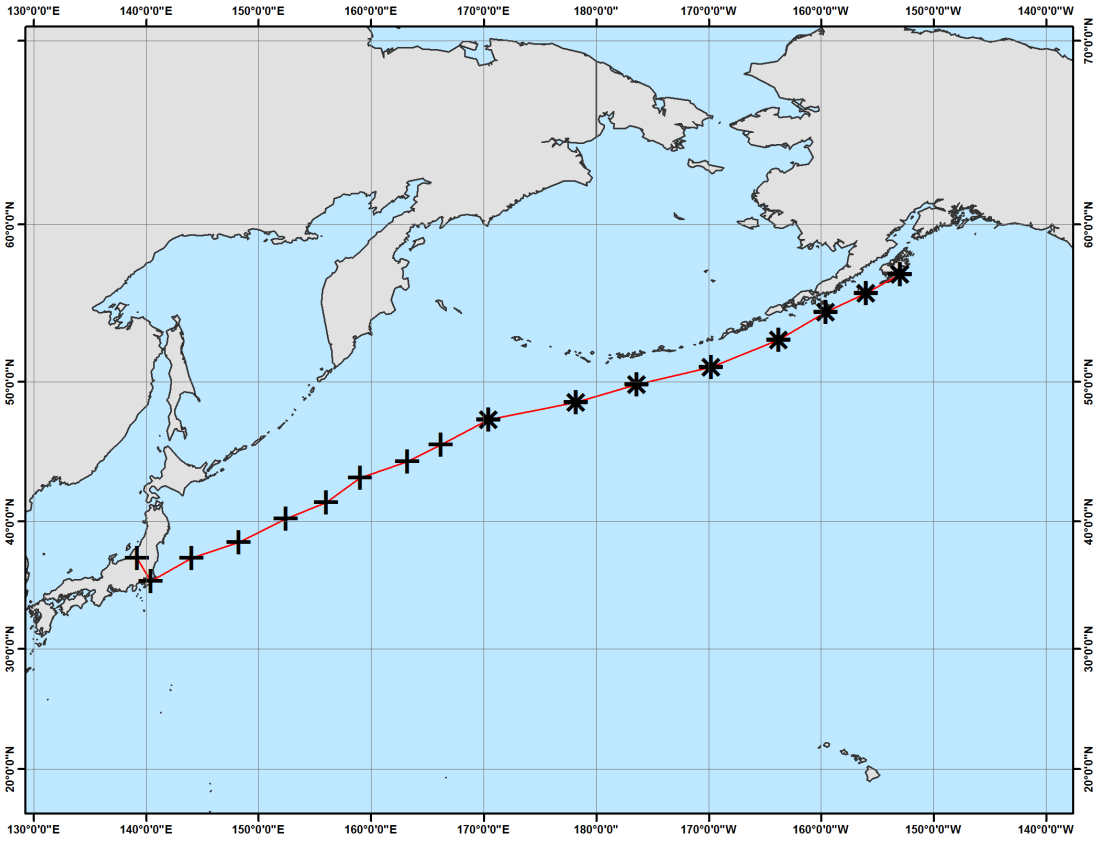

Figure 45. DRV01 observed propagation and intensification track (red line). Locations of propagation (+) and intensification (*) are marked every 6 hours (valid time 12 UTC 4 March 2010 – 12 UTC 8 March 2010). Observed DRV information from BW13 climatology.

1. DRV01 48hr Forecast

a. Location and Intensity

The location of the DRV01 48hr forecast was 529 km to the SW of the observed DRV01, exceeding the 500 km threshold. The strength of the forecast relative vorticity also registered as a "miss," with a value identified below the minimum strength threshold at 2.76 x 10^{-4} s^{-1}. Weak relative vorticity fields can be observed over most of the region within 500 km of the observed DRV01, with negative values at the specific location of the DRV01, as seen in Figure 46.

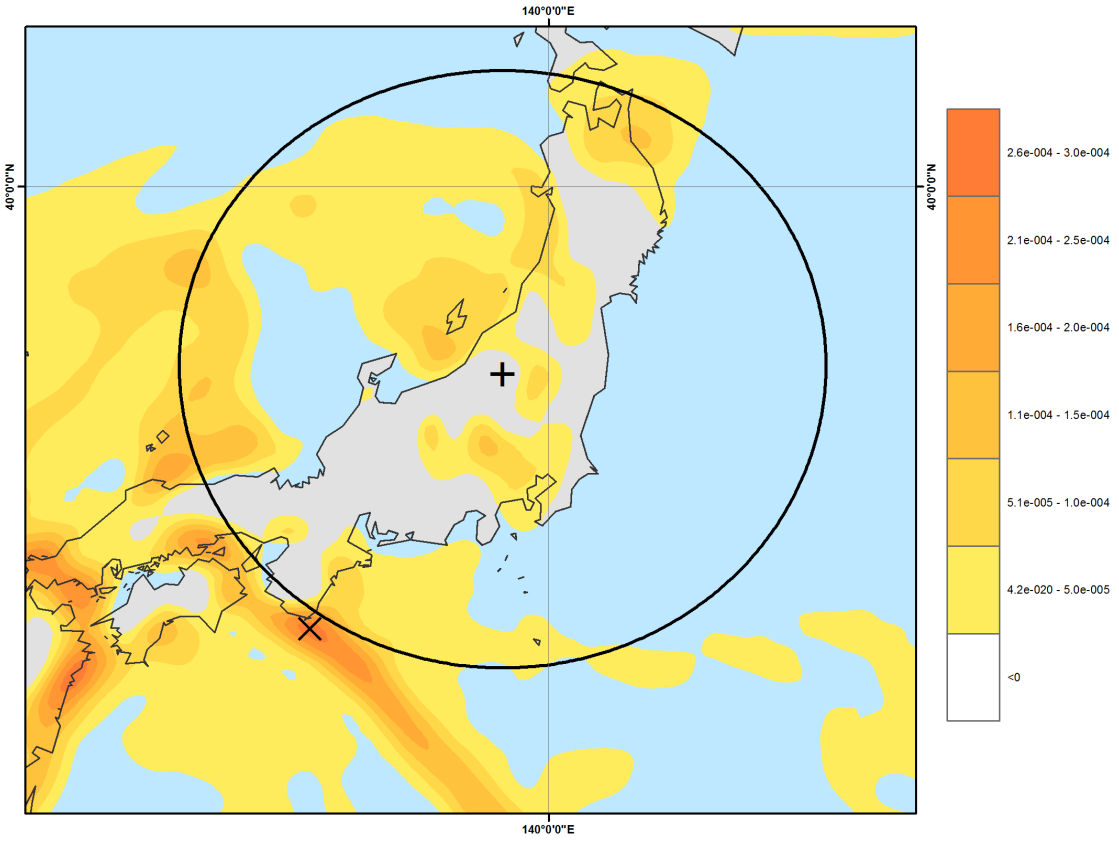

Figure 46. DRV01 48hr forecast (12 UTC 04 March 2010) plot of positive relative vorticity in the region of observed and forecast DRV locations. Shaded regions indicated areas of positive relative vorticity (magnitude identified by colorbar), observed DRV location represented by (+), forecast DRV location represented by (X), black circle represents 500 km radius around the observed DRV.

b. Baroclinicity

As seen in Figure 47, a strong baroclinic zone extends to the SE of the forecast DRV01 position, indicating an expected SE propagation path if the DRV were to establish in that location. The calculated gradient value of 6.38 K was classified as a "hit."

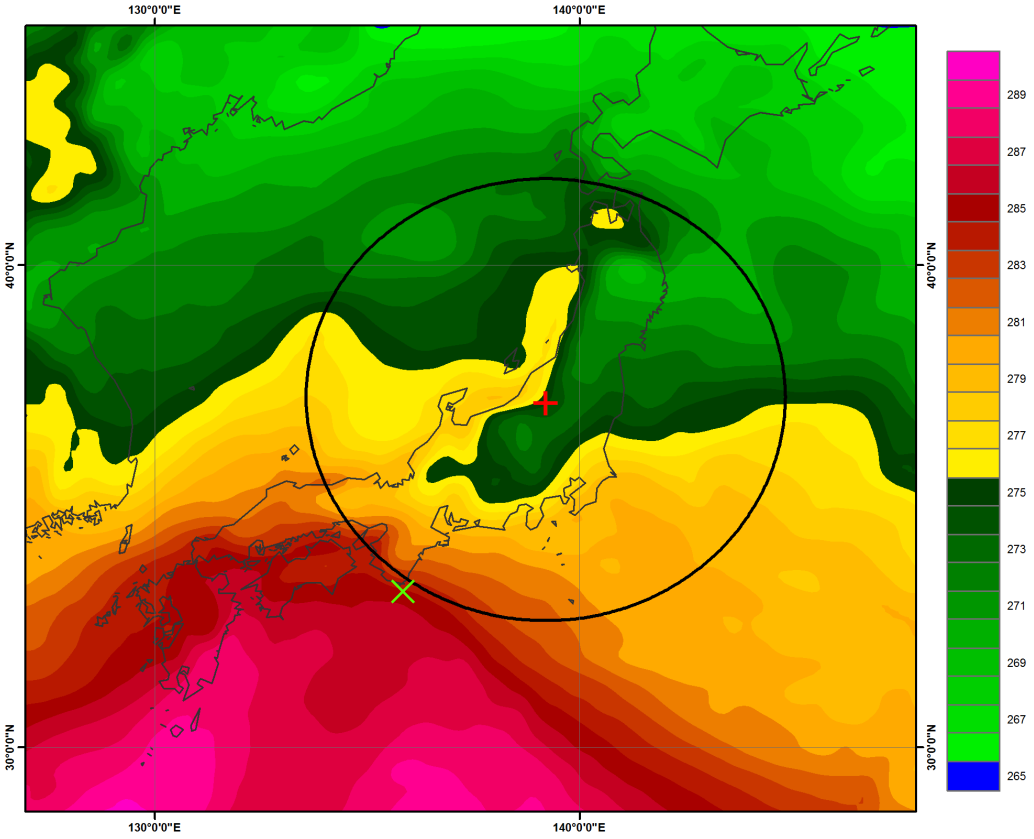

Figure 47. DRV01 48hr forecast (12 UTC 04 March 2010) plot of 925 hPa temperatures in the region of observed and forecast DRV locations. Shaded regions indicated temperature (magnitude identified by colorbar in degrees K), observed DRV location represented by (+), forecast DRV location represented by (X), black circle represents 500 km radius around the observed DRV.

c. Sufficient Moisture

Figure 48 illustrates the sufficient moisture around the DRV01 forecast location. A calculated value of 93.9 percent was classified as a "hit." The distribution of the moist air, with a large pool of moist air to the SW, S, and SE, is supportive of DRV growth.

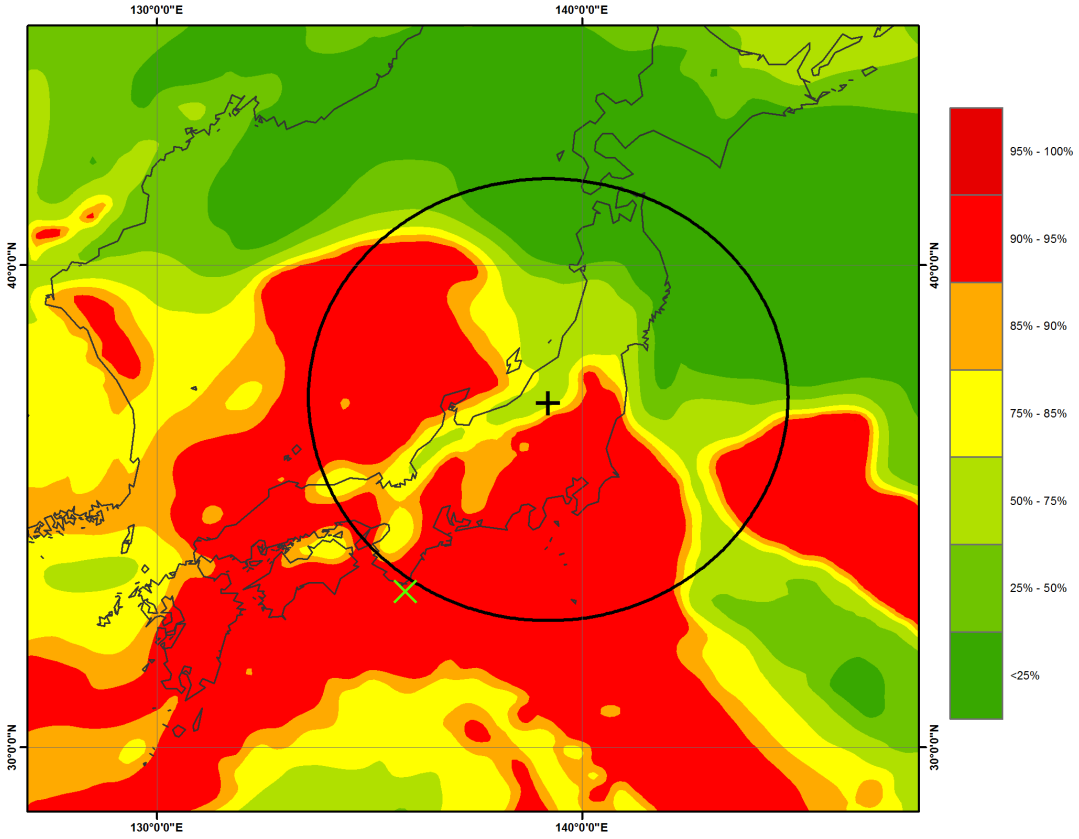

Figure 48. DRV01 48hr forecast (12 UTC 04 March 2010) plot of the 850 hPa relative humidity in the region of observed and forecast DRV locations. Shaded regions indicate relative humidity (magnitude identified by colorbar in percentages), observed DRV location represented by (+), forecast DRV location represented by (X), black circle represents 500 km radius around the observed DRV.

d. DRV01 48hr Forecast a "Miss"

While both a strong downstream region of baroclinicity and sufficient atmospheric moisture were forecast, the forecast for DRV01 failed both the location and intensity checks. As such the DRV01 48hr forecast is classified as a "miss." The generally weak field of relative vorticity indicates that the model struggled to forecast any strong disturbance formation at this lead time. Calculated values for the DRV01 48hr control forecast are presented in Table 5.

It should be noted that the presence of significant topography over the Japanese mainland does pose a significant complication for the identification of a DRV, especially considering the DRV was in its infancy at this time. The 850 and 925 hPa are likely below the actual surface at certain locations over Japan. It is entirely possible that the miss on the distance criteria is the direct result of these complications.

Lon	Lat	Rel. Vort. (s^{-1})	Dist. (km)	ΔT (K)	Rel. Humidity (percent)
135.84	33.302	2.76E-04	529.35	6.3809	93.9

Table 5. Calculated values for the DRV01 48hr control forecast. (Red values do not meet thresholds)

2. DRV01 60hr Forecast

a. Location and Intensity

Both the intensity and location of the DRV01 60hr forecast were determined to be "hits." The forecast intensity was well above the threshold with a value of 5.39 x 10^{-4} s^{-1}, indicating a developing cyclonic circulation. Forecast location was 353 km to the SW of the observed DRV01 position. While a hit, it should be noted that a distance of 353 km is still quite large for a 60 hour forecast.

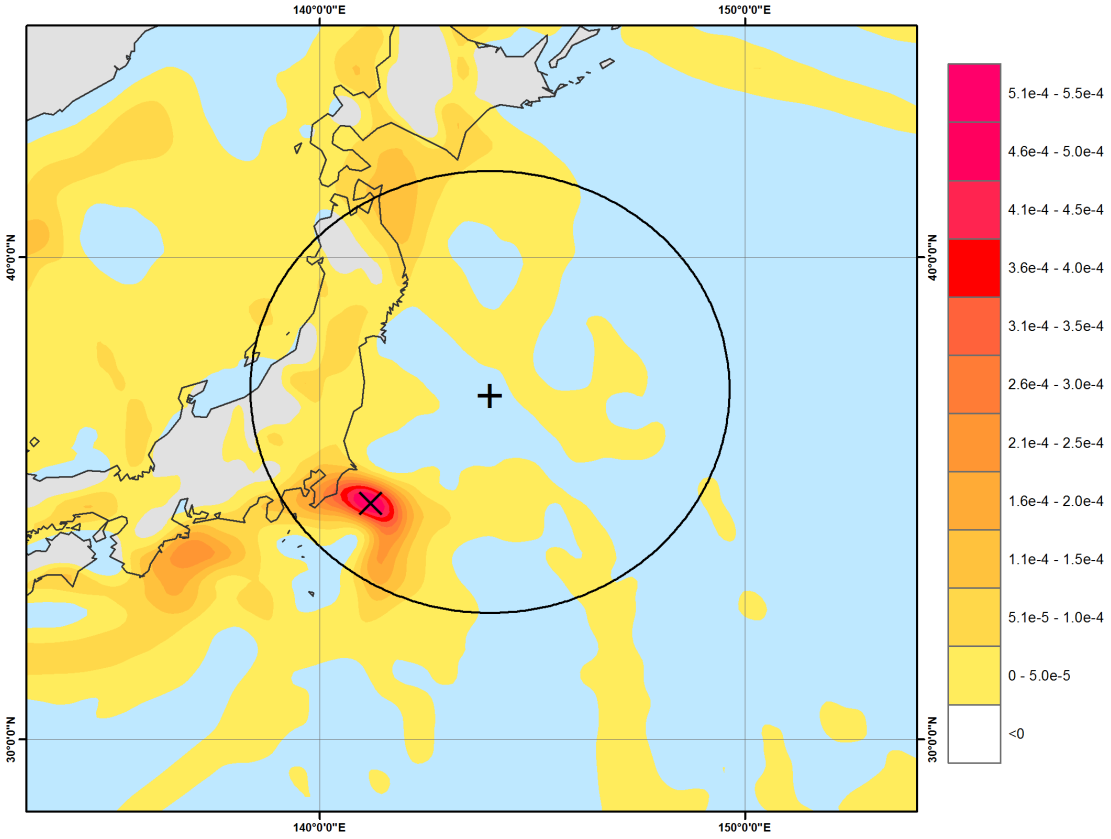

Figure 49. DRV01 60hr forecast (00 UTC 05 March 2010) plot of positive relative vorticity in the region of observed and forecast DRV locations. Shaded regions indicated areas of positive relative vorticity (magnitude identified by colorbar), observed DRV location represented by (+), forecast DRV location represented by (X), black circle represents 500 km radius around the observed DRV.

b. Baroclinicity

The forecast DRV01 baroclinicity is slightly below the threshold value (calculated at 4.86 K), thus constituting a miss. Examining the distribution of the temperature gradient in Figure 50, it is evident that the strongest gradient exists to the SE, but the search algorithm is looking for a strong gradient primarily to the E and NE due to the general propagation pattern of a typical DRV. Forecast temperature gradients to the east of the observed DRV01 were generally weak and trending to the SE, as well, without an easily identifiable strong low-level gradient. This result illustrates that the calculation of the low-level baroclinicity is likely sensitive to the orientation of the baroclinic zone.

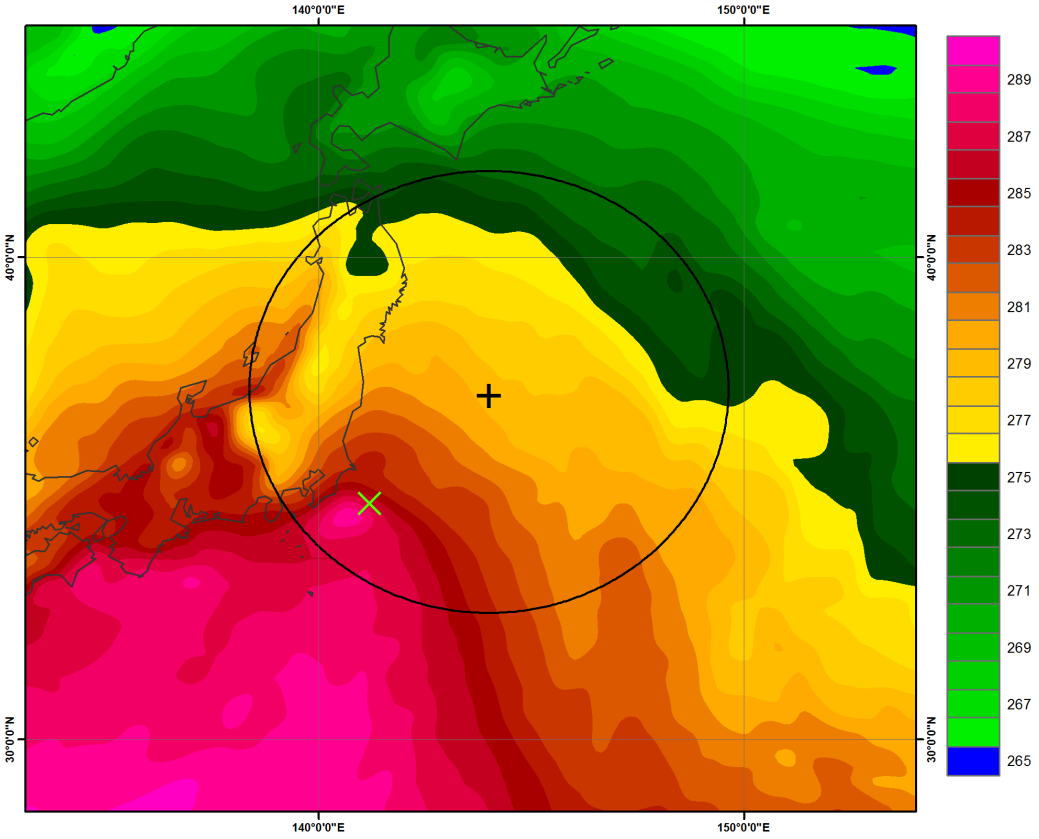

Figure 50. DRV01 60hr forecast (00 UTC 05 March 2010) plot of 925 hPa temperatures in the region of observed and forecast DRV locations. Shaded regions indicated temperature (magnitude identified by colorbar in degrees K), observed DRV location represented by (+), forecast DRV location represented by (X), black circle represents 500 km radius around the observed DRV.

c. Sufficient Moisture

Significant moisture was forecast for the entire region surrounding the observed and forecast DRV01, as seen in Figure 51. Calculated values of forecast DRV01 relative humidity were extremely high at 94.9 percent.

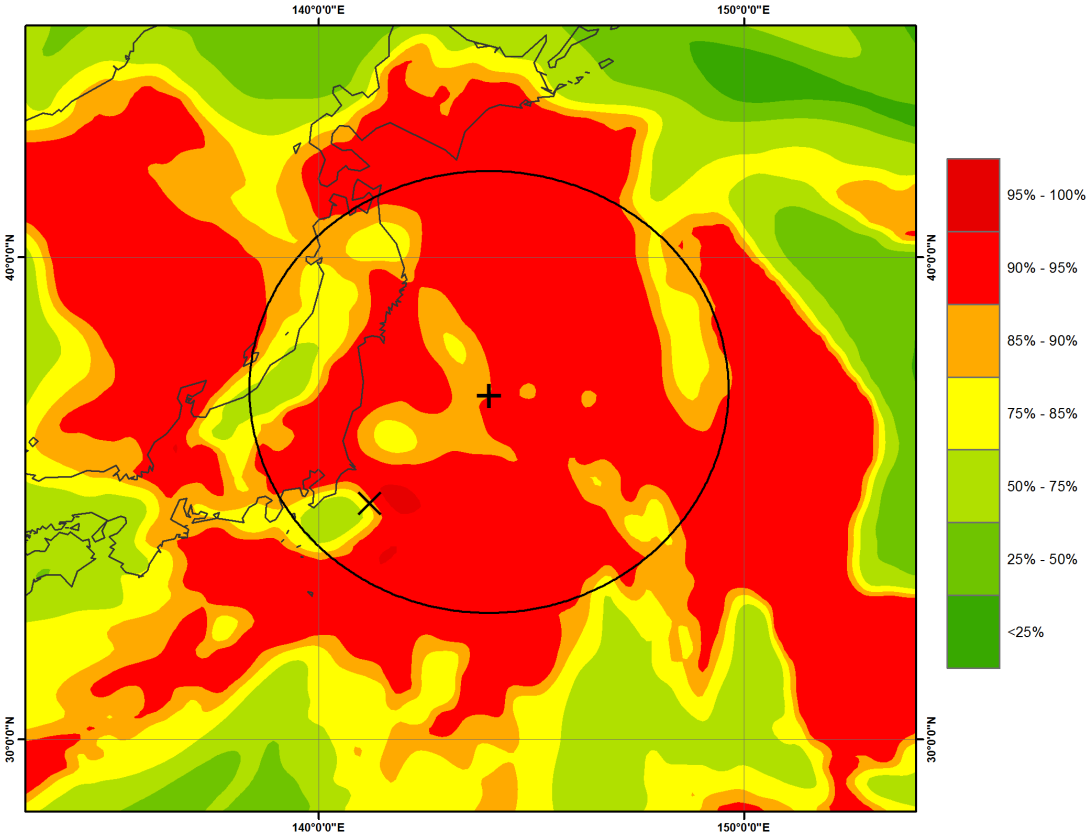

Figure 51. DRV01 60hr forecast (00 UTC 05 March 2010) plot of the 850 hPa relative humidity in the region of observed and forecast DRV locations. Shaded regions indicate relative humidity (magnitude identified by colorbar in percentages), observed DRV location represented by (+), forecast DRV location represented by (X), black circle represents 500 km radius around the observed DRV.

d. DRV01 60hr Forecast a "Miss"

While the DRV01 60hr forecast was evaluated as a "miss," the forecast only missed qualification as a DRV by a temperature gradient shortfall of 0.14 K. The intensity and structure of the forecast DRV01 appeared strikingly like a DRV, but exhibited a moderate location error to the SW of the actual DRV01 location. It is likely the SW tilt of the baroclinic zone is the culprit for the missed forecast. Calculated values of for the DRV01 60hr forecast are presented in Table 6.

Lon	Lat	Rel. Vort. (s^{-1})	Dist. (km)	ΔT (K)	Rel. Humidity (percent)
141.19	34.988	5.39E-04	352.64	4.8607	94.916

Table 6. Calculated values for the DRV01 60hr control forecast. (Red values do not meet thresholds)

3. DRV01 72hr Forecast

a. Location and Intensity

The location of the forecasted DRV01 remains to the SE of the observed position (760 km). The intensity is also significantly below the threshold value (2.27 x 10^{-4} s-^{1}). Significant areas of negative and weak positive vorticity dominate the region around the observed DRV01 (Figure 52). The forecast is therefore determined to be a "miss". Significant areas of negative and weak positive vorticity dominate the region around the observed DRV01 (Figure 52).

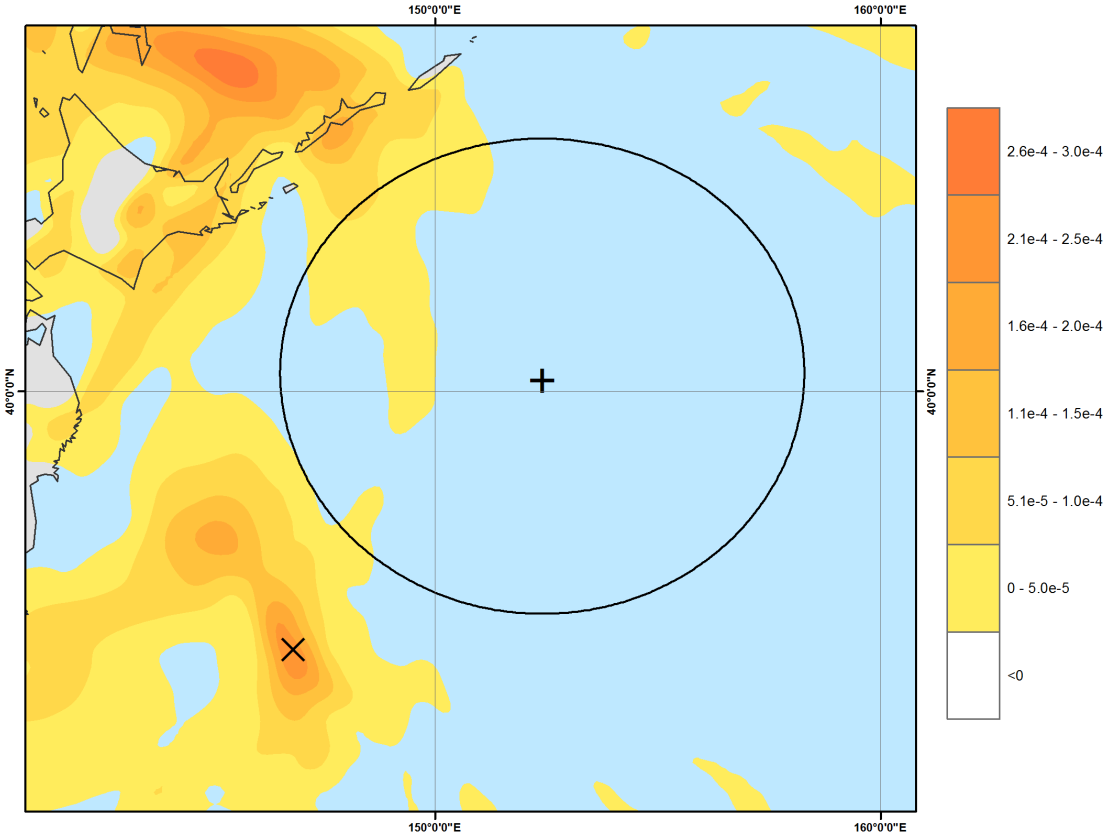

Figure 52. DRV01 72hr forecast (12 UTC 05 March 2010) plot of positive relative vorticity in the region of observed and forecast DRV locations. Shaded regions indicated areas of positive relative vorticity (magnitude identified by colorbar), observed DRV location represented by (+), forecast DRV location represented by (X), black circle represents 500 km radius around the observed DRV.

b. Baroclinicity

Calculated baroclinicity values for DRV01 at forecast time 72hrs are also determined to be a "miss." The calculated value of 3.15° K is well below the 5° K minimum. Analyzing the temperature gradient in Figure 53, the baroclinic front that the forecast DRV01 is located along is oriented N-S, which is nearly perpendicular to the W-E or SW-NE orientations associated with typical DRVs. The temperature gradient ahead of forecast DRV01 is also visibly weaker than the tight clustering of isotherms expected with a propagating DRV. The implication is that the environmental characteristics in the control simulation are not properly representing those observed.

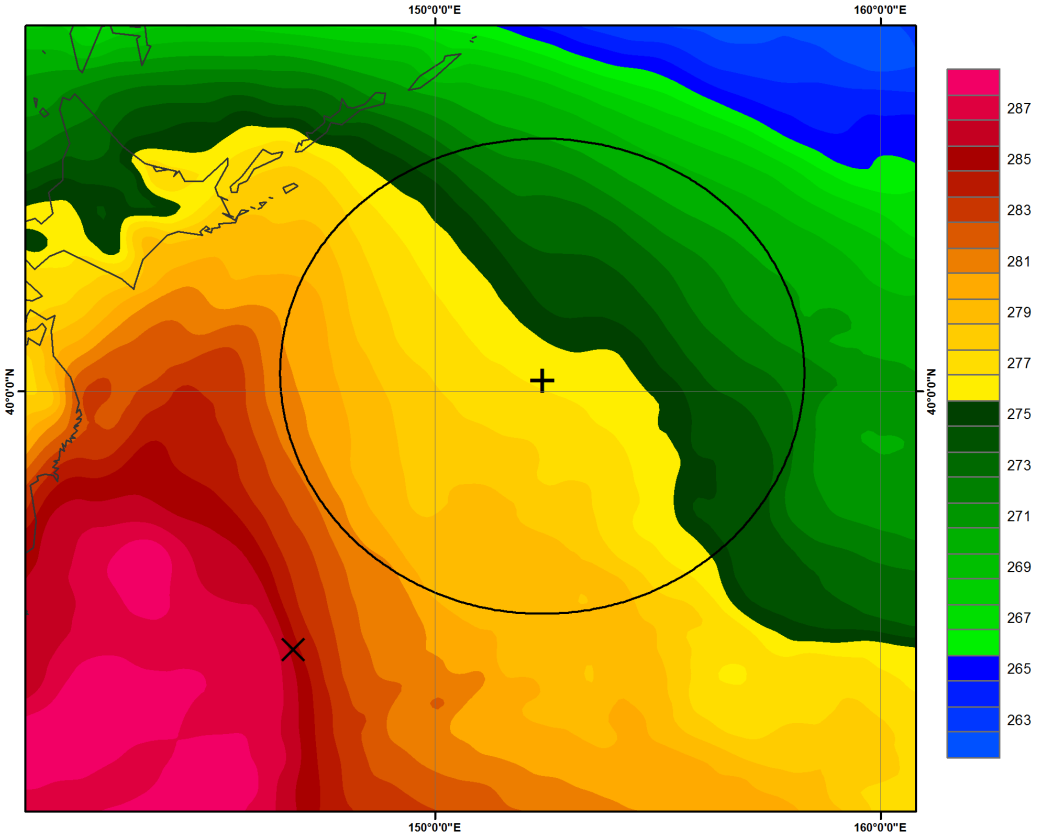

Figure 53. DRV01 72hr forecast (12 UTC 05 March 2010) plot of 925 hPa temperatures in the region of observed and forecast DRV locations. Shaded regions indicated temperature (magnitude identified by colorbar in degrees K), observed DRV location represented by (+), forecast DRV location represented by (X), black circle represents 500 km radius around the observed DRV.

c. Sufficient Moisture

Sufficient moisture calculations for forecast DRV01 are higher than minimum at 93.5 percent relative humidity for the mean of the 90 percentile. A plot of the 850 hPa relative humidity (Figure 54) indicates that a lack of nearly saturated air is not the primary issue in this case.

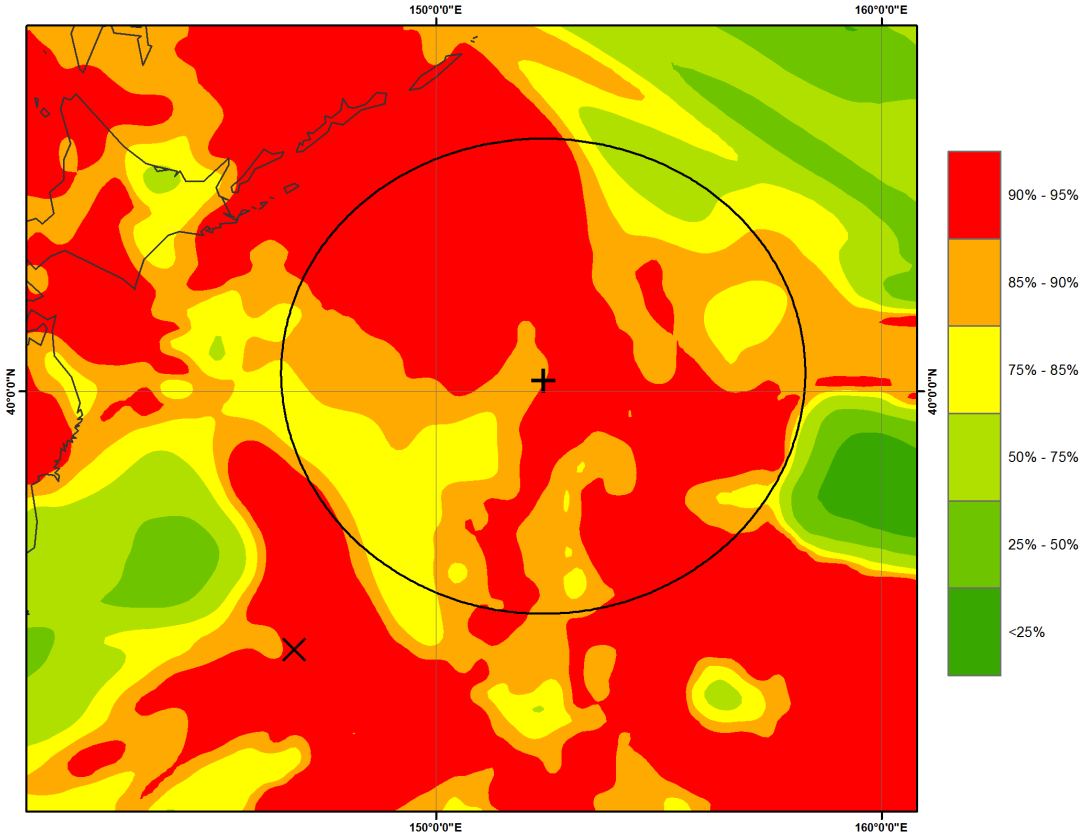

Figure 54. DRV01 72hr forecast (12 UTC 05 March 2010) plot of the 850 hPa relative humidity in the region of observed and forecast DRV locations. Shaded regions indicate relative humidity (magnitude identified by colorbar in percentages), observed DRV location represented by (+), forecast DRV location represented by (X), black circle represents 500 km radius around the observed DRV.

d. DRV01 72hr Forecast a "Miss"

The forecast intensity, location, and baroclinicity were all well outside of calculated cut-off values, which indicate the environmental characteristics predicted in the control forecast are not representative of those observed

Lon	Lat	Rel. Vort. (s^{-1})	Dist. (km)	ΔT (K)	Rel. Humidity (percent)
146.81	34.988	2.27E-04	759.97	3.1541	93.513

Table 7. Calculated values for the DRV01 72hr control forecast. (Red values do not meet thresholds)

4. Forecast DRV01 Summary and Conclusions

The tracks of the observed and predicted DRVs are shown in Figure 55. While there is some indication of the genesis of a DRV in the control forecast (as seen by the intensification of an isolated low-level relative vorticity maximum between the 48 and 60 hour forecasts). However, the identified disturbance appears unable to sustain itself. The magnitude of the maximum relative vorticity decreases significantly from the 60 to 72 hour forecast. The most likely conclusion from the data presented here is that the control forecast did a poor job of representing the environmental characteristics that are necessary for DRV growth. Sufficient moisture does appear to be present. The hypothesis would then be that the issue lies with the intensity and structure of the baroclinic zone.

It is also of note that there appears to be an issue with the identification and prediction of DRV genesis over land where there is significant orography. The south east propagation of the observed DRV during the first six hours is somewhat inconsistent with the conceptual picture of DRV evolution. The data presented in Figures 49 - 54 are more consistent with the DRV framework. The implication is that the initial identification of the observed DRV was the likely spurious and the direct result of topographic influences.

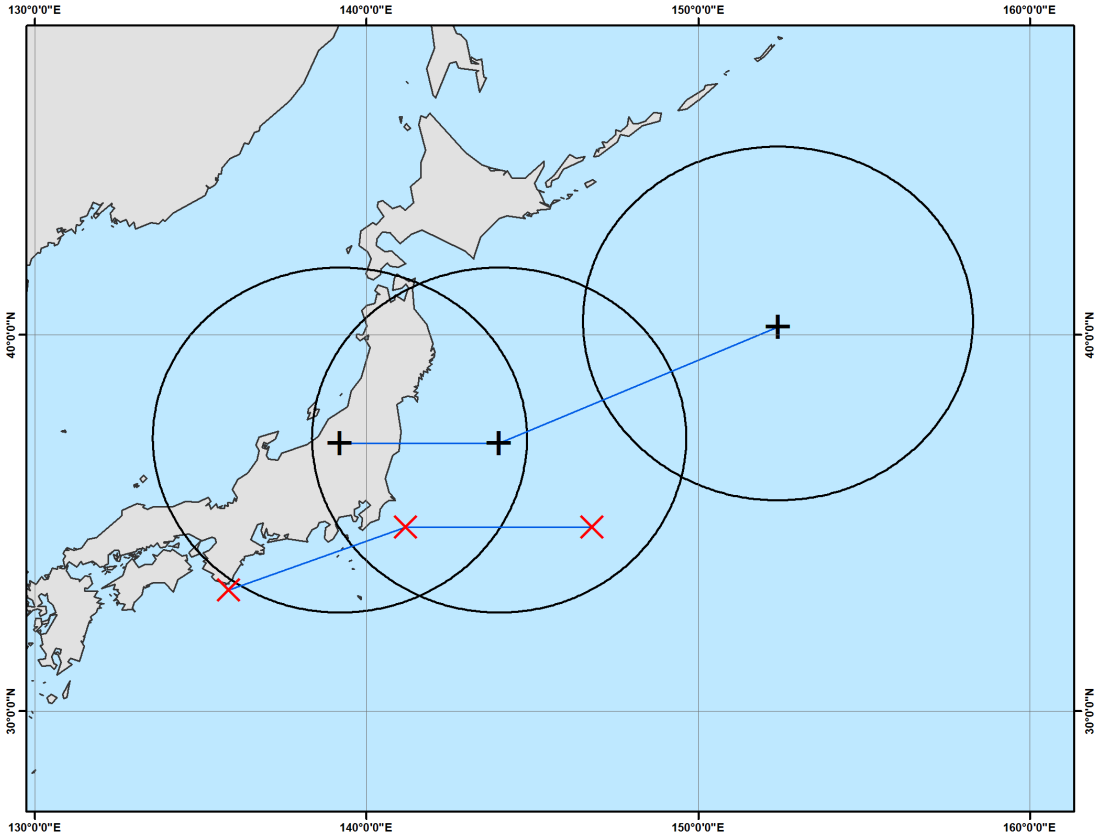

Figure 55. Test case 1 observed DRV (+) and forecast DRV (X) tracks in 12 hr time-steps over the initial 24 hours after formations. Black rings are 500 km radii around observed DRV locations. Black X symbols represent forecast "hits," while red X symbols represent forecast "misses" (Valid times: 12 UTC 4 March 2010, 00 UTC 5 March 2010, 12 UTC 5 March 2010).

C. TEST CASE 2

The test case 2 DRV, hereafter referred to as DRV02, was first observed over SW Japan, as seen in figure 56, at 1200 UTC 24 March 2010. Like DRV01, it was first identified over a land-mass and not over a warm, moist oceanic atmosphere (the more typical location for DRV genesis). After formation, DRV02 was observed just off the SE coast of Japan in a NE direction for 24 hrs before entering the intensification phase. While undergoing explosive deepening, DRV02 slowly changed its propagation path to the east before it entered the decay phase just south of the Aleutian Islands after passing over the International Date Line. A deepening rate of 1.5 Bergerons and a SLP minimum of 965.2 hPa were recorded.

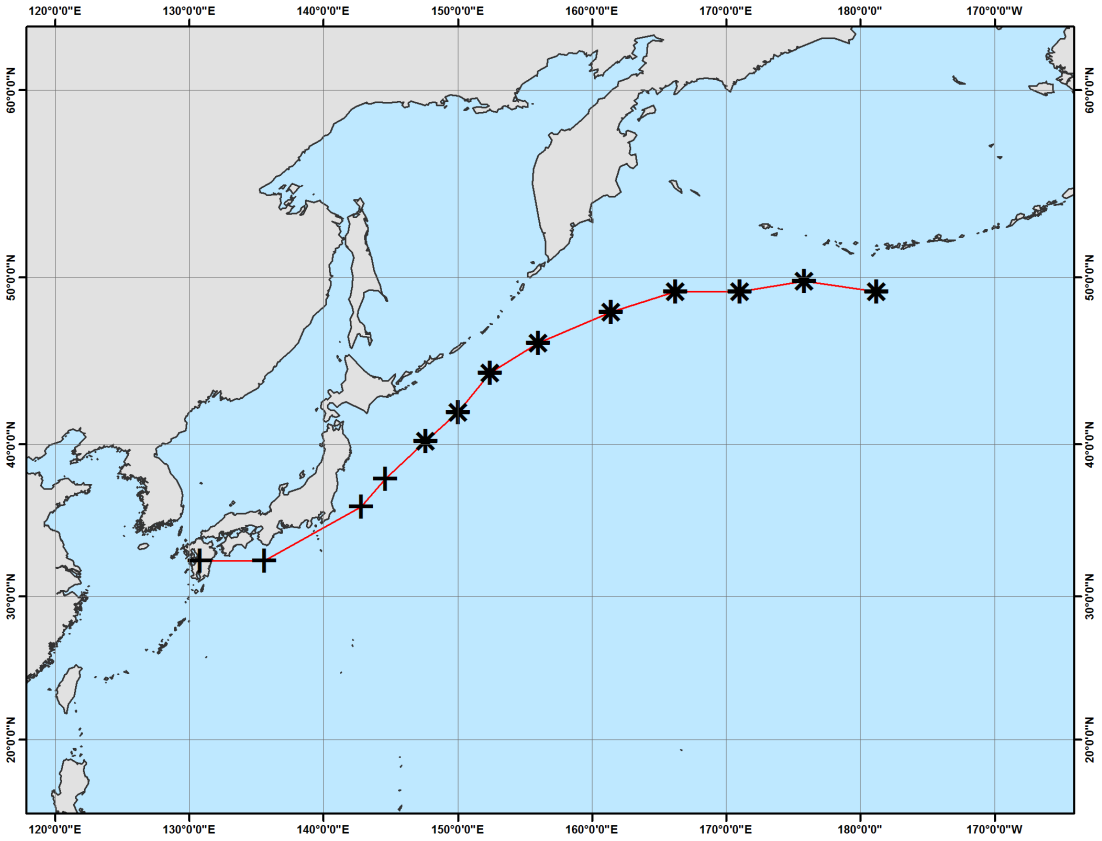

Figure 56. DRV02 observed propagation and intensification track (red line). Locations of propagation (+) and intensification (*) are marked every 6 hours (Valid time 12 UTC 24 March 2010 – 06 UTC 27 March 2010). Observed DRV information from BW13 climatology.

1. DRV02 48hr Forecast

a. Location and Intensity

At the time of formation, the DRV02 forecast identified a candidate DRV approximately 685 km to the east of the observed genesis position (Figure 57). It is possible, even likely, that the distance error is once again the result of topography. However, in addition to the location error, the relative vorticity maximum in the control forecast is significantly below the threshold value (2.34×10^{-4} s^{-1}).

The relative vorticity maximum is found within an elongated band of enhanced relative vorticity. This structure was noted by M12 for the tropical cyclone Chaba case

and, subsequently, has been observed in numerous DRV genesis cases (personal communication, Richard Moore). This result does raise a question as to the appropriateness of identifying solely the relative vorticity maximum (which will provide a single grid point). If the maximum falls with a band of enhanced vorticity of similar magnitude, the identified feature can be significantly displaced from the observed position. This issue would only be at work at or shortly after DRV genesis.

Two points can be gleaned by this analysis. Firstly, the prediction of a DRV-like feature at 48-hours appears quite reasonable in this case. Secondly, the choice of a moderate value of relative vorticity as a threshold may not be applicable for the DRV genesis.

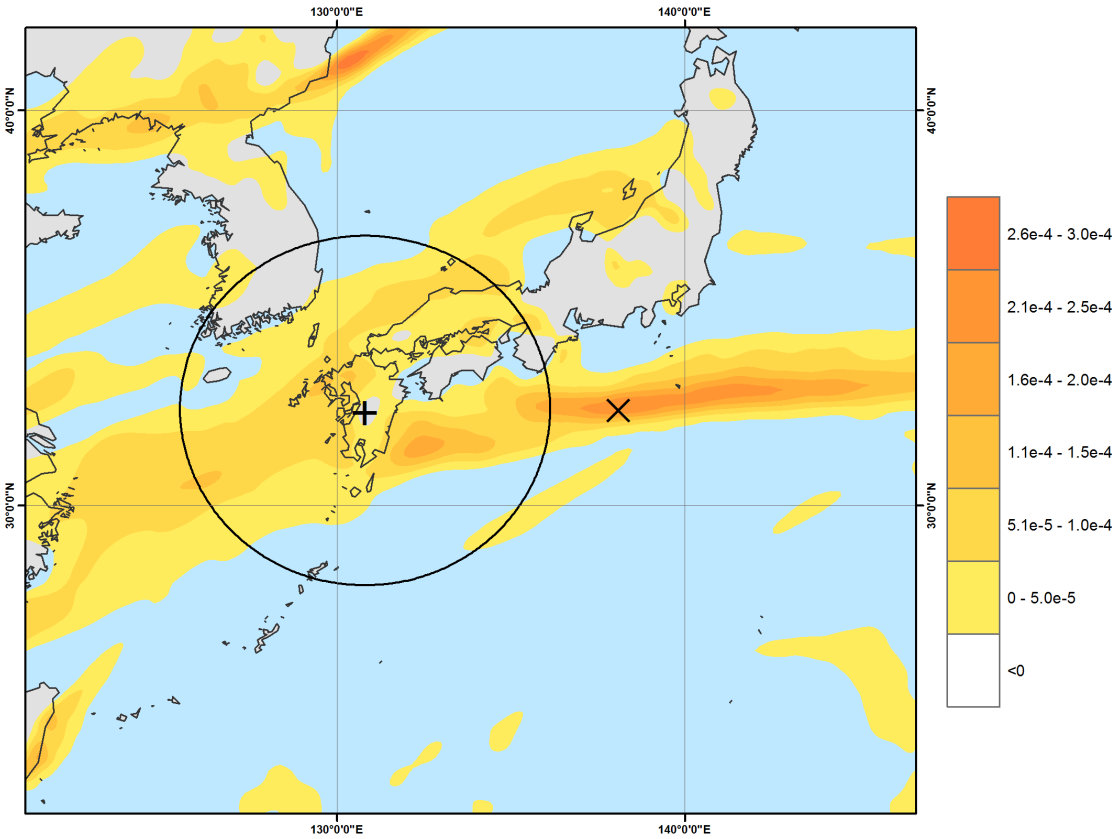

Figure 57. DRV02 48hr plot of positive relative vorticity in the region of observed and forecast DRV locations 12 UTC 24 March 2010. Shaded regions indicated areas of positive relative vorticity (magnitude identified by colorbar), observed DRV location represented by (+), forecast DRV location represented by (X), black circle represents 500 km radius around the observed DRV.

b. Baroclinicity

The calculated value of low-level baroclinicity is well above the threshold in the locations of both the observed and predicted positions (Figure 58). The value from the control forecast is 6.43 K. It should be noted that the orientation of the baroclinic zone in this case is more typical of that expected, in contrast to the previous example.

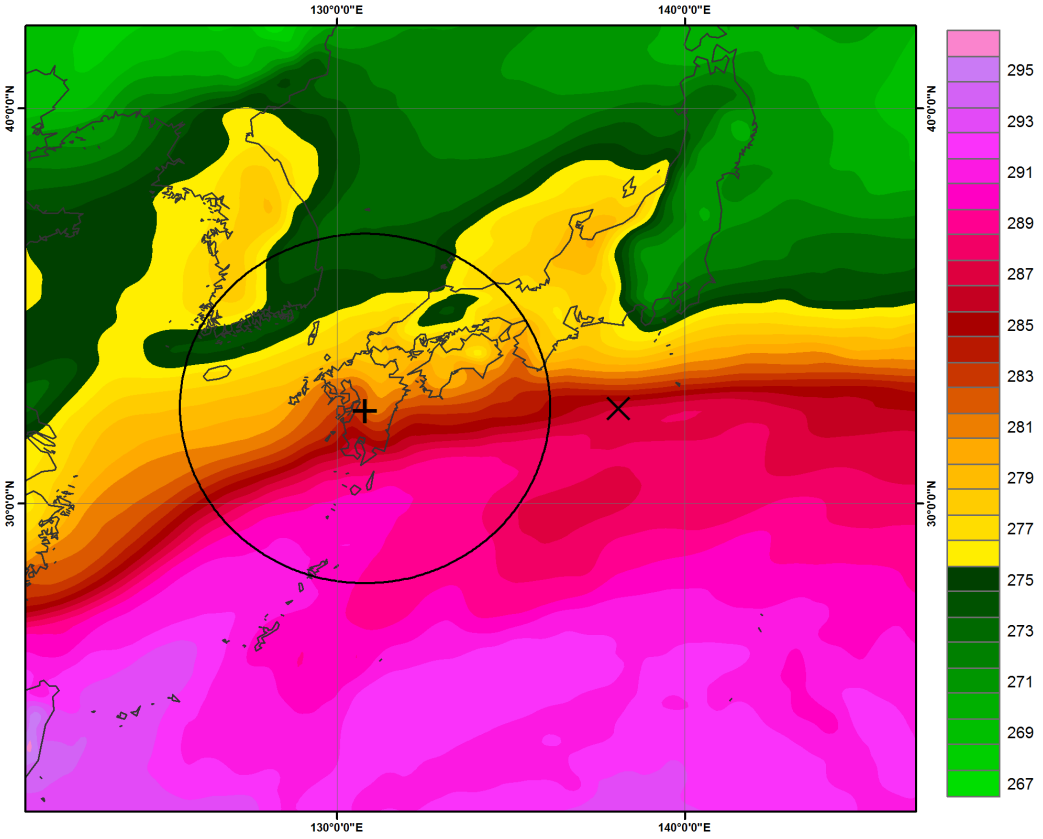

Figure 58. DRV02 48hr plot of 925 hPa temperatures in the region of observed and forecast DRV locations 12 UTC 24 March 2010. Shaded regions indicated temperature (magnitude identified by colorbar in degrees K), observed DRV location represented by (+), forecast DRV location represented by (X), black circle represents 500 km radius around the observed DRV.

c. Sufficient Moisture

Forty eight hour forecasted values of relative humidity were found to be sufficient to meet the moisture criteria (93.7 percent). The predicted structure is consistent with both the relative vorticity and baroclinicity fields presented above: a relatively narrow band of enhanced values are co-located with both parameters.

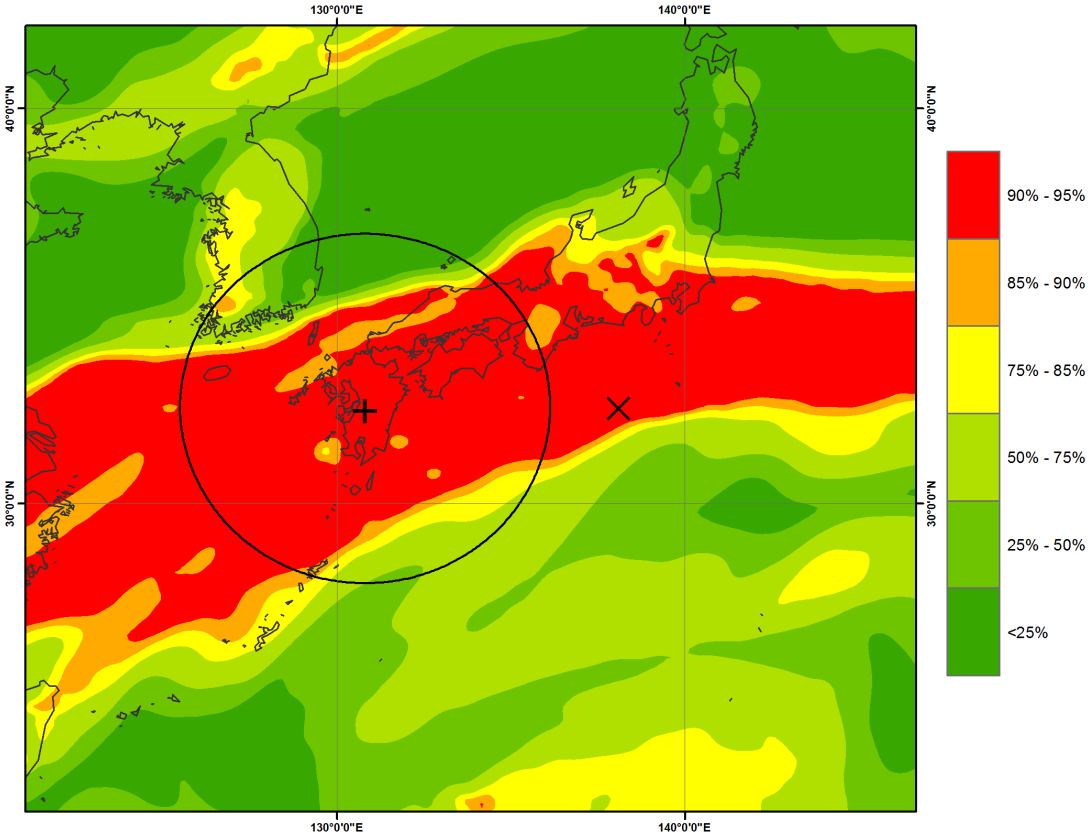

Figure 59. DRV02 48hr plot of the 850 hPa relative humidity in the region of observed and forecast DRV locations 12 UTC 24 March 2010. Shaded regions indicate relative humidity (magnitude identified by colorbar in percentages), observed DRV location represented by (+), forecast DRV location represented by (X), black circle represents 500 km radius around the observed DRV.

d. DRV02 48hr Forecast a "Miss"

The 48hr forecast for DRV02 is considered a "miss" because of the low values of relative vorticity and misplacement of the disturbance to the east of the observed genesis location. The control forecast does appear to show a structure that is conducive to DRV formation. However, at this early time, is unable to identify a coherent vortex.

The indication is that there is ascent along the entire band at this time and the formation of an isolated vortex (i.e. DRV genesis) is difficult to identify. It can be hypothesized that the reduced resolution TIGGE data is at a disadvantage when compared to the higher resolution operational analysis (both in the vertical and horizontal) in terms of identifying a nascent vortex.

Lon	Lat	Rel. Vort. (s^{-1})	Dist. (km)	ΔT (K)	Rel. Humidity (percent)
138.09	32.459	2.34E-04	685.87	6.4293	93.722

Table 8. Calculated values for the DRV02 48hr forecast.

2. DRV02 60hr Forecast

a. Location and Intensity

The DRV02 60hr forecast appears to do an excellent job of predicting both the intensity and disturbance placement (Figure 60). Forecast relative vorticity values are well above the threshold (4.78×10^{-4} s^{-1}) and distance to the observed DRV02 is 53 km. At this time, the band of enhanced vorticity seen at 48 hours has transformed into a more coherent feature that is intensifying.

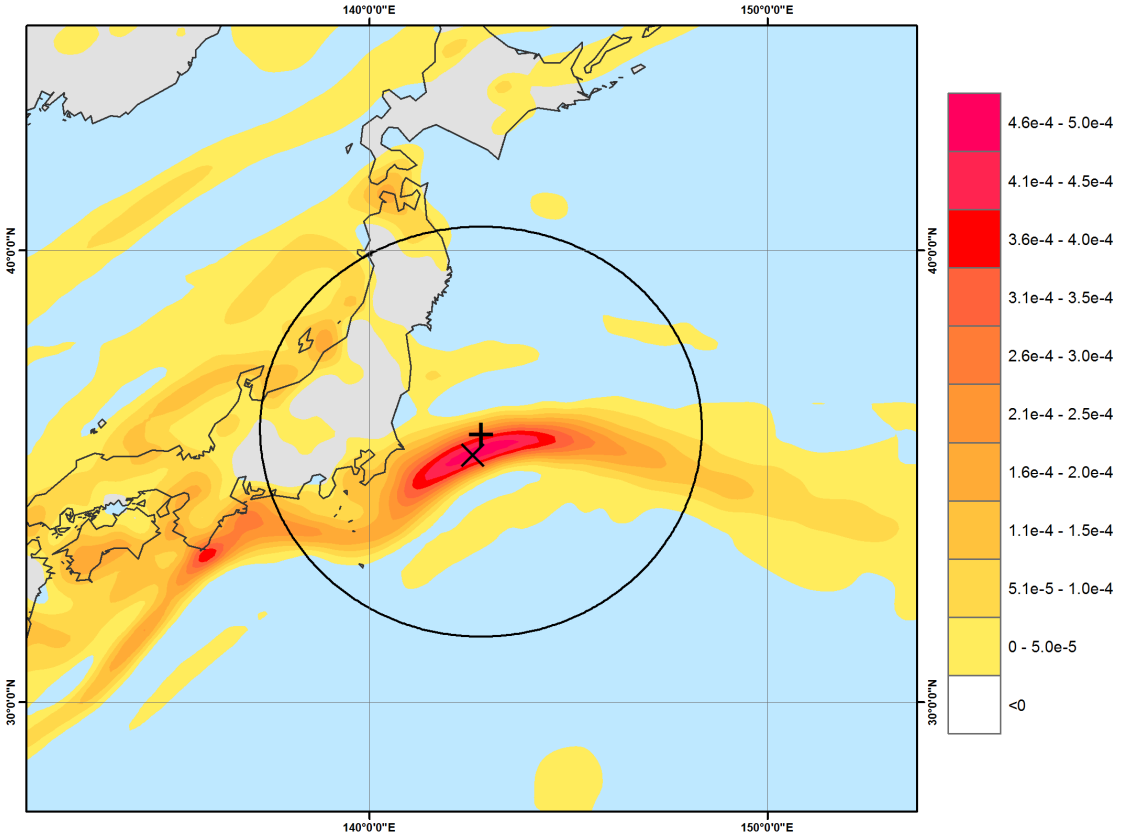

Figure 60. DRV02 60hr plot of positive relative vorticity in the region of observed and forecast DRV locations 00 UTC 25 March 2010. Shaded regions indicated areas of positive relative vorticity (magnitude identified by colorbar), observed DRV location represented by (+), forecast DRV location represented by (X), black circle represents 500 km radius around the observed DRV.

b. Baroclinicity

The forecast baroclinicity front for DRV02 at 60hrs is excellent, as well. Frontogenesis is observed as the baroclinicity has increased during the previous 12 hours.

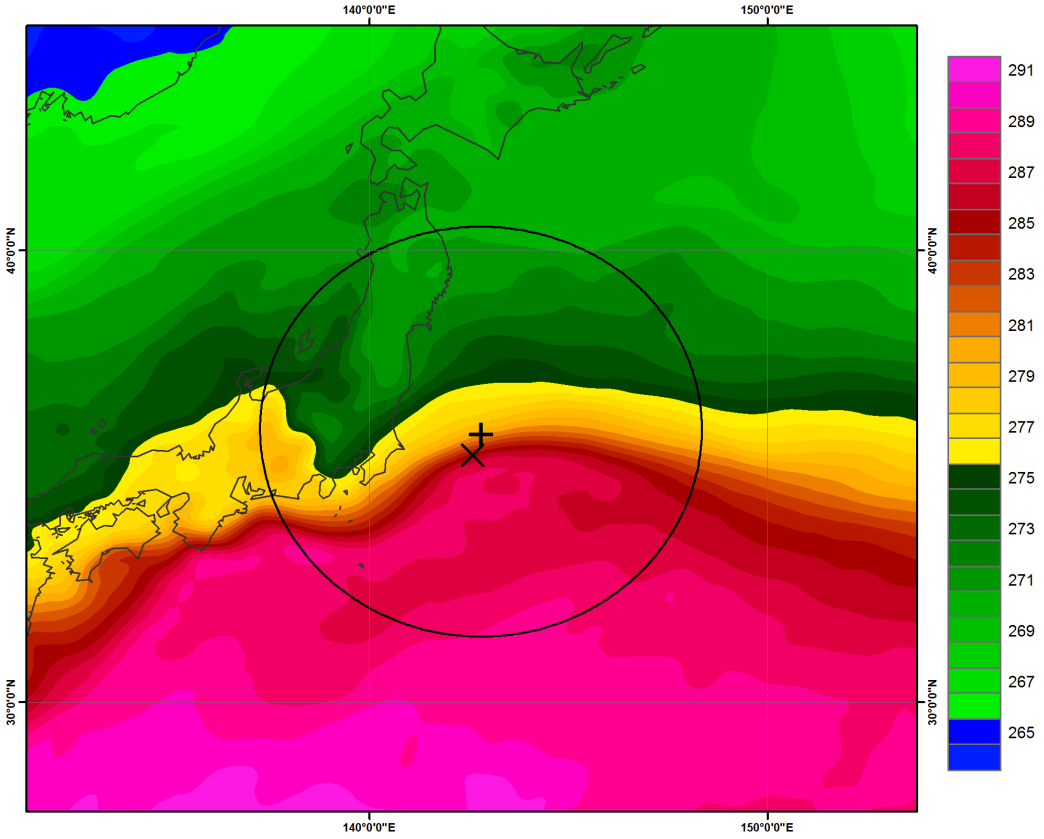

Figure 61. DRV02 60hr plot of 925 hPa temperatures in the region of observed and forecast DRV locations 00 UTC 25 March 2010. Shaded regions indicated temperature (magnitude identified by colorbar in degrees K), observed DRV location represented by (+), forecast DRV location represented by (X), black circle represents 500 km radius around the observed DRV.

c. Sufficient Moisture

DRV02 60hr forecast moisture is a "hit" with a calculated value of 94 percent for the region.

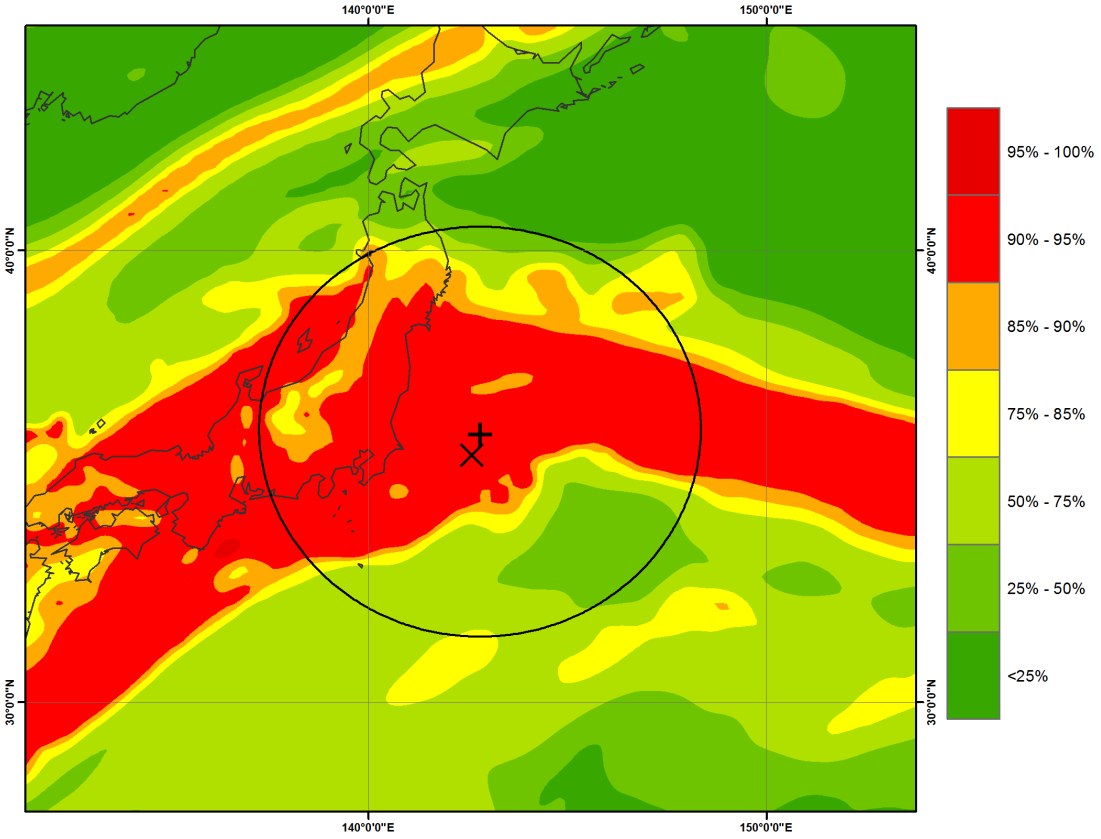

Figure 62. DRV02 60hr plot of the 850 hPa relative humidity in the region of observed and forecast DRV locations 00 UTC 25 March 2010. Shaded regions indicate relative humidity (magnitude identified by colorbar in percentages), observed DRV location represented by (+), forecast DRV location represented by (X), black circle represents 500 km radius around the observed DRV.

d. DRV02 60hr Forecast a "Hit"

The DRV02 60hr forecast agrees very well with the observed. All calculated parameters significantly exceed the necessary thresholds. This result thusly calls into question the identification, both observed and predicted, 12 hours earlier. Again, possible issues involve the topography and the predicted identification of a maximum value of relative vorticity when it falls within a band of enhanced values of similar magnitude.

Lon	Lat	Rel. Vort. (s^{-1})	Dist. (km)	ΔT (K)	Rel. Humidity (percent)
142.59	35.55	4.78E-04	53.263	8.41	93.994

Table 9. Calculated values for the DRV02 60hr forecast.

3. DRV02 72hr Forecast

a. Location and Intensity

The control forecast DRV02 at 72hrs identifies a growing disturbance, as measured by the magnitude of a low-level relative vorticity maximum (a 12 hour increase from 4.78 to 5.9 x 10^{-4} s^{-1}). However, it is of note that the discrepancy in the location of the DRV (error of 273 km) indicates a difference in the propagation speed of the observed and predicted DRVs. Idealized studies of DRV dynamics have shown that the propagation speed of a DRV is a function of the depth of the system, the strength of the baroclinic zone, and the amplitude of the DRV (MM04, MM05). More analysis would be necessary to identify the specific cause in this case.

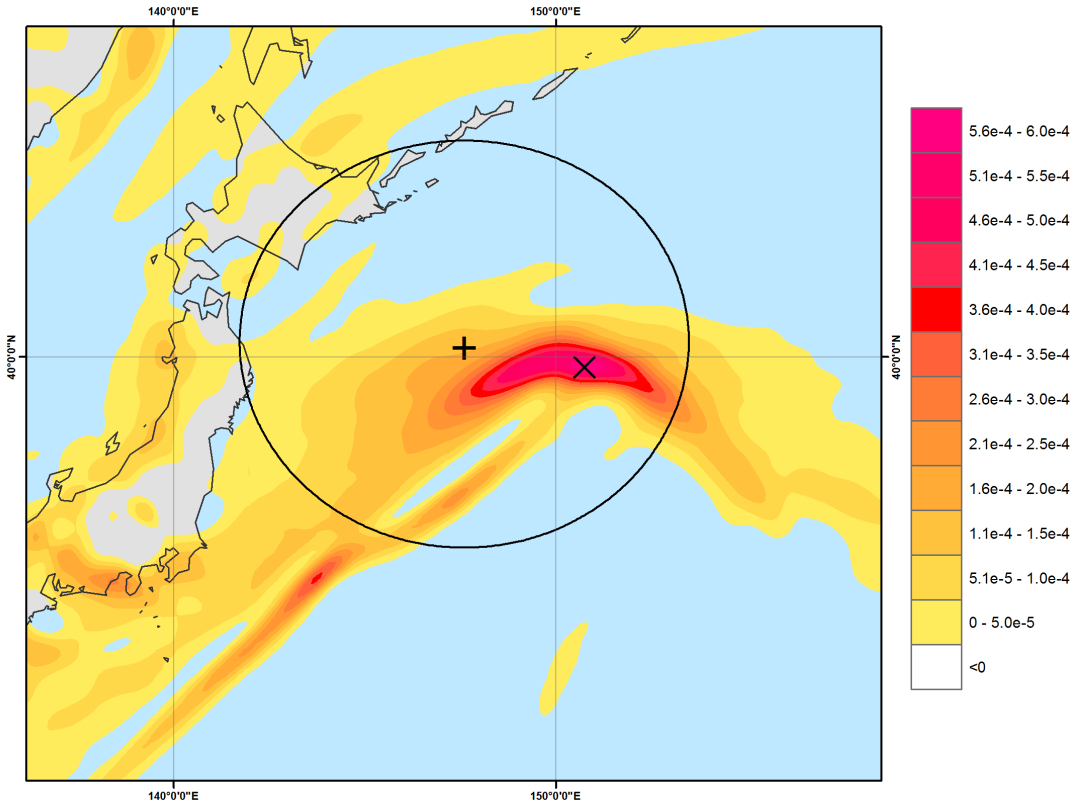

Figure 63. DRV02 72hr plot of positive relative vorticity in the region of observed and forecast DRV locations 12 UTC 25 March 2010. Shaded regions indicated areas of positive relative vorticity (magnitude identified by colorbar), observed DRV location represented by (+), forecast DRV location represented by (X), black circle represents 500 km radius around the observed DRV.

b. Baroclinicity

The frontogenesis has continued over the previous 12 hours (the calculated baroclinicity has increased from 8.41 K to 15.18 K). The latter value far exceeds the prescribed threshold.

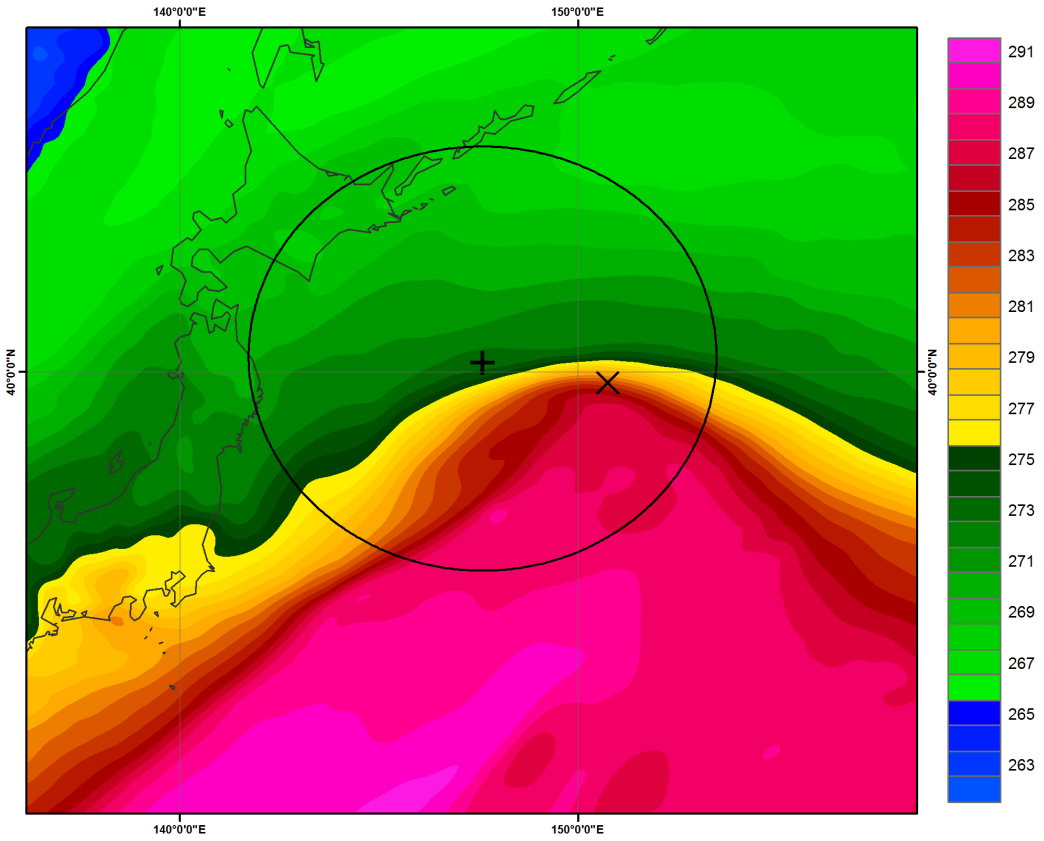

Figure 64. DRV02 72hr plot of 925 hPa temperatures in the region of observed and forecast DRV locations 12 UTC 25 March 2010. Shaded regions indicated temperature (magnitude identified by colorbar in degrees K), observed DRV location represented by (+), forecast DRV location represented by (X), black circle represents 500 km radius around the observed DRV.

c. Sufficient Moisture

Forecast moisture levels for the DRV02 72hr forecast are a "hit" with a calculated value of 94.6 percent. Visual inspection shows a large area of humid air to the S, SE, and

W of the forecast disturbance (Figure 65). The layout of the moist air is very good for fuelling DRV growth and maintenance.

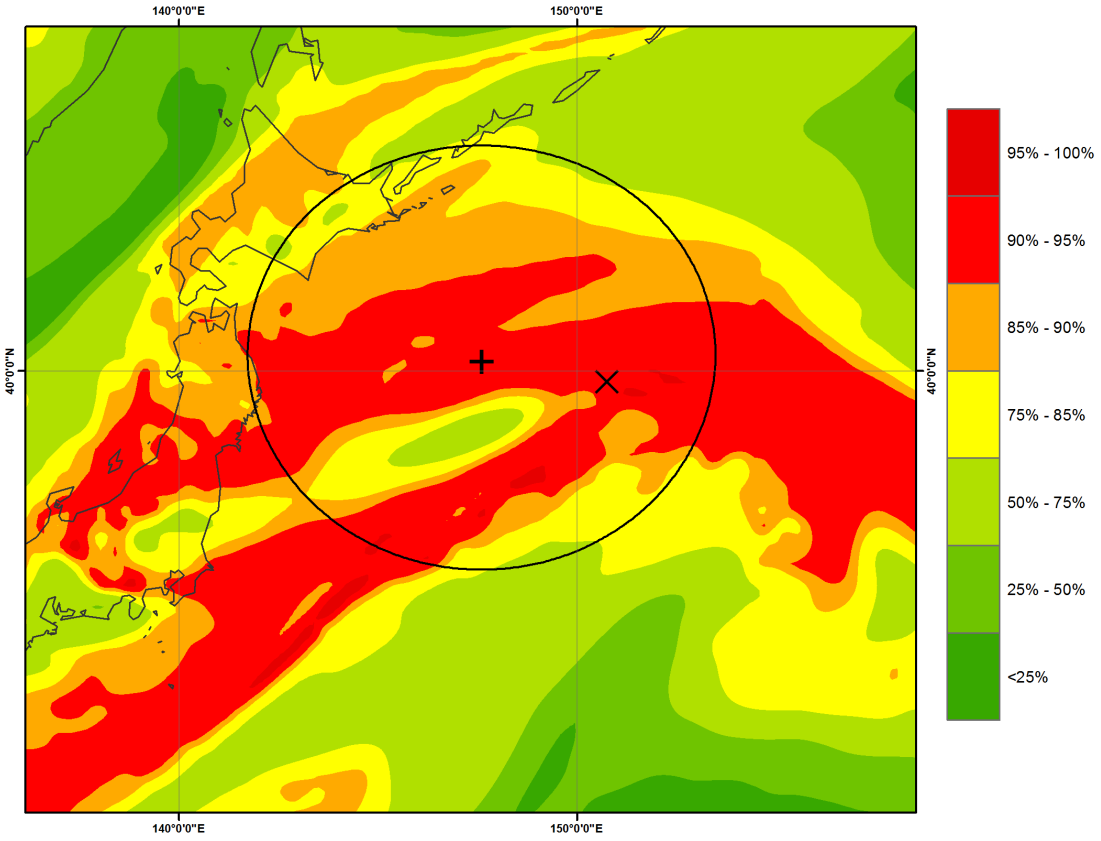

Figure 65. DRV02 72hr plot of the 850 hPa relative humidity in the region of observed and forecast DRV locations 12 UTC 25 March 2010. Shaded regions indicate relative humidity (magnitude identified by colorbar in percentages), observed DRV location represented by (+), forecast DRV location represented by (X), black circle represents 500 km radius around the observed DRV.

d. DRV02 72hr Forecast a "Hit"

The control forecast at 72 hours represents a hit. The increasing strength of the DRV, along with the increasing temperature gradient and relative humidity are all indications of a growing and propagating DRV. However, the 273 km discrepancy in

DRV location is significant (while still under the threshold of 500 km). The indication is that the propagation speed of the observed and predicted DRV are different in this case.

Lon	Lat	Rel. Vort. (s^{-1})	Dist. (km)	ΔT (K)	Rel. Humidity (percent)
150.75	39.766	5.90E-04	273.33	15.181	94.602

Table 10. Calculated values for the DRV02 72hr forecast.

4. Forecast DRV02 Summary and Conclusions

The initial forecast for test case 2 does a poor job identifying the location of the genesis of DRV02. In addition, the strength of the predicted disturbance is well below the threshold value.

These results highlight a number of issues regarding the forecast identification at or near the time of DRV genesis. The location issue may be the result of topographic influences (as mentioned with the previous case). In addition, it is possible that the identification algorithm may have problems when a DRV forms within a band of enhanced relative vorticity. As such, the choice of solely identifying the maximum value may not be appropriate at genesis time. It is also possible that the reduced resolution of the TIGGE data is important and that the relative vorticity threshold is too low for DRV genesis in certain cases.

The fact that the observed and predicted DRVs 12 hours after genesis agree very well indicates that a focus on the DRV genesis time (as seen in M12) may not be appropriate. It appears likely that the identification scheme used herein is tuned for later times after the emergence of a coherent, growing disturbance. .

Finally, when combining the results from the 60 and 72 hour forecast results, it is apparent the observed and predicted DRVs exhibit different propagation speeds. It has been shown that DRV propagation speed is a function of the depth of the system, the strength of the baroclinic zone, and the amplitude of the DRV (MM04, MM05). Further work would be necessary to identify the particular issue in this case. However, it is important to note that this issue will likely be exacerbated going forward in the DRV

evolution and may even be important in the subsequent explosive cyclogenesis. As such, this would be a very interesting case to examine in greater detail.

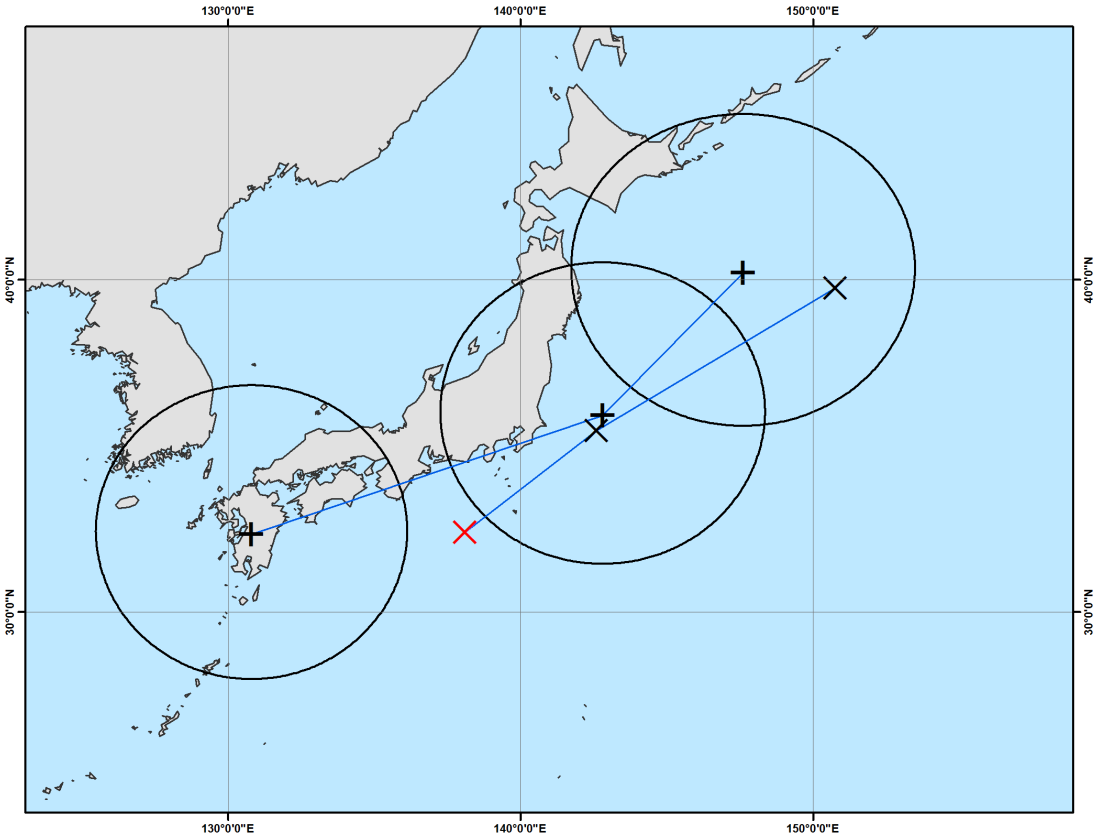

Figure 66. Test case 2 observed DRV (+) and forecast DRV (X) tracks in 12 hr time-steps over the initial 24 hours after formations. Black rings are 500 km radii around observed DRV locations. Black X symbols represent forecast "hits," while red X symbols represent forecast "misses" (Valid times: 12 UTC 24 March 2010, 00 UTC 25 March 2010, 12 UTC 25 March 2010).

D. TEST CASE 7

The test case 7 DRV, hereafter referred to as DRV07, was first observed over the western North Pacific (Figure 67) at 1200 UTC 5 October 2010. In contrast to the two cases presented above, DRV07 formed over the open ocean. A unique aspect of this case is the initial propagation of the disturbance in a southerly direction which, again,

highlights the importance of the orientation of the baroclinic zone. After genesis, DRV07 propagates ESE for 48 hours before entering the explosive intensification phase. After explosive intensification begins, DRV07 turns and follows a NE path towards the continental coast. Decay sets in after 42 hours of explosive deepening, at which point the disturbance is located roughly 200 km west of Graham Island, Canada. A deepening rate of 1.05 Bergerons and a SLP minimum of 972.3 hPa were recorded.

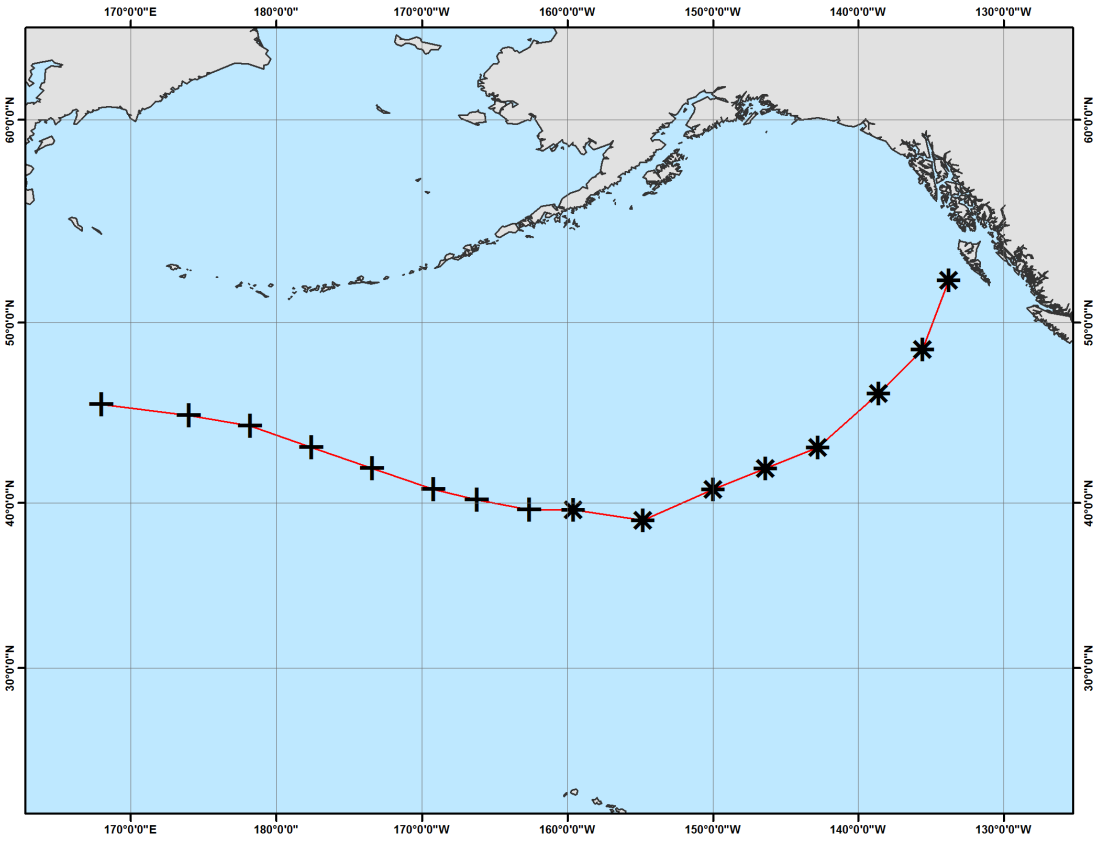

Figure 67. DRV07 observed propagation and intensification track (red line). Locations of propagation (+) and intensification (*) are marked every 6 hours (valid time: 12 UTC 5 October 2010 – 06 UTC 9 October 2010). Observed DRV information from BW13 climatology.

1. DRV07 48hr Forecast

a. Location and Intensity

The predicted location of the DRV agrees well with the observed (84 km discrepancy). The intensity also meets the relative vorticity criteria (3.81 x 10^{-4} s^{-1}). The orientation of the vorticity structure is somewhat unique (with a southwest to northeast access). As will be seen next, this is consistent with the orientation of the baroclinic zone.

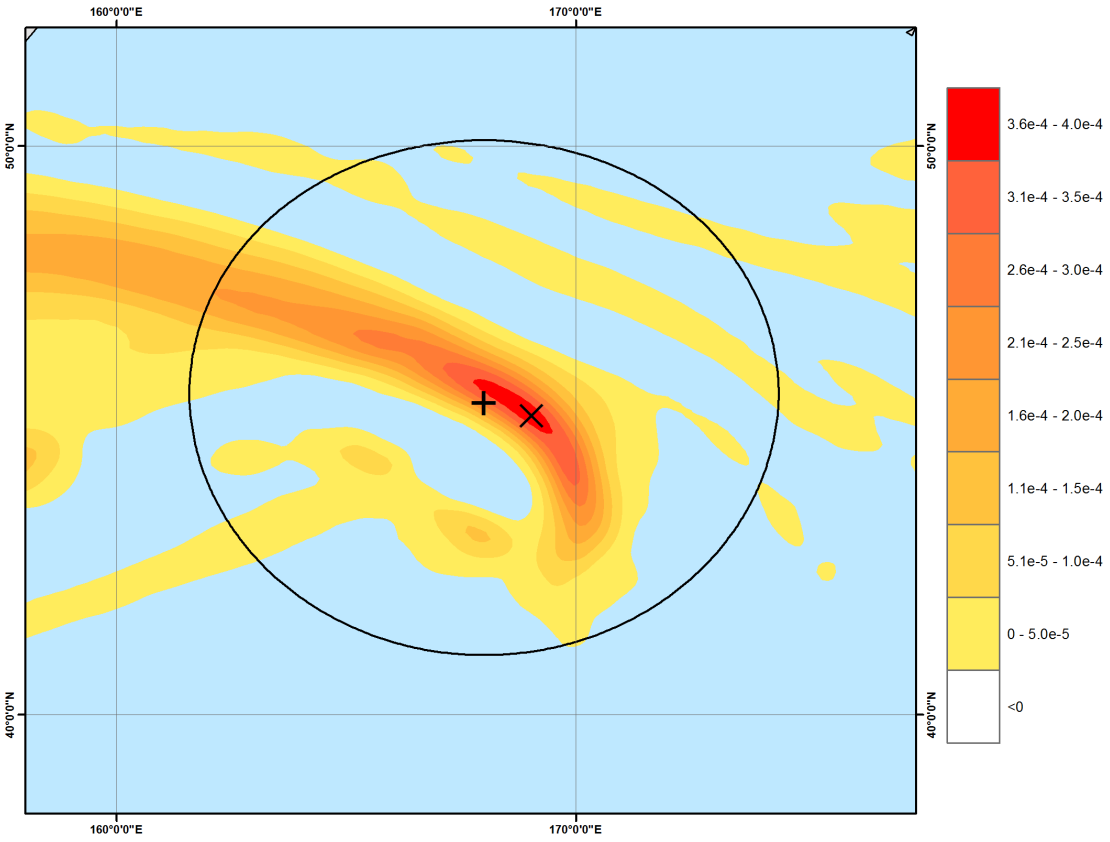

Figure 68. DRV07 48hr plot of positive relative vorticity in the region of observed and forecast DRV locations 12 UTC 5 October 2010. Shaded regions indicated areas of positive relative vorticity (magnitude identified by colorbar), observed DRV location represented by (+), forecast DRV location represented by (X), black circle represents 500 km radius around the observed DRV.

b. Baroclinicity

The magnitude of the calculated low-level baroclinicity far exceeds the threshold (7.8 K). When viewed in the context of expected baroclinic zone orientation, the result is interesting. As mentioned previously, the orientation in this case is not consistent with the conceptual picture of a DRV. Yet, the threshold value is easily surpassed. This is in contrast to test case one, where the orientation of the baroclinic zone actually resulted in a calculation of insufficient baroclinicity. In this case there is significant baroclinicity to the east and north of the predicted DRV location. That was not the case for test case one. It remains an open question as to whether this was a fundamental issue for the lack of growth in test case one.

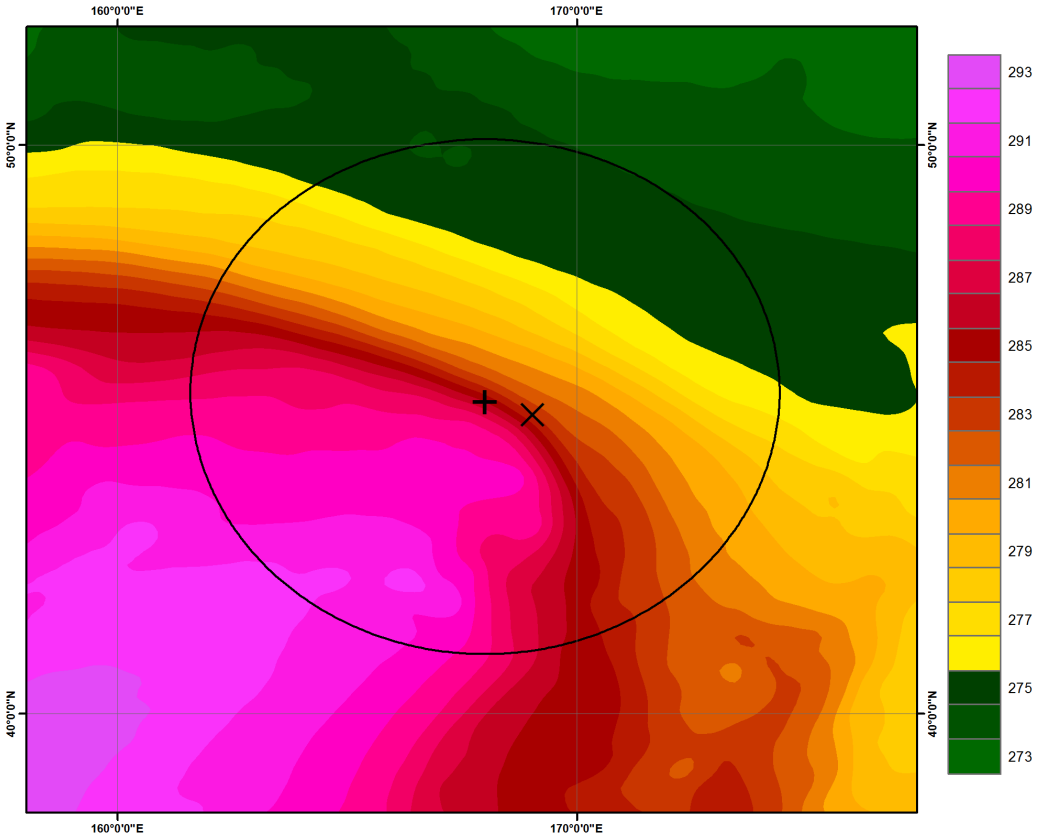

Figure 69. DRV07 48hr plot of 925 hPa temperatures in the region of observed and forecast DRV locations 12 UTC 5 October 2010. Shaded regions indicated temperature (magnitude identified by colorbar in degrees K), observed DRV location represented by (+), forecast DRV location represented by (X), black circle represents 500 km radius around the observed DRV.

c. Sufficient Moisture

The moisture criteria is easily met at this forecast lead time (94.14 percent).

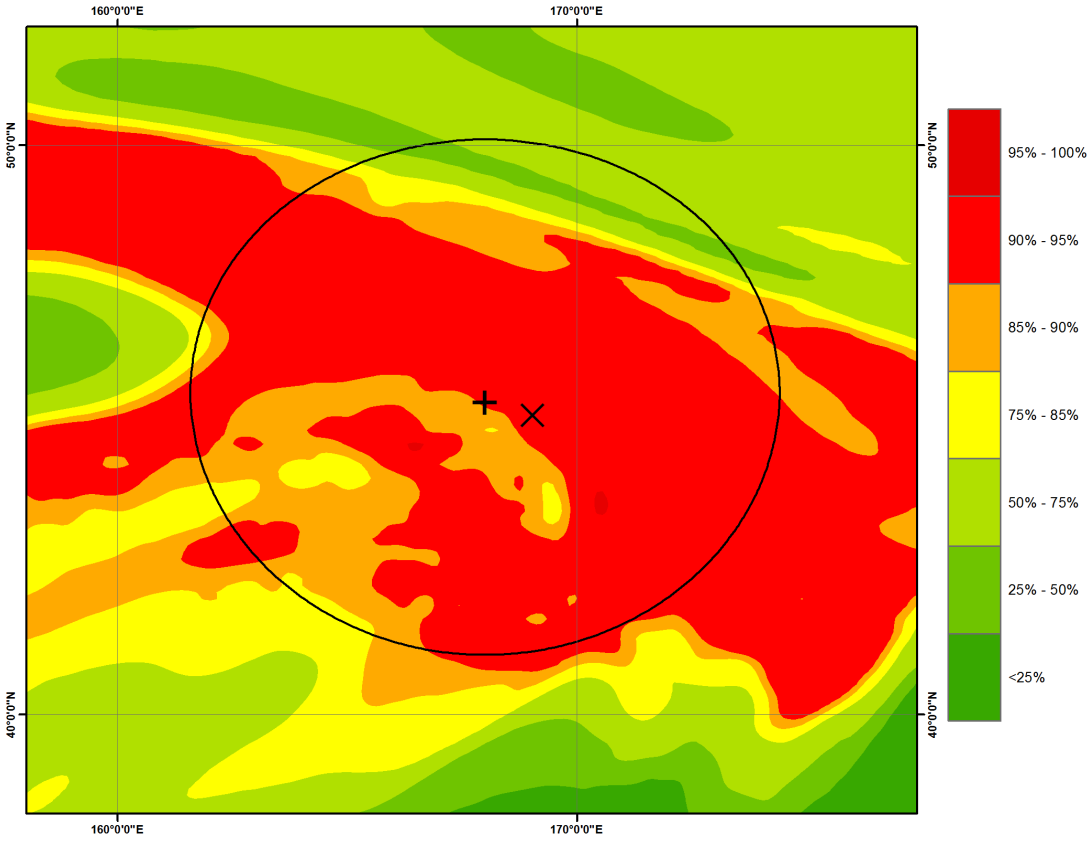

Figure 70. DRV07 48hr plot of the 850 hPa relative humidity in the region of observed and forecast DRV locations 12 UTC 5 October 2010. Shaded regions indicate relative humidity (magnitude identified by colorbar in percentages), observed DRV location represented by (+), forecast DRV location represented by (X), black circle represents 500 km radius around the observed DRV.

d. DRV07 48hr Forecast is a "Hit"

The DRV07 48hr forecast does an excellent job of locating the observed DRV at genesis time. All forecast calculated values meet minimum requirements (Table 11) and the disturbance location was well predicted. The DRV07 48hr forecast is also noteworthy as one of the few that were able to identify the DRV at the time of genesis. As noted

above and in the previous literature (MM05), DRV identification at genesis time appears to be a challenging problem.

Lon	Lat	Rel. Vort. (s^{-1})	Dist. (km)	ΔT (K)	Rel. Humidity (percent)
169.03	45.386	3.81E-04	84.033	7.7971	94.142

Table 11. Calculated values for the DRV07 48hr forecast.

2. DRV07 60hr Forecast

a. Location and Intensity

The forecast location for DRV07 at the 60hr lead time is well predicted, with a 60 km discrepancy (Figure 71). In contrast, the predicted intensity of the disturbance falls below the threshold (2.83×10^{-4} s^{-1}). The 12 hour evolution of the relative vorticity maxima predicts a weakening disturbance. However, given the very good agreement in the disturbance location, one might question if this is an instance where the threshold value for relative vorticity is too high call the tracked feature a DRV.

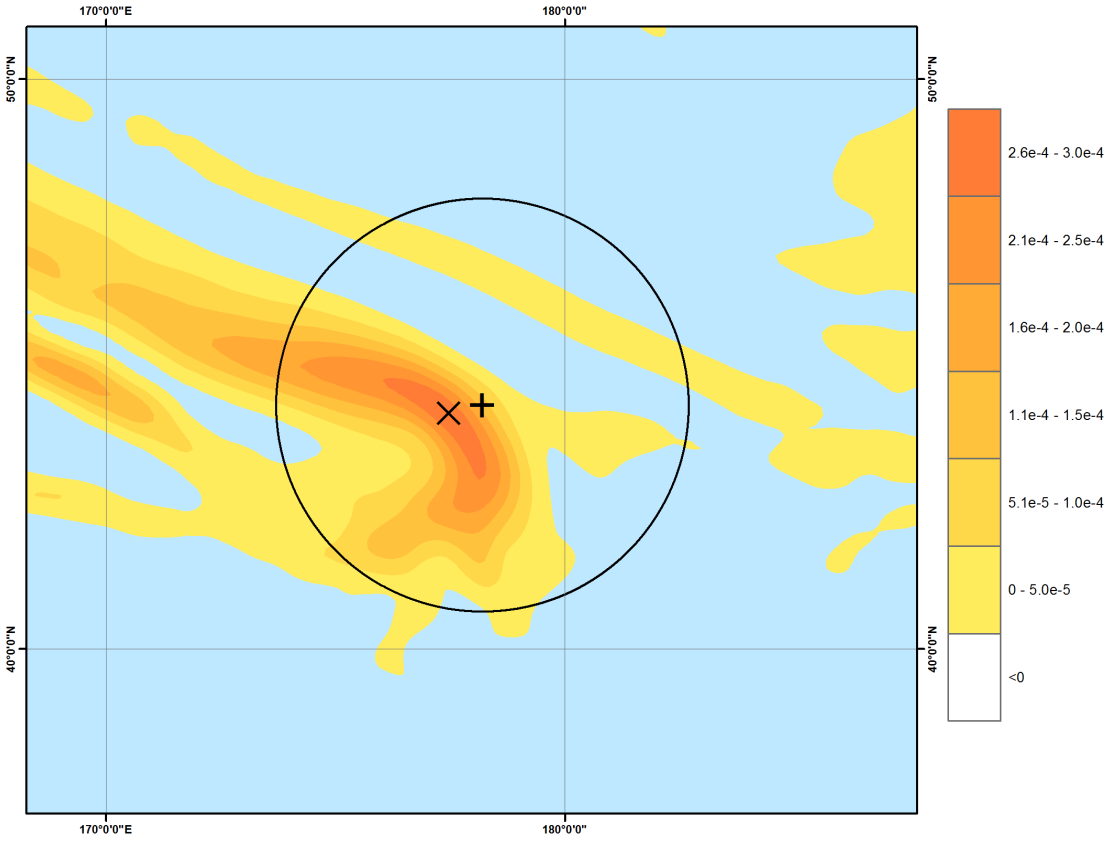

Figure 71. DRV07 60hr plot of positive relative vorticity in the region of observed and forecast DRV locations 00 UTC 6 October 2010. Shaded regions indicated areas of positive relative vorticity (magnitude identified by colorbar), observed DRV location represented by (+), forecast DRV location represented by (X), black circle represents 500 km radius around the observed DRV.

b. Baroclinicity

Like the forecast intensity, the baroclinicity forecast for DRV07 at the 60hr time-step has decreased (although it does fall above the threshold value). The decrease in value is likely two-fold, both an actual decrease in the environmental baroclinicity and a result of the unique orientation of the baroclinic zone. It should be noted that the decreased intensity is consistent with a decrease in baroclinicity (MM05).

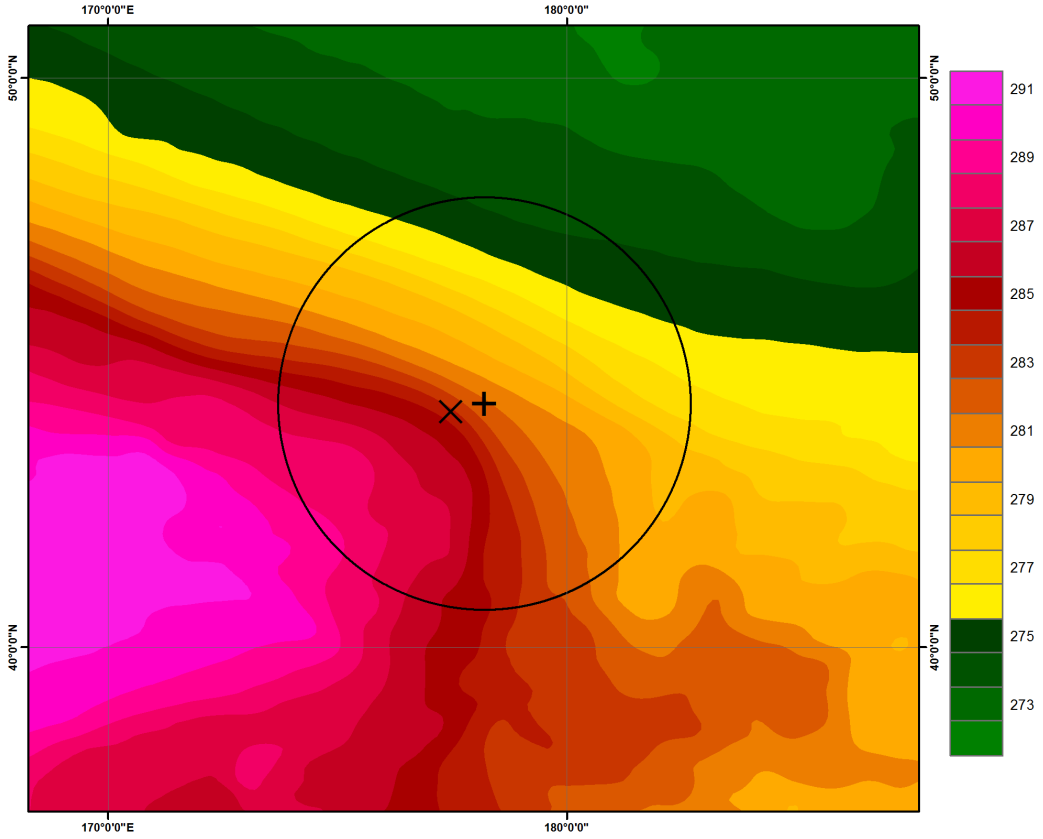

Figure 72. DRV07 60hr plot of 925 hPa temperatures in the region of observed and forecast DRV locations 00 UTC 6 October 2010. Shaded regions indicated temperature (magnitude identified by colorbar in degrees K), observed DRV location represented by (+), forecast DRV location represented by (X), black circle represents 500 km radius around the observed DRV.

c. Sufficient Moisture

The moisture threshold, as has been consistently seen, exceeds the threshold value (93.6 percent)

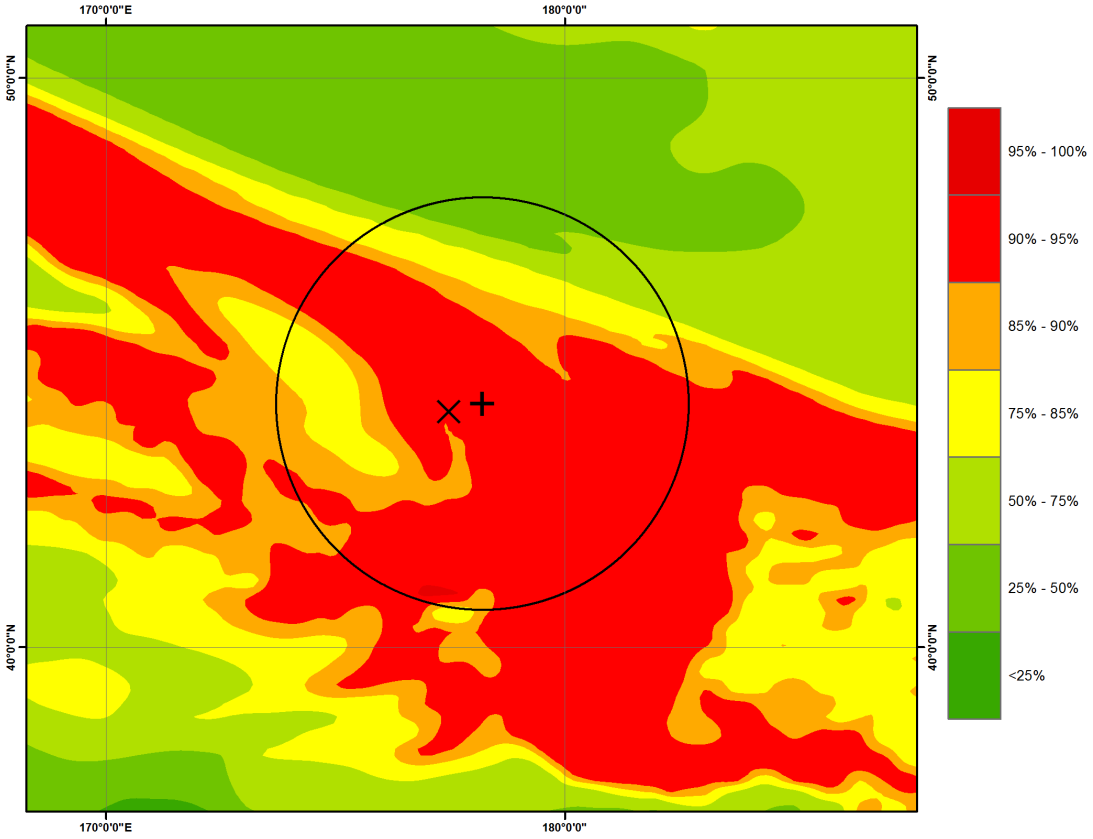

Figure 73. DRV07 60hr plot of the 850 hPa relative humidity in the region of observed and forecast DRV locations 00 UTC 6 October 2010. Shaded regions indicate relative humidity (magnitude identified by colorbar in percentages), observed DRV location represented by (+), forecast DRV location represented by (X), black circle represents 500 km radius around the observed DRV.

d. DRV07 60hr Forecast a "Miss"

The 60hr forecast for DRV07 did an excellent job of tracking the previously identified disturbance from the 48hr forecast. However, the predicted disturbance was shown to weaken over the 12 hour time period in conjunction with a decrease in the calculated baroclinicity.

Lon	Lat	Rel. Vort. (s^{-1})	Dist. (km)	ΔT (K)	Rel. Humidity (percent)
177.47	44.262	2.83E-04	60.298	5.7499	93.603

Table 12. Calculated values for the DRV07 60hr forecast.

3. DRV07 72hr Forecast

a. Location and Intensity

In contrast to the previous 12 hour time period, the predicted disturbance intensifies from the 60 to 72 hour forecast times (3.41 versus 2.83 x 10^{-4} s^{-1}). However, the relative vorticity threshold is not met in this case. It would be hard to argue the control forecast is not identifying a growing disturbance at this time. This calls into question the sensitivity of the identification algorithm to the relative vorticity threshold.

The location of the predicted disturbance is displaced to the west north west by 163 km. As with test case 2, there is a difference in the propagation speed of the predicted versus observed DRV. In contrast to the previous example, the predicted DRV is propagating more slowly than observed. Again, there are a number of possible reasons related to DRV and environmental characteristic that can lead to propagation errors (MM05).

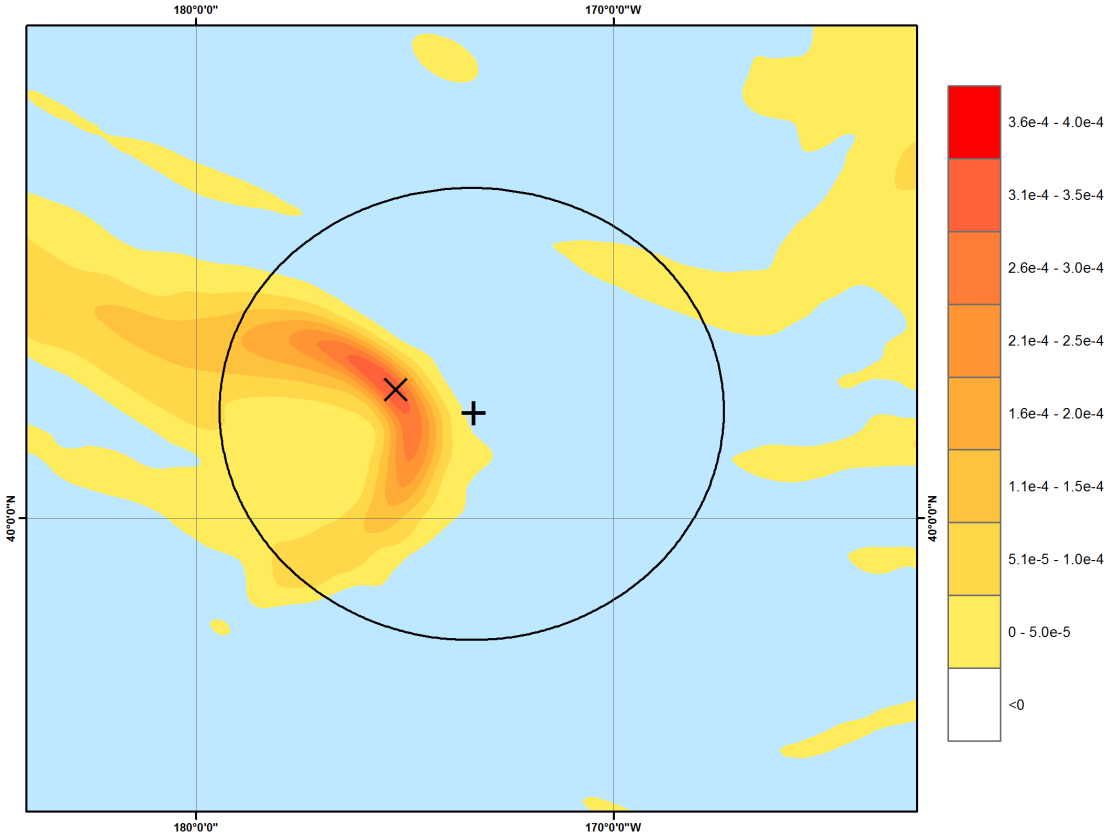

Figure 74. DRV07 72hr plot of positive relative vorticity in the region of observed and forecast DRV locations 12 UTC 6 October 2010. Shaded regions indicated areas of positive relative vorticity (magnitude identified by colorbar), observed DRV location represented by (+), forecast DRV location represented by (X), black circle represents 500 km radius around the observed DRV.

b. Baroclinicity

The forecast temperature gradients for DRV07 at the 72hr time-step are extremely similar in structure and calculated value (5.72 K) to the 60hr forecast. The structure of the baroclinic zone has generally moved along with the disturbance and still displays the NW-SE orientation (Figure 75). The calculate value exceeds the threshold.

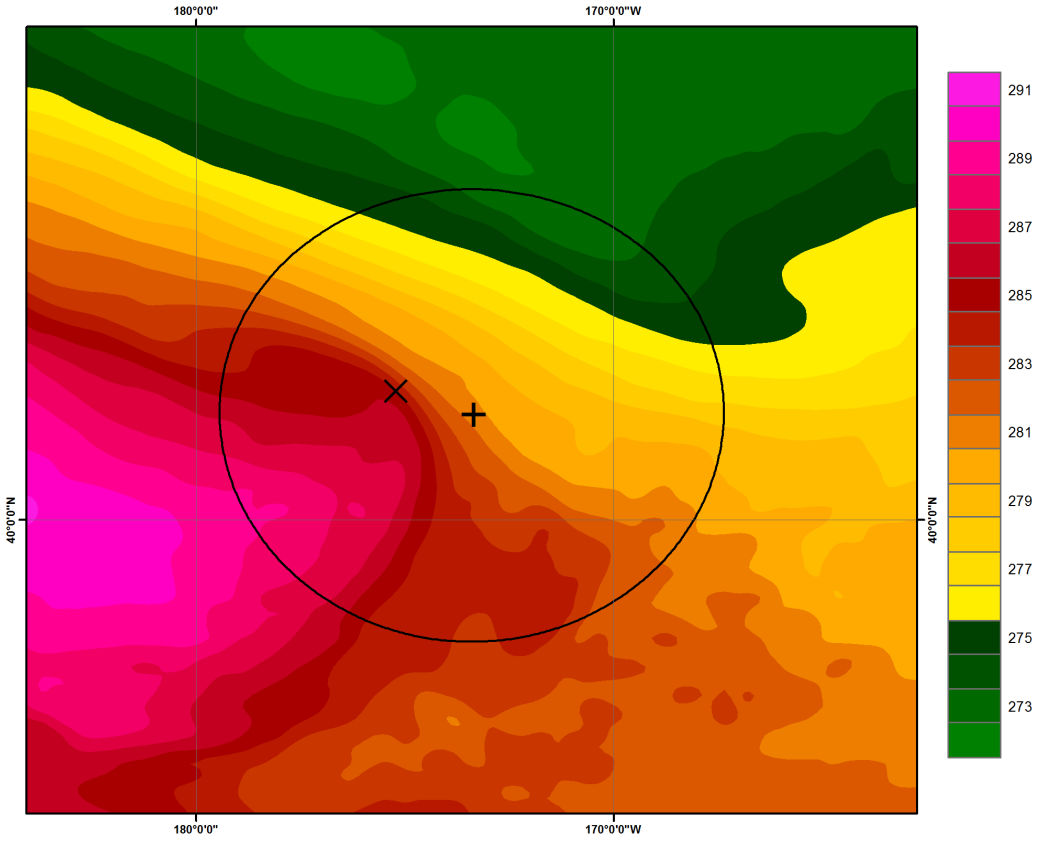

Figure 75. DRV07 72hr plot of 925 hPa temperatures in the region of observed and forecast DRV locations 12 UTC 6 October 2010. Shaded regions indicated temperature (magnitude identified by colorbar in degrees K), observed DRV location represented by (+), forecast DRV location represented by (X), black circle represents 500 km radius around the observed DRV.

c. Sufficient Moisture

Calculated moisture levels for the DRV07 72hr forecast are almost unchanged from the previous 2 forecasts. A calculation value of 93.7 percent exceeds the threshold.

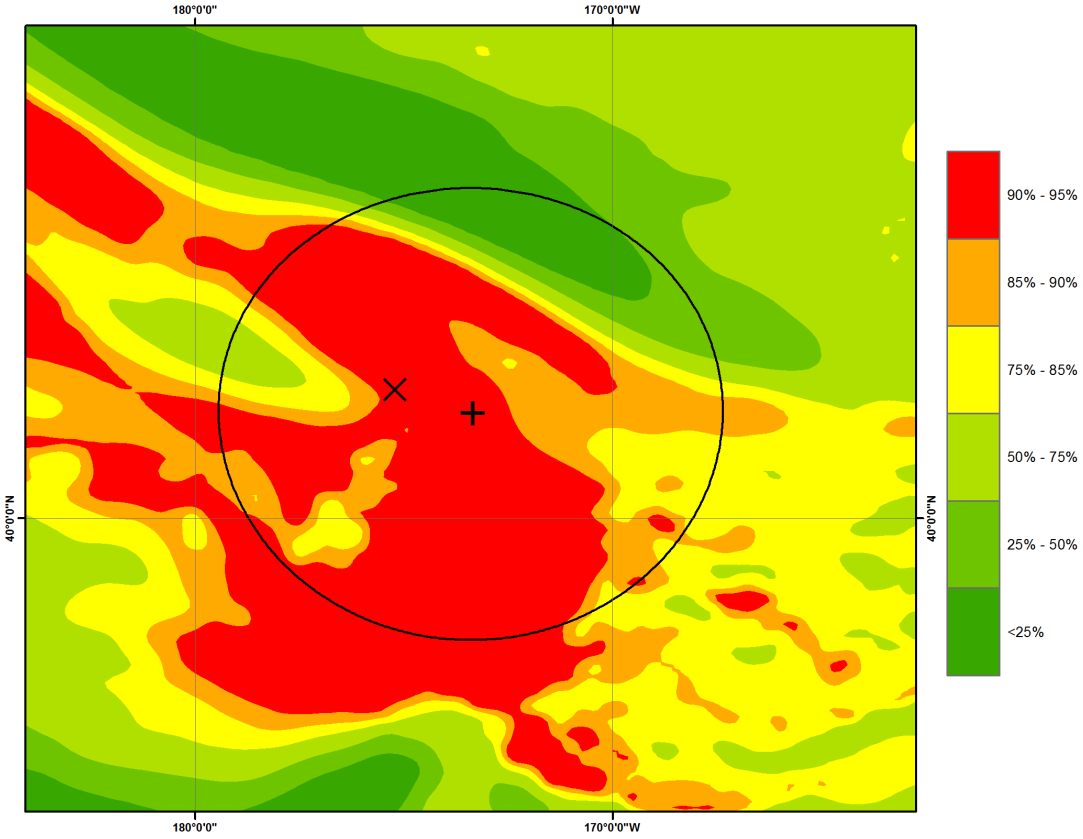

Figure 76. DRV07 72hr plot of the 850 hPa relative humidity in the region of observed and forecast DRV locations 12 UTC 6 October 2010. Shaded regions indicate relative humidity (magnitude identified by colorbar in percentages), observed DRV location represented by (+), forecast DRV location represented by (X), black circle represents 500 km radius around the observed DRV.

d. DRV07 72hr Forecast a "Miss"

The evolution from the 60 to 72 hour forecast predicts a growing disturbance that meets all the threshold criteria of the identification script, with the exception of the relative vorticity which is slightly below the criteria. It is also evident that the propagation speed of the observed and predicted DRVs are significantly different. While the slower propagation speed of the predicted DRV does not take it beyond the 500 km threshold, it is again important to note that the difference in propagation speed may very well impact the subsequent evolution of the system and the explosive cyclogenesis that was observed.

Lon	Lat	Rel. Vort. (s^{-1})	Dist. (km)	ΔT (K)	Rel. Humidity (percent)
184.78	42.576	3.41E-04	163.08	5.7193	93.721

Table 13. Calculated values for the DRV07 72hr forecast.

4. Forecast DRV07 Summary and Conclusions

As can be clearly seen in Figure 77, the forecast track for DRV07 was remarkable similar to the observed DRV07 track. The distances between the observed and forecast DRVs were less than any of the other 12 test cases.

The environmental conditions were clearly sufficient for DRV genesis and growth in this case. In contrast to test case 2, the uncharacteristic orientation of the baroclinic zone did not preclude the calculated value from exceeding the threshold value. However, consistent with test case 2, a distinct difference in propagation speed is evident. In addition, the difference was of opposite sign, with the predicted test case 2 disturbance propagating more quickly than observed (whereas the predicted disturbance in this case propagated less quickly).

The other feature of note is a forecast miss being the result of a slightly below threshold for the relative vorticity maximum. This calls in to question the sensitivity of DRV identification to the threshold value.

It might be hypothesized that, within the context of the comparison of an observed DRV from the climatology of BW13 and one predicted using the TIGGE control forecast, the efficacy of the ingredients based approach presented here is dependent on the strength and isolated nature of the DRV at genesis time.

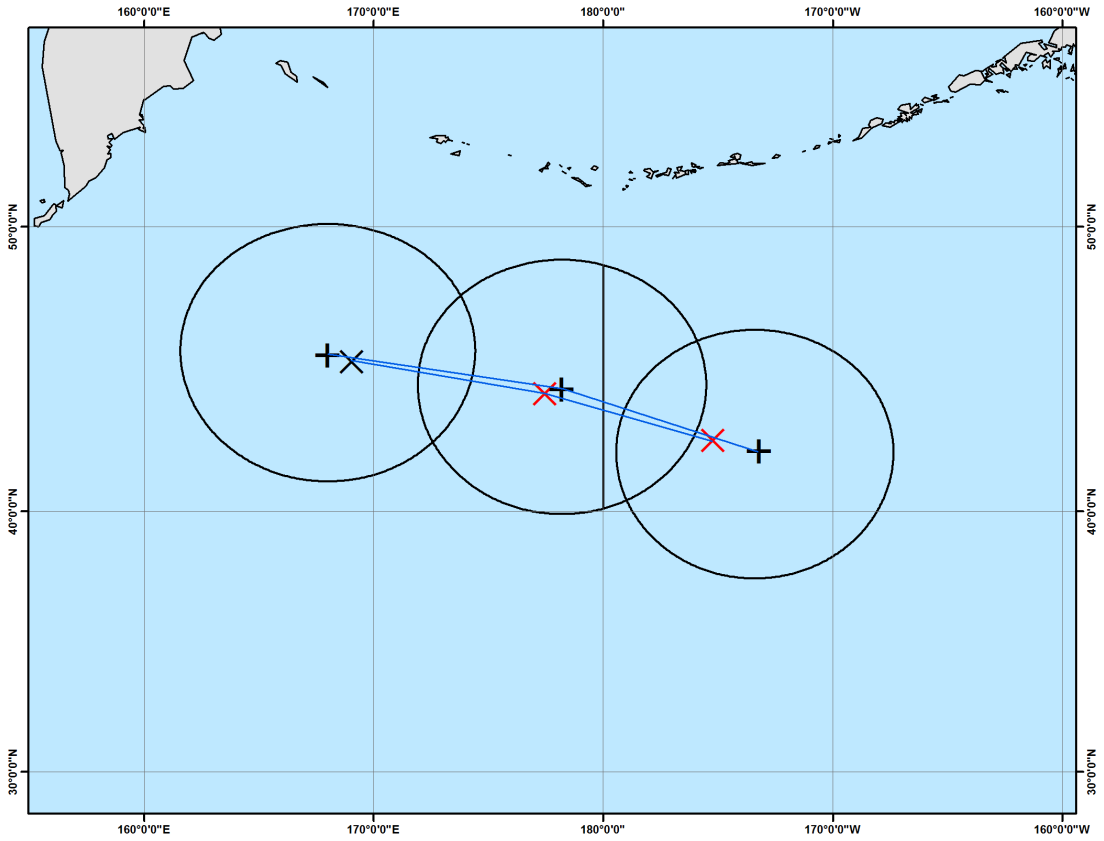

Figure 77. Test case 7 observed DRV (+) and forecast DRV (X) tracks in 12 hr time-steps over the initial 24 hours after formations. Black rings are 500 km radii around observed DRV locations. Black X symbols represent forecast "hits," while red X symbols represent forecast "misses" (valid times: 12 UTC 05 October 2010, 00 UTC 6 October 2010, 12 UTC 6 October 2010)

E. TEST CASE SUMMARY DISCUSSION

The examination of ensemble control forecasts for three cases and for multiple lead times presented in this chapter has provided significant insight into both the characteristics of predicted DRV genesis and evolution, as well as possible shortcomings of the identification criteria. General conclusions are:

- Significant topography can complicate the identification procedure (both in the case of the objective climatology of BW13 and that presented herein)

- The prediction of DRV genesis is challenging given the often weak signal of the precursor disturbance. This implies that forecasts valid at or shortly after genesis time may have considerable difficulty properly identifying a candidate DRV. It is also postulated that the resolution of the data source is especially important at these early times.

- The efficacy of disturbance identification is directly related to the intensity and structure (isolated vortex versus vorticity band) at or shortly after genesis time.

- The prediction of the propagation speed of a disturbance is difficult to accurately predict. It is hypothesized, but not proven, that a propagation error at a given time will be exacerbated as the forecast length increases and may directly impact the prediction of explosive cyclogenesis.

- In terms of the ingredients based approach, the predicted moisture content appears to always meet the threshold value and the orientation of the baroclinic zone may play an important role in evaluation the baroclinic component.

- Further examination of the sensitivity of the identification algorithm to the threshold values is needed.

THIS PAGE INTENTIONALLY LEFT BLANK

VI. ECMWF TIGGE CONTROL FORECASTS OF DRVS

A. EVALUATION OF THE 12 TEST CASE CONTROL FORECASTS

1. Forecast Evaluation Terminology

a. "Good" DRV Forecast

A "good" forecast will be defined as having met all four DRV identification criteria (intensity, location, baroclinicity, and moisture) for all three consecutive forecast times (48 hour, 60 hour, and 72 hour).

b. "Fair" DRV Forecast

A "fair" forecast will be defined as having met all four DRV identification criteria for 2 consecutive forecast times (48 hour and 60 hour; 60 hour and 72 hour). The "two consecutive forecasts" criteria is created with the assumption that the control forecast had difficulty with either DRV genesis or a later environmental uncertainty, but through at least 12 hours identified a propagating DRV.

c. "Poor" DRV Forecast

A "poor" forecast will be defined as any forecast not meeting the above criteria.

2. Overall Control Forecast Performance and Statistics

Of the 12 test cases, two were identified as "good," two were identified as "fair," and eight were identified as "poor" by the DRV identification script (Figure 78). As an overall performance indicator, these statistics indicate very poor performance overall for DRV forecasting at greater than 48 hour prior to storm generation.

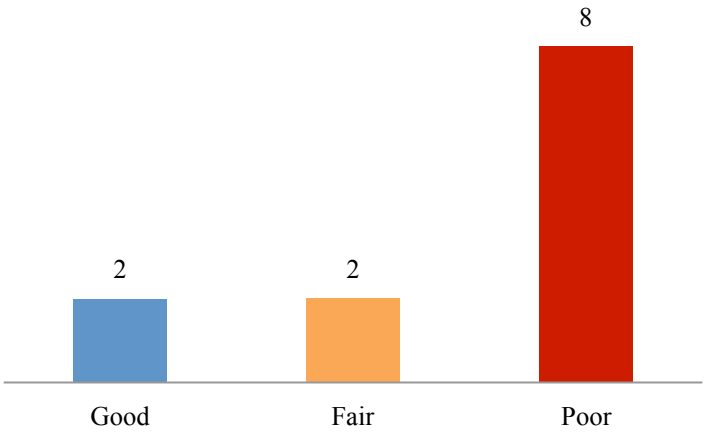

Figure 78. Control forecast performance for the 12 test cases.

To further explore possible causes for poor prediction of the early DRV phases, each forecast time will be evaluated, as will the individual identification metrics, in an effort to identify trends or outliers of significance.

a. Control Forecast "Hits" of Initial DRV Genesis

The success rate of forecasting DRVs at genesis in control model runs is low at approximately 33 percent (Figure 79).

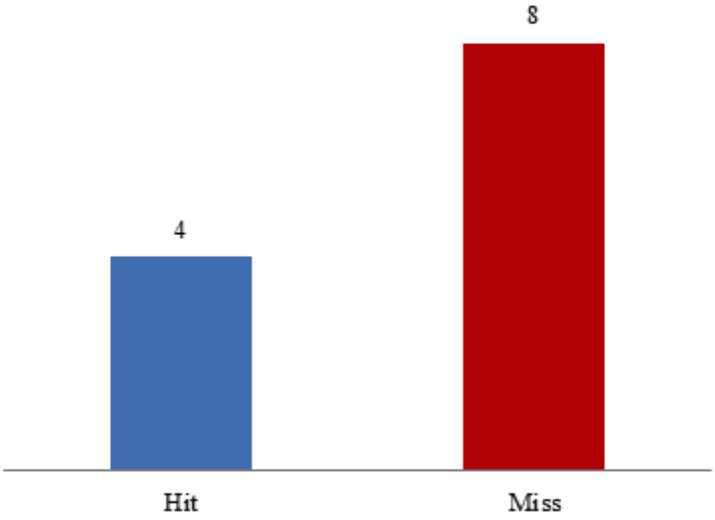

Figure 79. Performance of control forecasts of DRV genesis (48 hour forecast).

b. Control Forecast "Hits" After 12 Hours of Propagation

Interestingly, the success rate for the control 60 hour forecasts is identical to that for 48 hour control forecasts (Figure 80).

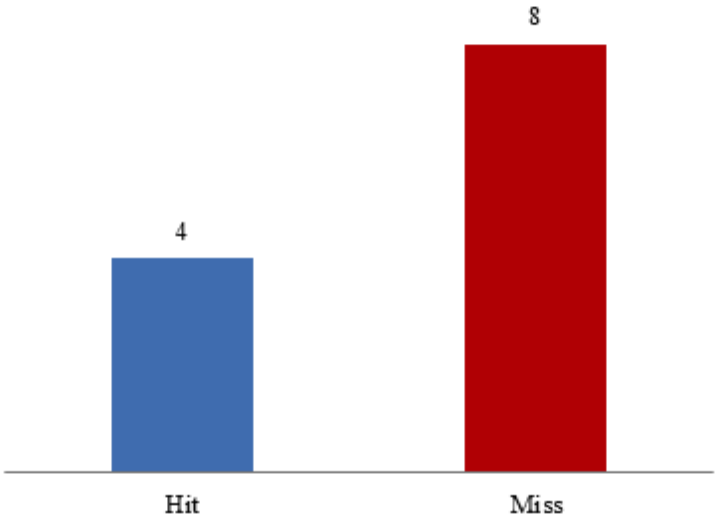

Figure 80. Performance of the 60 hour control forecasts.

c. Control Forecast "Hits" After 24 Hours of Propagation

Finally, computing the success rates for the final control forecast (72 hour) reveals the same success rate of 33 percent.

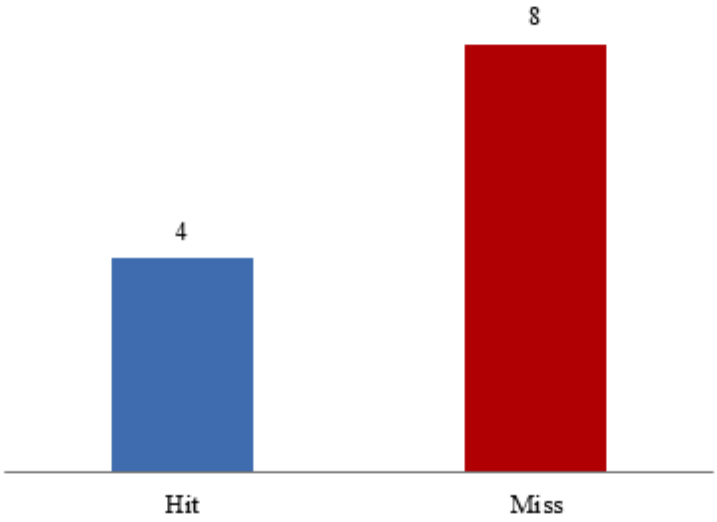

Figure 81. Performance of the 72 hour control forecasts.

d. Flat Control Forecast Performance over Time

The lack of a trend of the control model's forecasts is surprising. Initially, two hypotheses were expected with regard to forecast performance. The first being that DRV genesis would be difficult to forecast due to the often weak signal of the nascent DRV at or shortly after genesis time. This hypothesis was confirmed via the analysis in the previous chapter. The second hypothesis was that, while the control forecast identification of a DRV might initially improve in conjunction with a strengthening DRV, the model performance would subsequently degrade as the forecast length becomes larger. the longer forecasts are more susceptible to deviating from real environmental conditions. With both of these hypotheses in mind, the expected result was low performance for genesis (48 hour forecast), moderate-to-good performance in the mid-length forecast (60 hour forecast), and a decreased performance in the later forecast (72 hour forecast). The above analysis is not consistent with the expected results. It is possible that the small sample size of only 12 cases in insufficient to identify such a trend.

e. Compiled Hit/Miss Rate for all Control forecasts

The overall success rate for the 36 control forecasts evaluated using the DRV identification script was 33 percent (Figure 82). The low percentage of overall successful forecasts, combined with the majority (66.7 percent) of test cases being evaluated as "poor," leads to the conclusion that the genesis and early propagation phases of DRVs are difficult to properly predict.

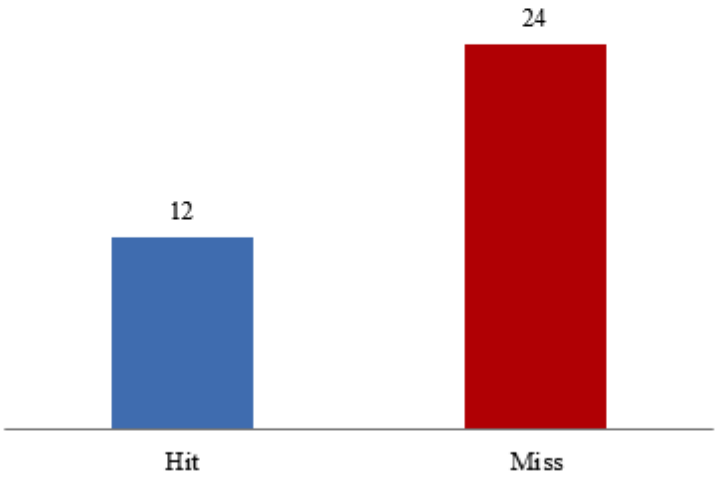

Figure 82. Performance of the 36 control forecasts.

Again, it is true that12 test cases represents a relatively small sample size. In addition, this is the first time this DRV identification script is being tested on multiple storms across different forecast times. As mentioned in the summary remarks in Chapter 4, further examination of the sensitivity of the identification algorithm to the threshold values is needed.

Further study of each variable, including which variables were most responsible for "hits" and "misses," will be carried out in the hope of achieving better understanding of the overall poor performance of the control forecasts.

3. Overview of Relative Vorticity Maxima Forecasts

a. Control Forecasts Meeting Relative Vorticity Thresholds

There was an even split of the 36 control forecasts that met the minimum threshold value for the identified relative vorticity maxima (Figure 83).

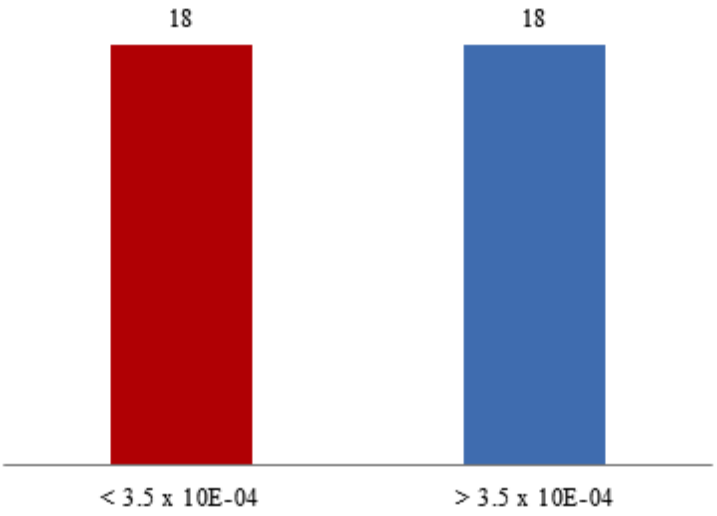

Figure 83. Histogram of the 36 control forecast relative vorticity maxima below (red; "miss") and above (blue; "hit") the threshold value of 3.5 x 10^{-4} s^{-1}.

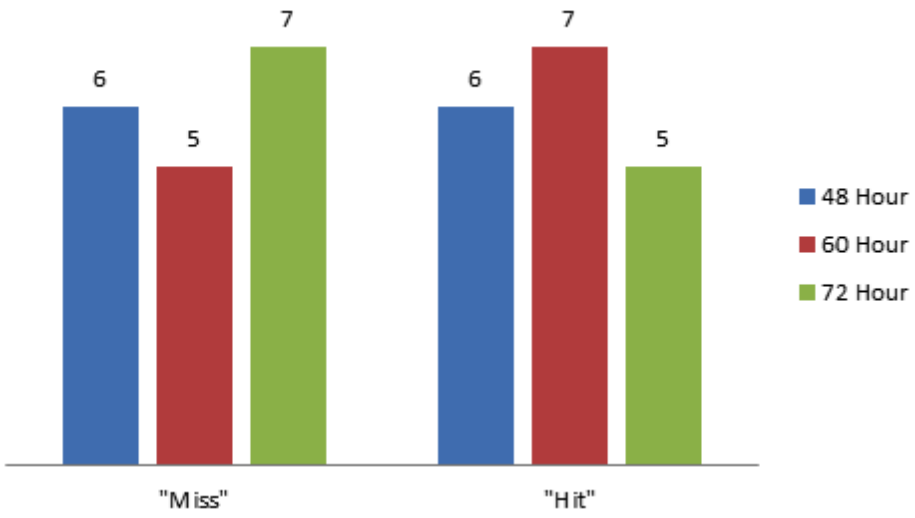

Figure 84. Histogram of the control forecast relative vorticity maxima "hits" and "misses" by forecast lead time (48, 60, and 72 hour).

b. Detailed Relative Vorticity Maxima Value Analysis

The range and frequency of occurrence of relative vorticity values are presented below in a histogram (Figure 85), the values appear to be skewed right with a distinct spike of values between 2.5 x 10^{-4} s^{-1} and 3.0 x 10^{-4} s^{-1}. Indeed, the majority of values fall between 2.0 x 10^{-4} s^{-1} and 3.5 x 10^{-4} s^{-1}; just below the relative vorticity maxima "hit"

threshold value. Relative vorticity maxima above the threshold value do not trend around a specific value range, but are spread over a larger range with multiple outliers of extremely strong relative vorticity.

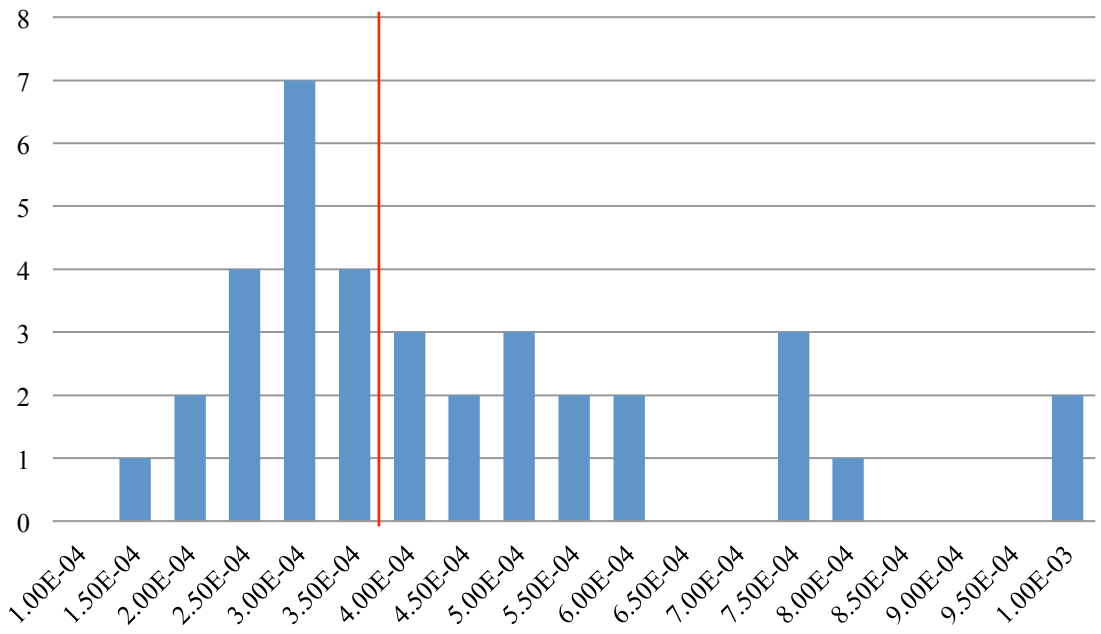

Figure 85. Histogram of control forecast relative vorticity maxima values with a 0.5 x 10^{-4} s^{-1} bin size. The numbers under each bar represent the upper value of the bin. The red line indicates the threshold cut-off for DRV identification.

The clear trend and clustering of control forecast values intuitively indicates two distinct possibilities: that there exists a bias for under-forecasting the intensity of DRV relative vorticity maxima or the DRV identification script threshold value is too high. It is impossible to discern with this limited study which is the reality, but is an ideal candidate for future research.

4. Overview of Control forecast Distance to Observed DRVs

a. Control forecasts Meeting Maximum Distance Thresholds

The majority (69.4 percent) of control forecast positions were located within 500 km of the observed DRVs (Figure 86) and registering as “hits” for the distance check.

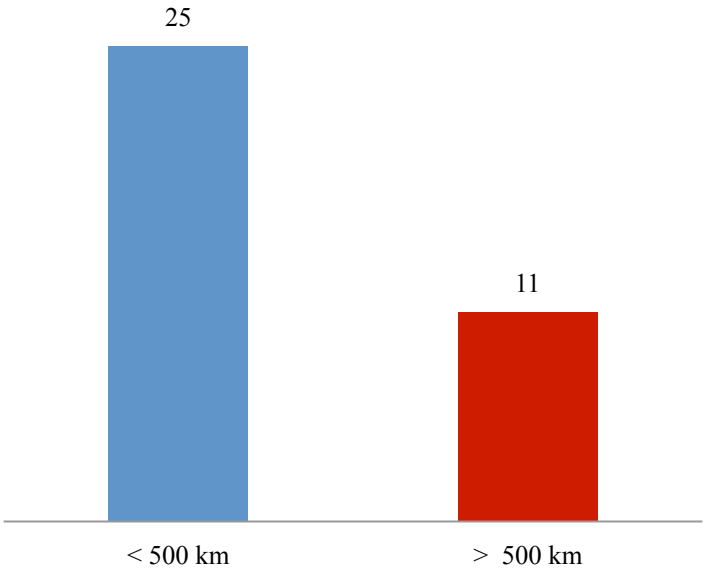

Figure 86. Histogram of the 36 control forecasts distance to observed DRVs. Forecasts less than 500 km (blue) are considered “hits,” while forecasts greater than 500 km (red) are considered “misses.”

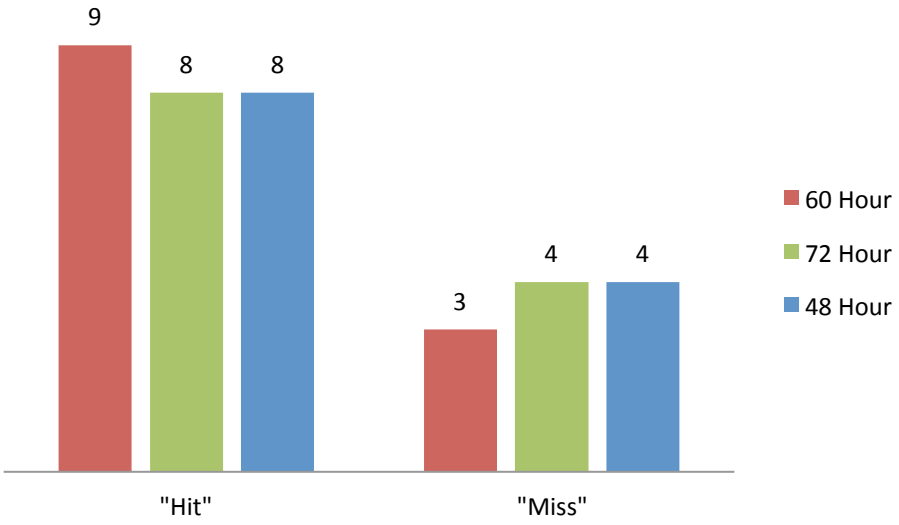

Figure 87. Histogram of the “hits” and “misses” of the control forecast distances to the observed DRVs at the three forecast lead times (48, 60, and 72 hour).

b. Detailed Analysis of Control Forecast Distance from Observed DRVs

Examination of a histogram of control forecast distances with a bin value of 100 km (Figure 88) highlights a possible dipole clustering of values, with the lower value clustering occurring from 0 - 200 km and the second clustering occurring from 300 - 700km. It is encouraging seeing the large number of forecast relative vorticity maxima with distances less than 200 km to the observed DRV, as well as only having two control forecasts locating relative vorticity maxima more than 800km from the observed position.

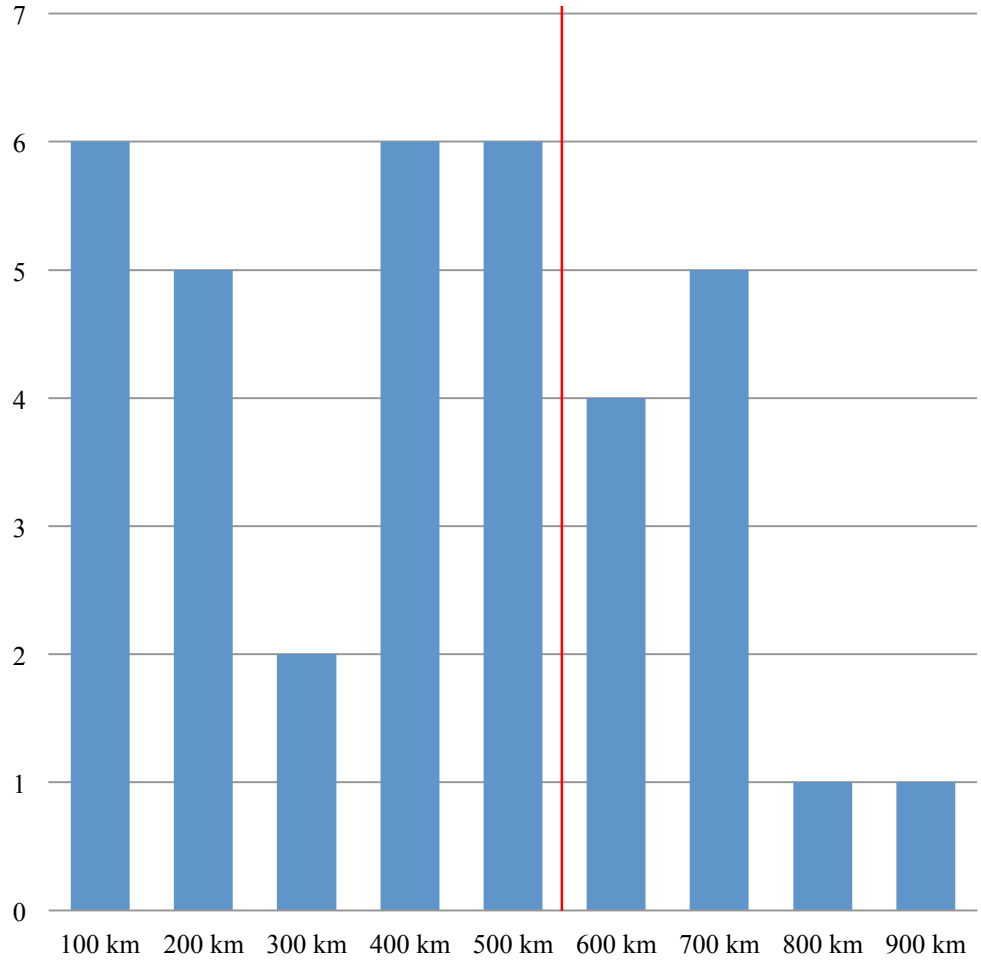

Figure 88. Histogram of control forecast distance to observed DRVs with a 100 km bin size. The numbers under each bar represent the upper value of the bin. The red line indicates the threshold cut-off for DRV identification.

Further analysis of the Figure 88 histogram reveals that the model does not appear to be displaying a particular bias, with generally even distributions out to 700 km. The broad distribution does allude to the forecasting models struggling with the proper identification of a relative vorticity maximum in the proper location.

The analysis generates no clear recommendations for modification to the DRV identification script (as a position error of more than 500 km is quite large for 48-72 hour forecasts). One possible consideration generated from the histogram would be to use the breakpoint between the 0 – 200 km cluster and 300 – 700 km cluster as a means of grading forecasts. This could prove beneficial to further differentiate good/fair/poor forecasts. For example, less than 200 km could be recognized as a "good" hit, less than 700 km as a "fair" hit, and beyond that distance it could be recorded as a "miss."

5. Overview of Control Forecast Baroclinicity Values

a. Control Forecasts Meeting Minimum Baroclinicity Thresholds

The majority (66.7 percent) of control forecasts met the minimum thresholds calculated by the DRV identification script (Figure 89).

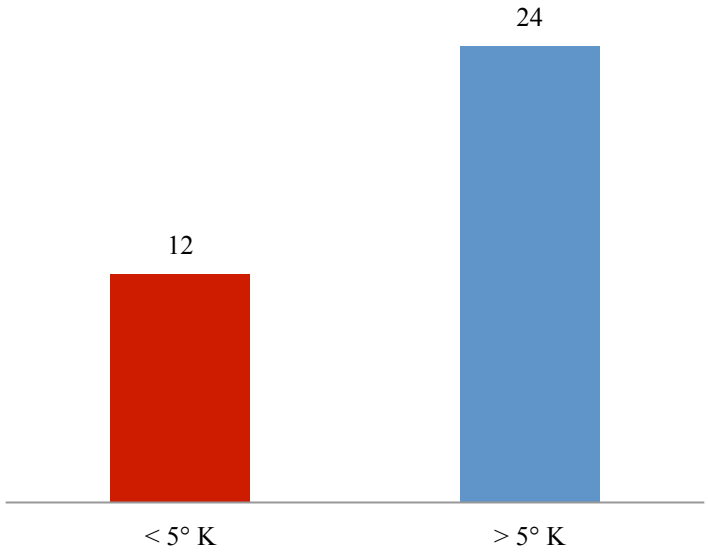

Figure 89. Histogram of the 36 control forecasts calculated baroclinicity values. Forecast calculations less than 5° K (red) are considered "misses," while forecasts greater than 5° K (blue) are considered "hits."

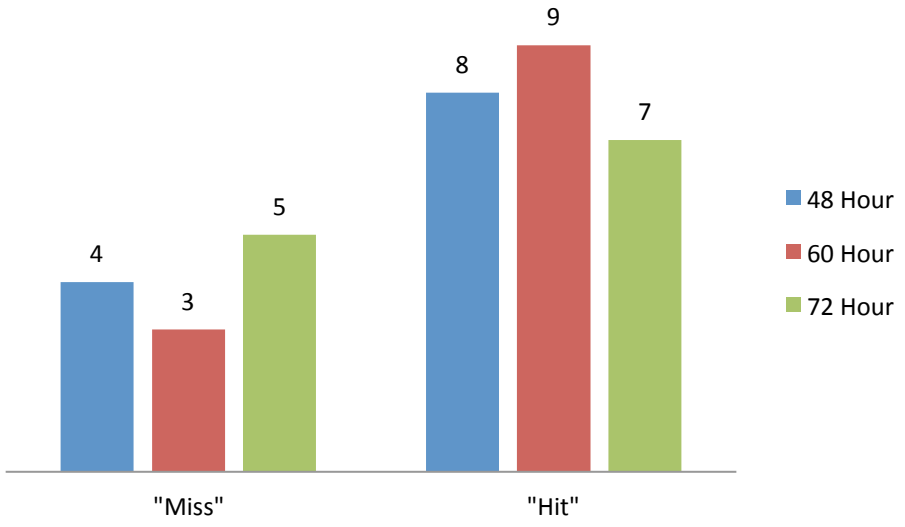

Figure 90. Histogram of "hits" and "misses" of the control forecasts calculated baroclinicity values by forecast lead times (48, 60, and 72 hour).

b. Detailed Analysis of Control Forecast Baroclinicity Values

Analysis of the detailed histogram of control forecast baroclinicity values reveals a central tendency around the threshold value of 5 K with an overall slightly positive skew to the data. With approximately 64 percent of all calculated baroclinicity values falling within +/- 2 K of the threshold value indicates that most downstream regions of from forecast relative vorticity maximum share similar temperature gradient magnitudes.

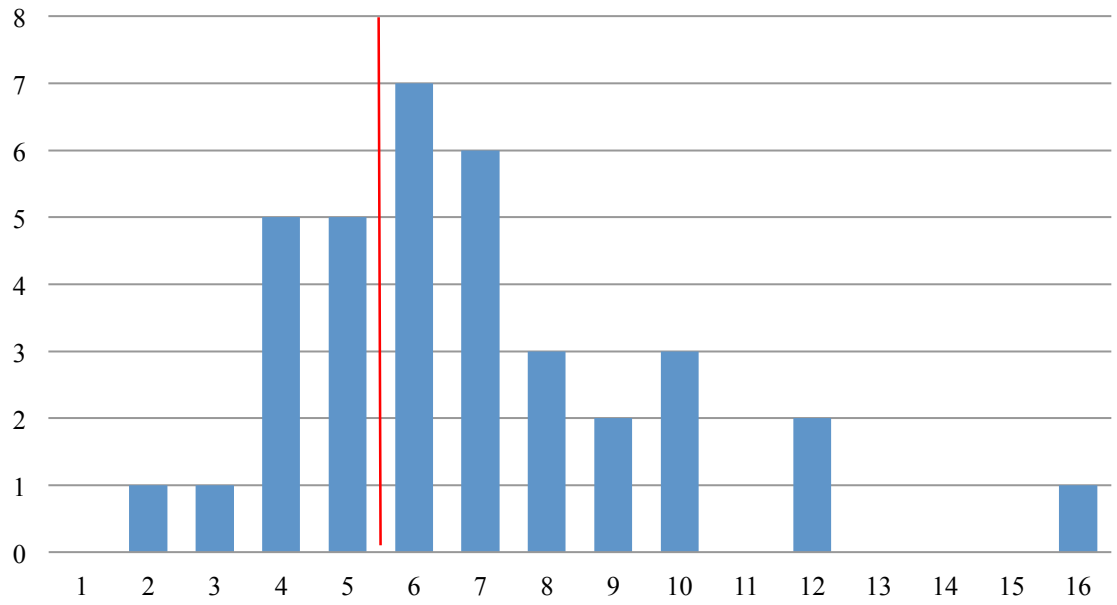

Figure 91. Histogram of control forecast baroclinicity values (in degrees K) with a one degree bin size. The numbers under each bar represent the upper value of the bin. The red line indicates the threshold cut-off for DRV identification.

There is no evidence of model bias in the control forecasts for downstream baroclinicity. It appears that the control forecasts models are doing a relatively good job of placing downstream baroclinic zones in relation to forecast relative vorticity maximum.

In regards to modifying the DRV identification script thresholds, there is no clear breakpoint in the analysis data until around 3 K, indicating that might possibly be a better

threshold of environments non-conducive to DRV formation. To first order, it seems reasonable to keep the calculation method used here to remain consistent with the study of BW13. However, it might prove useful to investigate a method that takes into account the orientation of the baroclinic zone, as this was shown to be important in Chapter 4.

6. Overview of Control Forecast Relative Humidity Calculations

a. Control Forecasts Meeting Minimum Relative Humidity Thresholds

All control forecast calculations of necessary relative humidity met minimum thresholds (Figure 92).

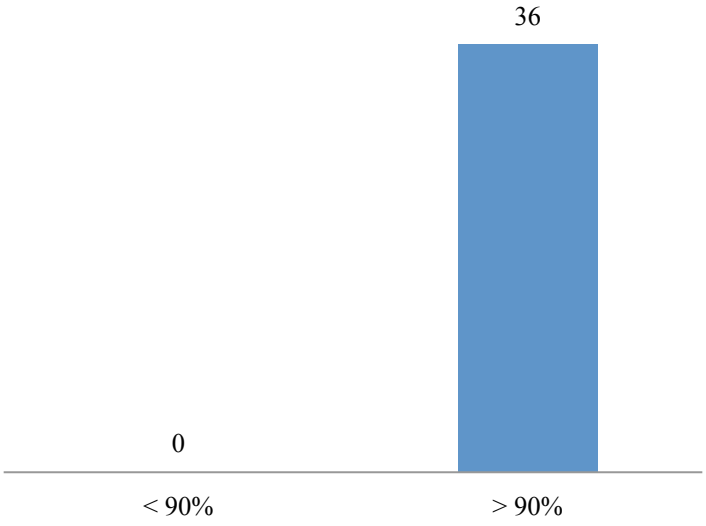

Figure 92. Histogram of the 36 control forecasts calculated relative humidity values. Forecast calculations less than 90 percent (red) are considered "misses," while forecasts greater than 90 percent (blue) are considered "hits."

b. Detailed Analysis of Control Forecast Relative Humidity Values

A further analysis of the control forecast relative humidity calculations reveals that the data is positively skewed with no calculated values below 93 percent (Figure 93). The vast majority of calculated relative humidity fields are 93 - 95 percent and well above the DRV identification threshold minimum value of 90 percent

The resulting calculations and distribution of the histogram appear to make the calculation redundant for DRV identification in control forecasts. Either the control models did a perfect job forecasting regional relative humidity conducive to DRV growth, or the minimum forecast value is set too low. In either case, the usefulness of the relative humidity calculation will be put further to the test when the DRV identification script analyzes the probabilistic forecasts.

It finally should be noted that if the baroclinicity calculation is modified to take into account the orientation of the baroclinic zone, it would make sense to also concurrently adjust the region for the relative humidity calculation.

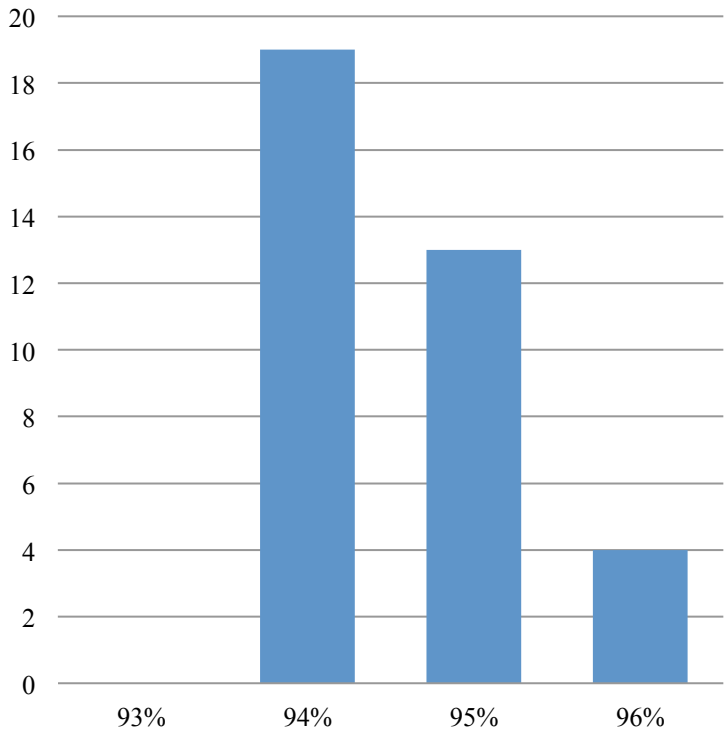

Figure 93. Histogram of control forecast calculated relative humidity values (in percentages) with a one percent bin size. The numbers under each bar represent the upper value of the bin. All values are above the threshold cut-off for DRV identification.

B. DRV IDENTIFICATION SCRIPT OUTPUTS AND SUMMARIES OF THE 12 TEST CASES

1. Test Case 1: "Poor"

Test case 1 failed all three forecast time-steps. The control forecast DRV is generally placed quite far from the observed locations, the brief growth of intensity at 60 hours is lost again at 72 hours, and baroclinicity values decreased over time, which is unsupportive of DRV growth.

Test Case	Fcst Hr	Lon	Lat	Rel. Vort.	Dist.	Barocl.	Rel. Hum.
1	48	135.84	33.302	2.76E-04	529.35	6.3809	93.9
1	60	141.19	34.988	5.39E-04	352.64	4.8607	94.916
1	72	146.81	34.988	2.27E-04	759.97	3.1541	93.513

Table 14. Test case 1 information and DRV identification script calculated variables. Red text indicates values outside the threshold cut-offs for DRV identification.

2. Test Case 2: "Fair"

Test case 2, as seen in Chapter 4.C, significantly misplaced and the initial forecast relative vorticity maximum position, but follow on forecasts at 60 hours and 72 hours were good-to-excellent and indicate that the control forecast was generating a storm system similar to the observed DRV.

Test Case	Fcst Hr	Lon	Lat	Rel. Vort.	Dist.	Barocl.	Rel. Hum.
2	48	138.09	32.459	2.34E-04	685.87	6.4293	93.722
2	60	142.59	35.55	4.78E-04	53.263	8.41	93.994
2	72	150.75	39.766	5.90E-04	273.33	15.181	94.602

Table 15. Test case 2 information and DRV identification script calculated variables. Red text indicates values outside the threshold cut-offs for DRV identification.

3. Test Case 3: "Poor"

Test case 3 control forecasts placed an extremely intense disturbance in the vicinity of the observed DRV genesis position. Unfortunately it also forecast a

downstream area of weak baroclinicity, which likely led to the significant weakening and subsequent misplacement of storm location. Decreasing intensity and baroclinicity values indicate a forecast of a decaying system.

Test Case	Fcst Hr	Lon	Lat	Rel. Vort.	Dist.	Barocl.	Rel. Hum.
3	48	128.81	26.838	9.62E-04	335.01	3.2446	95.296
3	60	136.13	26.838	2.86E-04	809.98	5.258	94.254
3	72	149.63	29.93	1.44E-04	607.66	3.6982	94.083

Table 16. Test case 3 information and DRV identification script calculated variables. Red text indicates values outside the threshold cut-offs for DRV identification.

4. Test Case 4: "Poor"

Test case 4 did an extremely poor job at forecasting the observed DRV at all forecast time-steps. All forecasted relative vorticity maximums lacked intensity and were located in zones lacking a strong baroclinic front.

Test Case	Fcst Hr	Lon	Lat	Rel. Vort.	Dist.	Barocl.	Rel. Hum.
4	48	129.38	38.361	1.82E-04	456.56	2.9145	93.378
4	60	136.97	38.642	2.75E-04	584.27	4.6634	95.039
4	72	158.63	42.014	3.31E-04	528.24	1.6053	94.304

Table 17. Test case 4 information and DRV identification script calculated variables. Red text indicates values outside the threshold cut-offs for DRV identification

5. Test Case 5: "Good"

Test case 5 is the first example of a "good" control forecast. Forecast relative vorticity maximum placement was consistently off by roughly the same amount, indicating the forecast was tracking a similarly evolving system to the observed DRV. High levels of forecast intensity and baroclinicity support the evaluation.

Test Case	Fcst Hr	Lon	Lat	Rel. Vort.	Dist.	Barocl.	Rel. Hum.
5	48	160.31	42.014	5.42E-04	352.68	9.1925	94.483
5	60	165.66	44.543	4.38E-04	419.29	11.67	93.674
5	72	170.44	46.792	4.73E-04	344.74	6.2471	93.332

Table 18. Test case 5 information and DRV identification script calculated variables. Red text indicates values outside the threshold cut-offs for DRV identification.

6. Test Case 6: "Poor"

Test case 6 appears to be an example of the control forecasts underperforming on the projection of intensity. A coherent and evolving disturbance remarkably close to the observed DRV seems to be apparent. Baroclinicity values are also extremely conducive to DRV genesis and evolution, but the under-predicted relative vorticity values show no indications of DRV-like intensity and growth.

Test Case	Fcst Hr	Lon	Lat	Rel. Vort.	Dist.	Barocl.	Rel. Hum.
6	48	149.06	39.204	2.87E-04	84.19	6.2178	93.563
6	60	157.22	43.419	2.42E-04	53.072	11.466	93.278
6	72	162.28	45.105	1.55E-04	174.89	9.6858	93.189

Table 19. Test case 6 information and DRV identification script calculated variables. Red text indicates values outside the threshold cut-offs for DRV identification.

7. Test Case 7: "Poor"

Test cast 7 was examined in detail in Chapter 4.D as a good "poor" control forecast. This can be easily understood from the output variables in Table 20. The forecast storm system is initially well placed, strong, and in a perfect environment for

intensification. Unfortunately, the 60 hour and 72 hour forecast intensities are slightly below threshold values and the two time-steps are identified as "misses."

Test Case	Fcst Hr	Lon	Lat	Rel. Vort.	Dist.	Barocl.	Rel. Hum.
7	48	169.03	45.386	3.81E-04	84.033	7.7971	94.142
7	60	177.47	44.262	2.83E-04	60.298	5.7499	93.603
7	72	184.78	42.576	3.41E-04	163.08	5.7193	93.721

Table 20. Test case 7 information and DRV identification script calculated variables. Red text indicates values outside the threshold cut-offs for DRV identification.

8. Test Case 8: "Fair"

Test case 8 is 0.04 K away from being a "good" forecast. The 48 hour control forecast created a baroclinic zone slightly too weak to be identified as conducive to DRV growth and the time-step was labelled a "miss." Otherwise test case 8 appears to be forecasting a DRV evolving similarly to the observed DRV with a rather large displacement error.

Test Case	Fcst Hr	Lon	Lat	Rel. Vort.	Dist.	Barocl.	Rel. Hum.
8	48	165.66	36.393	7.10E-04	464.74	4.9641	94.606
8	60	168.75	36.955	9.61E-04	403.11	5.75	94.355
8	72	178.03	38.642	5.92E-04	410.87	6.3993	94.464

Table 21. Test case 8 information and DRV identification script calculated variables. Red text indicates values outside the threshold cut-offs for DRV identification.

9. Test Case 9: "Poor"

Test case 9 forecasts suffer primarily from baroclinic zones that are judged too weak for DRV growth support. The initial forecast at DRV genesis is extremely misplaced and weak, but the 60 hour and 72 hour forecasts show increasing intensity and proximity to the observed DRV, yet are still short of a "hit" because of the poorly forecasted regions of downstream baroclinicity.

Test Case	Fcst Hr	Lon	Lat	Rel. Vort.	Dist.	Barocl.	Rel. Hum.
9	48	189	37.237	2.94E-04	660.81	4.9142	94.034
9	60	200.25	38.361	4.91E-04	283.12	3.4572	94.263
9	72	210.94	41.452	7.86E-04	94.1	3.3456	95.128

Table 22. Test case 9 information and DRV identification script calculated variables. Red text indicates values outside the threshold cut-offs for DRV identification.

10. Test Case 10: "Poor"

Over the course of the 48 hour, 60 hour, and 72 hour forecasts, the predicted disturbance track improves dramatically from 670 km to just 120 km. The forecast intensity never rises above minimum threshold standards, despite having a strong downstream baroclinic zone, and renders test case 10 a "poor" forecast.

Test Case	Fcst Hr	Lon	Lat	Rel. Vort.	Dist.	Barocl.	Rel. Hum.
10	48	156.09	34.145	2.01E-04	672.35	5.5618	93.52
10	60	161.16	34.707	3.13E-04	362.36	5.1656	93.532
10	72	168.19	34.707	3.09E-04	120.16	9.5173	93.785

Table 23. Test case 10 information and DRV identification script calculated variables. Red text indicates values outside the threshold cut-offs for DRV identification.

11. Test Case 11: "Poor"

Test case 11 represents the tropical cyclone Chaba case discussed in detail in M12. The initial 48 hour forecast for test case 11 is decent, meeting all criteria for DRV identification. Follow-on forecasts move the disturbance even further from observations and begin to weaken the system, most likely due to a weakened downstream field of baroclinicity in the 72 hour forecast. "Misses" of both the 60 hour and 72 hour forecast assess test case 11 as "poor."

Test Case	Fcst Hr	Lon	Lat	Rel. Vort.	Dist.	Barocl.	Rel. Hum.
11	48	138.94	32.178	3.81E-04	446.29	5.8888	93.826
11	60	144	33.583	3.90E-04	633.6	6.1527	93.666
11	72	159.47	36.674	2.92E-04	537.1	4.2705	93.724

Table 24. Test case 11 information and DRV identification script calculated variables. Red text indicates values outside the threshold cut-offs for DRV identification.

12. Test Case 12: "Good"

Test case 12 is the second example of a "good" control forecast, with excellent levels of intensity, relatively good tracking with the observed DRV, and strong downstream regions of baroclinicity for continued growth and development.

Test Case	Fcst Hr	Lon	Lat	Rel. Vort.	Dist.	Barocl.	Rel. Hum.
12	48	126	32.74	7.13E-04	115.95	8.2018	94.074
12	60	135	36.112	4.09E-04	394.4	7.1731	93.926
12	72	143.44	40.89	7.41E-04	158.43	7.9966	95.635

Table 25. Test case 12 information and DRV identification script calculated variables. Red text indicates values outside the threshold cut-offs for DRV identification.

C. SUMMARY OF CONTROL FORECAST PERFORMANCE

As defined by the identification script, the overall performance of the control forecasts for the 12 cases examined is quite poor. A DRV-like feature is properly identified only 33 percent of the time at all forecast lengths. It is apparent that the synoptic scale environment is more consistent with observed, as evidenced by the much higher hit rates for low-level baroclinicity and relative humidity. In contrast, the control forecasts appear to struggle to capture the mesoscale features of the observed DRV in terms of identifying a strong low-level vortex in the vicinity of the observed location.

A caveat to the above statements must be stated, however. It is distinctly possible the control forecasts are performing better than the results in this chapter would indicate. The predicted poor performance may be the result of deficiencies in the identification script. As has been previously mentioned, further examination of the relative vorticity threshold in particular should be undertaken

VII. ECMWF TIGGE PROBABILISTIC FORECASTS OF DRVS

A. OVERVIEW OF THE PROBABILISTIC APPROACH TO UNDERSTANDING THE UNCERTAINTY OF DRV FORECASTS

As the results of Chapter VI have clearly demonstrated, DRV prediction has so far proven problematic from a deterministic perspective. The overall performance of the ECMWF control forecasts was evaluated as "poor" with a hit rate of around 33 percent given leads times all under 72 hours.

In an effort to better understand both the poor control forecast performance and the uncertainty present in DRV predictability, a probabilistic approach is being pursued in the following sections of this chapter. Sea level pressure (SLP) mean and spread plots of the 51 ECMWF ensemble forecasts in the regions of the observed DRVs were created in an effort to define the general environmental variability associated with the areas of interest. The 50 perturbed ECMWF ensemble member forecasts were collected and statistically analyzed in the hope of better understanding the uncertainty of the predictability of DRVs by analyzing the calculated variable outputs across the initial 24 hour DRV lifespan.

B. 72 HOUR ECMWF 51 ENSEMBLE MEMBER FORECAST SEA LEVEL PRESSURE MEANS AND STANDARD DEVIATIONS

As a first step in obtaining a general awareness of the uncertainty the ECMWF ensemble system forecasts are producing in the vicinity of the observed DRVs, mean and spread plots of the sea level pressures at the 72 hour lead time were created. The 72 hour lead time was chosen for SLP study as the most likely to start of the three time periods studied associate SLP change with the developing DRVs (previous discussions within this study have shown SLP to be only moderately impacted early in DRV evolution).

A detailed examination at the magnitudes and locations of uncertainty will be investigated for each of the 12 test cases. To create the mean and spread plots in the following sections, the SLP mean and standard deviation of the 51 ECMWF ensemble forecasts were calculated and overlaid on maps with the mean represented by contours and magnitude of standard deviation by shading.

1. DRV01 72 Hour ECMWF Ensemble Forecast SLP Mean and Spread

The observed location of DRV01 is approximately 750 km to the southwest of an area of extreme uncertainty, with a wide lobe of heightened uncertainty intruding into the area of DRV01 from the northwest (Figure 94). The standard deviation value of approximately 5 hPa at the DRV01 position is moderately high and indicates there is a fair amount of spread and variability of ensemble member forecasts at this lead time. The ensemble forecast mean does not appear to be distinguishing any small scale features in the general flow pattern.

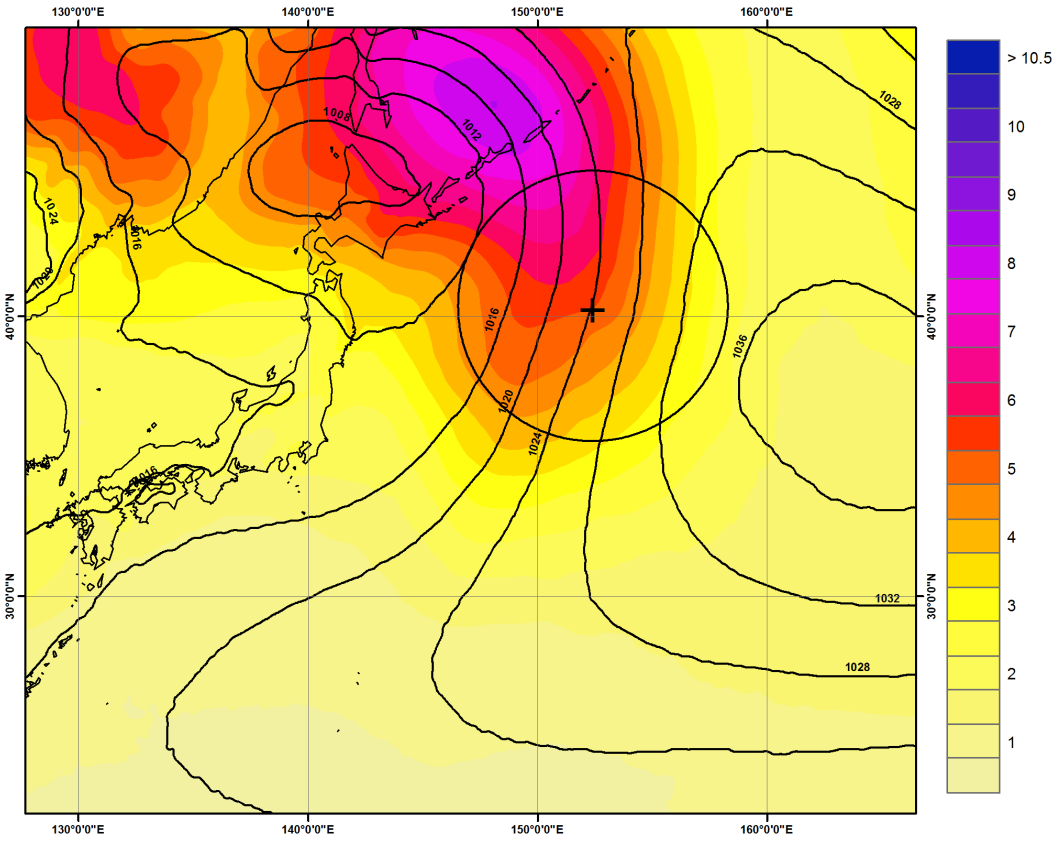

Figure 94. Test case 1 SLP mean and standard deviation spread map of the 72 hour ECMWF TIGGE probabilistic forecast (Valid time 12 UTC 5 March 2010). Climatology DRV location is annotated by "+" with a 500 km radius ring. Shading represents the standard deviation (colorbar; hPa) and black contours represent the mean (every four hPa) of the 51 ECMWF ensemble member forecasts of SLP for the 72 hour forecast time.

2. DRV02 72 Hour ECMWF Ensemble Forecast SLP Mean and Spread

The observed DRV02 position is co-located with an extraordinarily strong center of ensemble forecast variability. The mean SLP on the other hand is indicating a developing low in the region of the observed SLP, giving possible indication that despite the large amount of uncertainty, the ensemble is generally developing a developing low pressure disturbance in the vicinity of the observed DRV02 position.

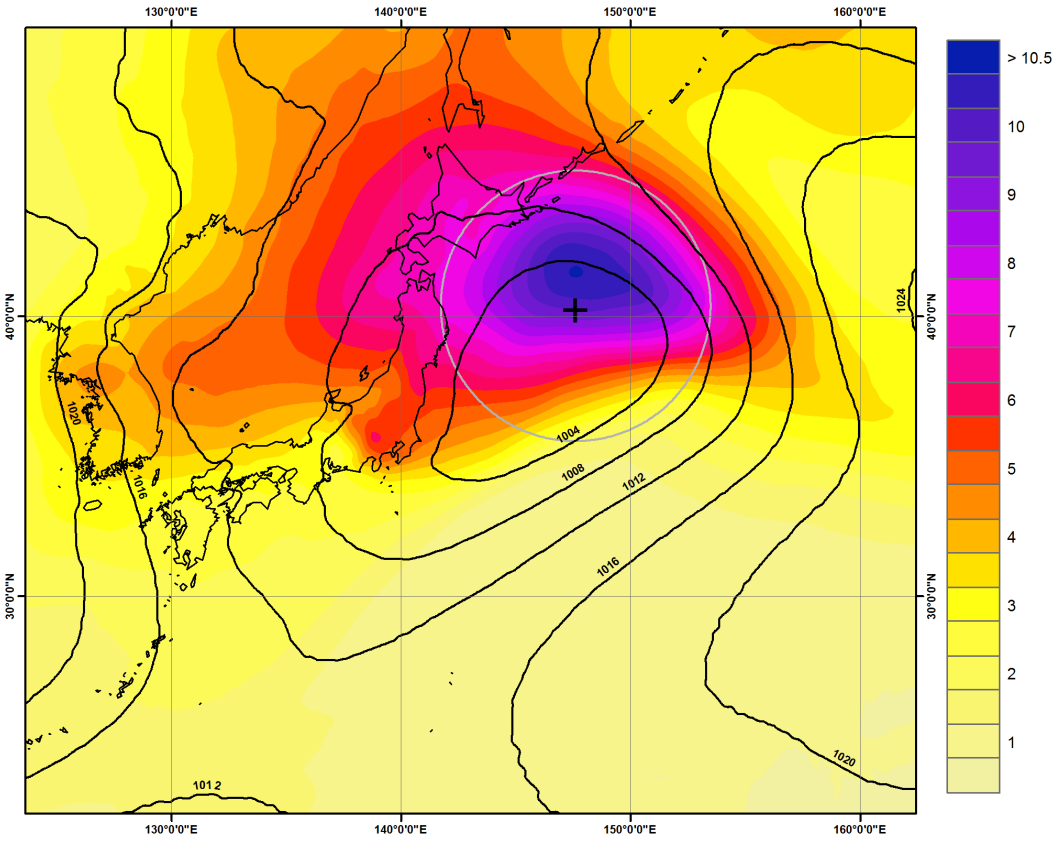

Figure 95. Test case 2 SLP mean and standard deviation spread map of the 72 hour ECMWF TIGGE probabilistic forecast (Valid time 12 UTC 25 March 2010). Climatology DRV location is annotated by "+" with a 500 km radius ring. Shading represents the standard deviation (colorbar; hPa) and black contours represent the mean (every four hPa) of the 51 ECMWF ensemble member forecasts of SLP for the 72 hour forecast time.

3. DRV03 72 Hour ECMWF Ensemble Forecast SLP Mean and Spread

The SLP mean for the 72 hour ECMWF ensemble forecast system appears to be developing a small scale disturbance in the vicinity of the observed DRV03. A moderate amount of uncertainty (standard deviation above 5 hPa) is co-located with both the observed DRV03 position and the short-wave disturbance.

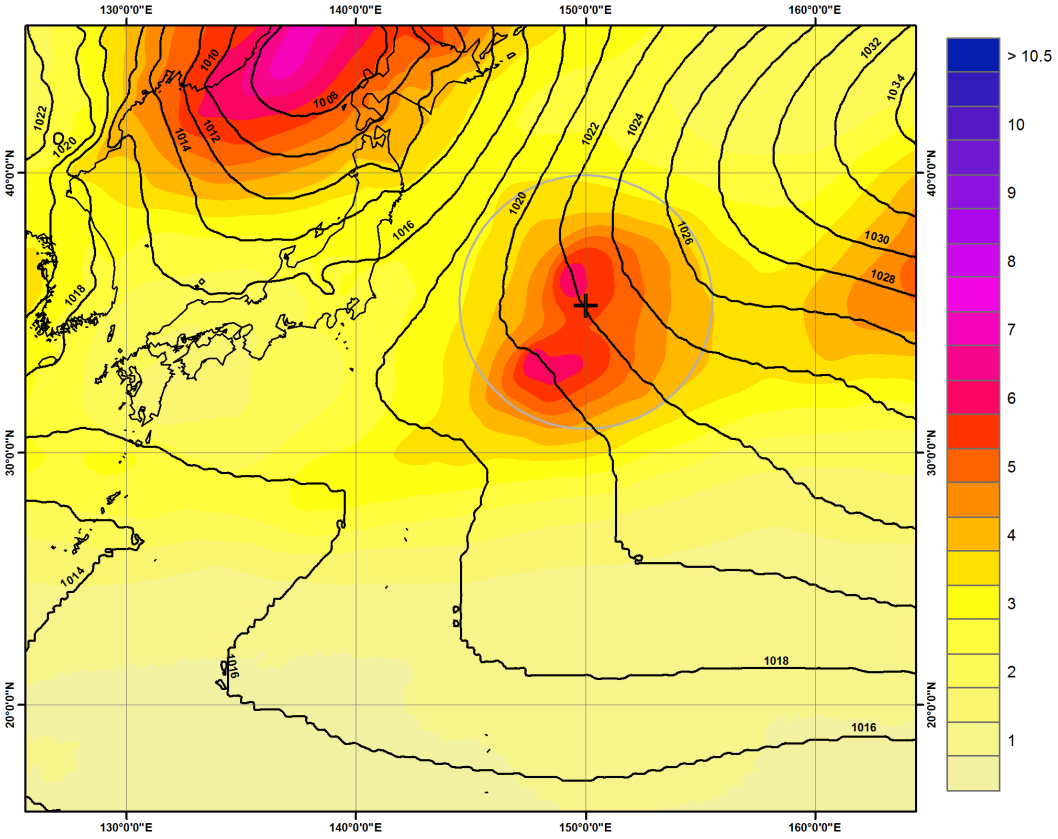

Figure 96. Test case 3 SLP mean and standard deviation spread map of the 72 hour ECMWF TIGGE probabilistic forecast (Valid time 00 UTC 6 April 2010). Climatology DRV location is annotated by "+" with a 500 km radius ring. Shading represents the standard deviation (colorbar; hPa) and black contours represent the mean (every two hPa) of the 51 ECMWF ensemble member forecasts of SLP for the 72 hour forecast time.

4. DRV04 72 Hour ECMWF Ensemble Forecast SLP Mean and Spread

The observed DRV04 position also appears to be located near a short-wave disturbance in the mean ensemble forecast SLP, but in this case there is very little variation in the vicinity of the disturbance, indicating good agreement between the ensemble members. This is the only test case that wasn't co-located with at least a moderate amount of ensemble forecast variability. This could be an outlier or a case of all ensemble forecasts completely misforecasting the actual SLP disturbance caused by the observed DRV. There is an indication of forecast low pressure system downstream of the observed DRV location and observed with a moderate amount of uncertainty, and it's possible the forecast DRV-related disturbance could be completely misplaced in the ensemble forecast system.

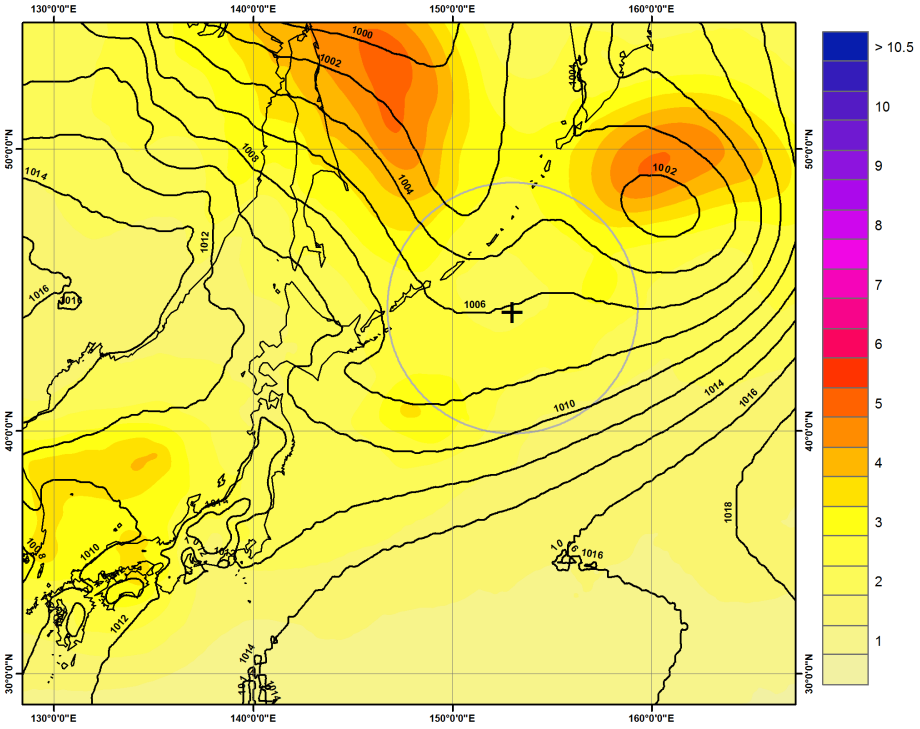

Figure 97. Test case 4 SLP mean and standard deviation spread map of the 72 hour ECMWF TIGGE probabilistic forecast (Valid time 12 UTC 7 September 2010). Climatology DRV location is annotated by "+" with a 500 km radius ring. Shading represents the standard deviation (colorbar; hPa) and black contours represent the mean (every two hPa) of the 51 ECMWF ensemble member forecasts of SLP for the 72 hour forecast time.

5. DRV05 72 Hour ECMWF Ensemble Forecast SLP Mean and Spread

DRV05, much like DRV02 above, is located in the vicinity of both a strong ensemble forecast mean SLP low pressure system and in an area of high uncertainty. A very high spread is observable to the north of the DRV05 position and could be responsible for a highly variable location of the ensemble forecast disturbance positioning.

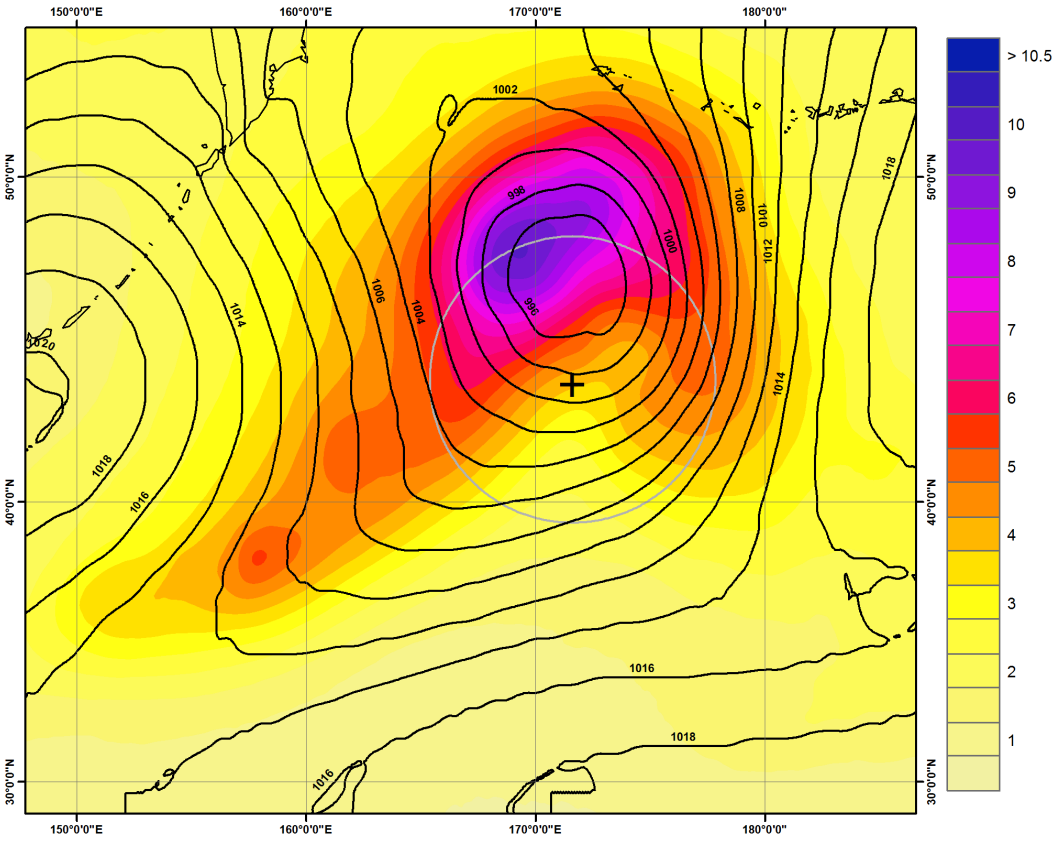

Figure 98. Test case 5 SLP mean and standard deviation spread map of the 72 hour ECMWF TIGGE probabilistic forecast (Valid time 00 UTC 15 September 2010). Climatology DRV location is annotated by "+" with a 500 km radius ring. Shading represents the standard deviation (colorbar; hPa) and black contours represent the mean (every two hPa) of the 51 ECMWF ensemble member forecasts of SLP for the 72 hour forecast time.

6. DRV06 72 Hour ECMWF Ensemble Forecast SLP Mean and Spread

DRV06 is located along an ensemble forecast mean short-wave trough, in an area of moderate uncertainty. Similar again to the test cases located along ensemble forecast short-wave disturbances, there is likely a general agreement between the ensemble members that a disturbance is moving through the region, but placement is likely highly variable, as indicated by the moderate values of SLP standard deviation in the same location.

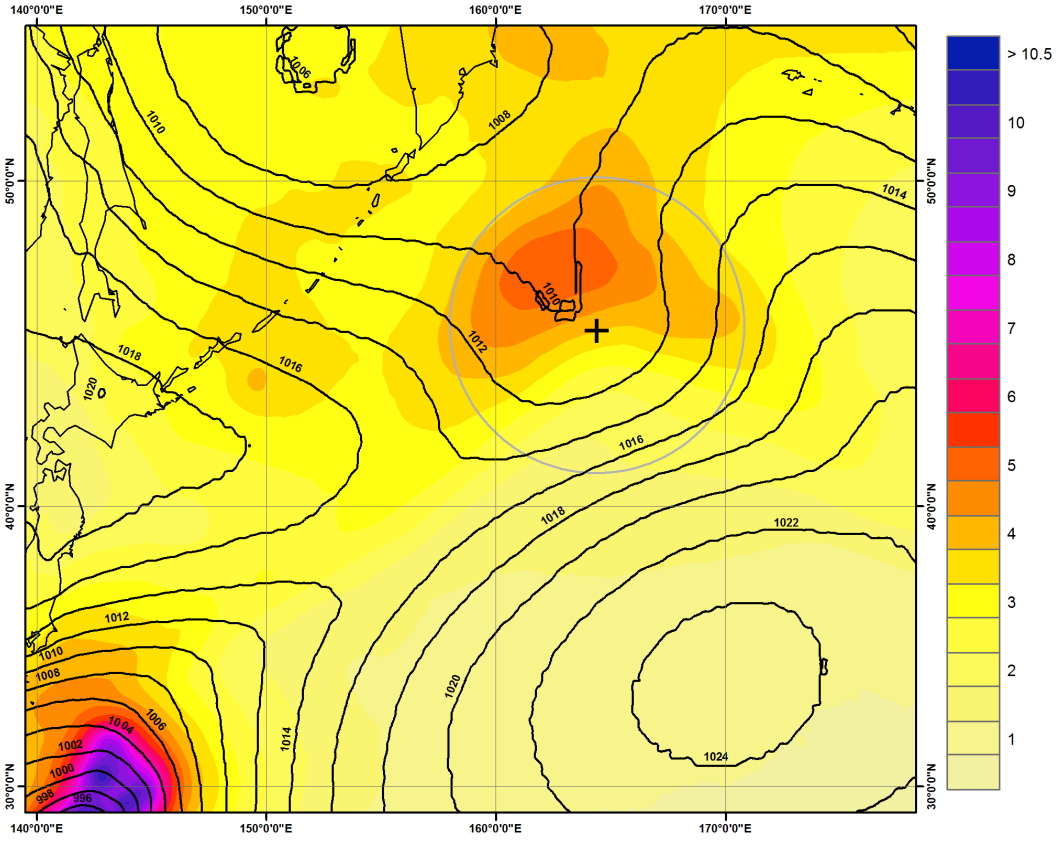

Figure 99. Test case 6 SLP mean and standard deviation spread map of the 72 hour ECMWF TIGGE probabilistic forecast (Valid time 12 UTC 24 September 2010). Climatology DRV location is annotated by "+" with a 500 km radius ring. Shading represents the standard deviation (colorbar; hPa) and black contours represent the mean (every two hPa) of the 51 ECMWF ensemble member forecasts of SLP for the 72 hour forecast time.

7. DRV07 72 Hour ECMWF Ensemble Forecast SLP Mean and Spread

The DRV07 ensemble forecast mean is locating a short-wave disturbance moving through the area of the observed DRV, but again, there the intensity and location of the disturbance are going to highly vary between the ensemble members. The area in the immediate vicinity of the observed DRV is showing moderate-high variability of the ensemble forecast SLP field, which again reaffirms the general spread of ensemble forecasts in the vicinity of DRVs in the studied test cases.

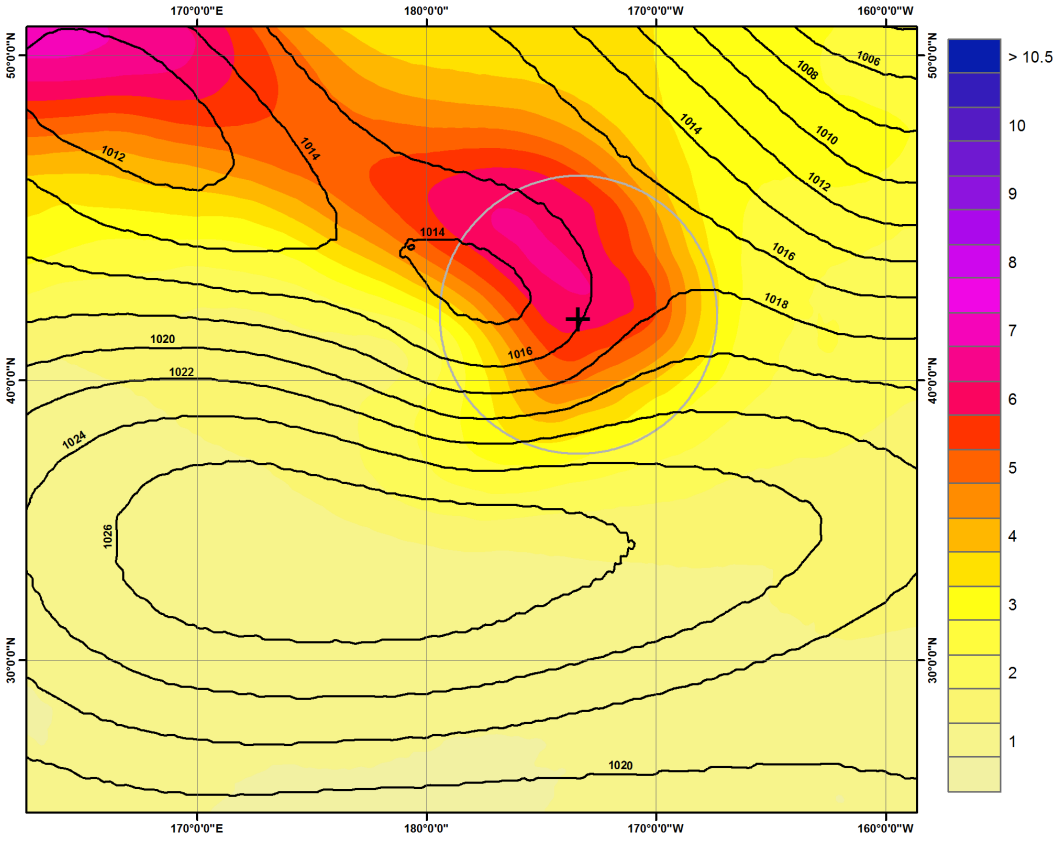

Figure 100. Test case 7 SLP mean and standard deviation spread map of the 72 hour ECMWF TIGGE probabilistic forecast (Valid time 12 UTC 06 October 2010). Climatology DRV location is annotated by "+" with a 500 km radius ring. Shading represents the standard deviation (colorbar; hPa) and black contours represent the mean (every two hPa) of the 51 ECMWF ensemble member forecasts of SLP for the 72 hour forecast time.

8. DRV08 72 Hour ECMWF Ensemble Forecast SLP Mean and Spread

The ensemble forecast mean SLP field is indicating a closed low in the vicinity of the observed DRV08. The closed low system is a good indication that the ensemble forecasts are generally identifying a disturbance in the vicinity of the observed DRV, but again there is moderate-high levels of SLP standard deviation in the ensemble forecast, indicated a high degree of uncertainty in magnitude and location of the positioning.

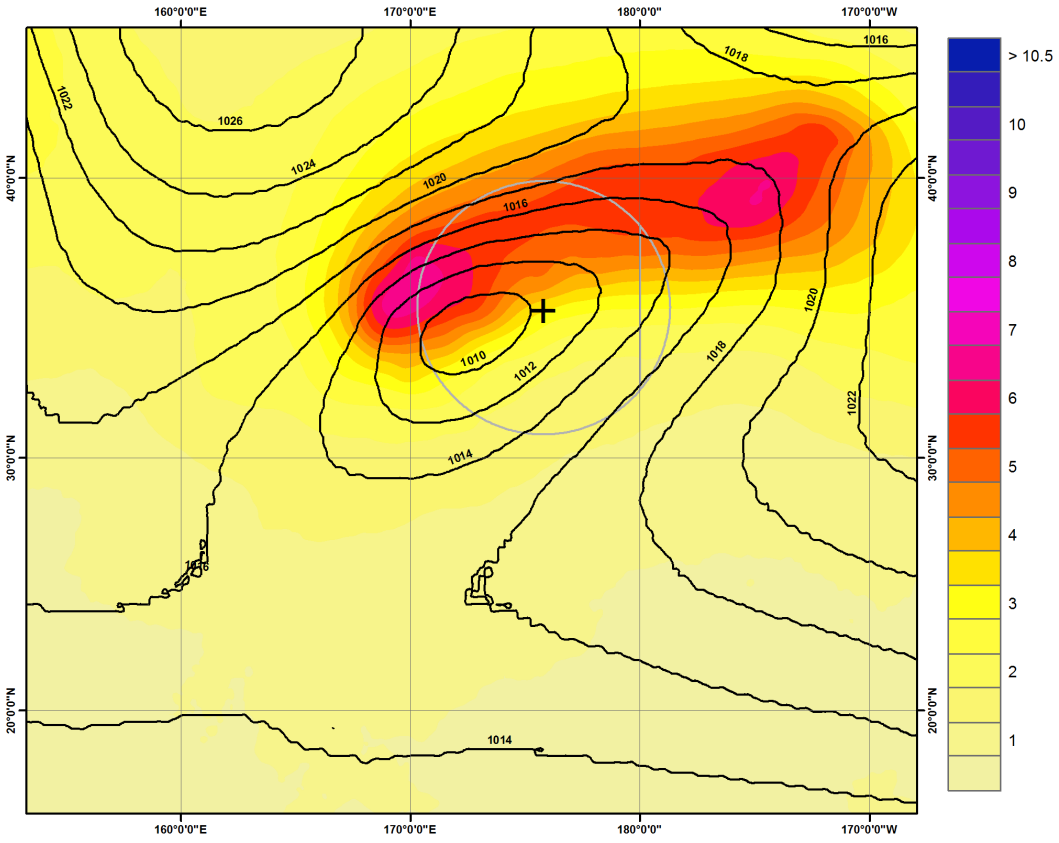

Figure 101. Test case 8 SLP mean and standard deviation spread map of the 72 hour ECMWF TIGGE probabilistic forecast (Valid time 12 UTC 10 October 2010). Climatology DRV location is annotated by "+" with a 500 km radius ring. Shading represents the standard deviation (colorbar; hPa) and black contours represent the mean (every two hPa) of the 51 ECMWF ensemble member forecasts of SLP for the 72 hour forecast time.

9. DRV09 72 Hour ECMWF Ensemble Forecast SLP Mean and Spread

The ensemble forecast SLP mean is exhibiting a short-wave disturbance with a closed low in the vicinity of the observed DRV09. The ensemble forecast maximum uncertainty and spread is co-located with the short-wave disturbance and closed low, again signaling a disagreement between ensemble forecasts on location and intensity of this disturbance pattern.

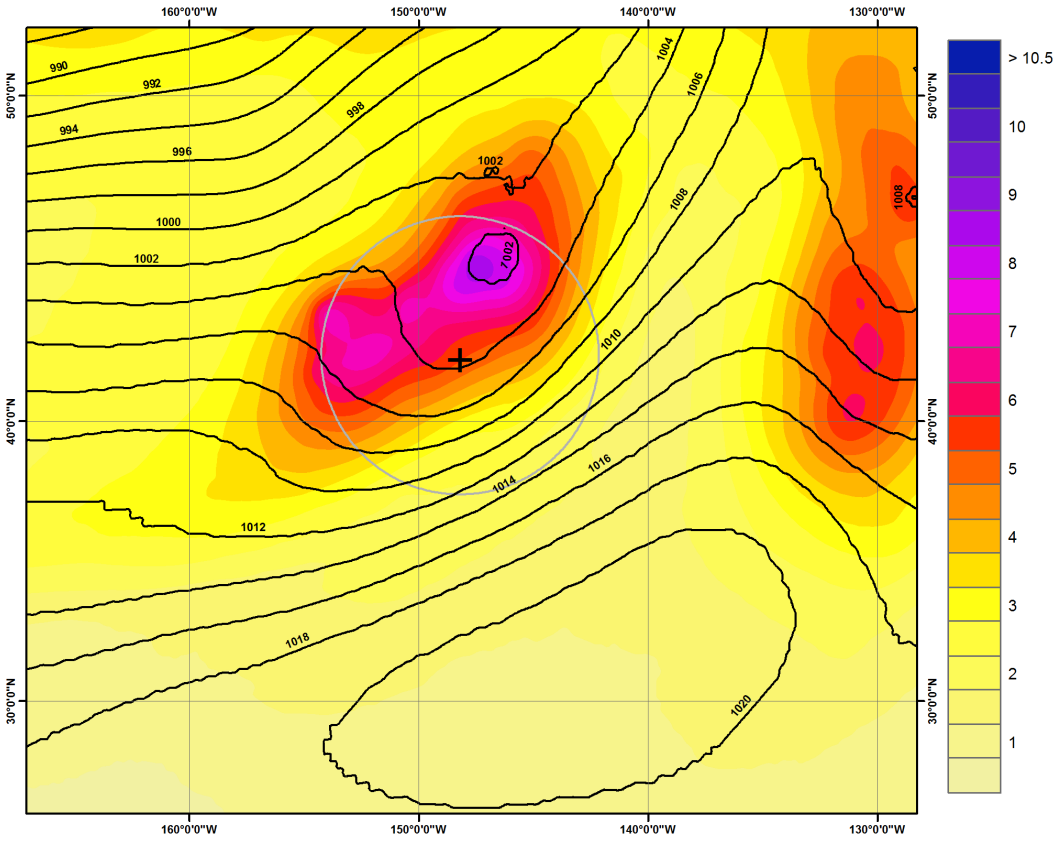

Figure 102. Test case 9 SLP mean and standard deviation spread map of the 72 hour ECMWF TIGGE probabilistic forecast (Valid time 00 UTC 22 October 2010). Climatology DRV location is annotated by "+" with a 500 km radius ring. Shading represents the standard deviation (colorbar; hPa) and black contours represent the mean (every two hPa) of the 51 ECMWF ensemble member forecasts of SLP for the 72 hour forecast time.

10. DRV10 72 Hour ECMWF Ensemble Forecast SLP Mean and Spread

The ensemble forecast mean SLPs in the vicinity of observed DRV10 are displaying an elongated area of closed SLP with an accompanying low-to-moderate area of uncertainty. The general pattern suggests the ensemble forecasts are not forecasting a specific disturbance in the vicinity, but perhaps an elongated band of general convection and instability. This pattern is unique in the test cases and would require further investigation to explain the exhibited structure.

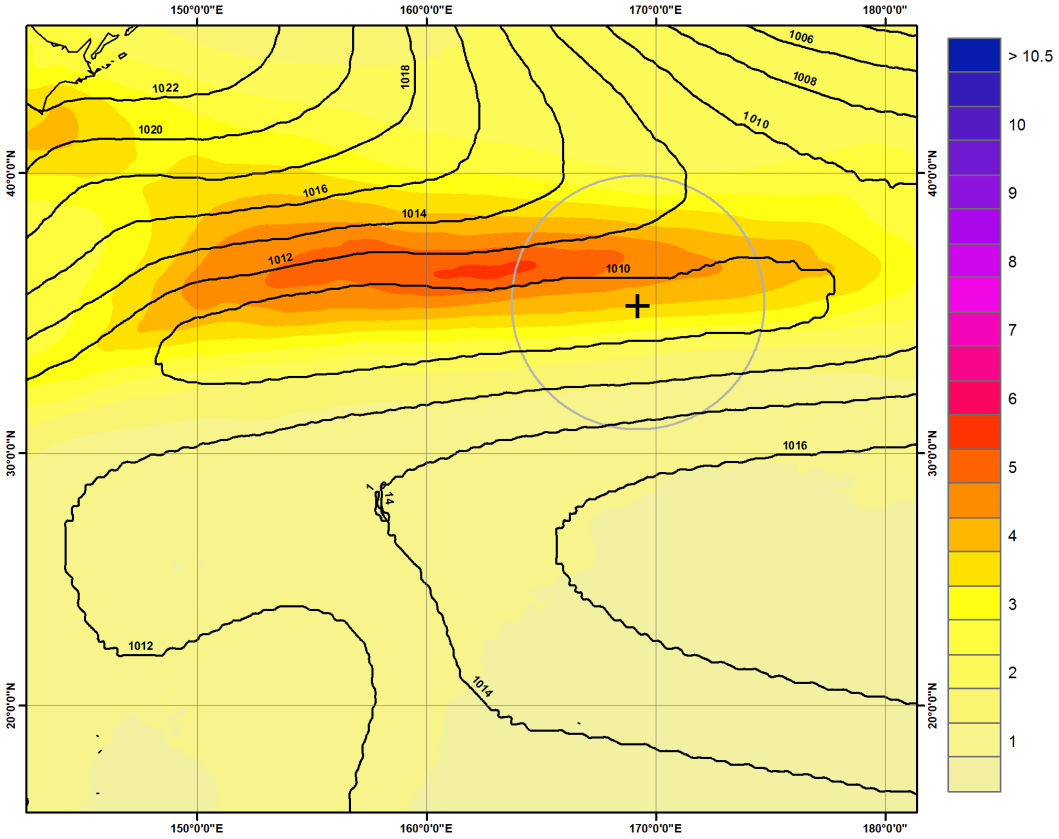

Figure 103. Test case 10 SLP mean and standard deviation spread map of the 72 hour ECMWF TIGGE probabilistic forecast (Valid time 00 UTC 22 October 2010). Climatology DRV location is annotated by "+" with a 500 km radius ring. Shading represents the standard deviation (colorbar; hPa) and black contours represent the mean (every two hPa) of the 51 ECMWF ensemble member forecasts of SLP for the 72 hour forecast time.

11. DRV11 72 Hour ECMWF Ensemble Forecast SLP Mean and Spread

The ensemble forecast SLP mean is displaying an area of moderate uncertainty above and inverted trough in the vicinity of the observed DRV. As examined in the test case for the TC Chaba, the control forecast identified relative vorticity maximum was to the south of the actual disturbance, likely a result of the baroclinic front placement, and this ensemble forecast uncertainty in the same general area could be an extension of that observation.

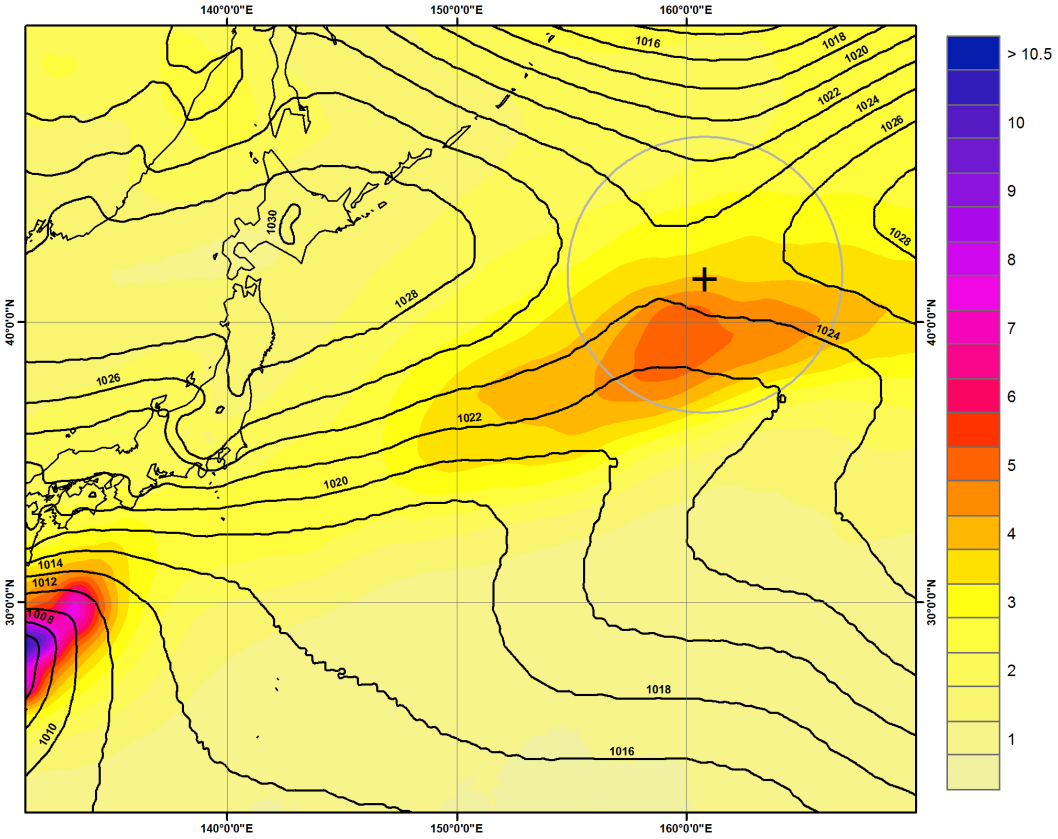

Figure 104. Test case 11 SLP mean and standard deviation spread map of the 72 hour ECMWF TIGGE probabilistic forecast (Valid time 12 UTC 29 October 2010). Climatology DRV location is annotated by "+" with a 500 km radius ring. Shading represents the standard deviation (colorbar; hPa) and black contours represent the mean (every two hPa) of the 51 ECMWF ensemble member forecasts of SLP for the 72 hour forecast time.

12. DRV12 72 Hour ECMWF Ensemble Forecast SLP Mean and Spread

The ensemble forecast SLP mean is locating a strong closed low disturbance neighboring the observed DRV position. This is a strong indication that there is general agreement between the ensemble forecasts that a disturbance exists, but the moderate-high values of ensemble forecast SLP standard deviation in overlapping the position of the closed low also reveal a discrepancy in ensemble agreement on location and intensity of the developing low-pressure system.

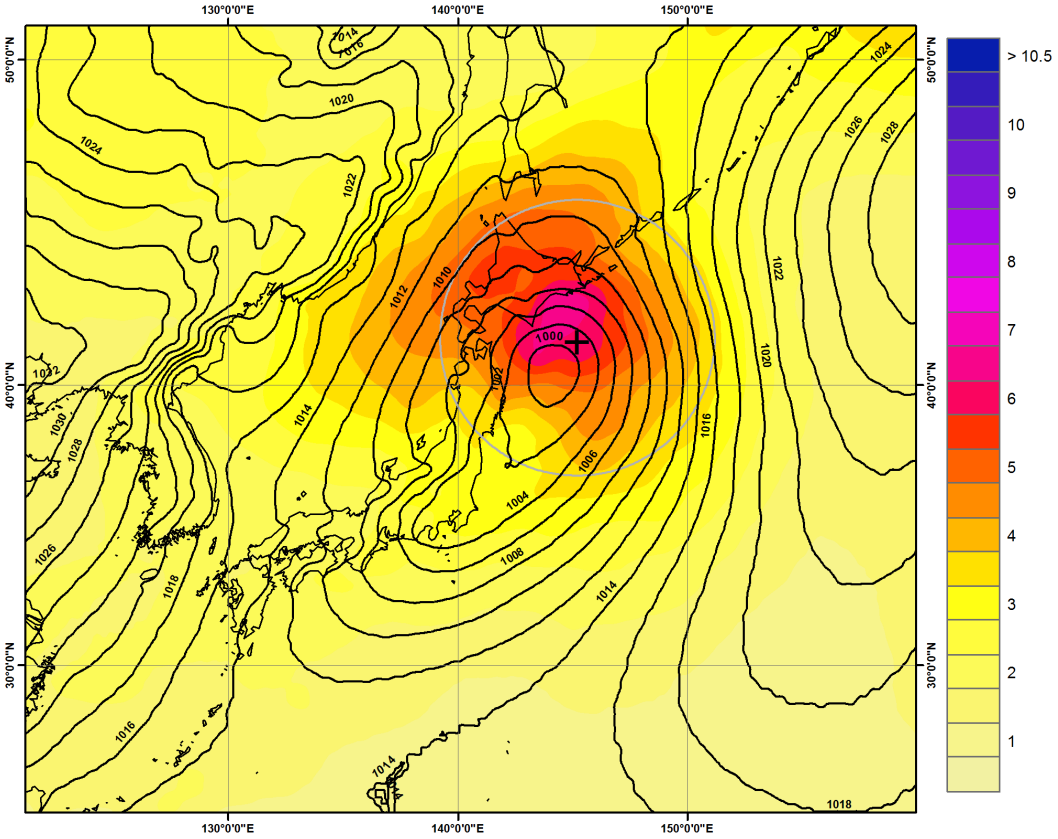

Figure 105. Test case 12 SLP mean and standard deviation spread map of the 72 hour ECMWF TIGGE probabilistic forecast (Valid time 00 UTC 14 December 2010). Climatology DRV location is annotated by "+" with a 500 km radius ring. Shading represents the standard deviation (colorbar; hPa) and black contours represent the mean (every two hPa) of the 51 ECMWF ensemble member forecasts of SLP for the 72 hour forecast time.

13. 72 Hour ECMWF Ensemble Forecast SLP Mean and Spread Summary

In almost all test cases the 72 hour ensemble forecast mean SLP mean indicated either a short-wave disturbance or closed low in the vicinity of the observed DRVs, indicating that the forecasts in general were forecasting a disturbance. The high variability of the ensemble forecast spread indicates a generally moderate-to-high level of uncertainty about the placement and the intensity of the disturbances.

This is of high interested when trying to understand the variability of DRV forecasting because the intensity and placement of features is key. As was investigated and discussed in Chapters 4 and 5, a misplacement of a baroclinic front or initial location of the disturbance can have a negative impact of the development of the disturbance in following forecast lead times.

C. OVERALL PERFORMANCE AND STATISTICS OF THE ECMWF TIGGE PROBABILISTIC FORECASTS

1. Perturbed Forecasts Summary

The ECMWF TIGGE ensemble data provides 1 control and 50 perturbed forecasts for each lead time of the 12 test cases. The control forecasts were analyzed and summarized in Chapter 6. The remaining 50 perturbed forecast members will be analyzed and summarized with the intention of achieving a better understanding of initial condition and control forecast uncertainty.

The resulting dataset is 600 perturbed forecasts at each of the three forecast times, with an end dataset size of 1800 perturbed forecasts. Finally, for the sake of organization and evaluation, the perturbed forecasts are sorted into aggregate cases that consist of the 48, 60, and 72 hour perturbed forecasts for each test case and each ensemble member, for a total of 600 perturbed aggregate cases.

In an effort to compare the overall performance of the perturbed forecasts with that of the control forecasts, the same criteria of “good,” “fair,” and “poor” performance metrics were applied from Chapter 6.

When analyzed over the 24 hour period from genesis through early propagation, 8.0 percent of the perturbed aggregate cases were found to meet the criteria of a "good" forecast, 15.8 percent met the criteria for "fair," and 76.2 percent were judged "poor" (Figure 106).

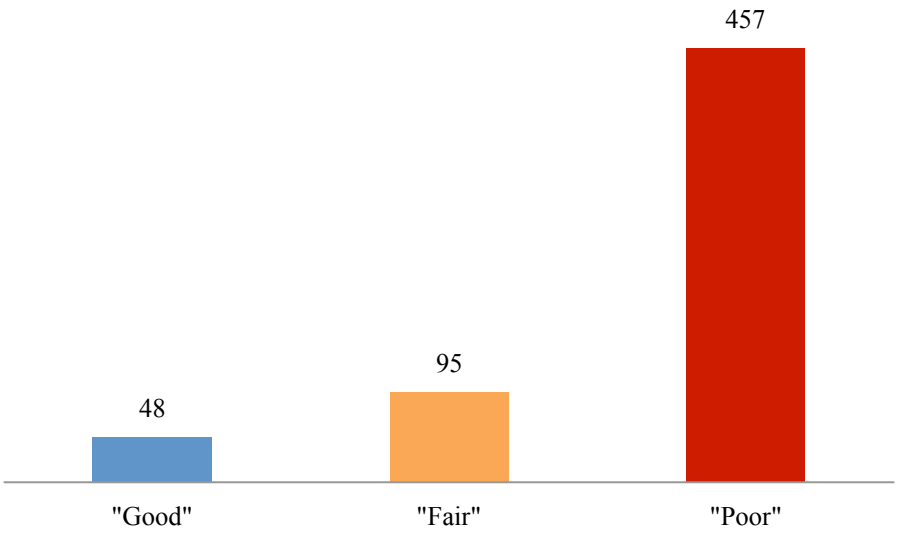

Figure 106. Perturbed forecast performance over the first 24 hours of a DRV lifespan for 600 perturbed aggregate cases.

These results are extremely similar to the evaluations of the 12 control forecast test cases. The noticeable difference between the perturbed forecast and control forecast evaluations is that the perturbed evaluations of "fair" forecasts was nearly double the number of "good" forecasts, whereas there were an equal number of "fair" and "good" evaluations of control test cases. Further investigation reveals that the percentage of "good" forecasts for the perturbed aggregate cases was nearly half the value of the control test case. The number of "fair" cases remained roughly the same between control and perturbation cases. The conclusion from these comparisons is that the control forecasts performance was likely above what should be realistically expected of early lifecycle DRV predictions. The small sample size of the control forecasts is likely culprit for the overestimation of "good" overall forecasts.

In a similar manner to the in-depth study of the DRV identification script output variables completed in chapter 6, the remainder of this chapter will be devoted to better understanding the spread and searching for any general trending, patterns, or bias of the perturbation forecasts.

2. Perturbed Forecast "Hits" of Initial DRV Genesis

Of the 600 perturbed forecasts at the time of observed DRV genesis (48 hour forecast) 23.7 percent we registered as "hits" (Figure 107). This is below the 33.3 percent initial detection in 48 hour control forecasts (Chapter 6). Again this large sample size is probably a better indicator of the general expected performance and indicates the 48 hour control forecasts likely slightly overestimated "hits" at DRV genesis.

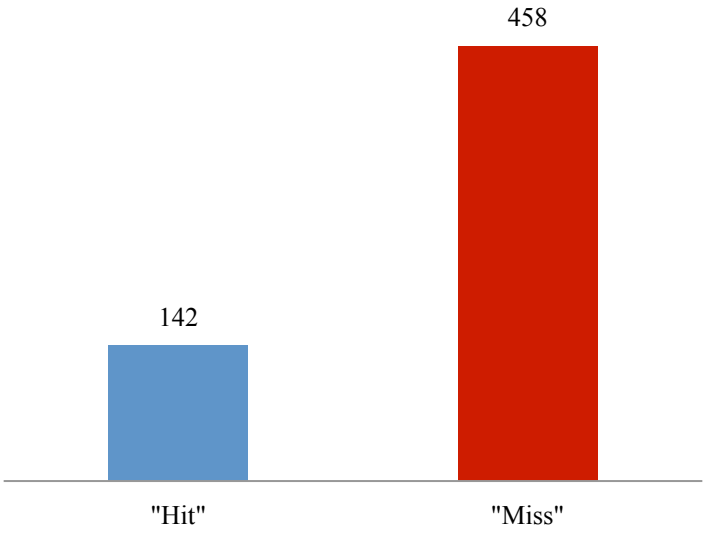

Figure 107. 48 hour perturbed forecast "hits" and "misses."

3. Perturbed Forecast "Hits" after 12 Hours of Propagation

The 60 hour perturbed forecasts exhibit a marked increase in DRV forecast skill with a jump to 31.2 percent; almost matching the 60 hour control forecast "hit" percentage of 33 percent noted in Chapter 5 (Figure 108). The similar "hit" percentage confirms the 60 hour control forecasts "hit" percentage as likely a good indication of expected "hit" chance.

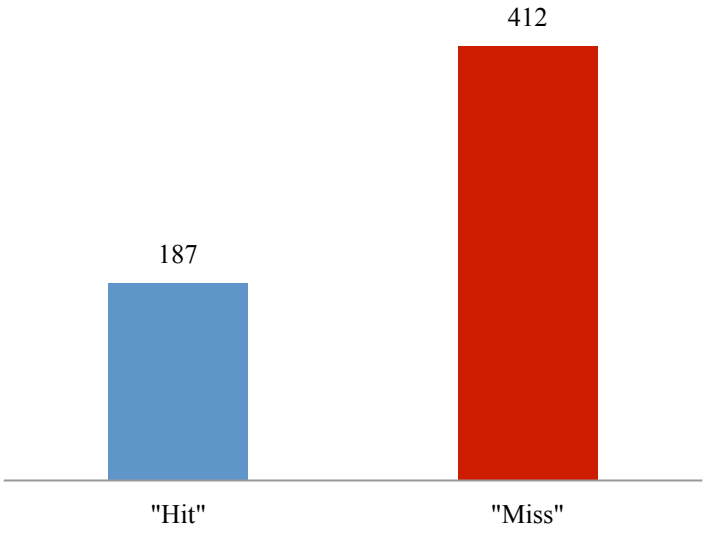

Figure 108. 60 hour perturbed forecast “hits” and “misses.”

4. Perturbed Forecast “Hits” After 24 Hours of Propagation

Perturbed forecasts “hits” again slightly increase over the previous 12 hour time-step. The 72 hour perturbed forecasts exhibited a 33 percent “hit”-rate (Figure 109), which was exactly the same percentage as the 72 hour control forecasts; a good indicator of the 72 hour control forecast “hit” rate as an acceptable result.

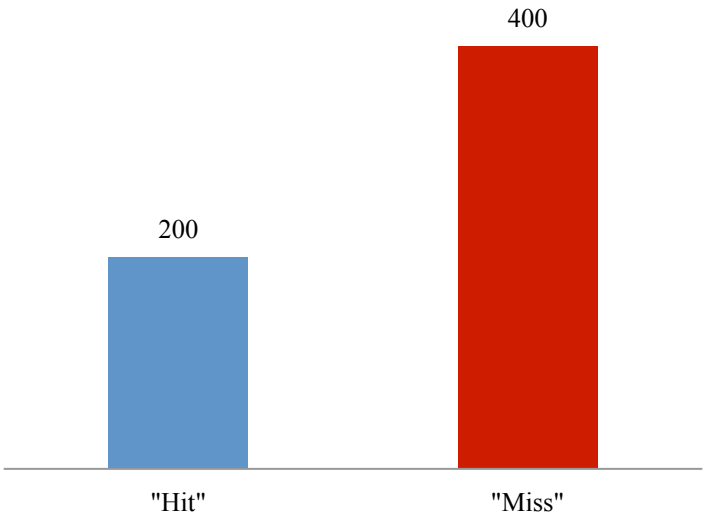

Figure 109. 72 hour perturbed forecast “hits” and “misses.”

5. Increasing "Hit"-rate over Time for Perturbed Forecasts

There was a slight, but noticeable, improvement in perturbed forecast "hit"-rate over the initial 24 hours of the 12 observed DRVs. This is likely a better indication of what to expect with regard to DRV forecasting in general (as is the lower overall "hit" rate of perturbed "hits"; Figure 110). Increasing storm strength and a more detectable signal at later periods of evolution also support the notion that the perturbation forecasts would potentially generate a storm that meets DRV thresholds further along the DRV lifespan, as discussed in the case studies in Chapter 2 and in-depth analysis of Chapter 4. The flat "hit" rate of the control forecasts through the 24 hour lead times was noted as not expected at the time and these results further confirm that they were most likely the result of the small sample size.

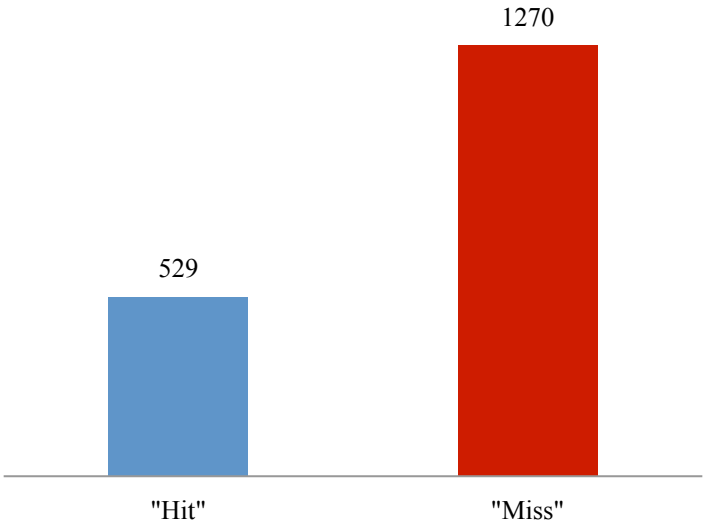

Figure 110. Performance of the 1800 perturbed forecasts.

D. OVERVIEW OF RELATIVE VORTICITY MAXIMA PERTURBATION FORECASTS

1. Perturbation Forecasts Meeting Relative Vorticity Thresholds

The number of perturbed forecasts meeting the minimum threshold for relative vorticity maximum value (59.2 percent) was overall higher than the control forecast

percentage (50%), again indicating the small sample size was most likely misrepresenting the expected number of forecasts that would be expected to meet threshold.

When broken down by forecast lead time, the perturbed forecasts show a moderate increase in detected "hits" at 60 hours and then a slight drop again 72 hours (the drop at 72 hours examined in detail in the next section). The increase in detected hits from genesis to 12 hour later is an expected result of the dynamics of the strengthening disturbance discussed in detail in the previous section.

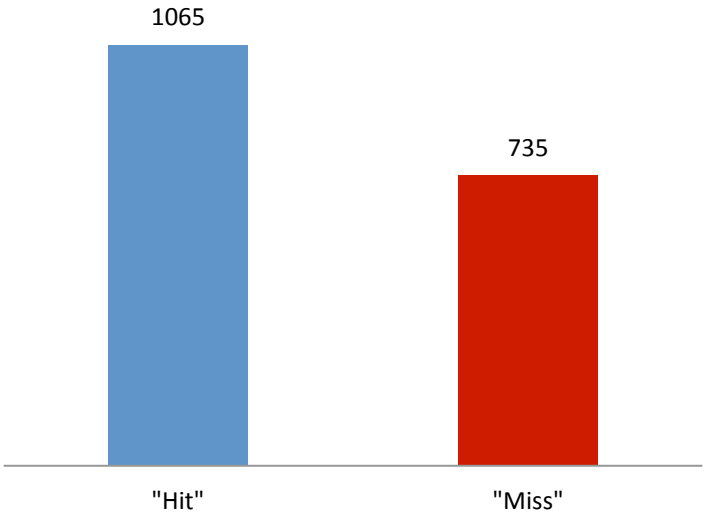

Figure 111. Histogram of the 1800 perturbation forecast's relative vorticity maxima below (red; "miss") and above (blue; "hit") the threshold value of 3.5 x 10^{-4} s^{-1}.

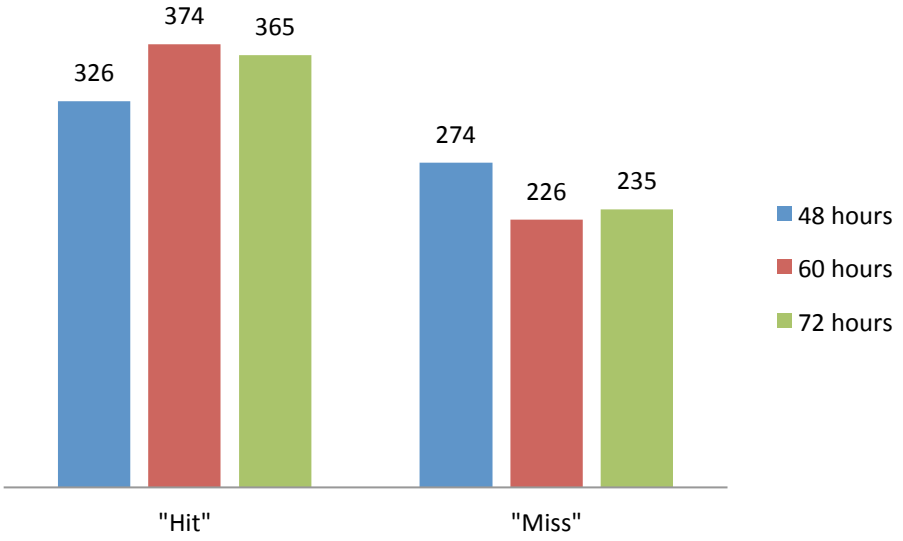

Figure 112. Histogram of the perturbation forecast's relative vorticity maxima at each forecast length. ("Hit" and "Miss" as defined above)

2. Detailed Perturbed Forecast Relative Vorticity Maxima Value Analysis

Examining the frequency distribution of the identified relative vorticity maxima (Figure 113), a few patterns emerge. The lower values with a high mode below threshold at the 48 hour forecast time indicate the weaker state of the identified disturbances and the decreased likelihood of detection. The strong mode below the threshold relative vorticity maximum value still exists at 60 hours, but there is now strong representation in the distribution above the threshold, as well. Finally at 72 hour, the forecasts spread significantly, indicating a much higher level of uncertainty at that forecast lead time.

The general trends of the mean and standard deviation of the relative vorticity maxima confirm what is observed in the frequency distribution graph. The steady mean value increase observed from the 48 hour perturbed forecast through the 72 hour perturbed forecast are matched by increasing standard deviations at each forecast lead time. This indicates increasing forecast strength, but also increasing uncertainty.

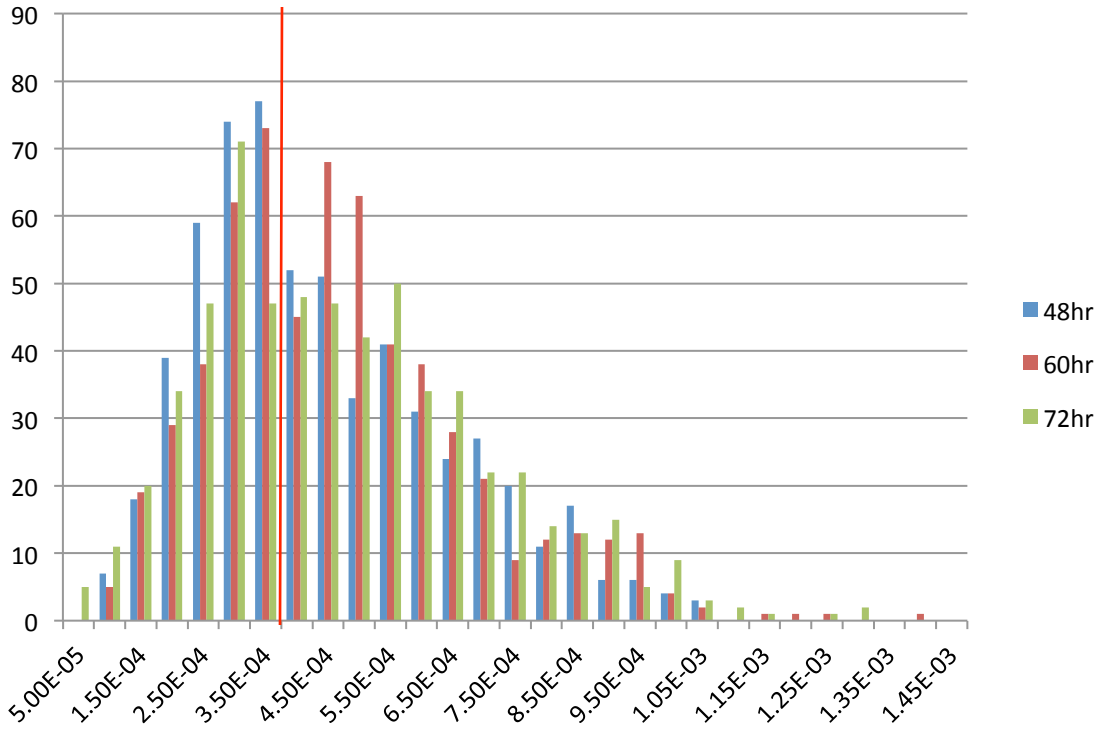

Figure 113. Histogram of perturbed forecast relative vorticity maxima values with a 0.5 x 10^{-4} s^{-1} bin size. The numbers under each bar represent the upper value of the bin. The red line indicates the threshold cut-off for DRV identification.

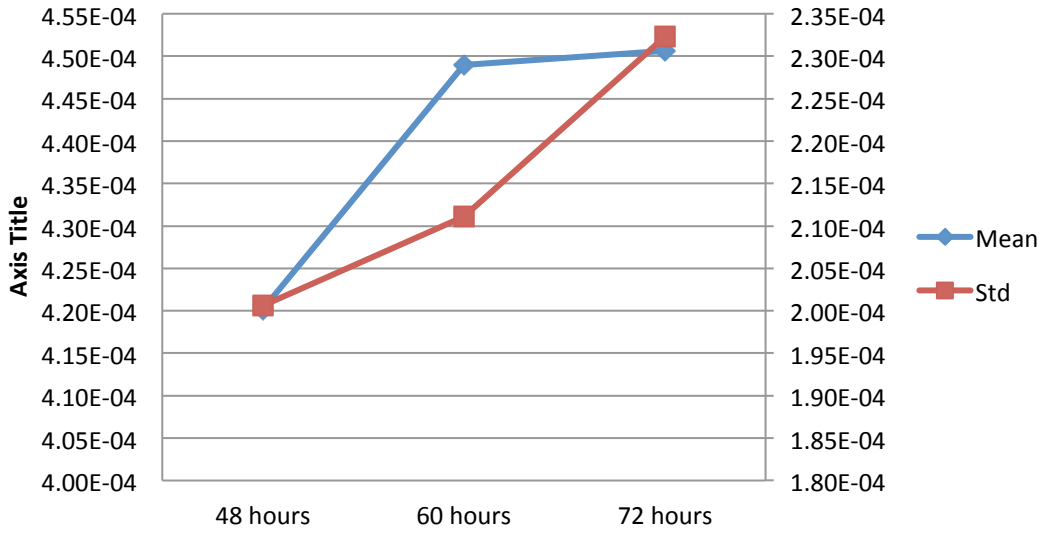

Figure 114. Perturbed forecast relative vorticity maxima mean and spread for 48, 60, and 72 hours.

E. OVERVIEW OF PERTURBED FORECAST DISTANCE TO OBSERVED DRVS

1. Perturbed Forecasts Meeting Maximum Distance Thresholds

Perturbed forecasts meeting maximum distance thresholds and registering as "hits" was found to be approximately 62.9 percent (Figure 115). This value was slightly below the control forecast percentage of 69.4, but again, is probably a more realistic result of what to expect given the larger sample size. Examination of hit rate by perturbation forecast lead time reveals relatively little variation (Figure 116).

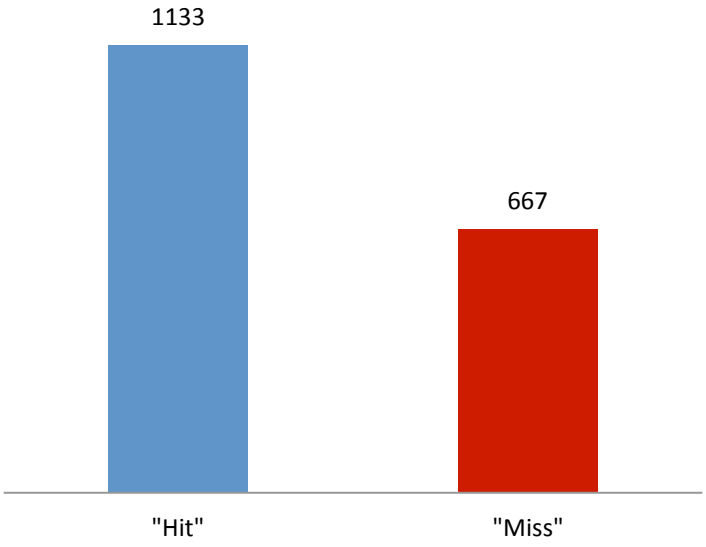

Figure 115. Histogram of the thresholds met for the 1800 perturbed forecast distances to observed DRVs. Forecasts less than 500 km (blue) are considered "hits," while forecasts greater than 500 km (red) are considered "misses."

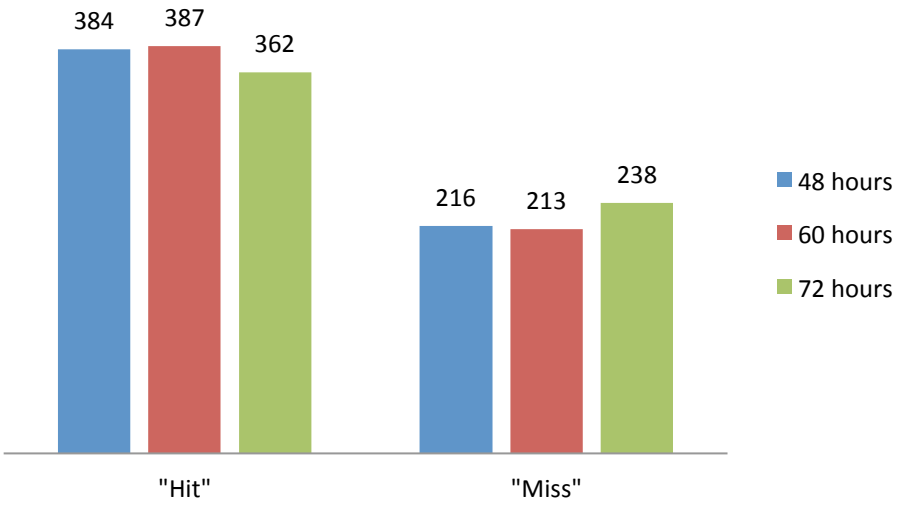

Figure 116. Histogram of the perturbation forecast distances threshold results at each forecast length. ("Hit" and "Miss" as defined above.)

2. Detailed Analysis of Perturbation Forecast Distances from Observed DRVs

Examination of the frequency distribution reveals a generally bimodal histogram with a very large spread (Figure 117). Even more so than the relative vorticity maxima frequency distribution, the distance distribution shows the large amount of uncertainty in DRV prediction. There are generally two identifiable value ranges of clustering: 150 – 350 km and 500 – 700 km. This is similar to what was observed in the control forecast histogram, but the lower distance clustering has increased in range.

Examining the mean and spread evolution from the 48 to 72 hour perturbed forecasts (Figure 118) indicates that both the mean perturbed forecast distance is increasing towards the threshold. The mean distance from observed DRV is already a relatively large displacement at around 395 km in the 48 hour perturbed forecasts, but the increase to over 420 km at 72 hours, with a standard deviation of over 200 km, indicates the uncertainty is growing with time.

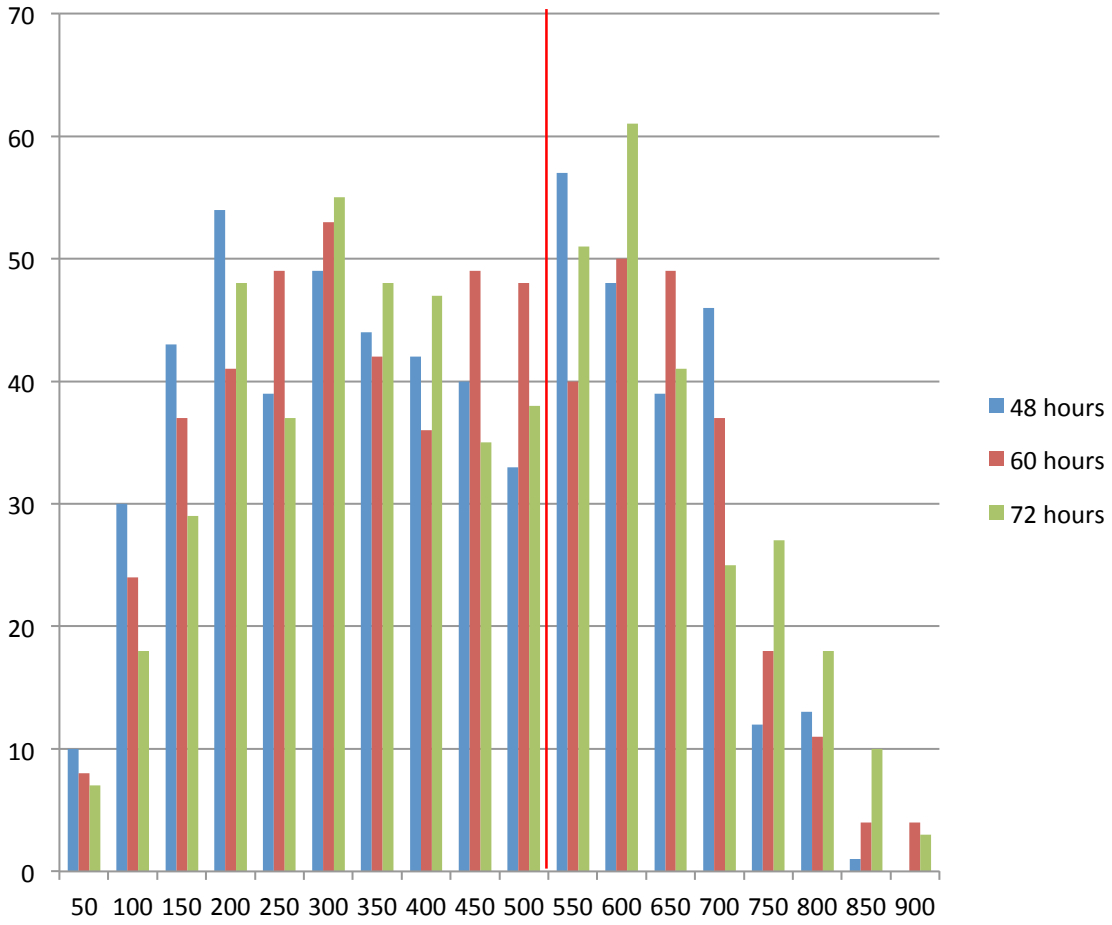

Figure 117. Histogram of perturbed forecast distances to observed DRVs with a 50 km bin size. The numbers under each bar represent the upper value of the bin (km). The red line indicates the threshold cut-off for DRV identification.

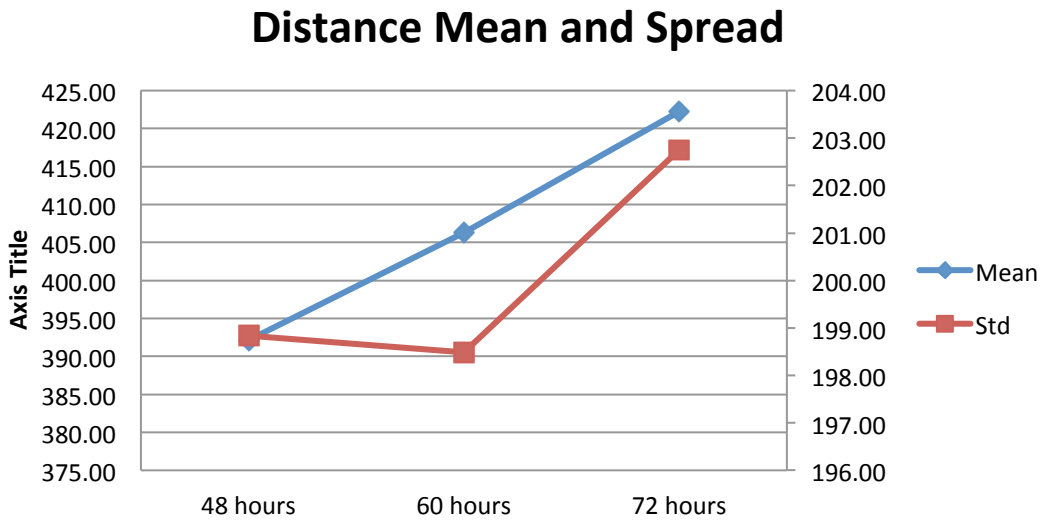

Figure 118. Perturbation forecast relative vorticity maximum distance from observed DRV mean and spread for 48, 60, and 72 hours.

F. OVERVIEW OF PERTURBATION FORECAST BAROCLINICITY VALUES

1. Perturbation Forecasts Meeting Minimum Baroclinicity Thresholds

The over perturbation forecast "hit" rate for meeting minimum baroclinicity thresholds was 63.3 percent, in pretty close agreement with the 66.7 percent of control forecasts that met the minimum threshold. This is a good indication that the general expected "hit" rate for forecasts early in a DRV lifecycle. Further investigating the "hit"-rates by perturbation forecast lead time reveals a slight 3 percent advantage at 60 hours, but it is not significant and is not a trending increase, as the forecast "hit" rate falls again at 72 hours.

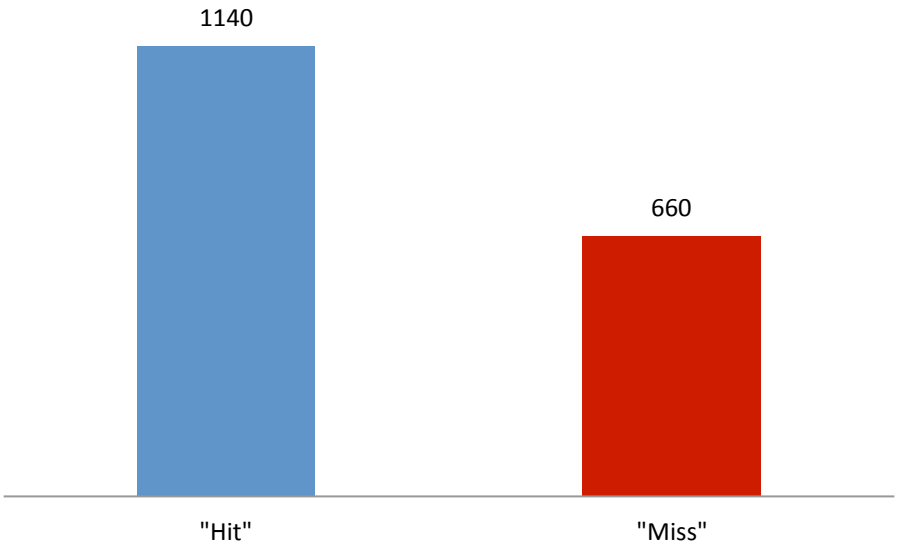

Figure 119. Histogram of the 1800 perturbation forecasts calculated baroclinicity values. Forecast calculations less than 5 K (red) are considered "misses," while forecasts greater than 5 K (blue) are considered "hits."

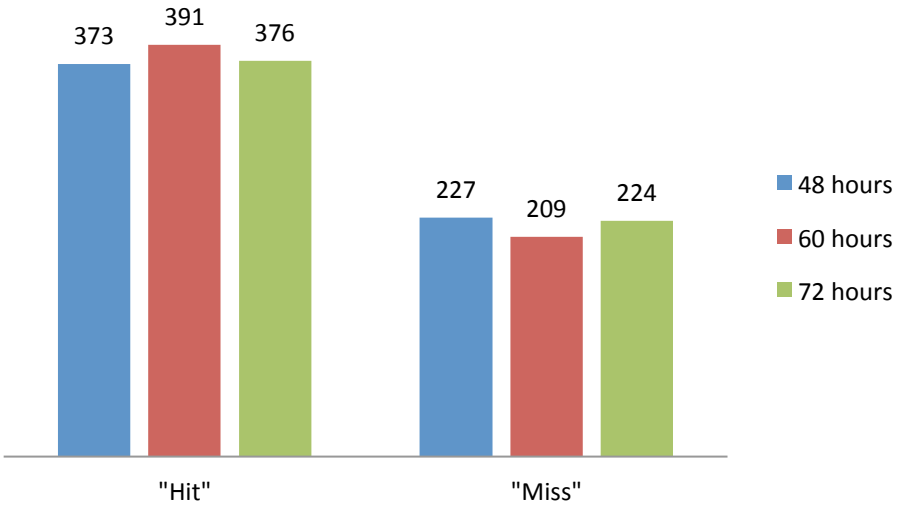

Figure 120. Histogram of the perturbation forecasts calculated baroclinicity values at each forecast length. (Thresholds same as above)

2. Detailed Analysis of Perturbation Forecast Baroclinicity Values

Analysis of the frequency distribution histogram of perturbation forecast baroclinicity values reveals a central tendency around the mean, with a general increase in the spread of values as the lead time increases (Figure 121).

An examination of the mean and spread trending over the perturbed forecast lead times reveals a positive trend in both values (Figure 122). The mean value is already above the threshold at the 48 hour forecast lead time and continues to well above threshold over the next to forecast lead times. In the same forecast time period the standard deviation is increasing, revealing a growth in uncertainty. The final value of standard deviation is quite high, indicating a fair amount of uncertainty in the perturbed forecasts by the 72 hour, which accounts for the decreased "hit" rates from the 60 hour perturbed forecasts despite the growth in mean baroclinicity values.

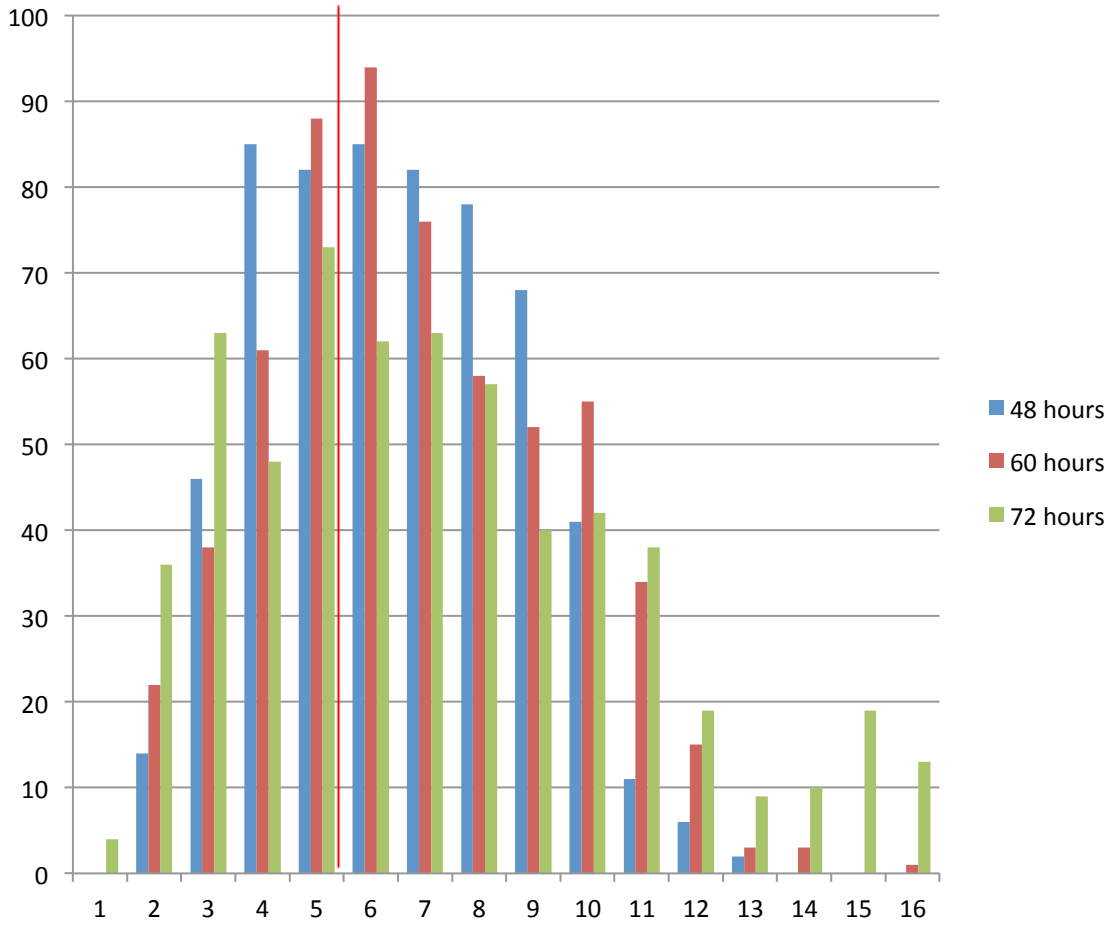

Figure 121. Histogram of perturbation forecast baroclinicity values (in degrees K) with a one degree bin size. The numbers under each bar represent the upper value of the bin. The red line indicates the threshold cut-off for DRV identification.

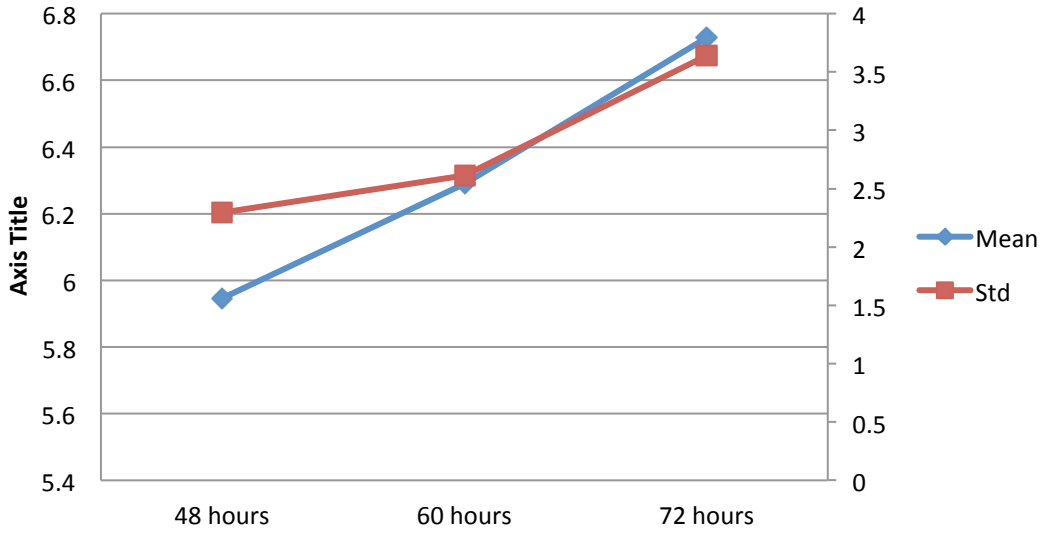

Figure 122. Perturbed forecast baroclinicity mean and spread for 48, 60, and 72 hours.

G. OVERVIEW OF PERTURBATION FORECAST RELATIVE HUMIDITY CALCULATIONS

1. Perturbation Forecasts Meeting Minimum Relative Humidity Thresholds

The vast majority (98.4 percent) of perturbed forecasts meet the minim threshold for relative humidity (Figure 123). Of the 1800 perturbation forecasts only 28 were below minimum and seem to happen with extreme infrequency. There appears to very little uncertainty to a relative humidity threshold being met in relation to the identified relative vorticity maximum locations.

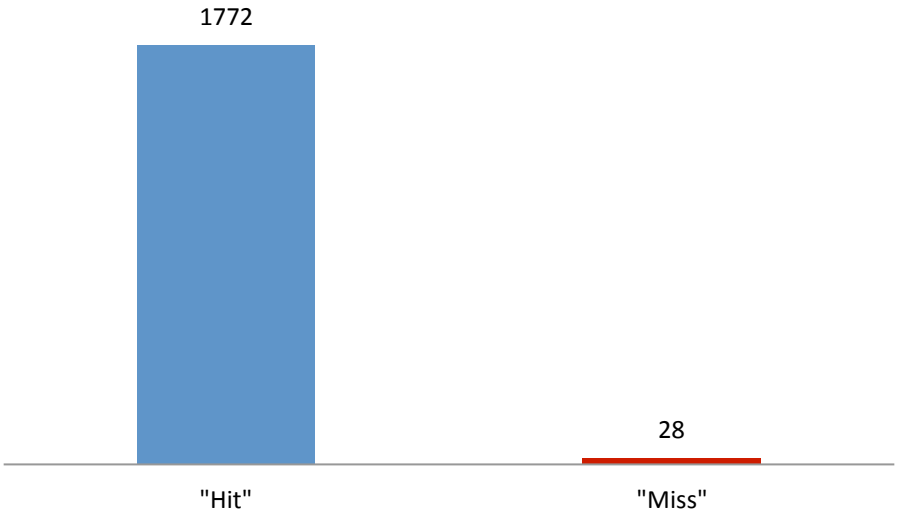

Figure 123. Histogram of the 1800 perturbation forecast calculated relative humidity values. Forecast calculations less than 90 percent (red) are considered "misses," while forecasts greater than 90 percent (blue) are considered "hits."

2. Detailed Analysis of Perturbation Forecast Relative Humidity Values

For verification of the lack of uncertainty, a more detailed frequency distribution histogram was examined (Figure 124). Besides a very small number of outliers, the majority of the calculated relative humidity values were above 93 percent, very similar to the observed distribution of the control forecasts in Chapter 5.

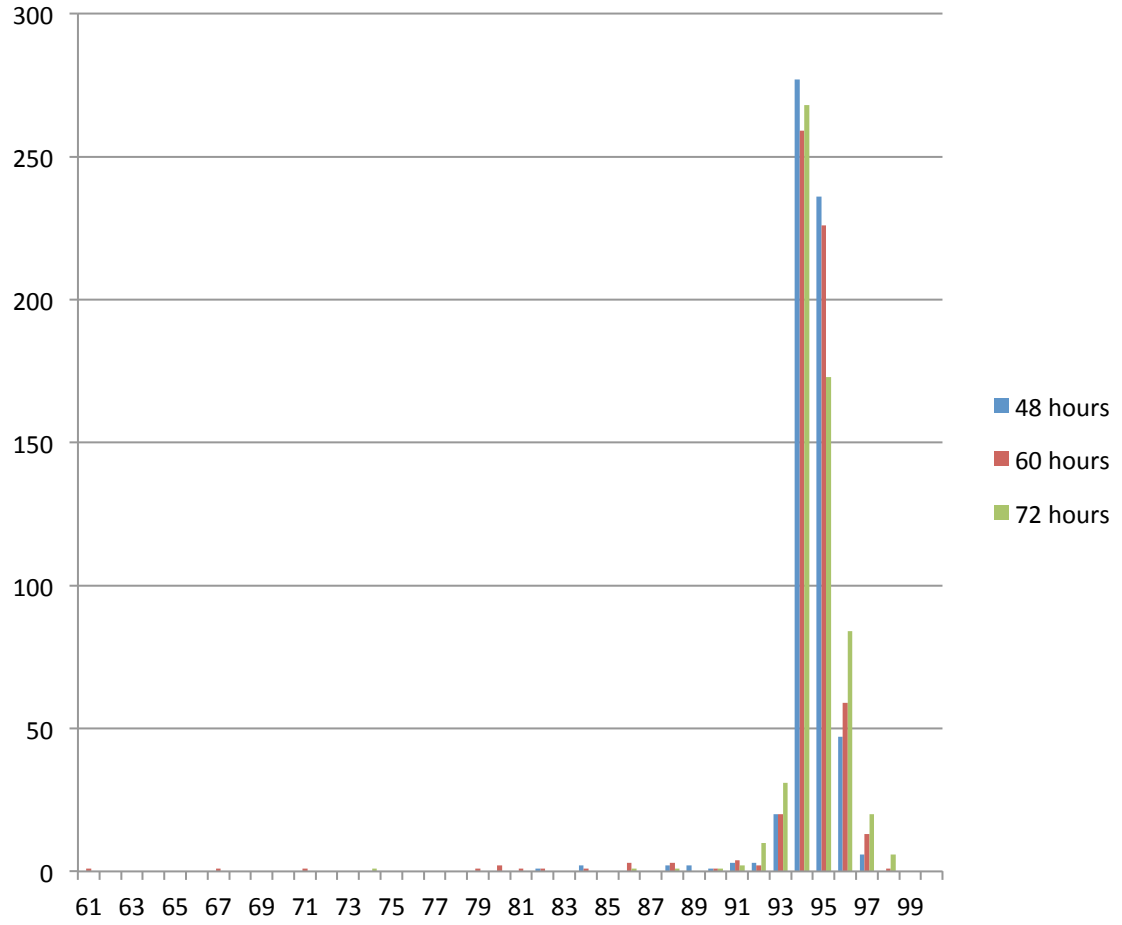

Figure 124. Histogram of perturbed forecast calculated relative humidity values (in percentages) with a one percent bin size. The numbers under each bar represent the upper value of the bin.

H. A MORE COMPREHENSIVE UNDERSTANDING OF THE UNCERTAINITY ASSOCIATED WITH DRV FORECASTS

The results of chapters 4-6 indicated that there is, on average, a large uncertainty associated with the predictability of DRV genesis and evolution (i.e., poor deterministic predictability). One might hypothesize that the general lack of in-situ data in the region of DRV genesis is deleterious to a deterministic forecast. In such situations where there is significant initial condition uncertainty, it is often valuable to use a probabilistic approach (i.e. an attempt to take into account initial condition uncertainty by perturbing ensemble members in a manner that accounts for the uncertainty).

Plots of the 72-hour sea level pressure mean and spread calculated from the ECMWF TIGGE appear to confirm the uncertainty of DRV prediction (large values of spread coincide with the observed location of the DRV). As such, it was deemed appropriate to evaluate the characteristics of DRV prediction in the context of the full ensemble.

The results confirm the general statement that DRV genesis and evolution is a difficult problem in the context of a deterministic forecast. The large spread indicates the predicted evolution is very sensitive to the initial conditions. It is also apparent that the observed solution does appear to be represented in the EPS solution space. It must be remembered that the goal of an ESP, in the context of DRV identification, is not to have 100% hit rate, but to evaluate the probability of DRV genesis and growth and to have the observed solution within the solution space of the EPS. That does appear to be the case here.

The goal of an ensemble prediction system is to attempt to account for initial condition uncertainty and evaluate the possible solution space that results when integrated forward.

The assumption is that the lack of in-situ data is deleterious to a deterministic forecast. In such situations where significant initial condition uncertainty is expected, it is often valuable to use a probabilistic approach (i.e. an attempt to take into account initial condition uncertainy). It therefore seems appropriate to apply a probabilistic approach. As indicated by both the SLP mean and spread plots and the statistics of the perturbed forecasts, there is a high level of uncertainty in almost all aspects of DRV forecasting. The 72 hour ensemble forecasting of the SLPs in the vicinity of the observed DRV in most cases placed a short-wave trough or closed low, but with the exception of a single case, exhibited high amounts of variability in the forecast. In a similar manner, all of the perturbation forecast output variables exhibited means within threshold, but the standard deviations were again very high. Both of these cases investigated in detail above, the mean and spread of the SLP and of the threshold values, highlight the vast amounts of uncertainty involved with the DRV forecasting and identification.

Comparing the perturbed and control forecast results reveal remarkable similarities. The comparable percentages of overall "hits" and "misses," as well as "hits" and "misses" of the individual threshold values, was quite remarkable. The overall spread of values and distribution was also similar. The probabilistic approach confirmed the large amount of initial uncertainty in the control forecasts, but unfortunately was not able to provide any clarity, as no new trends or patterns emerged from the perturbed forecast data.

On a final note, looking at the overall small number of "good" forecasts in both the control and perturbed forecasts, it's unlikely that if the analysis were continued beyond the first 24 hours of the DRV lifecycle, that the number of "good" forecasts would improve or even stay at the same level. It is very likely that a 48 hour initialization is not sufficient for forecasting DRVs, and to get even a modest amount of DRV test cases to track beyond 24 hours the initialization time would need to be moved closer to DRV genesis.

THIS PAGE INTENTIONALLY LEFT BLANK

VIII. DISCUSSION AND CONCLUSION

The overarching goal of this thesis was to add to the general knowledge and understanding of DRV predictability. Previous to this work, information regarding the performance of numerical models regarding the prediction of 'real world' DRVs was quite limited. It was hypothesized that the predictability of DRV genesis and evolution represented a difficult forecast problem. The work of MM05 summarized the issue as follows: 'Our findings here illustrate the challenges that DRV formation and evolution pose to the operational forecast community. It is clear that an accurate picture of both the background environment and the perturbation field is integral for an accurate forecast. An erroneous representation of the initial condition field will likely contribute to a poor forecast of DRV evolution or, at worst, lead to the failure of simulating DRV formation entirely. This inherent problem is exacerbated by the remoteness of the preferred regions of DRV genesis: due to their reliance on environmental moisture, DRVs often form and grow over oceanic regions where there is a distinct lack of observational data.'

The observed case of extreme winter storm Lothar (Wernli et al. 2002) and the study of an intense north Atlantic cyclone by Boettcher and Wernli (2011) documented two cases of high impact weather associated with a DRV where the forecast performance was found lacking. In addition, the study of M12 identified large forecast uncertainty of a DRV associated with recurving TC Chaba in the context of ensemble prediction. All of these cases lend credence to the hypothesis that DRV predictability is challenging. As such, they provide motivation to examine the issue in greater detail.

The work herein has leveraged and expanded upon previous research efforts. Given the hypothesis that there is large uncertainty associated with DRV genesis and evolution due to the inability to properly assess the initial state of the atmosphere, this work attempts to assess predictability in the context of an ensemble prediction system. ECMWF ensemble data from TIGGE is used to evaluate 12 cases of DRV genesis in the North Pacific during the year of 2010. All cases were chosen due to the high impact nature of the events: all chosen storms culminated in explosive cyclogenesis. While it has been shown previously that most DRVs exhibit minimal growth rates, a significant

number (15 percent) undergo explosive cyclogenesis. Of these, it is found that the DRV pathway to explosive cyclogenesis accounts for roughly 20 percent (North Pacific) of all cases of explosive deepening (BW13), a somewhat surprising result.

The work herein builds upon the studies of BW13 and M12. Both attempt to objectively identify DRV genesis and evolution using an ingredients-based approach. The work of BW13 incorporated high resolution ECMWF ensemble data to prepare a climatology of DRVs during the years 2001-2010. The work of M12 attempted to mimic the BW13 approach, utilizing BW13 climatological data and applying the methodology to data from ensemble data from a number of operational centers.

The reduced resolution in both the horizontal and vertical in the ECMWF TIGGE data necessitated alterations to the BW13 approach. Given the knowledge that a DRV did in fact exist in the operational analysis, the M12 approach limited the search area and did not attempt feature tracking. Other alterations were made, including the use of low-level averaged relative vorticity as the primary identification parameter (as opposed to sea level pressure minima and enhanced low-level PV) and no assessment of the upper-level forcing was conducted. Again, the assumption was that given the observed DRV, it was not necessary to evaluate upper-level forcing. Finally, the M12 identification script was slightly modulated to be more consistent with the BW13 calculations of environmental baroclinicity and moisture.

The improved identification algorithm was tested upon the TC Chaba DRV during the extent of its lifecycle from genesis through explosive deepening. The algorithm was applied to the analysis data (the 00 hour forecast of the ensemble control being used as the best guess to reality). The script performed very well throughout the entire lifecycle, lending credence to the identification code.

The TC Chaba DRV case was used also to perform an analysis of the deterministic forecast (i.e. the control simulation) over the lifecycle of a DRV and subsequent explosive deepening event. It was apparent the control forecast performed quite poorly. An in depth analysis of the parameter values provided by the identification script, combined with a visual inspection of the simulated fields, illustrated that, while there were instantaneous examples of a disturbance that had DRV-like characteristics,

there was no coherent disturbance over the observed time period. In addition, the repercussion of the poor forecast at early times was the inability to forecast the observed explosive deepening.

Following this initial assessment, three additional in depth analyses of control forecasts were performed. A number of additional insights were attained. They included the observations that: i) terrain effects over land can pose additional complications; ii) the prediction of DRV genesis, in particular, can be difficult due to the often weak signal in the chosen identification parameters; iii) the ability of the script to identify a DRV-like feature is related to the intensity of the feature; iv) the predictability of the propagation speed is difficult and a miscast of said propagation speed has important repercussions for the forecast at subsequent forecast times; and v) a further investigation of the appropriateness of the threshold values used should be undertaken.

To ascertain the performance of the deterministic forecasts as a whole, the DRV identification script was used to evaluate the control simulation forecasts for all 12 cases during the first 24 hours after DRV genesis. Each control forecast was determined to have been "good," "fair," or "poor" (as defined in Chapter 6). The overall performance of the deterministic forecasts was found to be lacking. Only two of the forecasts were determined to be "good," two were determined to be "fair," and the remaining eight were analyzed as "poor." Overall hit-rates for individual forecasts were lacking as well, with only 33 percent of control forecasts identified as "hits." Little sensitivity to forecast time was found. These results are consistent with the hypothesis that DRV predictability is a difficult problem, that the sensitivity to initial condition uncertainty is large and that, given such facts, a probabilistic approach that can account for initial condition uncertainty would likely be valuable.

The postulated large uncertainty was confirmed via an analysis of ECMWF ensemble mean sea level pressure and spread charts. In all but one case, a region of large uncertainty was identified in the region of the observed DRV.

Subsequently, the forecast "success" of the perturbed members of the ensemble system were evaluated in a similar manner as to that of the control simulations. The

results revealed remarkable similarities to those of the control simulation analysis. Approximately 23% of the ensemble members met the good or fair criteria.

The results regarding the assessment of the probabilistic approach indicate that the ensemble prediction system provides valuable information. It is useful to identify regions of high uncertainty. In addition, it should be noted that while hit rates were not large, a significant fraction of the ensemble members appear to be providing a reasonable facsimile of the observed evolution. Both of these facets are consistent with the goals of a probabilistic approach to forecasting. Given the results of this work in totality, it is apparent that DRV predictability is best attacked via a probabilistic approach.

While this work serves as a significant extension to previous work and represents the first systematic evaluation of DRV predictability beyond single case study analyses, there is much room for improvement. Suggestions for future work include:

- Sensitivity analysis of the chosen thresholds for the DRV identification script.
- Examination of the explosive deepening phase of DRV development
- Investigation of the impact of different forecast lead times
- Further expansion of the scope of this effort to include more cases and the analysis of ensemble data from other operational centers
- Evaluation of the cause of good / bad forecasts. Is there a systematic bias in the forecasting of any of the DRV characteristics or environmental requirements?

LIST OF REFERENCES

Boettcher, M., and Wernli H., 2011: Life cycle study of a diabatic Rossby wave as a precursor to rapid cyclogenesis in the North Atlantic - Dynamics and forecast performance. *Mon. Wea. Rev*., 139, 1861–1878.

_____, and _____, 2013: A 10-yr climatology of diabatic Rossby Waves in the Northern Hemisphere. *Mon. Wea. Rev*., 141, 1139-1154.

Conzemius, R. J., R. W. Moore, M. T. Montgomery and C. A. Davis, 2007: Mesoscale convective vortex formation in a weakly sheared moist neutral environment. J. *Atmos. Sci*., 64, 1443–1466.

Dunkerton, T. J., M. T. Montgomery, and Z. Wang, 2009: Tropical cyclogenesis in a tropical wave critical layer: easterly waves. *Atmos. Chem. Phys*., 9, 5587–5646.

European Centre for Medium-Range Forecasting, cited 2014: TIGGE – the THORPEX Interactive Grand Global Ensemble. [Available online at http://tigge.ecmwf.int/#info]

Fantini, M., and A. Buzzi, 1993: Numerical experiments on a possible mechanism on cyclogenesis in the Antarctic region. *Tellus*, 45A, 99–113.

Gyakum, J. R., P. J. Roebber, and T. A. Bullock, 1992: The role of antecedent surface vorticity development as a conditioning process in explosive cyclone intensification. *Mon. Wea. Rev*., 120, 1465–1489.

Holton, J. R., 1992: Synoptic-Scale Motions II: Baroclinic Instability. *An Introduction to Dynamic Meteorology*, R. Dmowska and J.R. Holton, Eds., Academic Press, 228–264.

Jiang, H. and D. J. Raymond, 1995: Simulation of a mature mesoscale convective system using a nonlinear balance model. *J. Atmos. Sci*., 52, 161–174.

Jones, S. C., P. A. Harr, J. Abraham, L. F. Bosart, P. J. Bowyer, J. L. Evans, D. E. Hanley, B. N. Hanstrum, R. E. Hart, F. Lalaurette, M. R. Sinclair, R. K. Smith and C. Thorncroft, 2003: The extratropical transition of tropical cyclones: forecast challenges, current understanding, and future directions. *Wea. Forecasting*, 18, 1052–1092.

Lorenz, E. N., 1955: Available potential energy and the maintenance of the general circulation. *Tellus*, 7, 157–167.

Mak, M., 1994: Cyclogenesis in a conditionally unstable moist baroclinic atmosphere. *Tellus*, 46A, 14–33.

Moore, R. W., H. A. Archambault, and P. Harr, 2012: The probabilistic prediction of diabatic Rossby vortex gensis associated with recurving western North Pacific TC Chaba (2010). Fourth International Workshop on the Extratropical Transition of Tropical Cyclones, Saint-Adèle, QC.

Moore, R. W., H. Archambault, and R. McTaggart-Cowan, 2013: DRV genesis associated with recurving tropical cyclones. Davos Atmosphere and Cryosphere Assembly, Davos, Switzerland.

Montgomery, M. T. and B. F. Farrell, 1991: Moist surface frontogenesis associated with interior potential vorticity anomalies in a semigeostrophic model. *J. Atmos. Sci*., 48, 343–367.

_____, and _____, 1992: Polar low dynamics. *J. Atmos. Sci*., 49, 2484–2505.

Moore, R. W., and M. T. Montgomery, 2004 (MM04): Reexamining the dynamics of short-scale, diabatic Rossby waves and their role in midlatitude cyclogenesis. *J. Atmos. Sci*., 61, 754–768.

_____, and _____, 2005 (MM05): Analysis of an idealized, three-dimensional diabatic Rossby Vortex: A coherent structure of the moist baroclinic atmosphere. *J. Atmos. Sci*., 61, 754–768.

_____, and _____, and H. C. Davies, 2008 (MMD08): The integral role of a diabatic Rossby vortex in a heavy snowfall event. *Mon. Wea. Rev*., 136, 1878–1897.

_____, and _____, and _____, 2012 (pending publication): Dynamical processes culminating in diabatic Rossby vortex genesis. Part I: An idealized numerical model study. *Mon. Wea. Rev*.

_____, and O. Martius, and H. C. Davies, 2008: Downstream development and Kona low genesis. *Geophys. Res. Lett*., 35, L20814, doi:10.1029/2008GL035502, 2008.

Norquist, D. C., E. E. Recker, and R. J. Reed, 1977: The energetics of African wave disturbances as observed during phase III of GATE. *Mon. Wea. Rev*., 105, 334–342.

Parker, D. J., and A. J. Thorpe, 1995 (PT95): Conditional convective heating in a baroclinic atmosphere: A model of convective frontogenesis. *J. Atmos*. Sci., 52, 1699–1711.

Petterssen S. and Smebye S. J., 1971 (PS71): On the development of extratropical cyclones, *Quart. J. R. Met. Soc*., 97, 457–482.

Raymond, D. J. and H. Jiang, 1990 (RJ90): A theory for long-lived mesoscale convective systems. *J. Atmos. Sci*., 47, 3067–3077.

Riviere, G., P. Arbogast, K. Maynard, and A. Joly, 2010: The essential ingredients leading to the explosive growth stage of the European wind storm Lothar of Christmas 1999. *Quart. J. Roy. Meteor*. Soc., 136, 638–652.

Sanders, F. and Gyakum, J. R., 1980 (SG80): Synoptic-dynamic climatology of the "Bomb". *Mon. Weather Rev*., 108, 1589–1606.

Shih, N., 2012: Formation and development of diabatic Rossby vortices in a 10 year climatology. Thesis, Meteorology Department, Naval Postgraduate School, 119pp.

Wernli, H., 2002: Diabatic Rossby Waves, *EGS XXVII General Assembly*, Nice, 21–26 April 2002, abstract #3957.

_____, S. Dirren, M. A. Liniger, and M. Zillig, 2002: Dynamical aspects of the life cycle of the winter storm "Lothar" (14–26 December 1999). Quart. J. Roy. *Meteor. Soc.*, 128, 405–427.

THIS PAGE INTENTIONALLY LEFT BLANK

INITIAL DISTRIBUTION LIST

1. Defense Technical Information Center
   Ft. Belvoir, Virginia

2. Dudley Knox Library
   Naval Postgraduate School
   Monterey, California